STUDIES FOR SEISMIC ZONATION OF THE SAN FRANCISCO BAY REGION

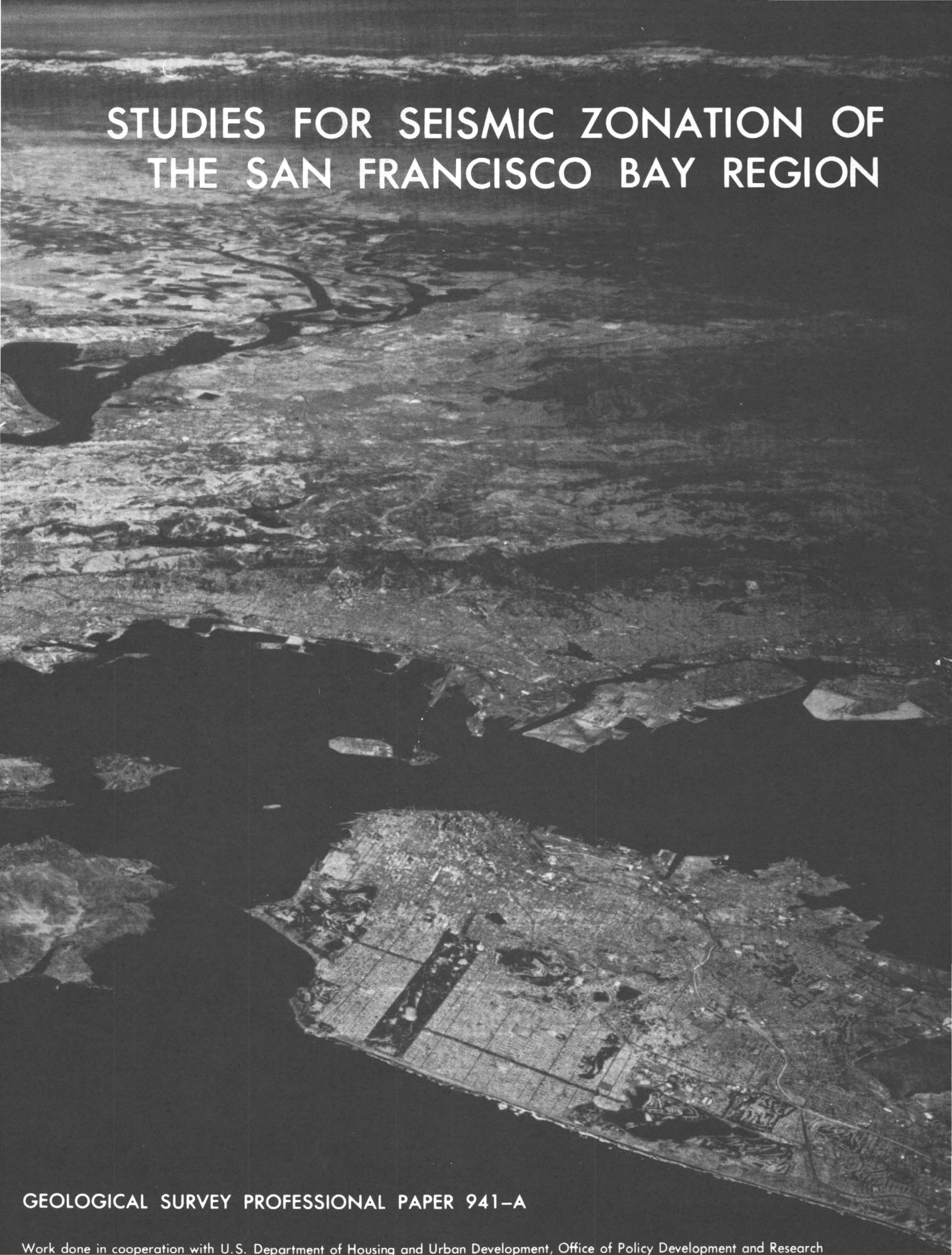

GEOLOGICAL SURVEY PROFESSIONAL PAPER 941–A

Work done in cooperation with U.S. Department of Housing and Urban Development, Office of Policy Development and Research

COVER PHOTOGRAPH of San Francisco Bay Region taken April 14, 1972, at altitude of 65,000 feet from U–2 aircraft. Courtesy National Aeronautics and Space Administration (Ames Research Center, Moffett Field, Calif.) Front shows city of San Francisco and Golden Gate at bottom, San Francisco Bay and city of Oakland in middle, Sacramento–San Joaquin Delta and crest of Sierra Nevada at top. Back shows Bolinas Lagoon and trace of San Andreas fault at bottom, San Pablo Bay in middle, Sacramento valley and crest of Sierra Nevada at top.

Studies for Seismic Zonation of the San Francisco Bay Region

Edited by R. D. BORCHERDT

BASIS FOR REDUCTION OF EARTHQUAKE HAZARDS, SAN FRANCISCO BAY REGION, CALIFORNIA

GEOLOGICAL SURVEY PROFESSIONAL PAPER 941-A

A series of closely related earth science studies that define the nature and severity of earthquake hazards associated with geologic conditions

Jointly supported by the U.S. Geological Survey and the Department of Housing & Urban Development, Office of Policy Development and Research, as a part of a program to develop and apply earth-science information in support of land-use planning and decisionmaking.

UNITED STATES GOVERNMENT PRINTING OFFICE, WASHINGTON: 1975

UNITED STATES DEPARTMENT OF THE INTERIOR

ROGERS C. B. MORTON, *Secretary*

GEOLOGICAL SURVEY

V. E. McKelvey, *Director*

Library of Congress catalog-card No. 75-15239

For sale by the Superintendent of Documents, U.S. Government Printing Office
Washington, D.C. 20402
Stock Number 024-001-02676-7

FOREWORD

Earthquake hazard reduction program

This report represents a milestone in the evolution of methods for reducing the hazards of earthquakes. The great Alaska earthquake of 1964 triggered an awareness among public officials of the seriousness of the earthquake hazard to many of the Nation's major cities. If the effects of the Alaska earthquake are used as a gage, it is clear that when a major earthquake hits California cities such as Los Angeles or San Francisco, casualties could be in the tens of thousands and damage could be in the tens of billions of dollars.

After the Alaska earthquake, the U.S. Geological Survey began to focus its diverse earth-science capabilities more specifically toward the goal of reducing earthquake hazards. The possible effectiveness of land-use planning to avoid the most serious hazards began to be recognized as a supplement to the common practice of incorporating earthquake-resistant designs into structures. For decades geologists had known, for example, that structures built astride the San Andreas fault were in jeopardy, but only in a few places had the fault been delineated in sufficient detail to serve as a guide to community officials and developers. Even if the fault data had been available, standard procedures were inadequate for translating the data into land-use plans or actions. Indeed, land-use planning was, and still is, in an early phase of evolution in the United States. No national land-use policy has been adopted.

In order to satisfy some of the most urgent needs for basic data, several projects were started after the Alaska earthquake. The entire 1,400-km (868-mi) length of the San Andreas fault was mapped for the first time on the best available topographic base maps. Nets of closely spaced seismic instruments were installed in an experimental field laboratory along the San Andreas fault to study the basic mechanisms of earthquakes and the patterns of energy radiation and attenuation as earthquake waves pass through different types of rocks and soil. New laboratory studies were initiated to explore the physical principles of earthquakes. Research demonstrated the feasibility of earthquake prediction and of earthquake control and modification.

The science of earthquakes is complex, requiring data and research in seismology, geology, soil mechanics, geophysics, hydrology, and engineering. Nevertheless, if earthquake hazards are to be reduced, earth-science data must be translated from scientific and technical language into a form that can be used effectively in the decisionmaking process.

The San Francisco Bay Region Environment and Resources Planning Study

Out of this recognition of the need to use earth-science information in regional planning and decisionmaking came an experimental program—the San Francisco Bay Region Environment and Resources Planning Study. The study, begun in January 1970, is jointly supported by the U.S. Geological Survey, Department of the Interior, and the Office of Policy Development and Research, Department of Housing and Urban Development. The Association of Bay Area Governments participates in the study and provides a liaison and communication link with other regional planning agencies and with county and local governments.

Although the study focuses on the nine-county 7,400-mi^2 San Francisco Bay region, it bears on a difficult issue that is of national concern—how best to accommodate orderly development and growth while conserving our natural resource base, insuring public health and safety, and minimizing degradation of our natural and manmade environment. The complexity, however, can be greatly reduced if we understand the natural characteristics of the land, the processes that shape it, its resource potential, and its natural hazards. These subjects are chiefly within the domain of the earth sciences: geology, geophysics, hydrology, and the soil sciences. Appropriate earth-science information, if available, can be rationally applied in guiding growth and development, but the existence of the information does not assure its effective use in the day-to-day decisions that shape development. Planners, elected officials, and the public rarely have the training or experience needed to recognize the significance of basic earth-science information, and many of the conventional methods of communicating earth-science information are ill suited to their needs.

The study is intended to aid the planning and decisionmaking community by (1) identifying important problems that are rooted in the earth sciences and related to growth and development in the bay region, (2) providing the earth-science information that is needed to solve these problems, (3) interpreting and publishing findings in forms understandable to and usable by nonscientists, (4) establishing new avenues of com-

munication between scientists and users, and (5) exploring alternate ways of applying earth-science information in planning and decisionmaking.

Since the study was started in 1970, it has produced more than 70 reports and maps. These cover a wide range of topics: reduction of flood and earthquake hazards, unstable slopes, engineering characteristics of hillside and lowland areas, mineral and water resources management, solid and liquid waste disposal, erosion and sedimentation problems, bay water circulation patterns, and others. The methods used in the study and the results it has produced have elicited broad interest and a wide range of applications from planners, government officials, industry, universities, and the general public.

Studies for seismic zonation of the San Francisco Bay region

This report brings together the results of a number of earth-science studies that provide a basis for reducing earthquake hazards.

The enormous amounts of energy released during large, or even moderate, earthquakes produce a complex chain of effects, most of which are potentially hazardous to man and his works. Many of these effects, such as fault displacement and ground shaking, are direct results of the earthquake. Others, like landsliding and liquefaction, result from the action of ground motion generated by earthquakes on unstable geologic units or structures. Still other effects result from the reaction of manmade structures to earthquake forces. Moreover, many of these effects are complexly interrelated in ways that make analysis difficult; ground shaking, for example, may be amplified or reduced by local geologic conditions, and the level of ground shaking may determine whether or not landslides are triggered or liquefaction induced.

The diversity and complexity of earthquake effects make the reduction of earthquake hazards extraordinarily difficult and require adoption of a coordinated and disciplined plan of attack. Such a plan must incorporate the efforts of many individuals and the skills and techniques of several professions. Earth scientists, structural and civil engineers, professional planners, elected officials, and private citizens are among those who are essential participants in the effort.

This report is designed to provide the earth-science basis for such a comprehensive approach to reducing earthquake hazards. It brings together and correlates significant results from several fields of geology and from seismology and engineering seismology. Because these results are derived from the natural processes brought into play by a damaging earthquake, they are a logical starting point for an attack on the problem.

The method outlined here for seismic zonation is applicable, with modifications, throughout the San Francisco Bay region and elsewhere in regions of high earthquake hazard. Its effectiveness, however, depends on the degree to which these results are used or applied. Although many of the research findings can be applied directly in hazard-reduction programs now underway, others suggest the need for continuing communication among participants in the hazard-reduction process and for the conduct of related research. Thus, while few readers will be prepared to apply all that is presented here, the contents should assist them in determining where additional expertise is needed.

CONTENTS

ILLUSTRATIONS

TABLES

BASIS FOR REDUCTION OF EARTHQUAKE HAZARDS,
SAN FRANCISCO BAY REGION, CALIFORNIA

STUDIES FOR SEISMIC ZONATION OF THE SAN FRANCISCO BAY REGION

ABSTRACT

Studies by 15 researchers in various earth-science and engineering disciplines suggest that seismic zonation of the San Francisco Bay region is feasible using existing geologic and geophysical knowledge. Seismic zonation is defined as the delineation of geographical areas with different potentials for surface faulting, ground shaking, flooding, liquefaction, and landsliding during future earthquakes of specific size and location. Seismic zonation, as defined, is a necessary foundation for the development of regional land-use policies to minimize future losses during earthquakes. The need for seismic zonation was clearly demonstrated by the large variations in damage resulting from the great California earthquake of April 18, 1906. In some areas of the San Francisco Bay region, the losses of life and property were catastrophic, whereas in other areas the losses were minor.

In an integrated sequence of papers, data required for seismic zonation are compiled and analyzed. Methodologies are emphasized for constructing the necessary tools from data currently available on a regional scale. Basic tools derived for seismic zonation are (1) a map showing active faults, (2) data on attenuation of shaking in bedrock, (3) geologic data, (4) a map showing qualitative estimates of ground response, (5) a map showing areas of potential inundation by tsunamis, (6) a map showing liquefaction potential, and (7) a map showing landslide susceptibility.

The map showing active faults delineates areas of potential faulting of the ground surface and the location of potential sources of strong ground shaking. Categorizing the faults according to geologic and geophysical evidence for recency of movement and fault length permits crude estimates of earthquake potential, maximum earthquake magnitude, and characteristics of future ground deformation. The San Andreas, Hayward, and Calaveras faults are considered to have the highest potential for large earthquakes, with estimates of maximum magnitude of 8.5, 8.2, and 6.5, respectively.

The data on attenuation of shaking with distance from the source suggest that duration and peak-amplitude parameters of ground motion can be predicted from empirical relations for sites on bedrock and firm alluvium at distances greater than 10, 20, and 40 km (6, 12, and 25 mi) for earthquakes of magnitude 5.0 to 5.9, 6.0 to 6.9, and 7.0 to 7.9, respectively. Data are not available for smaller distances and larger magnitudes; hence extrapolation based on numerical models of faulting is required.

Geologic data provide the basis for extrapolating results of local site studies to larger areas for purposes of seismic zonation. The unconsolidated sedimentary deposits of the San Francisco Bay region are differentiated into five geologic-genetic units based on geomorphic relations, soils, physical properties, fossils, and radiocarbon dates. Regrouping these units according to common sets of physical parameters such as thickness, density, sorting, data from standard penetration tests, and shear-wave velocities shows that certain groups of units are important for studying ground response, others for studing liquefaction, and still others for studying slope stability.

The map showing qualitative estimates of ground response delineates on a regional basis those areas for which the effects of ground shaking, as amplified by surficial deposits, are expected to be least, intermediate, and greatest. These expectations are based on analysis of the observed 1906 California earthquake intensities, accelerograms recorded from the 1957 San Francisco earthquake, amplifications of ground shaking measured at 99 sites, numerical models of ground response, and geologic data. Combining the data on the potential location and magnitude of future earthquakes, on the attenuation of strong shaking on bedrock, and on the estimated high-strain response of surficial deposits permits quantitative predictions of ground shaking at specific sites. Such predictions suggest that certain geologic units substantially amplify frequencies of ground shaking near the fundamental mode of the unit and that the peak amplification in some instances can be at least as high at high-strain levels as that at low-strain levels.

The map showing areas of potential inundation by tsunamis was prepared earlier by Ritter and Dupré (1972) and is mentioned here for completeness. The map delineates coastal areas and areas along the margins of San Francisco Bay likely to be inundated by an earthquake-generated wave of 6 m (20 ft) at Golden Gate Bridge.

The map showing landslide susceptibility delineates general areas where landsliding is considered likely. The map is based on the present distribution of landslide deposits, bedrock geology, and degree of slope. The parts of the San Francisco Bay region having the greatest susceptibility to landsliding are hilly areas underlain by weak bedrock units of slope greater than 15 percent.

Application of these seven basic tools along a demonstration profile for a postulated magnitude 6.5 earthquake on the San Andreas fault illustrates a methodology for seismic zonation of the San Francisco Bay region at the current state of the art. Pending completion of this suggested seismic zonation, a map showing maximum intensities delineates areas with potential earthquake problems, and the seven basic tools help identify the problems and their possible severity.

INTRODUCTION

The San Francisco Bay region (nine bay area counties) includes three major active faults and seven minor faults. Historically, 4 violent earthquakes and 33 smaller, but damaging, earthquakes have occurred on these faults. As a result, the San Francisco Bay region is considered one of the most earthquake-prone urbanized areas in the United States.

The most devastating earthquake to hit the San Francisco Bay region was that of April 18, 1906. Damage to property from the earthquake and the ensuing fires was estimated at $400 million (1906 value). Approximately 700 people lost their lives. The amount of damage from the earthquake was strongly dependent on the geologic character of the ground. For example, in the Telegraph Hill area of San Francisco, where rock is exposed at the surface, the effects of the earthquake were "weak," with "occasional fall of chimneys and damage to plaster, partitions, plumbing, and the like." But at a distance of less than one-quarter mile, in an area underlain by artificial fill and water-saturated mud, the effects of the earthquake were "violent," with "fairly general collapse of brick and frame structures when not unusually strong" (Wood, 1908). Comparison of the 1906 distribution of intensity (fig. 1) and the geologic map of San Francisco (fig. 2) demonstrates the need for zoning the region to account for variations in earthquake hazards originating from variations in geologic conditions.

The principal hazards to life and property from earthquakes in the San Francisco Bay region are potential failures of manmade structures, such as buildings, dams, waterlines, and bridges. Current urbanization implies that the effects of another 1906-type earthquake would be catastrophic. A recent study (Algermissen, 1972) predicts loss of life ranging from 2,300 to more than 100,000 people depending on time of day and the number of dam failures. The potential loss of property is estimated to be billions of dollars; the loss in productivity and earnings, substantially larger. Such potential losses can be minimized if manmade structures are adequately engineered to withstand future earthquakes.

Construction of earthquake-resistant structures requires the prudent and conscientious application of advanced engineering design techniques that consider the geologic setting of the surrounding region. In the past, the geologic setting has been considered principally on a site by site basis and only for major structures (such as high-rise buildings and nuclear power plants). For most structures, no consideration has been given to the influence of the geologic setting on potential earthquake damage. This situation is due partly to a past lack of knowledge, partly to the expense of assessing the geologic setting on a site by site basis, and partly to a lack of appropriate public policy to incorporate and enforce developments in the earth sciences and engineering.

The geologic setting of a region influences earthquake damage by controlling (1) the potential location and size of damaging earthquakes, (2) the potential for rupture of the ground surface by faulting, both slow creep and sudden movement, (3) the potential for damaging levels of ground shaking on different geologic units at various distances from the source of the earthquake, (4) the potential for flooding from dam failures, tsunamis, seiches, and tectonic changes of land level, and (5) the potential for shaking-induced ground failures such as landslides and those related to liquefaction.

This study summarizes the state-of-the-art for assessing these potential earthquake effects on a regional scale for purposes of seismic zonation. Such an evaluation of the geologic setting on a regional scale provides the necessary foundation for developing policies that will minimize future earthquake losses. It also provides a basis for incorporating geologic factors into codes for the routine design of earthquake-resistant structures.

The different sections of this report examine (1) faults and their earthquake potential, (2) estimation of bedrock motion at the ground surface, (3) geologic parameters for seismic zonation, (4) response of various geologic units to shaking, (5) liquefaction potential, and (6) landslide susceptibility. Seismic zonation requires the composite application of results from these studies for potential earthquakes of specific size and location. Such an application is demonstrated in terms of a profile showing effects predicted for a postulated earthquake (magnitude $\approx$6.5) on the San Andreas fault. This example illustrates the extent to which such effects as surface faulting, ground shaking, flooding, liquefaction, and landsliding can be predicted quantitatively on a regional scale for purposes of seismic zonation.

The nature of the seismic zonation problem suggests a broad audience ranging from the research earth scientist and engineer to the practicing land-use planner, engineer, and politician. Accordingly, the authors have directed much of their discussion toward a broad audience, with many results spanning a wide range of interests. The compilations and analyses presented in the first six papers are of most interest to earth scientists and engineers involved in research. The methodology presented in the seventh paper is of most interest to those involved in developing and implementing appropriate land-use and construction practices.

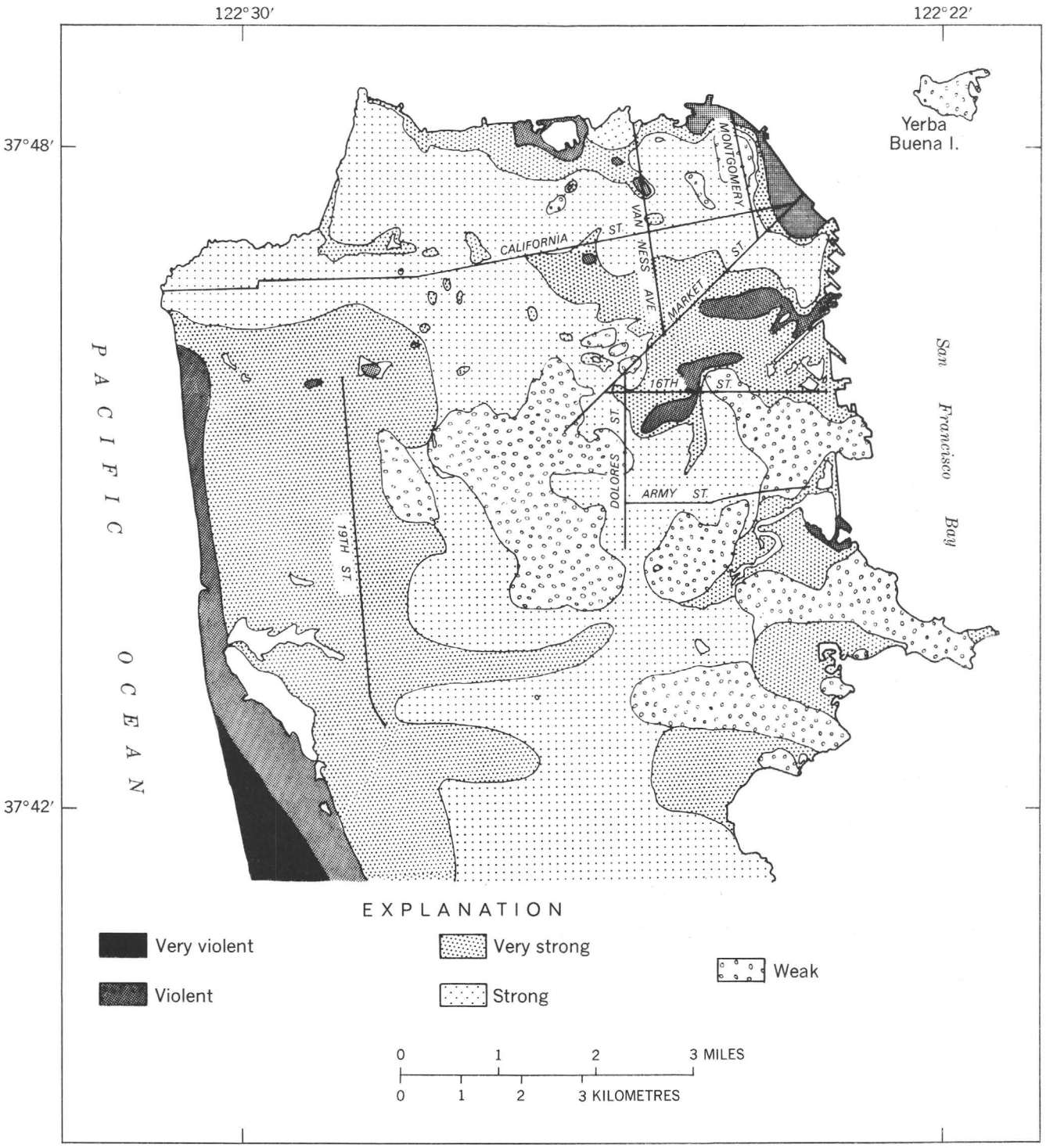

FIGURE 1.—Distribution of apparent intensity of the 1906 earthquake in San Francisco, Calif. (after Wood, 1908). Detailed description of 1906 intensity scale for San Francisco is presented at end of report. Compare with figure 2, which shows distribution of geologic report units.

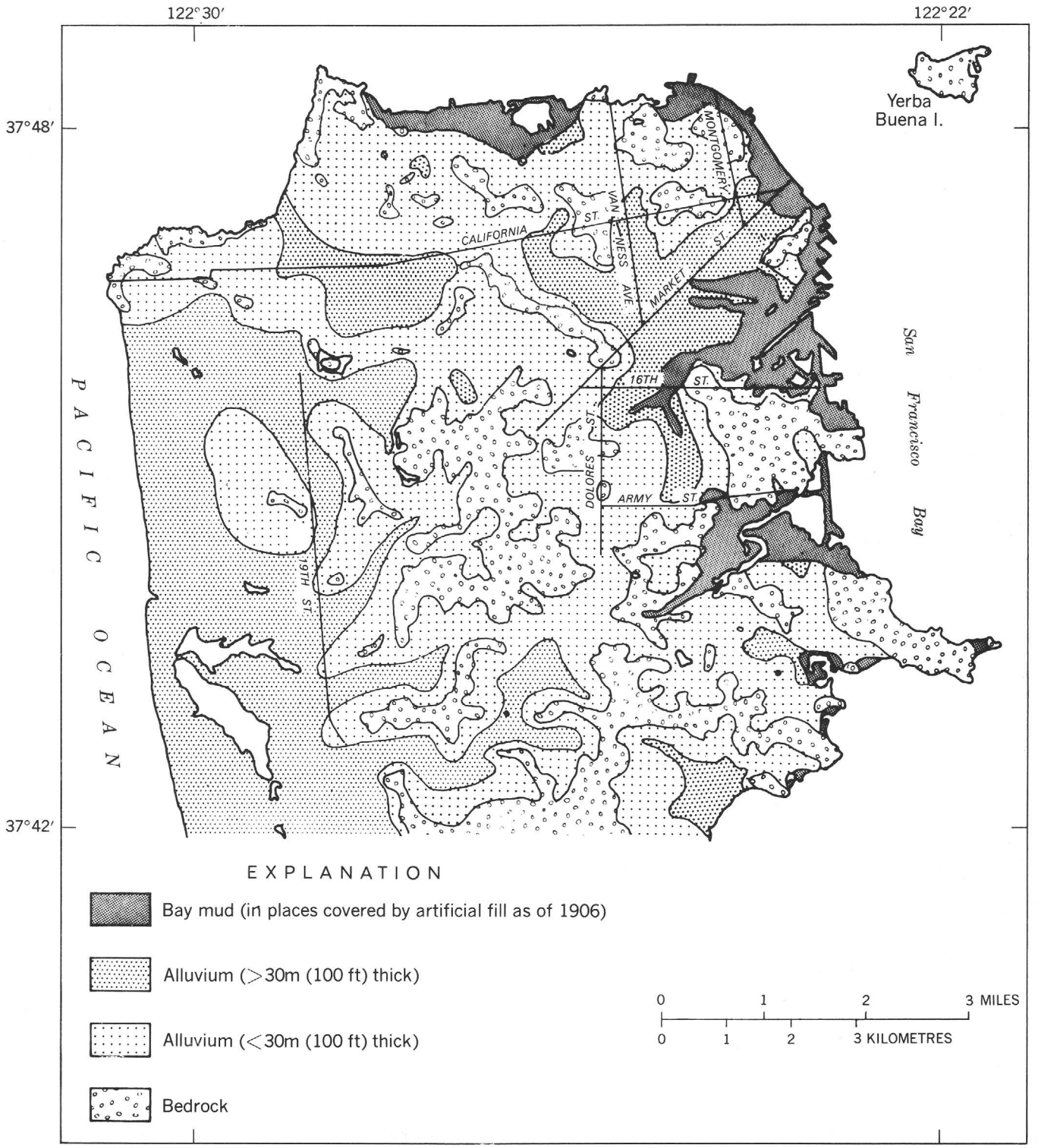

FIGURE 2.--Generalized geologic map, San Francisco, Calif. (compiled by K. R. Lajoie from data of Schlocker and others, 1958).

FAULTS AND FUTURE EARTHQUAKES

By R. L. WESSON, E. J. HELLEY, K. R. LAJOIE, and C. M. WENTWORTH

INTRODUCTION

The San Francisco Bay region is located within a broad complex of faults associated with the San Andreas fault system. Movement along these faults and the associated geologic deformation have produced the mountains and valleys of the California Coast Ranges that help make the bay region a scenic place to live. But this tectonic deformation is not entirely an asset. It continues today, producing small earthquakes that wake sleeping residents and earth movements that crack sidewalks and buildings. More importantly, continued deformation holds potential for generating catastrophic earthquakes, which result from the sudden movement of blocks of the earth's crust along faults.

All faults—and they are numerous in the bay region—have been surfaces of movement at least once in the geologic past. But which faults are likely to sustain future movement? And what will be the characteristics of this movement? The answers to these questions are critical to seismic zonation. If the answers can be found, land-use regulation and design and construction practices can be instituted to minimize the consequences of future movement. Our present methods are primarily empirical because physical laws governing earthquake behavior are still inadequately understood. Our judgment of whether or not a fault is likely to move in the near future is based on whether or not it is moving today or has moved in the recent geologic past. This determination is complicated because the geologic record of past movement is incomplete.

It is not now possible to determine with certainty if a fault will sustain movement in the future. We must assume that if a fault has been active over a considerable length of time (millions of years) and has been historically active or shows evidence of movement in the geologically recent past, it will most likely sustain movement in the future. Evidence from historically active faults both here and abroad indicates that this assumption is generally valid. Extensive studies of the geologic and tectonic settings of historic earthquakes, particularly those in California such as the great California earthquake of 1906, the Kern County earthquake of 1952, the Parkfield earthquake of 1966, and the San Fernando earthquake of 1971, reveal that the faults responsible for these earthquakes were characterized by at least one or more of the following features: (1) historic earthquakes with or without surface fault displacement, (2) ephemeral physiographic features such as sag ponds, offset streams, and linear ridges that suggest recent fault displacement, and (3) offset Holocene and Pleistocene deposits and geomorphic features. The presence of these characteristics provides a basis for determining which faults in the San Francisco Bay region are likely to sustain future movement. Faults along which these characteristics are developed are commonly termed "active faults."

Faults in the San Francisco Bay region that display features like those mentioned above are shown in figure 3*A*. They include the well-known San Andreas, Hayward, and Calaveras faults and many other less well-known faults potentially capable of causing substantial damage. The faults are classified according to the evidence available for recent or current movement. This evidence is summarized in table 1 and the sources of data are identified on figure 3*B*.

All the faults in the San Francisco Bay region are part of what is broadly termed the San Andreas fault system. Most of these faults trend northwestward, and most display a similar sense of movement. This movement shifts the rock mass on the southwest side of each fault relatively toward the northwest. Fault displacements occur suddenly during earthquakes or very slowly by a process called fault creep, and for most northwest-trending bay region faults, present-day movement is almost entirely horizontal. This kind of fault movement occurs on the San Andreas, Hayward, and Calaveras faults. It is technically described as strike slip, and faults with predominantly horizontal movement are termed "strike-slip" faults. Most strike-slip faults in the San Andreas system, including those just named, exhibit a right-lateral sense of movement; that is, to an observer looking along the fault zone, the rock mass to the right of the fault moves toward him (fig. 4). For left-lateral strike-slip faults, the horizontal movement is opposite in sense—the right-hand rock mass moves away from the observer.

A different sense of movement characterizes dip-slip or vertical-slip faults. Movement on them is predominantly vertical, and the rock mass on one side of a fault

surface is elevated relative to the opposite mass. Depending on the geometry of the fault surface and the sense of movement, these faults are termed "normal" or "reverse" (or thrust) faults (fig. 4). Although less common than strike slip, some dip-slip faults are recognized in the bay region. Many bay region faults are not yet well enough known to identify the sense of movement positively and unequivocally.

The faults in the San Francisco Bay region are grouped geographically and numbered in figure 3*B* and table 1. The groups include the following:

San Andreas fault—The San Andreas fault (1) trends through the Santa Cruz Mountains in the southern part of the bay region and along the coastal margin in the northern part. The 1906 earthquake made this one of the best known active faults in the world. Within the last few years, both local and State governments, through land-use regulation, have recognized the potential danger of this fault.

Hayward and related faults—The Hayward fault (2) trends northwestward along the base of the hills behind the East Bay cities from Fremont northwest to Richmond. North of San Pablo Bay, the Rodgers Creek and Healdsburg faults (3) continue along much the same trend. Farther north, three faults in the northeast of Alexander Valley (4, 5, and 6) continue the same trend. Segments of this fault system were responsible for damaging earthquakes in 1836, 1868, and 1969.

Calaveras and related faults—The Calaveras fault (7) diverges northward from the San Andreas fault south of Hollister and continues northward along the eastern margin of the Santa Clara Valley and into the Diablo Range. Related faults, some of which may be connected with the Calaveras, include the Pleasanton fault (8) near Pleasanton, the Concord fault (9) through Concord, the Green Valley fault (10) north of Suisun Bay, faults on the west side of Napa Valley (11), and the Silver Creek fault (12) southeast of San Jose.

Faults west of the San Andreas—Faults west of the San Andreas include the Zayante (13), San Gregorio (14), and the Seal Cove (15) faults. The Zayante lies west of the San Andreas but trends more westerly. The San Gregorio trends northward across the mouth of Monterey Bay and along the coast of San Mateo County. The Seal Cove and associated faults (15) north of Half Moon Bay may represent a northward continuation of this zone. The Pilarcitos fault (16) branches westward from the San Andreas fault on the San Francisco peninsula and may join the San Andreas beneath the Pacific Ocean south of San Francisco.

Faults along the east margin of the Santa Cruz Mountains—This group of faults is poorly exposed; it includes the Sargent (18), Black Mountain (19), Berrocal (20), Serra (21), and Vasona (22) and occurs in an irregular band roughly parallel to, and about 5 km (3 mi) east of, the San Andreas fault. Several of these are probably thrust faults with southwest-dipping fault surfaces.

Faults along the west margin of the Great Valley—Faults along the west margin of the Great Valley include the Rio Vista fault (24) and the Antioch fault (25), which trends through the town of Antioch. The Antioch fault may extend northwestward to the Montezuma Hills fault (26).

Faults in the Livermore Valley—Known faults in the Livermore Valley include the Livermore, Tesla, and Grenville faults (23).

Faults between San Andreas and Healdsburg–Rodgers Creek faults—Faults with trends more westerly than the San Andreas fault occur in the San Anselmo, Petaluma, and Santa Rosa areas (27, 28, 29, and 30).

Our knowledge of young fault movement in the San Francisco Bay region is still incomplete. Some of these faults may have moved more recently than is recognized, and other faults with as much potential for causing damaging earthquakes may be as yet unrecognized. This chapter is therefore a progress report, not a final definitive statement.

EVIDENCE SUGGESTING FUTURE MOVEMENT ALONG FAULTS

The process that leads earth scientists to believe that movement may occur along particular faults is one of determining which identifying characteristics result from historic fault movement and using these characteristics to evaluate the possibility of movement on those faults. What characteristics of the San Andreas fault were known prior to the 1906 earthquake? First, the fault was known to have produced surface displacement in earlier earthquakes in 1838 and 1890 (Lawson and others, 1908; Louderback, 1947). Second, the trace of the fault was characterized by such physiographic features as linear ridges and depressions, sag ponds, and scarps (Schuyler, 1898; Anderson, 1899). Third, the fault was known to offset geologic deposits of Pleistocene age (Lawson, 1893, 1895), formed within the last 3 million years. These and related characteristics are found worldwide along faults with historic movement. They are now accepted as evidence that a fault is likely to sustain future movement.

This evidence can be divided on the basis of its age into three categories: (1) historic fault displacement—at the surface, either suddenly in association with earthquakes or gradually as fault creep, or at depth, inferred from earthquakes that can be reliably attributed to the fault; (2) displacement during Holocene time (last 10,000 years)—faulted Holocene deposits and fault-produced topography of Holocene age; and (3) displacement during Quaternary time (last 3 million years)—faulted Pleistocene deposits and fault-produced topog-

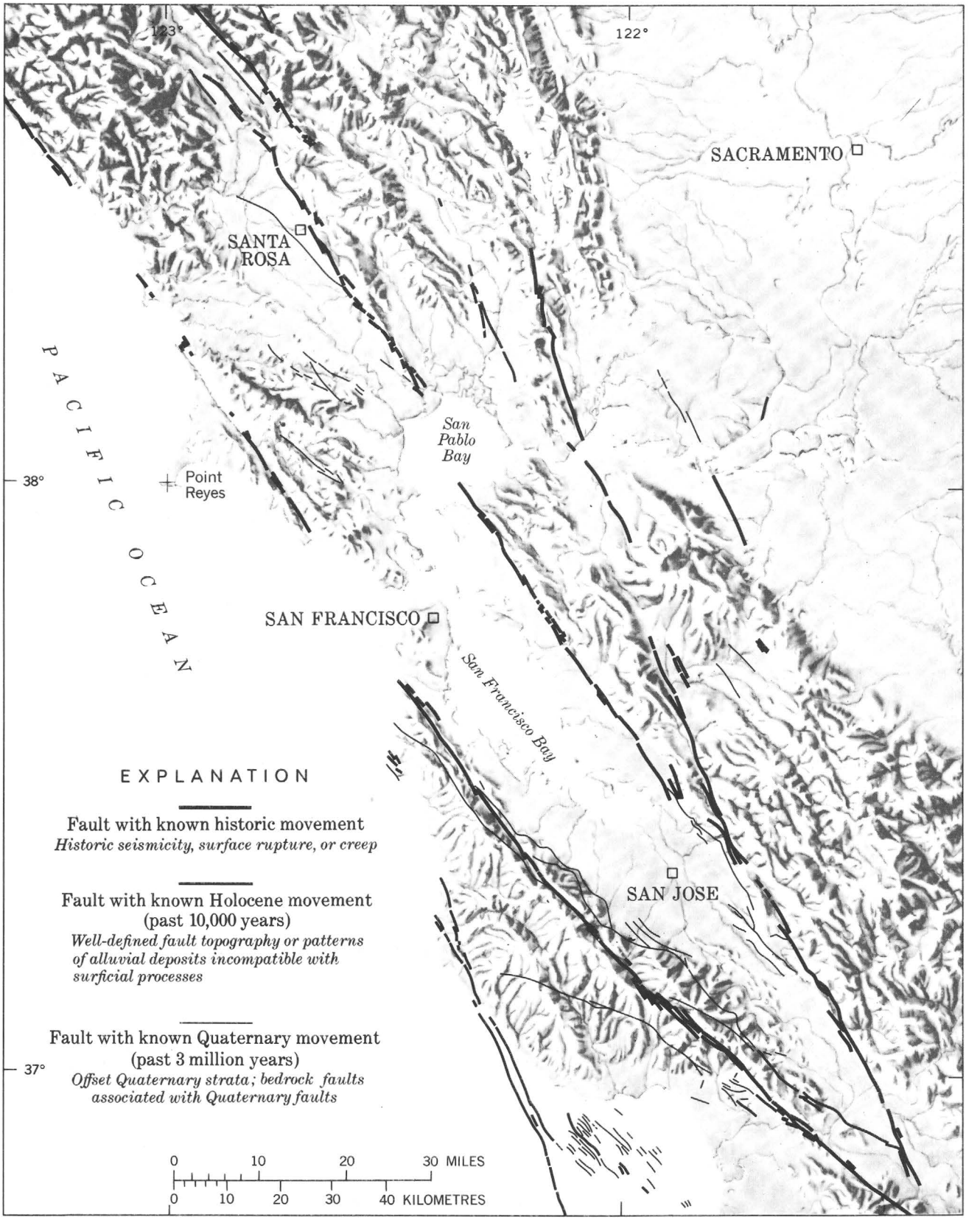

A

FIGURE 3.—*A*, Faults that may cause damaging earthquakes or surface displacement in the San Francisco Bay region. The most recent displacement on these faults is known to have occurred during historic time (past 150 years), during Holocene time (0–10,000 years before present), or during Quaternary time (0–3 million years before present). *B*, Sources of data, with explanation on facing page. Numbers on boxes are keyed to table 1, which summarizes the evidence for recent displacement.

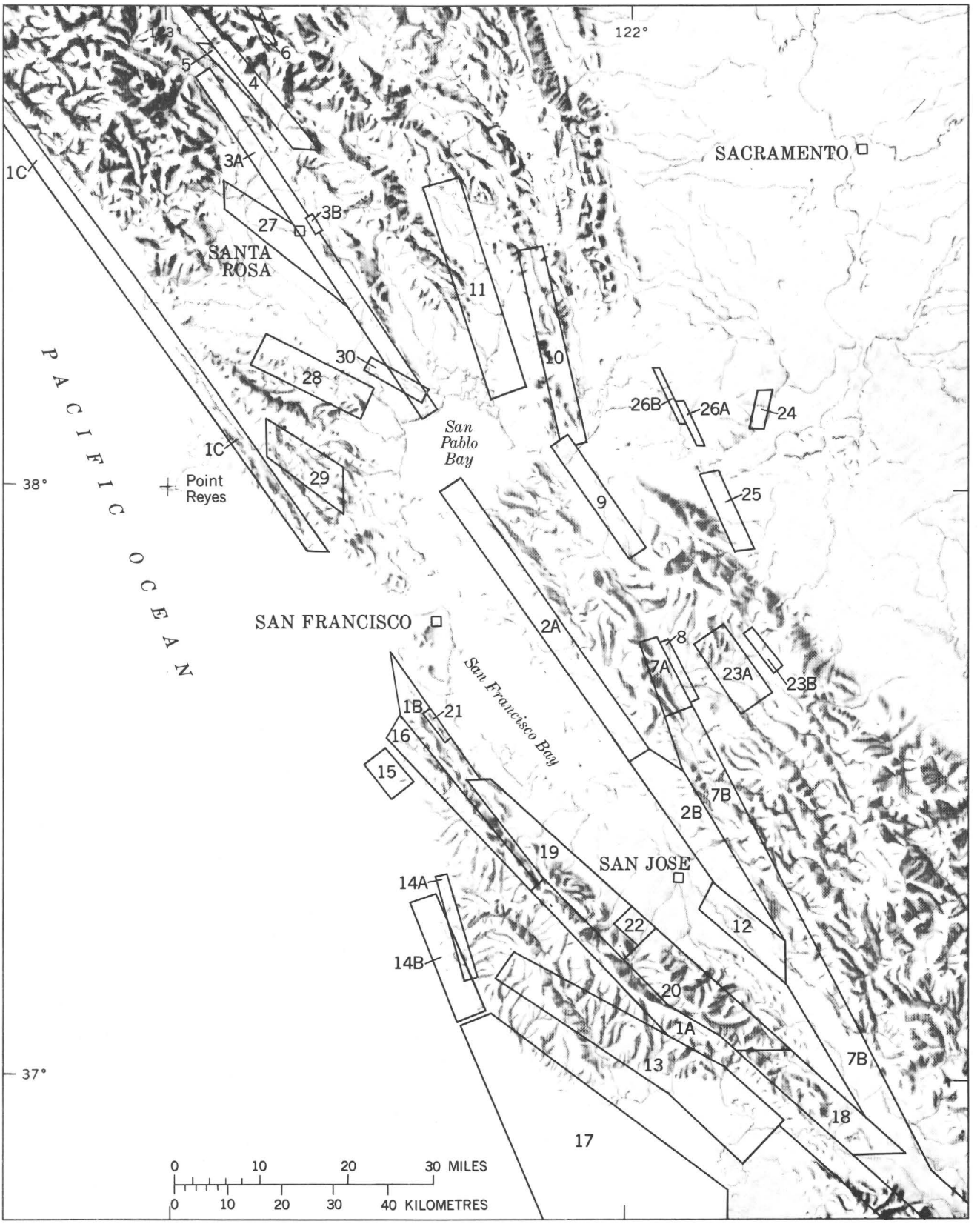

B

FIGURE 3.—Continued.

raphy of Pleistocene age. (The Holocene Epoch and preceding Pleistocene Epoch constitute the Quaternary Period.)

These categories form a framework that encompasses geophysical data, data on prehistoric and historic events, and geologic data. This framework can be used to distinguish recency of faulting on the basis of stratigraphic evidence, in the fashion of Wentworth, Ziony, and Buchanan (1970) and Ziony, Wentworth, and Buchanan (1973). The time span of each category overlaps younger ones, emphasizing that displacement more recent than the youngest identified may have occurred. Full use of this framework is possible only where much information is available, as in the San Francisco Bay region. In many places, information may be limited largely to historic data, topographic features, and sparse stratigraphic data.

Map No.	Fault name or locality	Sources of Data
1.	San Andreas	A. Sarna-Wojcicki, A., and Pampeyan, E. H. (unpub. data) B. Brown (1972) C. Brown and Wolfe (1972)
2.	Hayward	A. Radbruch (1967) B. Dibblee (1972b, c, d)
3.	Healdsburg-Rodgers Creek	A. Brown (1970a); Gealey (1951); Weaver (1949 B. Helley, E. J. (unpub. data)
4.	Northeast of Alexander	Radbruch-Hall, D. H. (unpub. data); Wentworth, C. W., and Frizzell, V. A., Jr. (unpub. data)
5.	Alexander Valley	Helley, E. J. (unpub. data)
6.	Big Sulphur Creek	McLaughlin, R. J. (unpub. data).
7.	Calaveras	A. Brown (1970a) B. Dibblee (1972a, b, d; 1973a, b, c, e)
8.	Pleasanton	Radbruch (1968a)
9.	Concord	Sharp (1973)
10.	Green Valley	Brown (1970a); Brown, R. D., Jr., and Frizzell, V. A., Jr.(unpub. data)
11.	West side Napa Valley	Fox and others (1973)
12.	Silver Creek	Dibblee (1972b; 1973c)
13.	Zayante	Hall, N. T. (unpub. data)
14.	San Gregorio	A. Brown (1972) B. Weber and Lajoie (1974)
15.	Seal Cove	Lajoie, K. L., and Brown, R. D., Jr. (unpub. data)
16.	Pilarcitos	Smith (1960); Lajoie, K. L.(unpub. data)
17.	Monterey Bay	Greene and others (1973)
18.	Sargent	McLaughlin (1973)
19.	Black Mountain	McLaughlin and others (1971); McLaughlin, R. J.(unpub. data)
20.	Berrocal	McLaughlin and others (1971); McLaughlin, R. J. (unpub. data)
21.	Serra	Bonilla (1965)
22.	Vasona	McLaughlin, R. J. (unpub. data)
23.	Livermore Valley	A. California Department of Water Resources (1966) B. Burke, D. B. (unpub. data)
24.	Rio Vista	Reiche (1950)
25.	Antioch	Burke and Helley (1973)
26.	Montezuma Hills	A. Burke, D. B. (unpub. data) B. Sims and others (1973)
27.	Southeast of Santa Rosa	Helley, E. J., and Fox, K. F., Jr. (unpub. data)
28.	Burdell Mountain	Wentworth, C. W. (unpub. data)
29.	San Geronimo Valley	Wright, R. H., and Sorg, D. (unpub. data)
30.	Tolay	Wentworth, C. W. (unpub. data)

FIGURE 3.—Continued.

EVIDENCE FOR HISTORIC DISPLACEMENT

Evidence for historic displacement along faults in the bay region comes from the historic record of surface faulting and studies of recent seismicity. These studies are based partly on data collected from networks of closely spaced seismograph stations and are providing precise locations and focal-mechanism solutions for small earthquakes as well as accurate measurements of fault creep.

SURFACE FAULT DISPLACEMENT DURING EARTHQUAKES

Six earthquakes in the San Francisco Bay area have been accompanied by documented surface fault displacement (table 2). These earthquakes occurred on the San Andreas, Hayward, and Calaveras faults (fig. 5). By far the most extensive and best described ground rupture occurred with the 1906 earthquake along the San Andreas fault (Lawson and others, 1908). During this earthquake, surface displacement across the fault was as much as 5 m (16 ft)[1] (fig. 6*A*). The pattern of disturbed ground along the fault, typical of surface displacement during earthquakes on strike-slip faults, is frequently described as a giant mole track (fig. 6*B*). Ground rupture along the Hayward fault accompanied the earthquake of 1868 (Lawson and others, 1908; Radbruch, 1967), and surface displacement due to fault slip accompanied four other earthquakes in 1836, 1838, 1861, and 1890 (table 2). At least three additional earthquakes in the San Francisco Bay area (1800, 1865, 1911) were large enough to have caused surface displacement, although none was described.

FAULT CREEP

Tectonic fault creep consists of gradual relative movement across a fault at rates as large as a few centimetres (an inch or two) per year. It is less

[1]A larger displacement, 6 m (20 ft), is commonly cited as the maximum. This figure appears to be based on observations by G. K. Gilbert (in Lawson and others, 1908) of fault displacement of a road near the south end of Tomales Bay. Gilbert's field notes and his published description of this locality (Lawson and others, 1908, p. 71) suggest that some of this displacement was nontectonic and resulted from the shifting of road fill resting on marshy ground. Four unequivocal fault offsets located about 2 km (1½ mi) south of the road locality averaged about 4.70 m (15.25 ft) according to Gilbert (Lawson and others, 1908, p. 71).

TABLE 1.—*Faults with*

Map number (fig. 3B)	Fault or group of faults	Evidence for displacement				
		Historic displacement			Holocene displacement	
		Surface fault displacement associated with earthquakes	Fault creep	Small earthquakes	Offset Holocene deposits	Geomorphic features
1	San Andreas	Yes (see Lawson and others (1908); Louderback, (1947); Brown and others (1967)).	Yes (see Steinbrugge and Zacher (1960); Tocher (1960)).	Yes (see Brown and Lee (1971)).	Yes	Yes (see Brown (1970a,b); Brown and Wolfe (1972); U.S. Geological Survey (unpub. data)).
	Hayward and related faults:					
2	Hayward	Yes (see Lawson and others (1908); Louderback (1947); Radbruch (1967)).	Yes (see Radbruch and others (1966); Cluff and Steinbrugge (1966).	Yes (see Brown and Lee (1971)).	Yes (see Helley, Lajoie, and Burke (1972; unpub. data)).	Yes (see Radbruch (1968a)).
3	Healdsburg–Rodgers Creek.	None known	None known	Yes (see Unger and Eaton (1970); McEvilly (1970)).	Yes (E. J. Helley (unpub. data)).	Yes (R. D. Brown unpub. data)).
4	Northeast of Alexander Valley.	None known	Probably (D. H. Radbruch-Hall (unpub. data)).	Possibly (see Wesson and others (1972a, b; 1973a, b)).	None observed	Yes (C. M. Wentworth and V. A. Frizzell, Jr. (unpub. data)).
5	Alexander Valley	None known	None known	None known	None observed	Yes (E. J. Helley (unpub. data)).
6	Big Sulfur Creek	None known	None known		Yes	Yes
	Calaveras and related (?) faults:					
7	Calaveras	Yes (see Radbruch (1968a)).[1]	Yes (see Radbruch (1968a)).[1]	Yes (see Brown and Lee (1971)).	Yes	Yes (see Radbruch (1968a)).
8	Pleasanton	None observed	Possibly (see Radbruch (1968a); Gibson and Wollenberg (1968)).	Possibly (see Lee and others (1971)).	Possibly (see Gibson and Wollenberg (1968)).	Yes (see Brown (1970a); Gibson and Wollenberg (1968)).
9	Concord	None known	Yes (see Sharp (1973)).	Possibly (see Sharp (1973); Lee and others (1972a,b,c,); Wesson and others, (1972a,b; 1973)).	Yes (E. J. Helley (unpub. data)).	Yes (see Sharp (1973)).
10	Green Valley	None known	Possibly (M. G. Bonilla, R. D. Brown, and C. M. Wentworth (unpub. data); V. A. Frizzell, Jr., and R. V. Sharp (unpub. data); Dooley (1973)).	Possibly (see Lee and others (1972a,b,c); Wesson and others (1972a,b,c; 1973)).	Possibly (M. G. Bonilla, R. D. Brown, and C. M. Wentworth (unpub. data)).	Yes (see Brown (1970a); Dooley (1973); V. A. Frizzell, Jr. (unpub. data)).
11	Western side of Napa Valley.	None known	None known	Possibly, but not within resolution of data (see Lee and others (1972a,b,c); Wesson and others (1972a,b, c)).	Yes (see Fox and others (1973); E. J. Helley (unpub. data)).	Yes (see Fox and others (1973); E. J. Helley (unpub. data)).
12	Silver Creek	None known	Possibly (Lowney/ Kaldveer Assoc. (unpub. report, 1971)).	Possibly (see Wesson and others (1972a,b; 1973); Lee and others (1972a,b,c)).	Possibly (Lowney/ Kaldveer Assoc. (unpub. report, 1971)).	Yes (see Brown (1970a)).
	Faults west of the San Andreas:					
13	Zayante	None known	None known	Possibly (see Wesson and others (1972a,b; 1973)).	Possibly (see Hall and others (in press, 1975))	Yes
14	San Gregorio	None known	None known	Yes (see Greene and others (1973); Griggs (1973)).	Yes (see Greene and others (1973); G. Weber (unpub. data)).	Yes (see Greene and others (1973); G. Weber, J. Tinsley, and K. R. Lajoie (unpub. data)).
15	Seal Cove	None known	None known	None known	None known on main strand; yes on associated strand (K. R. Lajoie, J. Tinsley, and G. Weber (unpub. data)).	Yes (see Glen, (1959); Jack (1968); K. R. Lajoie, J. Tinsley, and G. Weber (unpub. data)).
16	Pilarcitos	Possibly (see Lawson and others (1908)).	None known	None known	None known	Yes (see Smith (1960); K. R. Lajoie (unpub. data)).
17	Faults in Monterey Bay.	None known	None known	Possibly (see Greene and and others (1973); Griggs (1973)).	Yes (see Greene and others (1973)).	Yes (see Greene and others (1973)).
	Faults along the eastern margin of Santa Cruz Mountains:					
18	Sargent	None known	None known	Yes (see Brown and Lee (1971)).	Yes (see McLaughlin (1973)).	Yes (see Allen (1946); Brown (1970a); McLaughlin (1973)).
19	Black Mountain	None known	None known	Probably (see Lee and others (1972a,b,c); W. H. K. Lee and P. Bauer (unpub. data)).	None observed	None observed
20	Berrocal	None known	None known	Possibly (see Lee and others (1972a,b,c); Wesson and others (1972a,b,c; 1973)).	None observed	Yes (R. J. McLaughlin (unpub. data)).
21	Serra	None known	None known	None known	None observed	None observed
22	Vasona	None known	None known	Possibly	None observed	None observed
23	Livermore Valley (several faults in the eastern Livermore Valley show various types of evidence for Quaternary displacement, including ground-water anomalies in young alluvium, creep, and small earthquakes. At present, however, these faults are poorly delineated. (See Bernreuter and Tokarz (1972); John Blume and Associates (unpub. report); California Department of Water Resources (1966); Hansen (1964); M. G. Bonilla and J. E. Schoellhamer (unpub. data); Gibson and Wollenberg (1968).					
	Faults along the western margin of Great Valley:					
24	Rio Vista	None known	None known	None known	Yes (see Reiche (1950)).	Yes (see Reiche (1950)).
25	Antioch	None known	Probably (see Burke and Helley (1973)).	Probably (see McEvilly and Casaday (1967)).	Yes (see Burke and Helley (1973)).	Yes (see Burke and Helley (1973)).

Footnotes are at end of table.

Quaternary displacement

Quaternary displacement	Additional factors for assessing earthquake potential					
Offset Quaternary deposits	Estimated recurrence interval (in years) for maximum earthquake, inferred from geologic slip rate[7]	Magnitude of largest historic earthquake	Total known fault length (in kilometres) (estimate of maximum magnitude earthquake in parentheses[8])		Present ability to predict pattern of surface faulting	Comments
Yes (see Cummings (1968)).	100–1,000 (for magnitude 7–8+)	8.3 (see Lawson and others (1908)).[2,3]	1,200 (8½)[9]		Generally good, locally very good.	Right-lateral strike-slip fault, maximum displacement in 1906, 6 m (20 ft).
Yes	10–100 (for magnitude 6–7)	7±½ (see Slemmons (1967)).[2,3]	72 (7.0)	Geyserville to Milpitas, 163 (7.5)	Generally good, locally very good.	
Yes (R. D. Brown and E. J. Helley (unpub. data)).		5.7 (see McEvilly (1970)).[4]	72 (7.0)		Generally good, locally very good.	Right-lateral strike-slip faults.
None observed		3–4 (see Lee and others (1972a,b,c); Wesson and others (1972a,b; 1973)).	35 (6.6)		Locally very good, abundant evidence, fault not well mapped.	
None observed		None known[2]	13 (?)		Locally very good. Fault not well mapped.	
Yes (R. McLaughlin (unpub. data)).		None known[12]	6.4		Locally very good.	
Yes	10–100 (for magnitude 6–7)	6	115 (Hollister to San Ramon) (7.3)		Generally fair, locally very good to very poor.	Right-lateral strike-slip faults. Northward extension of Green Valley probable.
Yes (see Gibson and Wollenberg (1968)).		4.3 (see Lee and others (1971)).[4]	9 (?)			
None observed		5.4 (see Sharp (1973); Murphy and Cloud (1957)).[5]	18 (?) 22 (includes extension across Carquinez straits) (6.3)		Locally very good.	
Yes (M. G. Bonilla and C. M. Wentworth (unpub. data); Dooley (1973)).		2–3 (see Lee and others (1972a,b,c); Wesson and others (1972a,b; 1973)).[5] 4–5, on possible northward estension (R. L. Wesson (unpub. data)).[5]	38 (6.6)		Locally very good.	
Yes (see Fox and others (1973); E. J. Helley (unpub. data)).		2–3 (see Lee and others (1972a,b,c); Wesson and others (1972a,b; 1973)).[5]	17 (?)		Poor.	
Yes (see Dibblee (1972a,b,c)).		3.5 (R. L. Wesson and others (unpub. data)).[4]	20 (minimum estimate) (6.2)		Poor.	Northward extension toward San Jose not well known.
Yes		Not known	82 (7.4)		Poor.	
Yes (see Greene and others (1973); Brabb (1970)).		6.1 (see Richter (1958)).[5,10]	135 (7.4)	200 (includes possible northward extension to San Andreas fault, connecting at Bolinas) (7.6)[11]	Locally very good.	Right-lateral strike-slip fault. Southward extension.
Yes (see Jack (1968); Cooper (1971); K. R. Lajoie, J. Tinsley, and G. Weber (unpub. data)).		None known[12]	3 (?)		Locally very good.	
Yes (see Cummings (1968)).		None known[12]	43 (6.7)			
Yes (see Greene and others (1973)).		6.1 (see Richter (1958)).[5,10]	42 (across entire bay) (6.7)			Southward extension on shore probable.
Yes (see McLaughlin (1973)).		5.0 (see McEvilly (1966)).[4]	95 (Portola Valley to Hollister) (7.4) 33 (Mount Madonna to Hollister) (6.7) 55 (Lake Elsman to Hollister) (6.9)		Locally good.	Steep southwest-dipping right-lateral fault, up on southwest side, dip decreases to northwest.
Yes (see Dibblee (1966); Pampeyan (1970); R. McLaughlin (unpub. data)).		3.6 (see Lee and others (1972)).[4]	31 (Portola Valley to Los Gatos) (6.7)		Poor.	Westward-dipping thrust fault.
Yes (R. J. McLaughlin and D. Sorg (unpub. data)).		4.5? (R. L. Wesson (unpub. data)).[5]	33 (Los Gatos to Mount Madonna) (6.7)		Poor.	Westward-dipping thrust fault.
Yes (see Bonilla (1965)).		None known[12]	4 (?)		Very good.	Westward-dipping thrust fault.
Possibly		2–3 (see Lee and others (1972a,b,c); Wesson and others (1972a,b; 1973)).[5]	14 (?)		Poor.	
Yes (see Reiche (1950)).		None known[12]	5 (?)		Poor.	No longer exposed, buried by dredged material.
Yes (see Burke and Helley (1973)).		4.9 (see McEvilly and Casaday (1967); 1899 earthquake[6]; Tocher (1959)).[4]	14 (?) 37 (including en echelon northward extension) (6.6)		Locally very good.	Right-lateral strike-slip fault.

TABLE 1.—*Faults with*

Map number (fig. 3B)	Fault or group of faults	Evidence for displacement				
		Historic displacement			Holocene displacement	
		Surface fault displacement associated with earthquakes	Fault creep	Small earthquakes	Offset Holocene deposits	Geomorphic features
26	Montezuma Hills	None known	None known	Yes (see Wesson and others (1972a,b,c; 1973)).	Possibly	Yes (D. B. Burke (unpub. data)).
	Faults between San Andreas and Healdsburg–Rodgers Creek faults:					
27	Southeast of Santa Rosa.	None known	None known	None known	None observed	Yes (E. J. Helley (unpub. data)).
28	Burdell Mountain	None known	None known	None known	None observed	Yes (C. M. Wentworth (unpub. data)).
29	San Geronimo Valley.	None known	None known	None known	None observed	Yes (R. H. Wright (unpub. data); Berkland (1969)).
30	Tolay	None known	None known	None known	None observed	Yes (C. M. Wentworth (unpub, data)).

[1]Cited paper contains numerous additional references.
[2]Magnitude uncertain or estimated.
[3]Ground rupture along surface trace of fault associated with earthquake.
[4]Instrumental location of epicenter and focal mechanism suggest occurrence on named fault.
[5]Instrumental location of epicenter compatible with, but not compelling evidence for, location on named fault.
[6]Location of epicenter based on data from felt earthquakes and is compatible with occurrence on named fault.
[7]Recurrence intervals for maximum magnitudes (from Wallace, 1970).
[8]Maximum magnitude estimated assuming (1) total length of fault is known and (2) half the total length would break in maximum earthquake. The maximum magnitude is calculated

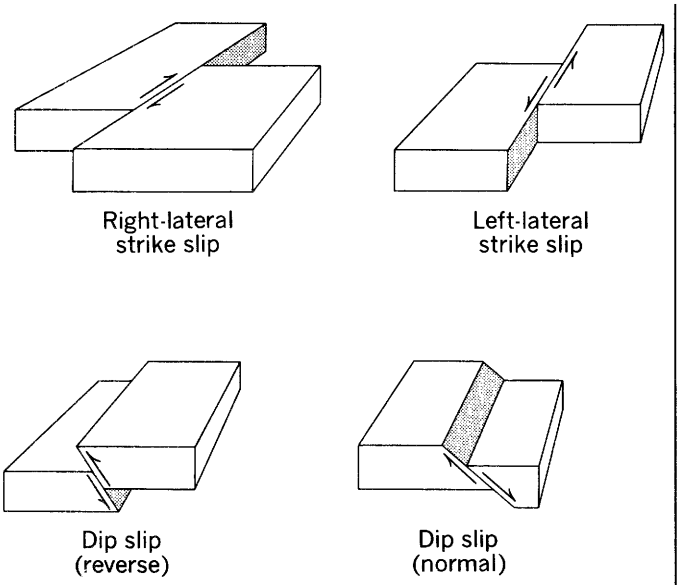

FIGURE 4.—Four types of fault movement, characterized by the sense of movement relative to the fault and to the horizontal. Most faults in the bay region show right-lateral strike slip, the characteristic sense of movement for the San Andreas fault. Movement on oblique-slip faults has both strike- and dip-slip components.

spectacular than the sudden fault movements that accompany earthquakes. Fault creep is most obvious where it breaks or offsets streets, curbs, sidewalks, and other structures (fig. 7). Such breaks and offsets, where mapped through populated areas, define linear trends that approximate those of underlying bedrock faults. Fault creep was first measured in central California in 1956 along the San Andreas fault south of Hollister (Steinbrugge and Zacher, 1960; Tocher, 1960), although its existence was predicted many years before (Louderback, 1942). Fault creep has now been documented for long sections of the San Andreas fault (Brown and Wallace, 1968; Nason, 1971; Savage and Burford, 1973) and the Hayward fault (Cluff and Steinbrugge, 1966; Bonilla, 1966; Blanchard and Laverty, 1966; Radbruch and Lennert, 1966; Bolt and Marion, 1966; Radbruch, 1968b; Nason, 1971) and at several localities along the Calaveras fault (Rogers and Nason, 1971). Evidence for fault creep has been described along the Concord fault (Sharp, 1973) and along the Antioch fault (Burke and Helley, 1973). Fault creep is now recognized as a common and widespread characteristic of active faults in the San Francisco Bay region (fig. 8).

SMALL EARTHQUAKES

Small earthquakes provide convincing evidence of contemporary fault movement where (1) many are alined along a fault, (2) the sense of movement inferred from them is systematic, and (3) that sense of movement agrees with the sense of movement derived from geologic data.

An abundance of small earthquakes does not, by itself, demonstrate that a fault has the potential to generate a large earthquake, but in California several recent earthquakes in the magnitude range from 5.0 to 7.7 were preceded by many small earthquakes clustered near the larger one (Wesson and Ellsworth, 1973).

To demonstrate that small earthquakes are related to a given fault requires both relatively large numbers of earthquakes and the ability to locate them accurately. Accurate location depends primarily on the number and distribution of seismograph stations and also on the ability to correct for the complexities of wave propagation in the earth's crust (Wesson and others, 1973b). Most of the accurately located earthquakes in the San Francisco Bay region can be assigned to faults with historic or geologic evidence for recent movement (fig. 9).

Quaternary displacement

Quaternary displacement	Additional factors for assessing earthquake potential				
Offset Quaternary deposits	Estimated recurrence interval (in years) for maximum earthquake, inferred from geologic slip rate[7]	Magnitude of largest historic earthquake	Total known fault length (in kilometres) (estimate of maximum magnitude earthquake in parentheses[8])	Present ability to predict pattern of surface faulting	Comments
Yes (D. B. Burke (unpub. data)).		None known	16 (?)	Locally good.	
Yes (E. J. Helley (unpub. data)).		None known[12]	27 (6.4)	Poor.	Primarily right-lateral strike-slip faults, but also have significant reverse displacement. Northeast side up along more westerly reaches.
Yes (C. M. Wentworth and E. J. Helley (unpub. data)).		None known[12]	19 (?)	Locally good.	
None observed		None known[12]	15 (?)	Locally good. Fault not well mapped.	
None observed		None known[12]	11 (?)	Fault not well mapped.	

by taking the arithmetic average of three estimates using the empirical relations of Tocher (1958) $M=0.9 \log_{10}(L)+5.6$, Iida (1965) $M=0.76 \log_{10}(L)+6.07$, and either Bonilla and Buchanan (1970) $M=2.57 \log_{10}(L)+2.79$ for strike-slip faults or Bonilla and Buchanan (1970) $M=2.96 \log_{10}(L)+1.85$ for other faults, where M is magnitude and L is one-half the fault length in kilometres. Both the assumptions and the empirical magnitude-fault length relations are to some degree uncertain; therefore, the estimated maximum magnitude must be regarded as no more than a crude estimate. Only faults longer than 20 km (12 mi) were considered.

[9]Maximum magnitude for the San Andreas fault is assumed to be equal to the magnitude of a historic earthquake in 1906.

[10]Uncertainty in location of epicenter permits assignment of earthquake (October 22, 1926) to either the Monterey Bay or San Gregorio fault zone.

[11]Greene and others (1973), using a variety of magnitude–fault length relations, estimated maximum magnitudes between 7.2 and 7.9 for this fault zone.

[12]No significant earthquake can be assigned reliably to this fault on basis of present data.

TABLE 2.—*Historic surface fault displacements associated with earthquakes in the San Francisco Bay region*

Date	Fault	Rupture length	Locality	References
June 10, 1836	Hayward	Unknown	Hayward	Louderback (1947).
Late June, 1838	San Andreas	Unknown	Woodside	Louderback (1947).
July 3, 1861	Calaveras	Unknown	29 km (18 mi) northwest of Calaveras Reservoir, west side San Ramon Valley, Dublin.	Brewer (1930); Trask (1964); Witney (1865); Lawson and others (1908); Radbruch (1968b).
October 22, 1868	Hayward	>30 km (20 mi)	Warm Springs northward to San Leandro, possibly as far north as Berkeley.	Lawson and others (1908).
April 24, 1890	San Andreas	>10 km? (6 mi)	San Juan Bautista to Pajaro Gap?.	Lawson and others (1908).
April 18, 1906	San Andreas	>430 km (270 mi)	San Juan Bautista northward to Shelter Cove or Point Delgada.	Lawson and others (1908).

EVIDENCE FOR HOLOCENE DISPLACEMENT

Holocene deposits are those formed during the last 10,000 years, during which climatic and sea level conditions have been similar to those now prevailing. These deposits are common where depositional processes are still active, in such places as stream flood plains and terraces, alluvial fan surfaces, low coastal terraces, marshes, and beaches. The age of these deposits is determined in various ways, but the most reliable age assignments depend ultimately on radiocarbon dating.

Where Holocene deposits are displaced or offset by faults, the fault surface—and the movement that produced it—must be younger than the deposits. Although the age of landforms such as hills, terraces, valleys, and stream channels is more difficult to determine, some can be shown to have formed during Holocene time. Where landforms of known Holocene age are cut or displaced by a fault, they too provide evidence that establishes the time of fault movement. Faults that cut or displace Holocene deposits or Holocene landforms must have moved within the last 10,000 years, a long time by conventional calendars but a brief and very recent episode in geologic time. Major geologic processes like faulting are long lived, lasting millions or tens of millions of years. Thus it is prudent to consider a fault that has moved within the past 10,000 years as still active and as a factor to be weighed carefully in planning for the future.

OFFSET HOLOCENE DEPOSITS

Holocene deposits in the San Francisco Bay region consist primarily of stream and marine terrace deposits, alluvial fan deposits, the muds deposited in San Francisco Bay, beach deposits, and slope wash or colluvium. These deposits can be identified and dated by their surface morphology and the type of soil profiles developed upon them, by the presence of shells or bones from modern species, by the presence of aboriginal

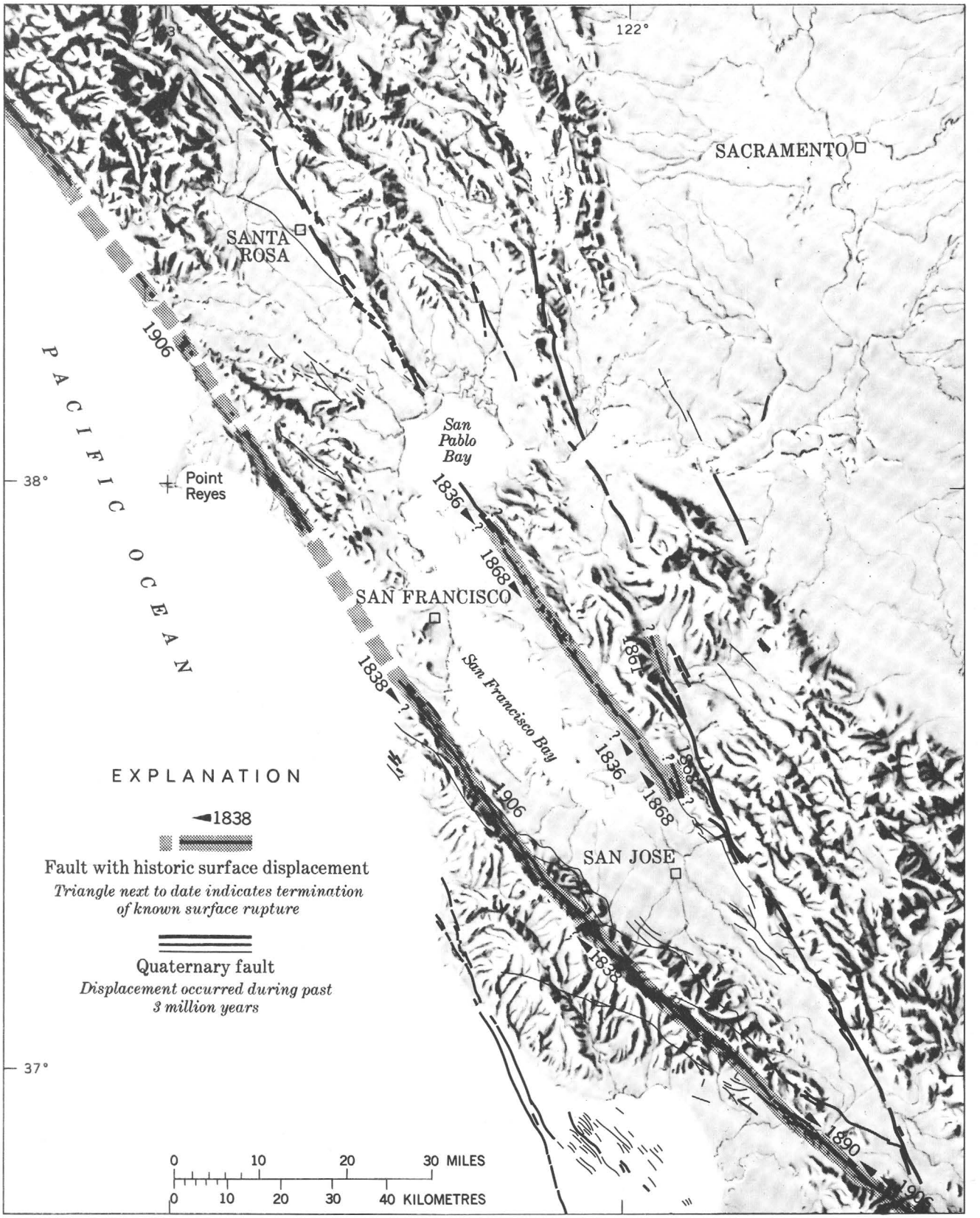

FIGURE 5.—Zones of surface fault displacement associated with earthquakes in the San Francisco Bay region during historic times (see table 2). See figure 3*A* for explanation of symbols used for Quaternary faults.

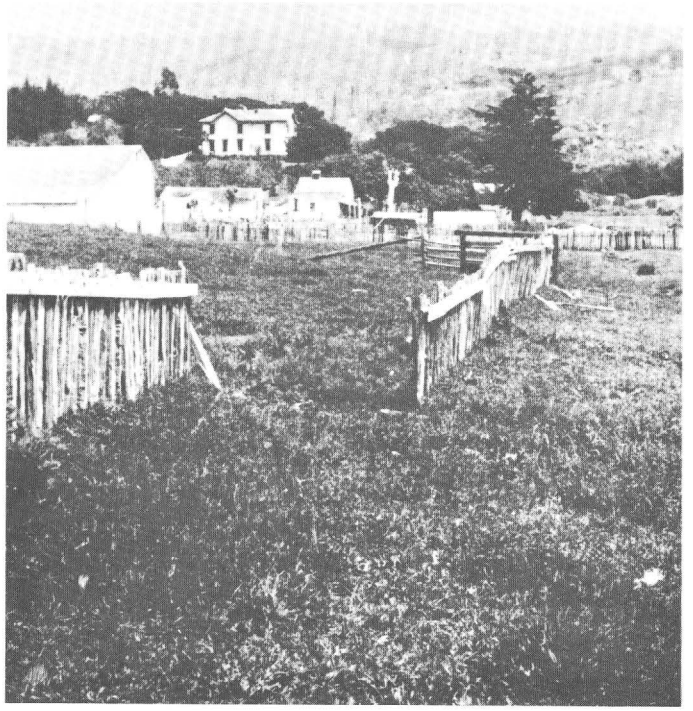

FIGURE 6.—Examples of surface displacement that accompanied the 1906 earthquake. *A*, Fence offset 2½ m (8 ft) by right-lateral displacement on San Andreas fault. Trace of fault approximately perpendicular to fence. One kilometre (½ mi) northwest of Woodville, Marin County. Camera was alined with straight part of fence at right (in middle ground) to illustrate the zone of flexure beyond the abrupt offset. Total offset including flexure was about 3.5 m (11 ft) (from Lawson and others, 1908, plate 49A). *B*, "Mole track" produced by right-lateral displacement on San Andreas fault 1½ km (1 mi) northwest of Olema, Marin County (from Lawson and others, 1908, plate 40A). View northwest.

artifacts or skeletal remains, or by radiocarbon dating of enclosed organic materials (Helley and Brabb, 1971;

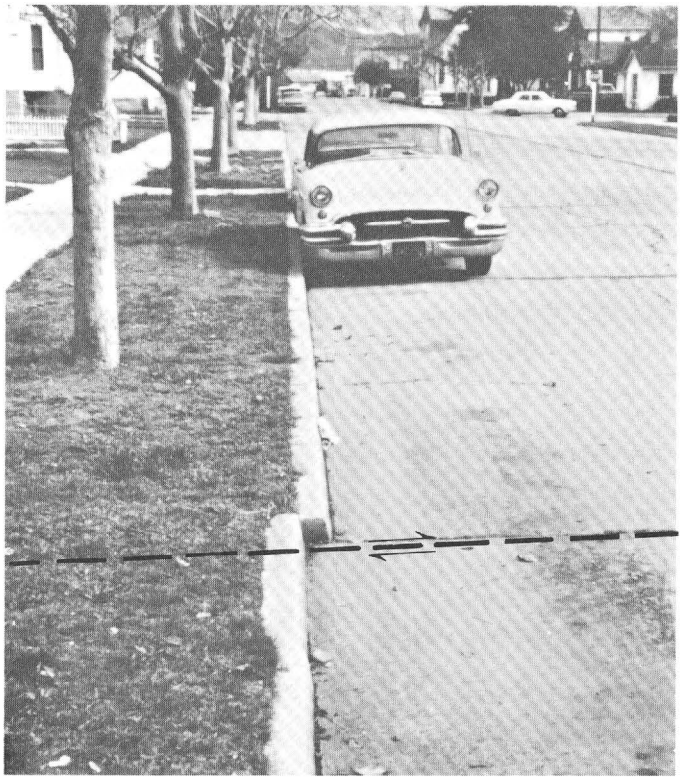

FIGURE 7.—North curb on Sixth Street in Hollister, Calif., offset by right-lateral fault creep on the Calaveras fault. General trend of fault trace indicated by dashed line. Date of street construction is 1925±2 years. Fault trend and date of street construction from Rogers and Nason (1971, figure 7). View east.

Helley and others, 1972; Wright, 1971). Holocene faulting of these deposits is expressed as linear scarps on modern flood plains, anomalously straight contacts of fluvial deposits, and the disruption of surface and subsurface hydrologic processes along relatively straight lines. The study of trenches dug across suspected fault zones is one of the most useful techniques for determining the recency of fault movement; however, it is not infallible and does require careful attention in locating the trench, preparing the trench walls, logging the exposed stratigraphic and structural relations, and dating any amenable material. Most important, a trench must expose geologic relations that provide unequivocal evidence of the relative age of fault movement.

A sketch of a trench wall (fig. 10) through the fault break of the 1968 Borrego Mountain earthquake in southern California provides an example of this technique. The relative movement along this fault zone is primarily strike slip, with a small dip-slip component. This dip-slip movement offsets the deposits vertically across the fault. The amount of this offset was measured at four stratigraphic levels in the trench. The progres-

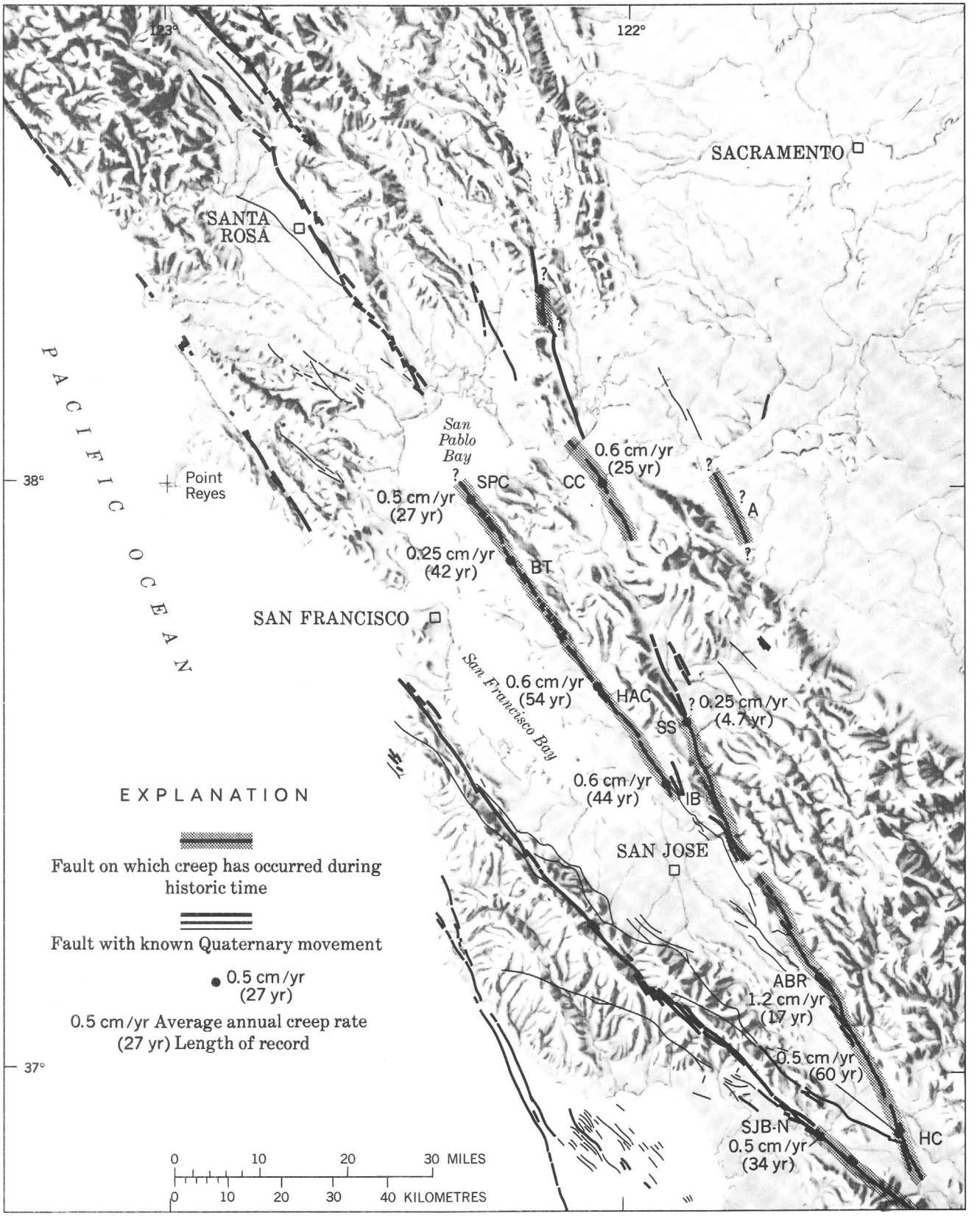

FIGURE 8.—Distribution of documented fault creep along faults in the San Francisco Bay region. Creep rate on the Hayward, Calaveras, and San Andreas faults from Nason (1971). SPC, offset curb in San Pablo; CC, offset curb in Concord; A, Antioch fault; BT, offset tunnel in Berkeley; HAC, offset curb in Hayward; IB, offset building in Irvington; SS, deformed survey array in Sunol; ABR, offset bridge at Anderson reservoir; HC, offset curb in Hollister; and SJB–N, offset fence north of San Juan Bautista. Creep rate on Concord fault from Sharp (1973). No data available for creep rate on Antioch fault (Burke and Helley, 1973). See figure 3*A* for explanation of symbols used for Quaternary faults.

sively older beds show greater offset, and a graph of the offsets against radiometric age indicates a rate of vertical deformation. Analysis of this data not only provided abundant evidence for pre-1968 Holocene movement, but also permitted a quantitative estimate of the rate of deformation.

PHYSIOGRAPHIC FEATURES

Faults that are surfaces of contemporary or youthful movement can also be identified by how they interact with other geologic processes. A fault undergoing tectonic creep or one with recent episodes of abrupt displacement causes subtle but distinctive changes in the terrain it crosses. For a series of similar repetitive events, these changes are additive. Anomalous and very distinctive patterns are produced where active faults cross streams, landslides, basins that are concurrently undergoing deposition, and other ongoing geologic processes. The alined features that produce such patterns include scarps, trenches, notches, ridges, stream offsets, sag ponds, and lines of springs or vegetation (figs. 11, 12). Some of these features are direct results of fault movememt, but some have more complex origins.

The absence of identifiable fault topography in places along the fault zone does not necessarily imply lack of recent displacement. The preservation of such features depends on the local rates of erosion and deposition, which vary greatly from place to place. Landslides and downslope movement of soil, as well as many other geologic processes, can effectively bury or erase the physiographic evidence of fault displacement within a few years.

Although topographic features caused by fault movement seldom can be dated precisely, many can be dated approximately by geologic interpretation. In the bay region, many certainly were formed during Holocene time and therefore indicate the youngest category of prehistoric fault movement. Recently, the dating of sediments in some sag ponds along the San Andreas fault in the San Francisco Bay region (Andrei Sarna-Wojcicki, written commun., 1973) has confirmed their previously tentative age assignment as Holocene.

EVIDENCE FOR QUATERNARY DISPLACEMENT

Displaced deposits of Pleistocene age and some fault-produced physiographic features record fault movements that took place between 10,000 and 3 million years ago. Faults that display such evidence are here considered Quaternary faults (fig. 3*A*)—they clearly have moved in Pleistocene time and may have moved during Holocene time.

Pleistocene deposits in the San Francisco Bay region consist of alluvial fan and stream terrace deposits 10,000 years old and older, marine terrace deposits 70,000 to 1 million(?) years old, older San Francisco Bay mud, and semi-indurated, structurally deformed continental sand and gravel deposits. The Pleistocene deposits are differentiated and dated approximately by their relation to present drainage, degree of erosional dissection, relative development of soil profile, degree of induration and weathering, fossil assemblages and radiometric ages. Many faults that cut these deposits are expressed as subdued linear surface features or as near-surface ground-water barriers.

Emergent wave-cut marine terraces and their associated deposits record Quaternary faulting and associated warping along the coast. In some places approximate rates of deformation can be inferred from the relations shown by sequences of deformed terraces (fig. 13).

ESTIMATING THE RATE OF FUTURE MOVEMENT ALONG FAULTS AND THE CHARACTERISTICS OF ASSOCIATED EARTHQUAKES

When the evidence suggests that future fault movement is likely, questions arise about the frequency and characteristics of the expected earthquakes. What proportion of the future movement will be associated with large earthquakes, and what proportion will occur as creep? What will be the characteristics of surface fault displacement? How much displacement may occur in a given event? But even more important are questions regarding the size of future earthquakes and the intensity of shaking. Until earthquake processes are better understood, the past must be used as the primary guide to the future in considering these questions.

Present estimates of the maximum size and frequency of earthquakes along a given fault are based on (1) the geologically determined rate of slip and historic records of ground deformation, (2) the seismic history of the fault and the surrounding tectonic regime, (3) geologic evaluation of the tectonic setting, and (4) the empirically derived relation between magnitude of earthquakes and fault length or other parameters.

GEOLOGICALLY DETERMINED SLIP RATES

The offset of distinctive rock units establishes the rate of fault movement only within fairly wide bounds. Commonly these offsets average the rate of movement over millions of years and cannot be used to distinguish between sudden slip and creep. Data for the San Andreas fault suggest an average slip rate of 1–2 cm/yr (0.4–0.8 in./yr) over the last 20 million years (Dickinson and Grantz, 1968). But to predict movements in the immediate future, the most recent few hundreds to thousands of years are the most important.

The history and rate of fault movement have been obtained within this brief time period in a few special circumstances in southern California using absolute age dating techniques. Clark, Grantz, and Rubin (1972)

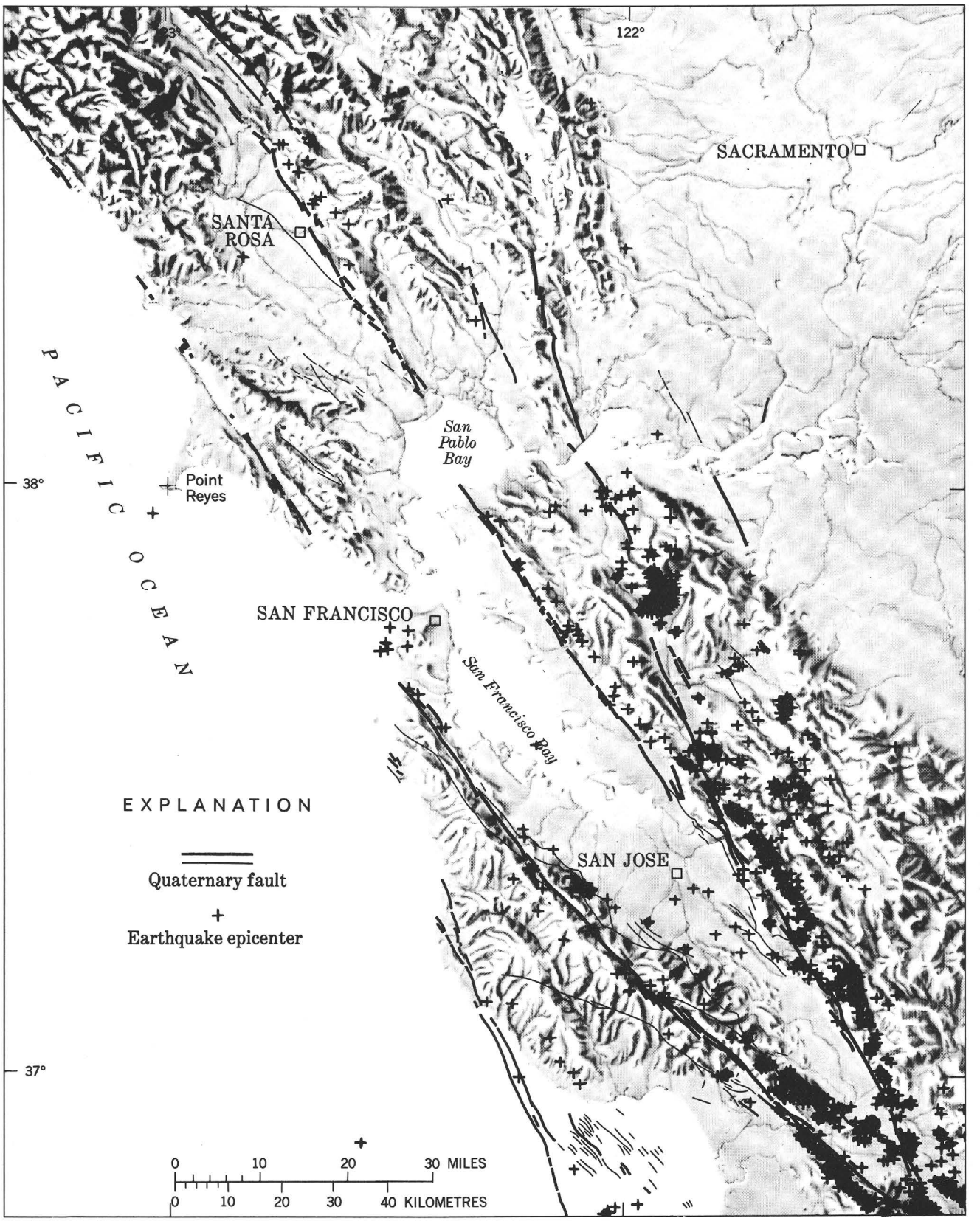
123°
122°
SACRAMENTO
SANTA ROSA
PACIFIC OCEAN
San Pablo Bay
38°
Point Reyes
SAN FRANCISCO
San Francisco Bay
EXPLANATION
Quaternary fault
Earthquake epicenter
SAN JOSE
37°
0 10 20 30 MILES
0 10 20 30 40 KILOMETRES

A

were able to establish closely the slip rate along the Coyote Creek fault in southern California by radiometrically dating sediments of Holocene Lake Cahuilla (fig. 10). The 1971 San Fernando earthquake led to similar investigations (Bonilla, 1974) that provide evidence bearing on recurrence intervals on another fault. Such investigations can allow joint estimates of the magnitude and frequency of prehistoric earthquakes. For example, Clark, Grantz, and Rubin (1972) estimated that an earthquake with a similar amount and type of displacement, and presumably a similar magnitude, to that of the 1968 earthquake would be required along each segment of the Coyote Creek fault about every 200 years to account for the movement accumulated over the past 3,000 years. Comparable observations are not yet available in the San Francisco Bay region but are likely as more data are obtained.

A major problem in estimating magnitudes and recurrence intervals is to allow for fault movement due to creep or to other aseismic processes. Wallace (1970) estimated magnitudes and recurrence intervals for maximum expectable earthquakes along parts of the San Andreas fault system by relating to a particular tectonic model the long-term slip rate inferred from geologic observations and the measured offsets from earthquakes and creep. This model assumes that the presently observed creep rates represent the longer term rates and predicts that the higher the rate of tectonic creep, the longer the recurrence interval for an earthquake of a given magnitude. The recurrence intervals and maximum magnitudes obtained in this way for the San Andreas (100–1,000 years for magnitude 8+) and Calaveras (10–100 years for magnitude 6–7) faults are no more than a general guide to the frequency of potentially hazardous earthquakes; they represent only one of several possible interpretations of the creep-earthquake relation, but they are a step toward answering the questions of expected magnitude and frequency. Eventually it may be possible to combine the geologic data on past rates of movement and fault creep with geodetic measurements of contemporary movements (for example, Savage and Burford, 1973) to obtain more accurate estimates of recurrence intervals.

SEISMIC HISTORY

The historic record of seismicity helps in estimating characteristics of future earthquakes by providing a measure of the magnitude of earthquakes that can occur along a given fault. In California the 200 years of written history and 40 years of reasonably good instrumental records are a small sample of the events on all active faults, but the usefulness of the available record can be expanded by assuming that similar faults are capable of sustaining similar earthquakes. Thus one can assume that an earthquake with a magnitude comparable to the 1868 earthquake along the Hayward

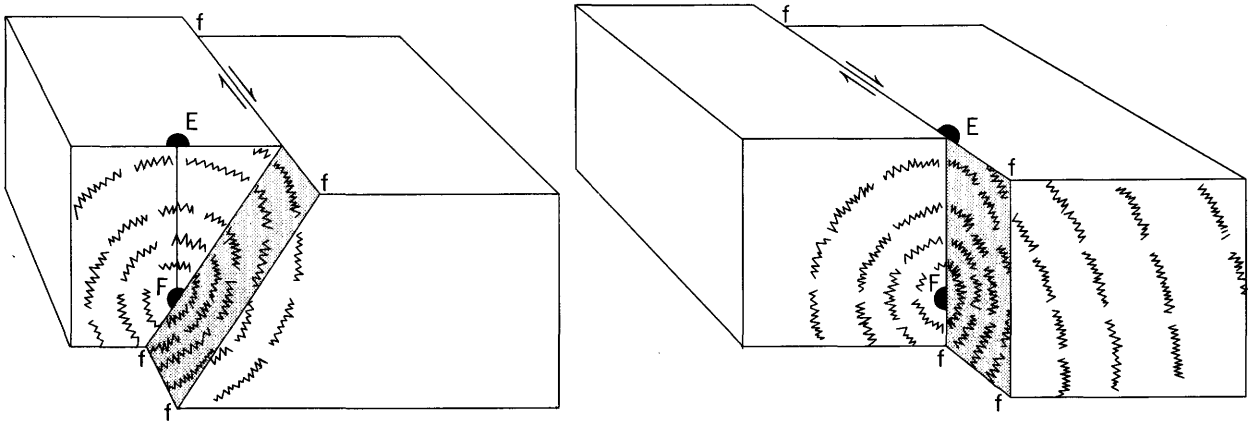

B

FIGURE 9.—*A*, Epicenters of earthquakes in San Francisco Bay region, 1969–72, with magnitudes ≥1.0 (Lee and others, 1972 (three references); Wesson and others, 1972a and b, 1973a, 1974). The pattern of epicenters is incomplete because distribution of seismograph stations is uneven and has changed with time. Most epicenters lying in elongate concentrations parallel to major faults were most likely associated with earthquakes on these faults. The location of these epicenters off the fault traces stems from the necessarily simplified crustal model used in the location procedure. See figure 3*A* for explanation of Quaternary fault symbols. *B*, Relation between fault surface, earthquake epicenter, and earthquake focus. F, earthquake focus or hypocenter (that point, generally at some depth within the earth's crust, from which the seismic energy appears to radiate); E, earthquake epicenter (a point on the earth's surface that is vertically above the focus); f, fault surface (shaded) (a fracture surface along which failure and accompanying dislocation have displaced adjacent blocks of the earth's crust). In both diagrams arrows indicate a right-lateral strike-slip sense of movement, as on the San Andreas fault.

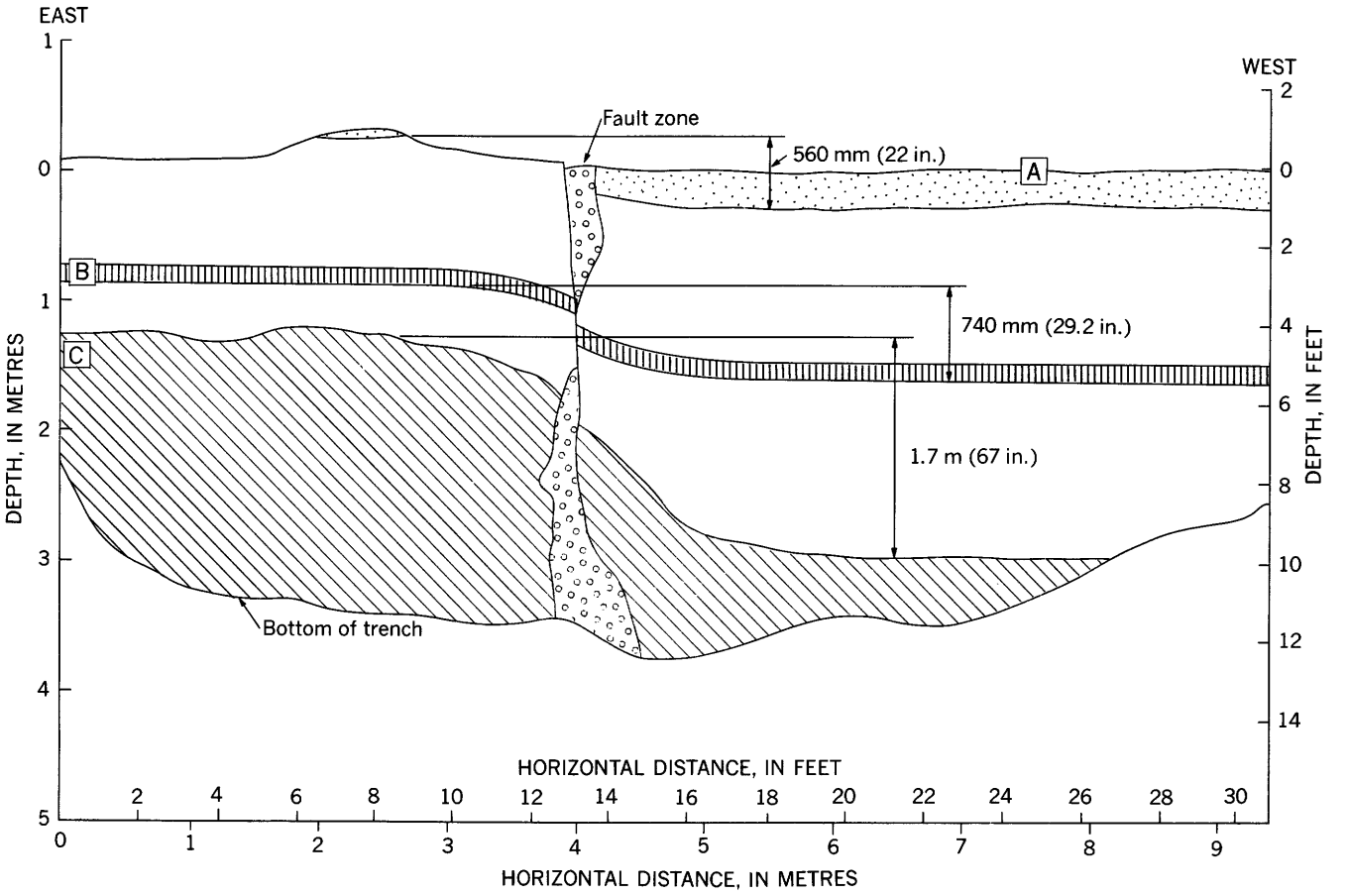
EAST
WEST
Fault zone
560 mm (22 in.)
740 mm (29.2 in.)
1.7 m (67 in.)
A
B
C
Bottom of trench
DEPTH, IN METRES
DEPTH, IN FEET
HORIZONTAL DISTANCE, IN FEET
HORIZONTAL DISTANCE, IN METRES

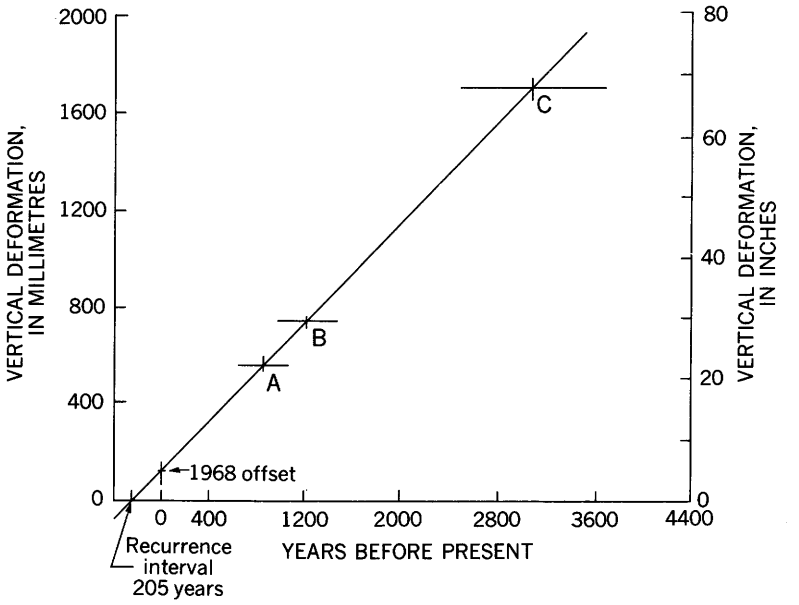
VERTICAL DEFORMATION, IN MILLIMETRES
VERTICAL DEFORMATION, IN INCHES
A
B
C
1968 offset
Recurrence interval 205 years
YEARS BEFORE PRESENT

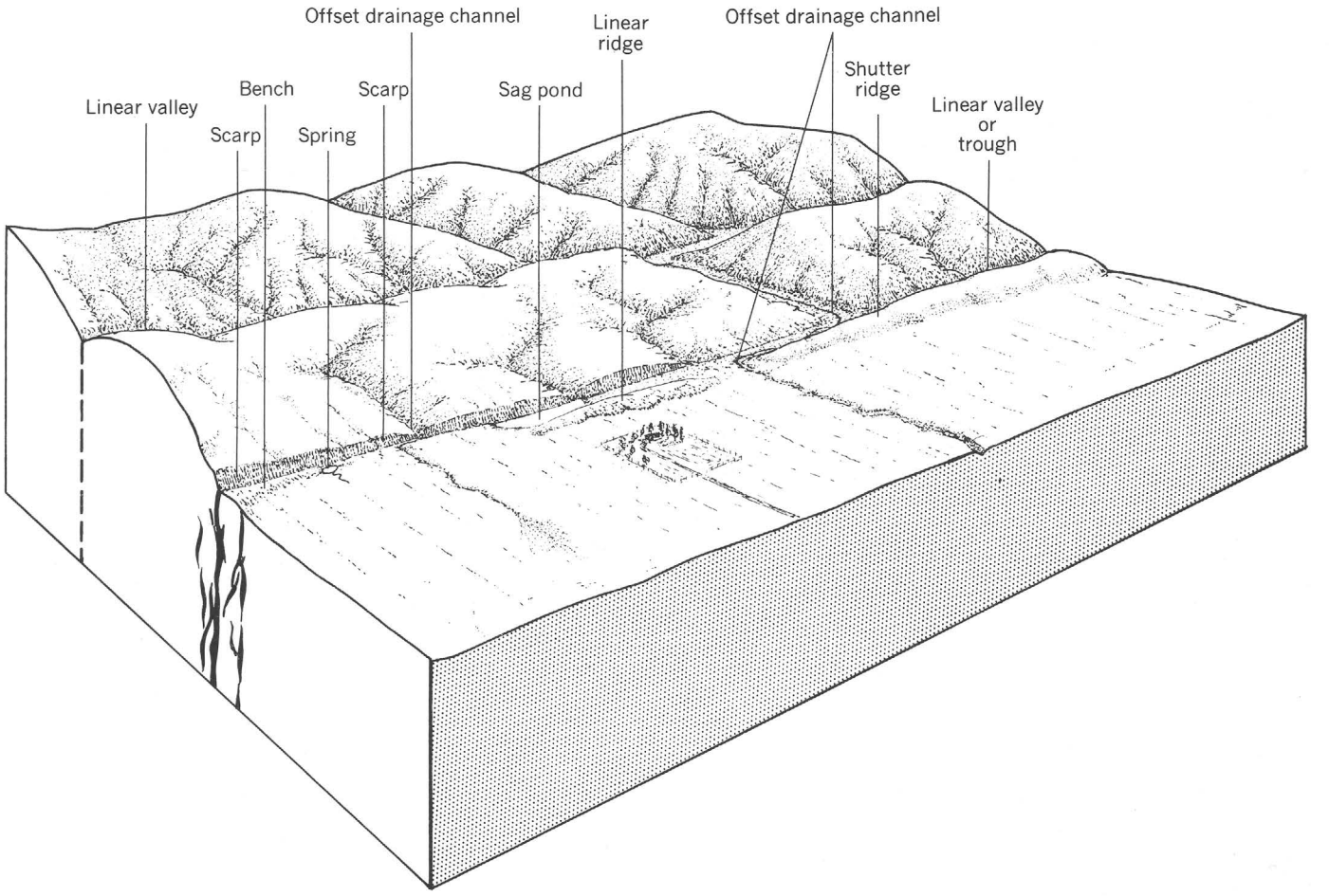

FIGURE 11.—Block diagram showing landforms developed along recently active strike-slip faults.

fault could occur along the San Gregorio fault because of similarities in tectonic regime, fault geometry, surface expression, and seismic characteristics (Greene and others, 1973).

This kind of assumption is given added credibility by historical records of earthquakes in other seismically active parts of the world (Iran, Japan, Turkey) where historic data cover a much greater time span than in California.

FIGURE 10. —Simplified sketch of trench wall showing vertical deformation of initially flat-lying sediments and sedimentary contacts associated with predominantly horizontal movement on the Coyote Creek fault, southern California (from Clark and others, 1972, fig. 83). The trench, dug shortly after the 1968 Borrego Mountain earthquake, crosses a branching break of the fault zone along which about 50 mm (2 in.) of vertical displacement and about the same amount of horizontal displacement took place during the earthquake. Deposits at points A, B, and C were dated radiometrically. The vertical displacement of the sedimentary contacts plotted against the age of the corresponding deposits yields an average rate of vertical deformation of about 0.5 mm/yr (0.02 in./yr) for the past 3,000 years. This suggests a recurrence interval for earthquakes the size of the 1968 event of about 200 years (Clark and others, 1972).

EMPIRICAL MAGNITUDE—FAULT LENGTH RELATIONS

Several empirical relations between earthquake magnitude and the length of associated surface ruptures along faults have been derived (Bonilla, 1970; Bonilla and Buchanan, 1970; Albee and Smith, 1967; Iida, 1965; Tocher, 1958; Bolt, 1973). These magnitude-fault length relations may be used as crude estimates of the maximum-magnitude earthquake that might be expected from a particular fault, if the length of the fault is well known (fig. 14).

The broad scatter shown by the data is partly due to (1) the variety of field conditions in the areas where the observations of faulting were made, (2) the inadequacy of the length of surface fault rupture as a measure of the length of faulting at depth, and (3) theoretical considerations (Dieterich, 1973; Thatcher and Hanks, 1973).

Another difficult problem is the inability to determine, for faults lacking historic ruptures, the proportion of a given fault zone that might be involved in any one earthquake (Wentworth and others, 1973). Despite these serious limitations, magnitude-fault length relations are widely used to estimate the size of the maximum expectable earthquake on known faults.

Estimates of maximum magnitude for various San Francisco Bay region faults are shown in table 1. These estimates are based on the assumption that half the total fault length can break in any one earthquake; however, some of the faults present special problems. For example, lengths of 135 km (84 mi) or 200 km (125 mi) can be assumed for the San Gregorio fault (No. 14, fig. 3), depending on whether the Seal Cove fault and its offshore extension (No. 15, fig. 3) are considered as part

A

FIGURE 12.—Physiographic features of recent faulting along a segment of the San Andreas fault near the Carrizo Plain, southern California. *A*, Aerial view west-southwestward. Low sun angle enhances physiographic features. See *B* for location. *B*, Part of strip map of San Andreas fault showing topographic features such as offset drainage channels, linear ridges and valleys, and linear scarps associated with recent faulting. View in *A* shown by stippled area (from Vedder and Wallace, 1970).

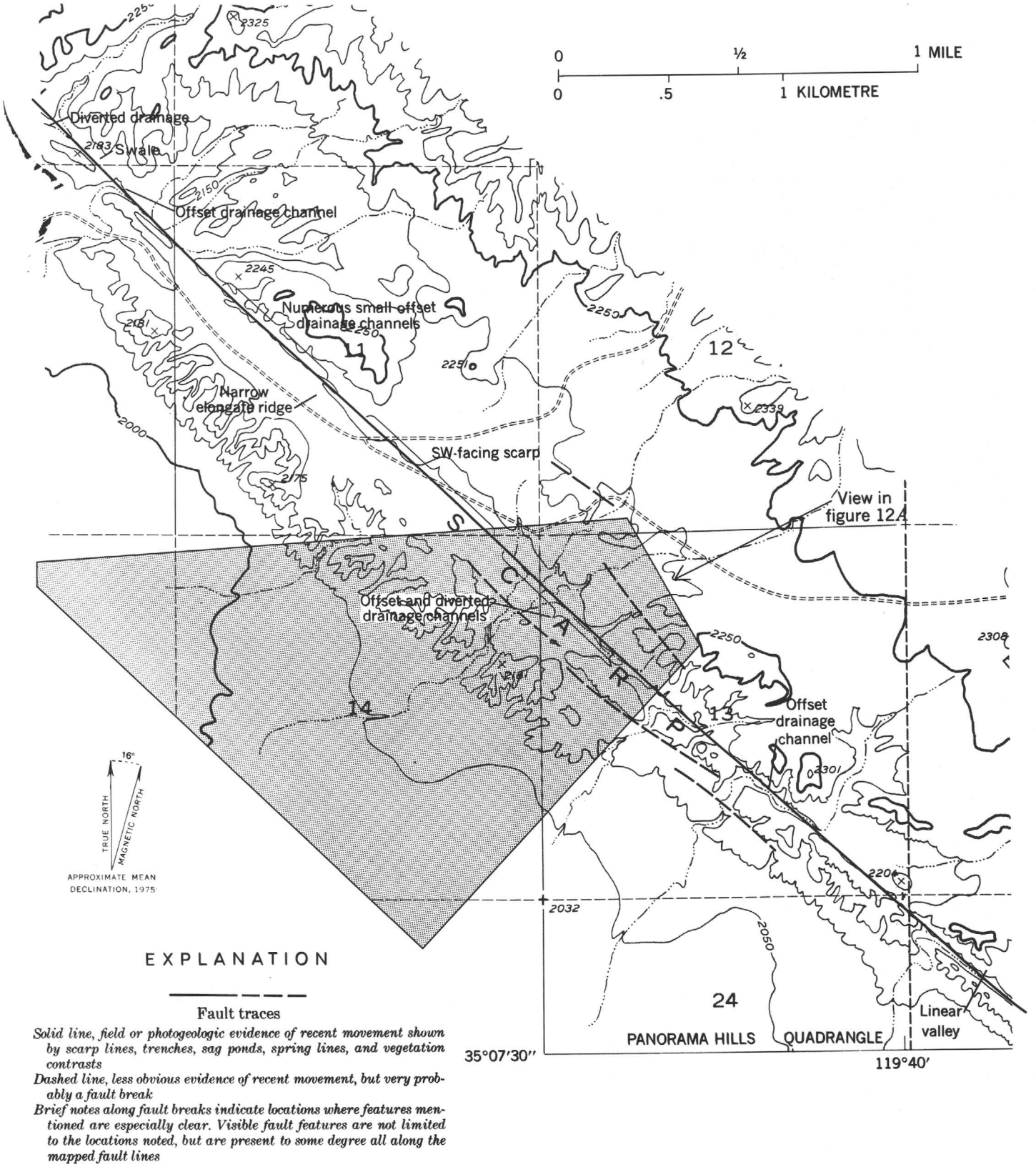

B

FIGURE 12.—Continued.

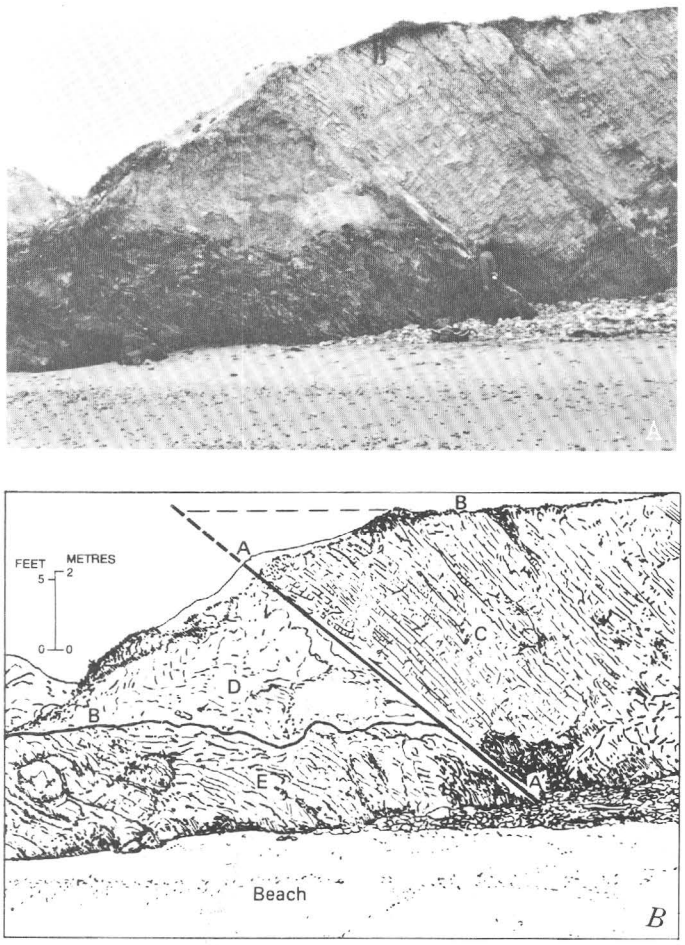

FIGURE 13.—*A*, Faulted wave-cut platform of probable Sangamon age (70,000–120,000 years before present) near Point Año Nuevo, San Mateo County, Calif. *B*, Sketch showing geologic relations. Movement along strand of San Gregorio fault (No.14, fig. 3 and table 1) has displaced wave-cut platform (B) about 5.2 m (17 ft) and thrust Miocene siliceous shale (C); over unconsolidated Sangamon marine terrace deposits (D) and highly sheared Miocene shale (E). Terrace deposits overlying the steeply dipping siliceous shales in the upthrown block (C) have been removed by erosion. Neither the age of the most recent displacement nor the amount of lateral displacement associated with the thrust displacement on this fault is known. The youngest features displaced are the wave-cut platform and overlying terrace deposits, which are probably 70,000–120,000 years old. Therefore, the displacement is younger than that age. Displacement along a related subparallel fault strand 1.2 km (0.8 mi) east of this site has also offset this same wave-cut platform and deformed alluvial deposits dated at 9,510±140 years before present (Weber and Lajoie, 1974).

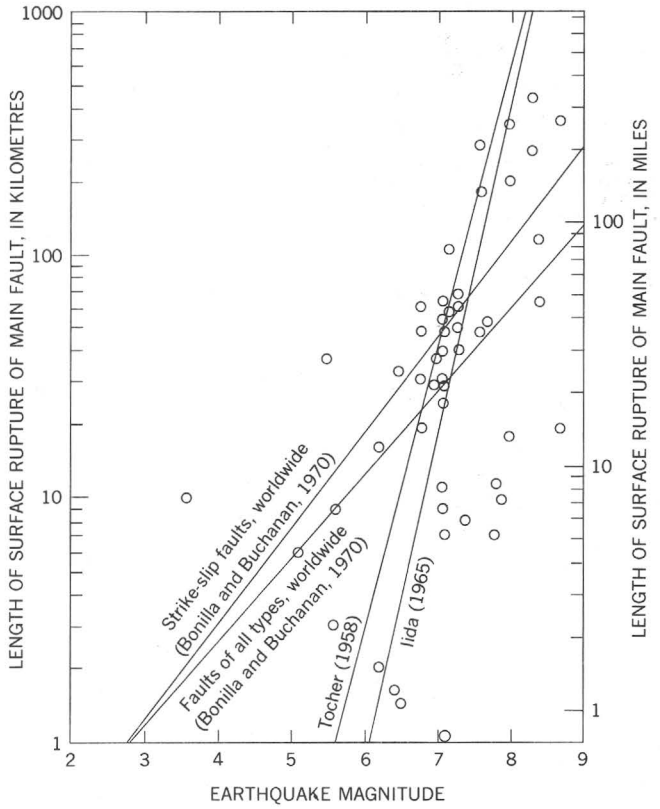

FIGURE 14.—Length of observed surface rupture in relation to earthquake magnitude (Bonilla and Buchanan, 1970). Observations of rupture length often underestimate the actual source dimension of the earthquake because (1) the rupture expressed at the surface may represent only a small part of the total rupture or (2) the surface rupture may be obscured by vegetation or water. Shown for comparison are four suggested magnitude-fault length relations: Bonilla and Buchanan (1970), best fit to all the data plotted (world); Bonilla and Buchanan (1970), best fit to all the data from strike-slip faults; and Iida (1965) and Tocher (1958), best fit to subsets of the data.

of the San Gregorio. These alternate assumptions give estimates of about magnitude 7.4 and 7.7, respectively (Greene and others, 1973).

In summary, accurate estimates of the maximum-magnitude earthquake for any given fault zone cannot be made at present. Consideration of the available data in the manner described above yields reasonable approximations. Maximum magnitude is not the whole story, because damaging earthquakes of lesser magnitude commonly occur with greater frequency. In fact, statistics indicate that over the last 40 years the number of earthquakes smaller than a given magnitude increases by a factor of about 10 for each unit decrease in magnitude. Thus, the frequency of occurrence of various sizes of earthquakes is also required to appraise the potential hazards of various faults.

ESTIMATING THE CHARACTERISTICS OF GROUND DEFORMATION ASSOCIATED WITH FUTURE MOVEMENT ALONG FAULTS

At the time of the great California earthquake in 1906, the San Andreas fault broke almost instantaneously along at least 430 km (270 mi) of its length and offset the ground surface as much as 5 m (16 ft). The main line of rupture followed preexisting fault-controlled topography and was accompanied by subsidiary faulting and tectonic distortion of the ground

that at least locally extended as far as 1 km to several kilometres (thousands of feet to several miles) from the main fault (Lawson and others, 1908). Data from this and numerous other historic faulting events in the world give a basis for estimating the location, character, and maximum amount of ground deformation along many of the faults in the San Francisco Bay region.

Of principal concern in fault-related ground deformation are (1) detailed prediction of the pattern of surface faulting, especially the width of the zone, (2) the amount of displacement across the surface traces of faults, and (3) tectonic distortion of the ground, including uplift, subsidence, and horizontal distortion.

PATTERN OF SURFACE FAULTING

The pattern of surface faulting, especially along the strike-slip faults, involves a main fault zone of varying but generally narrow width along which the principal offsets occur and lesser branch and secondary faults that extend to, or occur at, considerable distance from the main zone (figs. 12, 15). Reverse faults commonly produce more complex rupture zones, and the zones typically are broader and less regular in plan (fig. 16).

Major displacements can be expected along lineaments defined by recognizable fault-caused topographic features (figs. 12, 15). Studies of several surface faulting events indicate that historic ground ruptures closely follow mappable geomorphic features that delineate preexisting fault traces (1857 Fort Tejon—Wallace, 1968; 1906 San Francisco—Lawson and others, 1908, Wallace, 1969; 1966 Parkfield—Brown and Vedder, 1967; 1968 Borrego Mountain—Clark and others, 1972, Clark, 1972; 1971 San Fernando—Yerkes and others, 1974; 1973 Managua— Brown and others, 1973); these observations suggest that patterns of surface faulting are predictable. Clark (1972) estimated, for example, that along about 50 percent of the length of the surface rupture from the Borrego Mountain earthquake of 1968, the position of the main surface fractures could have been predicted to within about 100 m (300 ft) before the earthquake. In the San Francisco Bay region, the San Andreas, Hayward, Concord, Antioch, and a few other faults are mapped in sufficient detail to accurately show the location of fault traces and of the expected future displacements (Brown and Wolfe, 1972; Brown, 1972; Radbruch, 1968a; McLaughlin, 1971; Sharp, 1973; Burke and Helley, 1973). Much of this map information is adequate to influence decisions on structural design and land use.

The confidence with which surface traces can be mapped at a scale of 1:24,000 (1 cm=240 m; 1 inch=2,000 feet) varies considerably depending on frequency and amount of Quarternary displacement, the style of fault movement, and rate of destruction of geomorphic features (controlled largely by climate and local geology and topography). Recent fault traces along strike-slip faults such as the San Andreas can be mapped more confidently than those on faults with dip-slip movement. Consequently, dip-slip faults with youthful movement are only now being recognized in regions where active strike-slip faults have long been known.

ZONE WIDTH

Although the most obvious fault displacement tends to be localized along recognizable and mappable fault lineaments, some permanent ground deformation from fault movement extends outward from the main fault trace. This deformation, manifested as fractures, relatively small surface faults, and local warping, defines an irregular zone that parallels and includes the more obvious and more continuous traces of the main fault.

The width of this zone of surface deformation varies with the type of faulting, earthquake magnitude, the local geologic setting, and perhaps other factors. An example of this variation for strike-slip faulting associated with the Borrego Mountain earthquake is shown in table 3 (Clark, 1972). Because the zone width is so variable and because it seldom can be well defined by surface morphology prior to a major fault event, detailed site studies are usually required for accurate delineation of the zone. Such detailed site information is not yet widely available. In its absence, estimated zone widths are often based on comparison with known patterns of deformation associated with well-documented modern fault geometry accompanying major earthquakes.

Data on zone widths for North American earthquakes in the magnitude range from 5.5 to about 8.5 were analyzed by Bonilla (1970). The data are sparse because only a few events are well documented, but they indicate the general range in width of zones that can be anticipated. For strike-slip faults, the maximum half-width of the zone, from the centerline of the main fault zone to the outer edge of the deformation zone, is about 92 m (300 ft). For dip-slip faults the zone is as much as 900 m (3,000 ft). These values are probably conservative estimates except for very large earthquakes. They have been suggested as the basis for some kinds of planning decisions (Brown, 1972; Hall and others, 1974), but they should be used cautiously and where possible should be supplemented by site investigations. Some evidence from studies of worldwide data suggests that maximum zone width for strike-slip faults may be significantly greater than that cited above and that deformation zones of strike-slip faults may be as wide as those associated with dip-slip faults (U.S. Geological Survey, 1971b, p. A169).

The designation of deformation zones by these criteria is relatively simple where a single fault trace can be used as the center of the zone. Where multiple, parallel, or overlapping fault traces are recognized, the zone width is established by measuring out a half-width from the two outermost fault traces.

Surface offset may also extend well beyond the main rupture zone as branch faults and secondary ruptures on faults that are not visibly connected to the main zone and at considerable distance from it. Large branch and secondary faults probably will be recognized as problem faults in their own right on the basis of geologic evidence, but smaller ones or those with less frequent displacement may not. Secondary and branch faults

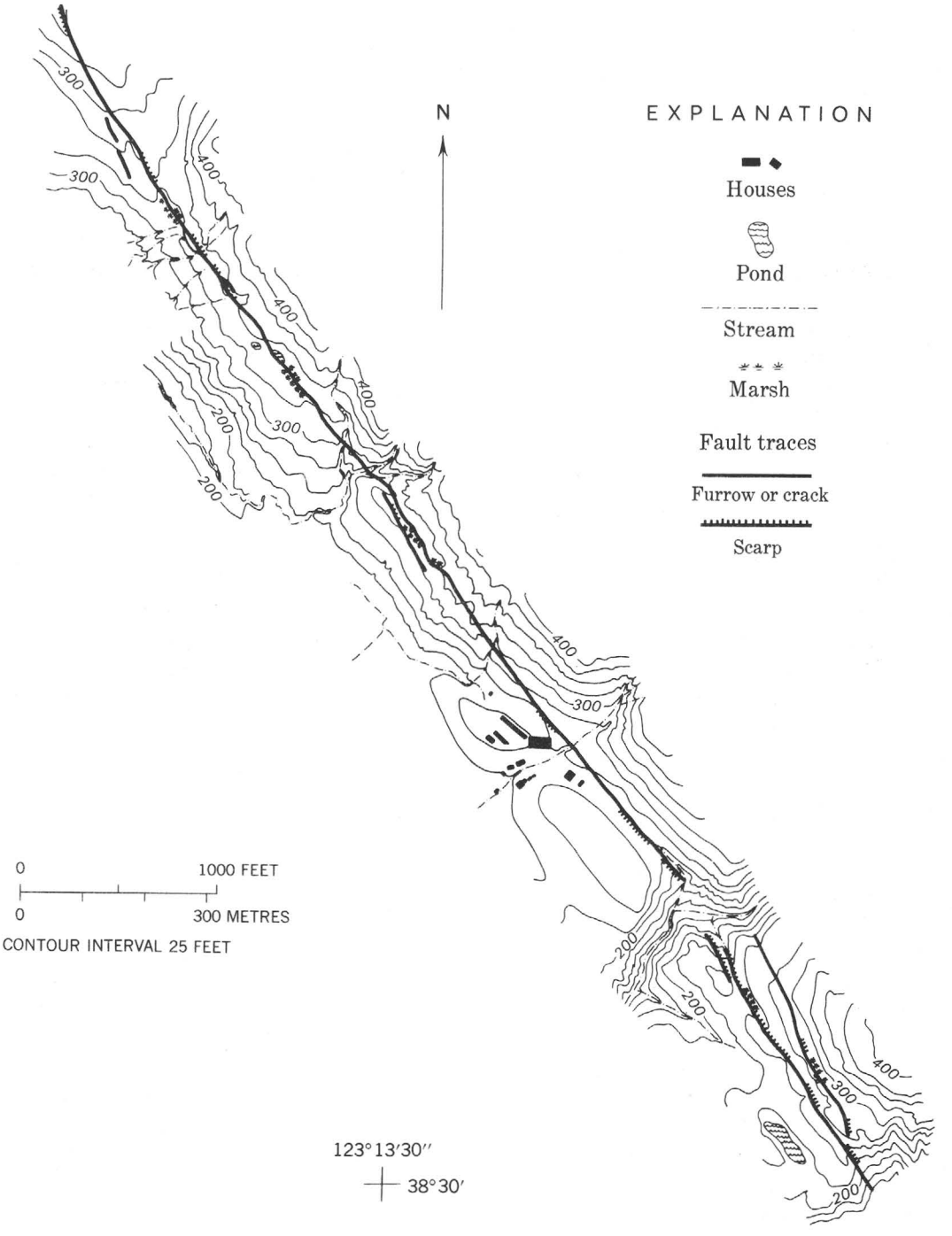

FIGURE 15.—Surface rupture associated with the 1906 earthquake along part of the San Andreas fault near Fort Ross, Calif., showing primary and secondary fault segments. Map simplified from P. Matthes (Lawson and others, 1908).

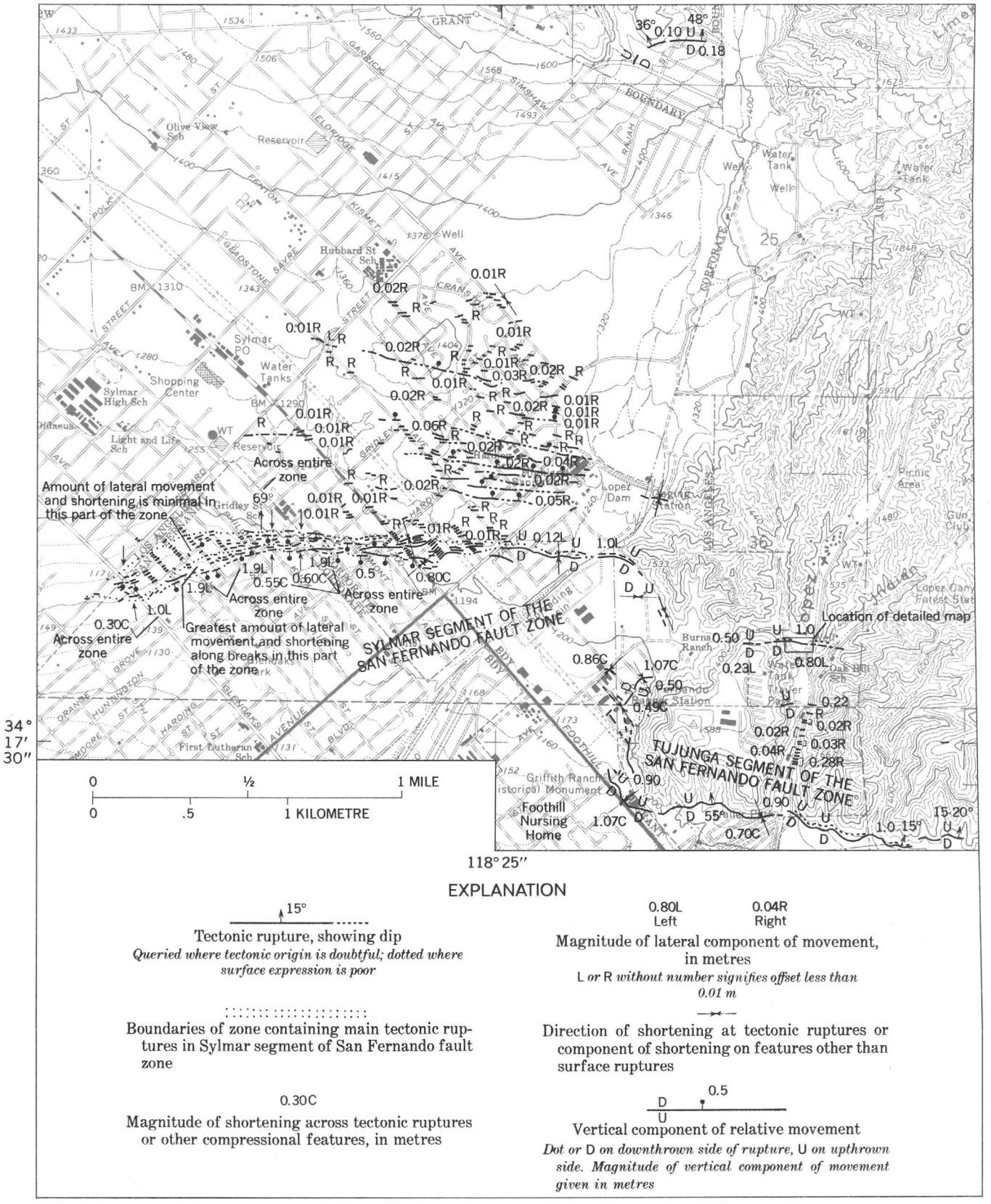

FIGURE 16.—Part of detailed map of surface ruptures associated with the 1971 San Fernando earthquake (U.S. Geological Survey, 1971a, fig. 2). The greater complexity of this pattern relative to that of the 1906 earthquake (fig. 15) reflects the difference in type of faulting (reverse slip for 1971, strike slip for 1906) and the properties of the near-surface materials.

TABLE 3.—*Width of the main rupture zone along the Coyote Creek fault resulting from the 1968 Borrego Mountain earthquake*

Width of rupture		Cumulative length		Percentage of total length of rupture
m	ft	km	mi	
0–50	0– 150	19.7	12.2	64
50– 100	150– 300	2.7	1.7	9
100– 500	300–1,600	5.4	3.4	17
500–1,000	1,600–3,300	1.0	0.6	3
>1,000	>3,300	2.2	1.4	7

historically have shown measurable displacements at distances of as much as 10 km (6 mi) from the main fault zone.

AMOUNT OF DISPLACEMENT

Approximate limits on the amount of surface fault displacement associated with future earthquakes can be estimated from data on past events and estimates of the maximum earthquake magnitude of which a fault is capable. Maximum offsets in historic faulting events in the San Francisco Bay region range from a centimetre (½ in.) or so in some creep events to 5 m (16 ft) on the San Andreas fault in 1906 (Lawson and others, 1908). Wallace (1968) suggested that offset on the San Andreas fault in southern California during the 1857 Fort Tejon earthquake was about 10 m (30 ft), and so 5 m (16 ft) cannot be assumed as the maximum possible for magnitude 8 earthquakes in the San Francisco region. Other documented evidence in the bay region is limited to the 0.9 m (3 ft) of horizontal and 0.3 m (1 ft) of vertical offset that occurred on the Hayward fault in 1868. None of the reverse or thrust faults in the region are known to have undergone historic surface offset that can be used as a guide to future events.

These data together with other historic data comparing earthquake magnitude and maximum fault offset (Bonilla and Buchanan, 1970; Clark, 1972; U.S. Geological Survey, 1971b) suggest upper bounds for maximum displacements on strike-slip faults of 10 m (30 ft) for magnitude 8, 6 m (20 ft) for magnitude 7, 2 m (6 ft) for magnitude 6, and 0.5 m (2 ft) for magnitude 5. The available historic data for the strike-slip faults in the San Francisco Bay region (Bonilla, 1970) suggest that the vertical displacement along these faults may be at most about one-third of these values but commonly is less than one-tenth.

TECTONIC GROUND DISTORTION

In addition to discrete rupture along fault traces, large areas of the ground surface can be more subtly, but also permanently, affected by vertical and horizontal distortions of the earth's crust, including gross uplift and subsidence. These effects are related geometrically to the main fault offset but may extend for tens of kilometres (or tens of miles) from the fault. These distortions include bending, warping, and changes in elevation (Bonilla, 1970; Sharp and Clark, 1972). The 1964 Alaska earthquake (magnitude 8.5) caused crustal deformation over an area of perhaps 285,000 km^2 (11,000 mi^2), producing a maximum uplift of 12 m (38 ft) and a maximum downwarp of 2½ m (7½ ft) (Plafker, 1969). This may be an extreme example, and the amount of distortion may reflect the fact that it was related to thrust faulting; however, similar distortions of smaller magnitude and extent have been observed with several other earthquakes. Studies of the widespread surface distortion associated with the 1971 San Fernando earthquake suggest that its general character could have been predicted from the Quaternary geologic history of the area (Yerkes and others, 1974). Commonly the maximum distortion is adjacent to the fault, and it gradually decreases with distance away from the fault.

Such distortions must be expected to accompany any large earthquake in the San Francisco Bay region. Because the most hazardous faults in the bay region are characterized by predominantly horizontal movement, the amount of tectonic uplift or subsidence probably will be less than a metre (about 3 ft). However, significant changes in elevation or slope can be caused by dip-slip faulting or by other mechanisms of surface distortion such as landslides.

IMPLICATIONS FOR REDUCING EARTHQUAKE HAZARDS

Which faults are capable of generating damaging earthquakes? What will be the frequency and character of the earthquakes? What will be the pattern and character of surface fault displacement associated with earthquakes? These questions are central to the practical aspects of reducing the hazards associated with earthquakes. The answers are still incomplete, but the information available now can substantially reduce loss of life and property in future large earthquakes. Nevertheless, the San Francisco Bay region faults discussed are all believed capable of future movement.

Future loss can be reduced through planning that recognizes (1) that earthquakes on these faults will be the sources of locally severe and widespread shaking and (2) that surface fault displacement and associated deformation will be localized along these faults. Current knowledge provides an ample basis for this kind of land-use planning, the formulation of local building codes, and similar governmental decisions. Because the most severe ground deformation is typically restricted to a zone several tens to hundreds of metres wide along the fault trace, limitations in land use or requirements for special engineering design to reduce loss need affect only a small area, compared with

the area for which precautions against severe seismic shaking should be taken.

The response that follows recognition of a particular fault hazard can vary greatly. One sort of response may be appropriate for facilities such as nuclear reactors, hospitals, and schools, quite another for parks, recreation areas, or other less potentially hazardous uses. For potentially hazardous land uses, prudence demands a conservative response even though the evidence for current and youthful fault movement is relatively weak. But any fault showing evidence for late Quaternary or more recent movement must be regarded as capable of future movement and should be carefully evaluated in any kind of land-use or planning decision. Faults showing evidence for older Quaternary displacement must be regarded with extreme caution, especially if they are near sites under consideration for potentially hazardous facilities.

The likelihood that earthquakes of various sizes will occur may be taken into account by considering several levels of performance of structures during an earthquake. One level might be represented by survival of the structures without impairment of function or safety, and another level might permit substantial structural damage but not so much as to represent catastrophic failure. In the siting and design of nuclear power reactors, for example, an expectable "operating basis earthquake" and a maximum expectable "safe shutdown earthquake" are considered (Atomic Energy Commission, 1973) so that capital investment and generating capacity are protected at reasonable cost but so that catastrophe can be avoided in the event that full potentials of the fault are realized during the life of the structure. Similar procedures can be applied to other structures with less extreme impact on public safety.

The immediate implications of fault creep for any engineering structure astride the trace of a creeping fault are clear; many structures in the bay region, particularly where the Hayward fault passes through the densely populated east side of the bay, exhibit damage from fault creep. But fault creep also may or may not imply a high level of stress in the earth's crust. What this means in terms of the potential for a large earthquake is not yet known and is currently the subject of vigorous debate (see, for example, Savage and Burford, 1973; Nason, 1971). Whether tectonic creep sufficiently relieves stress to inhibit the occurrence of a large earthquake, whether creep is a precursor of a large earthquake, or whether the actual situation is some combination of these is uncertain at present. But fault creep and large earthquakes can occur on the same segment of a fault; the sections of the Hayward fault responsible for large damaging earthquakes in 1836 and 1868 have been creeping at an average rate of about 1 cm (½ in.) per year for at least the last 54 years (Nason, 1971).

Planning and land-use decisions at site, local, and regional scales should take into account the broader zone of deformation as well as fault traces themselves. Until proved otherwise by geologic site investigations, prudence suggests zone widths of 184 m (600 ft) for the largest strike-slip faults and 1,800 m (6,000 ft) for the largest dip-slip faults. In the San Francisco Bay region, most dip-slip faults are relatively short (less than 16 km or 10 mi), and for these, narrower zone widths are appropriate. Hall, Sarna-Wojcicki, and Dupré (1974) have assigned zone widths of 850 m (2,800 ft) to the Zayante fault, an oblique-slip fault in Santa Cruz County.

The level of potential hazard from branch and secondary faults is less than that associated with the main fault, but for some facilities it may be essential to perform geologic site investigations to insure that branch and secondary faults are not a problem.

Tentative upper bounds on the maximum surface fault displacement for an earthquake of a given magnitude are 10 m for magnitude 8, 6 m for magnitude 7, 2 m for magnitude 6, and 0.5 m for magnitude 5.

In the San Francisco Bay region, the impact of permanent tectonic distortion of the earth's surface may be small in comparison with the damage caused by shaking, landslides, and other effects. Vertical movements present problems along shorelines and on canals and pipelines. Horizontal distortions may cause problems for pipelines as well but may also cause havoc in the definitions of land ownership.

SUMMARY

A well-designed program to reduce hazards from earthquakes requires concerted and coordinated effort both by the scientific and engineering disciplines and by those public agents having social and political responsibilities. It also requires an information base that can be used as input to engineering analysis and to policy decisions. The most fundamental segment of that information base deals with (1) the location of faults capable of generating damaging earthquakes, (2) the magnitude of earthquakes anticipated on these faults, (3) the amount of fault displacement anticipated, (4) the nature and areal distribution of deformation accompanying earthquakes or fault movement, and (5) the frequency of recurrence of earthquakes on a known fault.

The evaluation presented in this chapter reflects our current assessment of these topics for the San Francisco Bay region, and it suggests an approach that can be applied to other areas with high earthquake risk. The results are encouraging for those who wish to imple-

ment a program of earthquake hazard reduction, but they also indicate a need for further effort and for attention to new discoveries.

About 30 faults in the bay region are potentially capable of producing damaging earthquakes. Most of these can be accurately located, and those that are the largest and potentially most destructive can be very well located. Detailed maps, suitable for most planning and decisionmaking purposes, are available for many of these faults.

Magnitudes of historic earthquakes are known for more than half of the recognized faults. These data indicate that at least eight moderate or large-magnitude events have occurred on known bay region faults and that one very large earthquake (magnitude 8.3) was located on the San Andreas fault. Current methods of estimating maximum magnitude in the absence of historic data are still crude, but they provide an approximate measure of the size of earthquake that can be expected on faults that have no historic record of damaging earthquakes.

Fault displacement of as much as 5 m (16 ft) was recorded after the 1906 earthquake on the San Andreas, and maximum horizontal displacement of as much as 10 m (30 ft) is judged possible with a magnitude 8 earthquake on a strike-slip fault. Estimated upper bounds for displacement (horizontal) accompanying smaller earthquakes on strike-slip faults in the bay region are 6 m (20 ft) for magnitude 7, 2 m (6 ft) for magnitude 6, and 0.5 m (2 ft) for magnitude 5. Vertical displacements associated with earthquakes on strike-slip faults are likely to be less than one-third of the horizontal displacement. Displacement associated with dip-slip faults is more difficult to evaluate, but these evidently are fewer and shorter in the bay region than strike-slip faults.

The nature and areal distribution of deformation related to fault movement includes (1) permanent ground deformation localized as a zone along the fault and (2) systematic deformation of the earth's surface on a regional or subregional scale.

Accurate delineation of the width of the zone of deformation along the fault is best accomplished through careful geologic site studies including, where necessary, trenching, excavation, or other subsurface investigations. Where such data are not available, zone width can be crudely estimated by analogy with measured zones of deformation that have accompanied historic faulting. This method suggests that, for strike-slip faults, permanent ground deformation may be expected to extend for 92 m (300 ft) on either side of a recognizable strike-slip fault trace and 425 m (1400 ft) on either side of a recognizable dip-slip fault trace (Hall and others, 1974). Designation of deformation zones on this basis is admittedly a stop-gap measure and should be re-evaluated with the availability of new geologic data at the site.

Regional or subregional deformation of the earth's crust commonly accompanies major earthquakes. It is manifested predominantly as upwarping or subsidence for dip-slip faults and predominantly as horizontal distortion for strike-slip faults. In the bay region horizontal distortion appears to be the predominant process, although some local vertical warping (about 0.5 m or 1.5 ft) accompanied the 1906 earthquake on the San Andreas. The magnitude of this process and its potential hazard for the bay region are not completely known, but it appears to be less important in evaluation of earthquake hazards than other earthquake effects.

The frequency of recurrence of earthquakes is perhaps the most difficult to assess of all these topics. Until more geologic data are available, recurrence estimates are tentative at best and depend heavily on our knowledge of recurrence of historic earthquakes. The historic record in the bay region is little more than 150 years old, a woefully inadequate sample for faults that have been active for millions or tens of millions of years. But even that record shows a crude pattern of damaging earthquakes on major bay region faults. Attempts to determine recurrence intervals for bay region earthquakes are further complicated by the unresolved relation between fault creep and damaging earthquakes because several bay region faults exhibit fault creep along parts of their length. Despite the need for more accurate data on frequency of recurrence, the phenomenon of recurrence is well established.

Many important questions are still unanswered, but enough is known now to move positively toward reducing the hazard from future earthquakes. Some steps in this direction are obvious. All residents would agree that schools and hospitals should not be located astride the traces of major faults; most would accept requirements for geologic site studies in the deformation zones along major faults; and many would agree on siting restrictions that would locate major highway interchanges, dams, or power plants away from faults that may generate earthquakes. These kinds of actions are ultimately a product of the democratic process, and they depend as much on social and economic values as on our scientific knowledge.

Other steps toward reducing earthquake hazards cannot be taken without more information than is given here. Building codes, for example, are an important mechanism for protecting life and property from earthquakes. But such codes require specific information on the nature of seismic shaking, possible modes of structural response, and other factors that go far beyond the initial geologic process that causes the earthquake. These and other problems relating to hazard reduction are treated in subsequent sections of this report.

ESTIMATION OF BEDROCK MOTION AT THE GROUND SURFACE

By R. A. PAGE, D. M. BOORE, and J. H. DIETERICH

INTRODUCTION

In terms of human and economic losses, seismic shaking is the most significant factor contributing to the overall earthquake hazard. Shaking contributes to losses not only directly through vibratory damage to manmade structures but also indirectly through triggering of secondary effects such as landslides or other modes of ground failure. Thus, an important element in seismic zonation on a regional basis is the geographical assessment of potential ground shaking.

The intensity and character of ground shaking depends upon earthquake source parameters such as magnitude, driving stress causing the fault to slip, and dimensions of the slip surface, as well as upon distance from the fault. In addition, experience shows that surficial geologic materials may influence the level and nature of ground motion. Hence, the problem of evaluating the potential of seismic shaking divides naturally into two parts: estimation of bedrock motion at the ground surface, which is the subject of this paper, and estimation of the response of surficial geologic units to bedrock motion, which is discussed by Borcherdt, Joyner, and others (this report).

FACTORS INFLUENCING DAMAGE POTENTIAL OF GROUND MOTION

Three factors, amplitude, frequency content, and duration, govern the damage potential of ground motion and thus must be included in any scheme to characterize ground motion for purposes of design or hazard assessment. Damage tends to increase with the amplitude of bedrock motion; however, the relation between damage and amplitude is generally complex because of the response of surficial geologic deposits and manmade structures to large ground motions. Frequency content is a critical factor because structures, and in some cases surficial deposits, may respond in a resonant manner depending upon the frequency content of the ground motion. Relatively large deformations and stresses can occur in a structure or unconsolidated surficial deposit if the shaking includes significant amounts of energy at frequencies close to the natural resonant frequencies of the system. Duration of shaking, which is perhaps the least widely recognized factor influencing damage from shaking, is important because failure mechanisms in structures and unconsolidated surficial deposits commonly are dependent upon the cumulative number of induced stress cycles as well as the amplitudes of the stress. For example, had the duration of strong shaking during the San Fernando, Calif., earthquake of 1971 been longer, the earthquake damage and loss of life caused by shaking would have been greater than it was, as several critical structures were very near failure (Housner and Jennings, 1972).

CHARACTERIZATION OF BEDROCK MOTION

Ground motion can be characterized in a number of ways. The most complete characterization is a time history of ground movement, that is, a specification of ground motion in three independent spatial coordinates for every instant of time in terms of acceleration, velocity, or displacement. As basic data for the dynamic analysis of structural designs, time histories are a valuable tool to the seismic engineer. For purposes of seismic zonation, however, a more compact characterization of the ground motion is desirable. For sites underlain by bedrock, one such characterization employs four physical parameters scaled or computed from standard strong-motion seismograms: maximum ground acceleration, maximum ground velocity, maximum ground displacement, and duration of shaking above some threshold amplitude. On a typical strong-motion recording of an earthquake at distances within which damage is sustained (see fig. 17), the peak ground acceleration commonly occurs at frequencies in the range 2 to 10 Hz, whereas the dominant frequencies of velocity and displacement are in the ranges 0.5 to 2 Hz and 0.06 to 0.5 Hz, respectively. Thus, specification of the peak amplitudes for acceleration, velocity, and displacement also conveys information about the frequency content of the motion.

The strategy for predicting ground motion (Borcherdt, Brabb, and others, this report) involves two

steps: first, estimation of bedrock motion at the ground surface and, second, modification of that motion to account for the dynamic response of surficial geologic deposits. For use as input to the second step, we want to express ground motion in terms of the Fourier amplitude spectrum of ground acceleration. We cannot estimate the Fourier spectrum directly from peak ground-motion parameters and duration of ground motion; however, an upper bound to the spectrum is given by the zero-damped velocity response spectrum (Hudson, 1962), for which a smooth estimate can be obtained from the peak ground-motion parameters using an empirical technique described by Newmark and Hall (1969).

The velocity response spectrum is a common tool for seismic design. It is defined by the maximum response velocities of a suite of linear, damped, single-degree-of-freedom oscillators subjected to a specified time history of motion. A velocity response spectrum for a given level of damping is thus a plot of maximum velocity as a function of oscillator period or frequency (see fig. 18). The usefulness of the response spectrum for design purposes stems from the ability to model structures by comparable oscillators and to estimate stresses induced by the ground motion from knowledge of the response spectrum and of the equivalent natural frequencies and damping of the structure.

The relation between the Fourier and zero-damped velocity response spectra is illustrated (fig. 18) for one horizontal component of the Pacoima damsite recording of the 1971 San Fernando earthquake. Figure 18 also illustrates the graphical method of Newmark and Hall (1969) for constructing smooth response spectra from peak ground-motion parameters. The first step is to plot lines of constant acceleration, velocity, and displacement (dot-dashed lines, fig. 18) equal to the maximum values of ground motion (1.25 *g*, 115 cm/s (43 in./s), and 43 cm (17.8 in.), respectively). To obtain the smooth response spectrum, these lines are then shifted upward (dashed lines, fig. 18) on the plot by multiplying the ground-motion values by factors (4.8, 3.0, and 1.7, respectively) that reflect the dynamic amplification of the ground motion by the oscillator and the duration of ground motion. The amplification factors are dependent on the level of damping of the oscillator and, at low levels of damping, on the duration of shaking. In this example, the amplification factors are chosen to produce the illustrated fit between the smooth tripartite response spectrum (dashed line) and the computed zero-damped response spectrum (heavy solid line). These factors are derived for a magnitude 6.6 earthquake; larger factors would be appropriate for a larger magnitude, and hence longer duration, earthquake.

SCALING OF GROUND-MOTION PARAMETERS WITH DISTANCE AND EARTHQUAKE MAGNITUDE

Since 1966, the increase in the amount and quality of strong-motion data obtained within 50 km (31 mi) of the causative fault during moderate-sized earthquakes (magnitude 5.0 to 6.9) has made it possible to predict on a statistical basis peak ground-motion values for earthquakes smaller than magnitude 7.0 at distances greater than 10 to 20 km (6 to 12 mi) for sites on competent geologic materials ranging from bedrock to firm alluvium. The increase in the quantity of strong-motion data comes largely from increased numbers of strong-motion recorders placed in operation in recent years by the Seismological Field Survey of the National Oceanic and Atmospheric Administration (now the Seismic Engineering Branch of the U.S. Geological Survey). Even with the greater number of recorders, however, no strong-motion seismograms have been obtained within 40 km (25 mi) of a magnitude 7 earthquake and within more than 100 km (62 mi) of a magnitude 8 shock. The quality of the strong-motion data also has improved in the sense that detailed aftershock investigations and field studies after recent moderate-sized earthquakes have delineated the inferred slip surface for the main earthquake and have made possible more accurate estimates of distances of strong-motion sites from the causative fault.

To determine the scaling factors for ground-motion parameters with distance, we must know the distance from a recording site to the source of the seismic energy responsible for the peak recorded motion. Lacking such information for most earthquakes, we approximate that quantity by the shortest distance to the slipped fault surface. Close to a fault the approximation may be poor because the source of peak motions may not be the point on the fault closest to the recording site (Lindh and Boore, 1973; Boore and Zoback, 1974; Hanks, 1974; Trifunac, 1974). For this reason, there is considerable uncertainty in empirical relations between ground-motion parameters and distance close to the fault (at distances less than the width or depth of the fault), even for earthquakes for which some near-fault data exist (shocks smaller than magnitude 7).

PEAK GROUND ACCELERATION

A plot of peak horizontal ground acceleration against shortest distance to the slipped fault (fig. 19) reveals that acceleration increases with magnitude at all distances for which data exist and that the rate of attenuation with distance is similar for all magnitudes at distances beyond 10 to 40 km (6 to 25 mi). Although

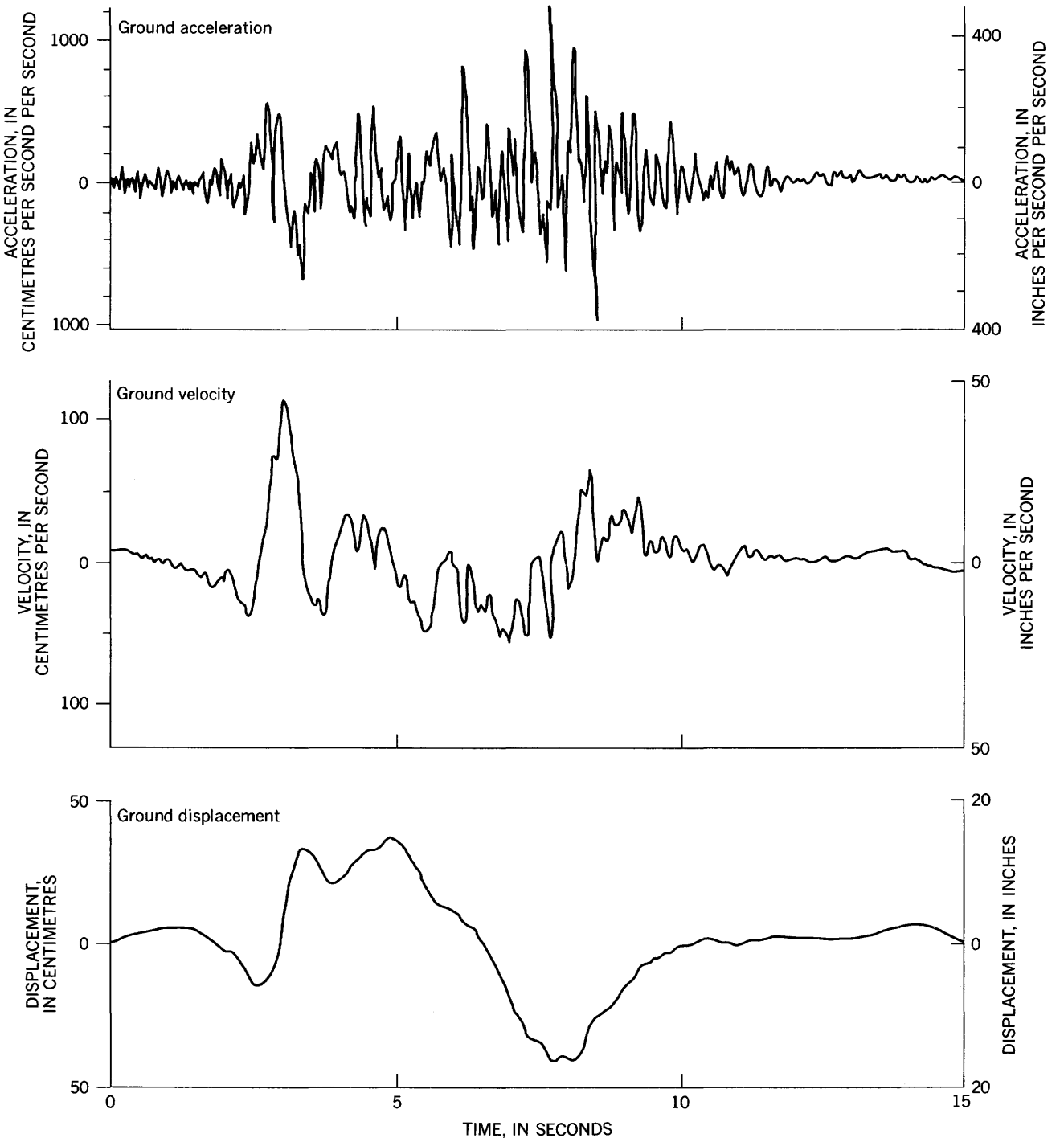

FIGURE 17.—Records of N. 14° E. component of horizontal ground motion at Pacoima damsite for San Fernando, Calif., earthquake of February 9, 1971 (after Trifunac and Hudson, 1971). Velocity (center) and displacement (bottom) records are obtained by integrating acceleration record (top) once and twice, respectively.

there is considerable scatter in the data for a particular range of distance and magnitude, the systematic trends are obvious. Distances are known to an accuracy of about 2 to 3 km (1 to 2 mi) for most events of magnitude 5.0–5.9 and 6.0–6.9, and to within 5 km (3 mi) for events of magnitude 7.0–7.9, with one exception for which a minimum value is plotted. If peak-acceleration data taken from the literature are plotted without regard to the measure of distance (that is, whether the distance is to the epicenter, hypocenter, or closest point on the slipped surface) or without regard to accuracy of the distance, the scatter at distances less than 30 km (20 mi)

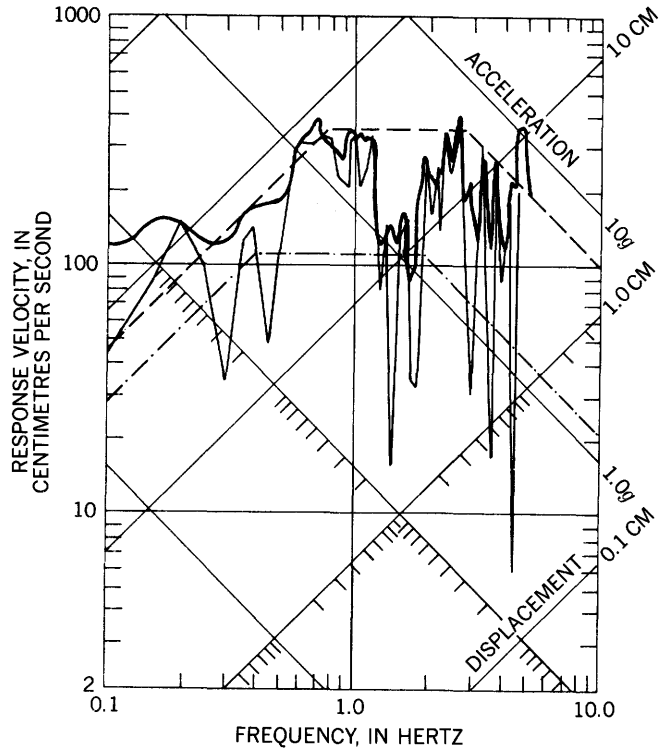

FIGURE 18.—Comparison of spectra for N. 14° E. component of ground motion at Pacoima damsite for San Fernando, Calif., earthquake of February 9, 1971. Amplitude at a given frequency may be read in terms of velocity (vertical axis), acceleration (bottom left to top right axis), or displacement (bottom right to top left axis). Zero-damped velocity response spectrum (heavy solid line) envelopes Fourier spectrum of ground acceleration (light solid line). Derivation of smooth tripartite response spectrum (dashed lines) from peak ground-motion values (dot-dashed lines) is described in text.

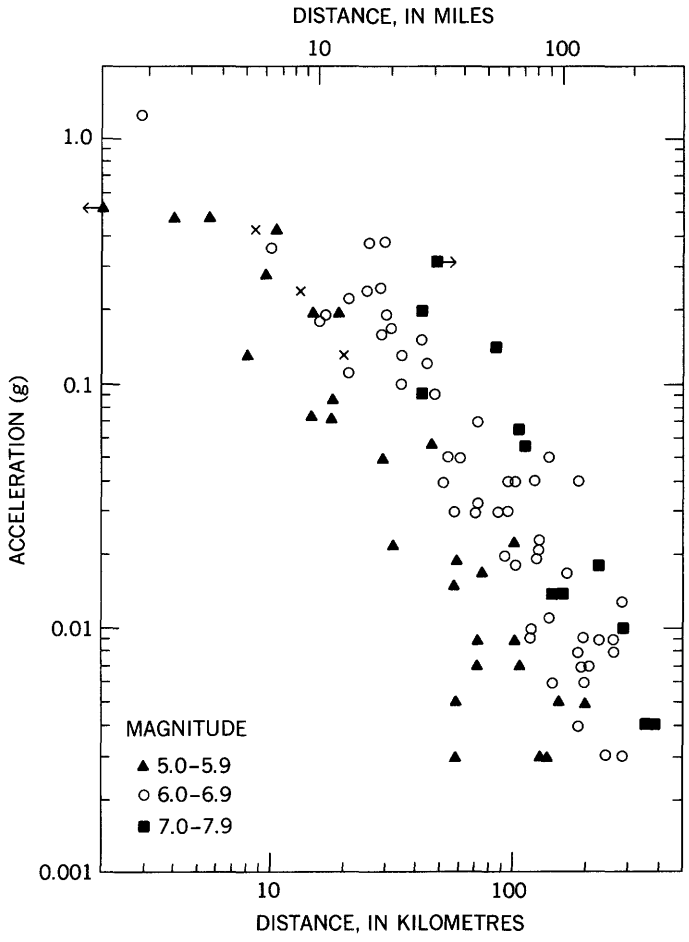

FIGURE 19.—Peak horizontal ground acceleration in relation to shortest distance to slipped fault as a function of magnitude. Acceleration expressed in terms of gravitational acceleration, *g*. Data from free-field sites, including buildings up to two stories high. Most data from Page, Boore, Joyner, and Coulter (1972, table 4). Arrow pointing to left signifies distance to fault is actually smaller than shown; arrow to right signifies distance is greater. Crosses are interpolated values for postulated earthquakes (see Borcherdt, Brabb, and others, this report).

is at least twice that observed in figure 19 (compare Page and others, 1972, fig. 4) and tends to obscure the marked attenuation of acceleration within this distance range.

The site conditions corresponding to the data shown in figure 19 range from crystalline rock to thick sections of firm alluvium. To estimate the effect of surficial conditions on peak ground acceleration, the data are replotted separately for the magnitude intervals 5.0–5.9 and 6.0–6.9 (figs. 20, 21) with a twofold classification of site geology. A site underlain by less than 5 m (16 ft) of alluvium is classified as a rock site, whereas a site underlain by a greater thickness is labeled an alluvium site. Within the range of surficial materials and levels of ground motion sampled (figs. 20, 21), site geology appears to contribute no more to the observed variation in peak acceleration than other factors that are yet to be thoroughly investigated, such as variations in driving stress and dimensions of the fault surface for earthquakes of equivalent magnitudes and variations in the propagation of seismic waves. At sites close to the fault, where ground shaking is sufficient to cause significant damage to ordinary structures, surficial deposits may substantially influence peak accelerations. As more near-fault strong-motion records of damaging levels of shaking are obtained, we anticipate that the effects of site geology upon peak acceleration will become clear. For example, on weak foundation materials such as the bay mud and Holocene alluvium in the San Francisco Bay region (see Lajoie and Helley, and Borcherdt, Joyner, and others, this report), we expect that for some sites peak levels of acceleration will be limited by the ability of the geologic materials to transmit the intense motion from the bedrock to the ground surface. Although the peak accelerations, which are generally a measure of the ground-motion amplitude at the higher frequencies, may be reduced for such sites from those

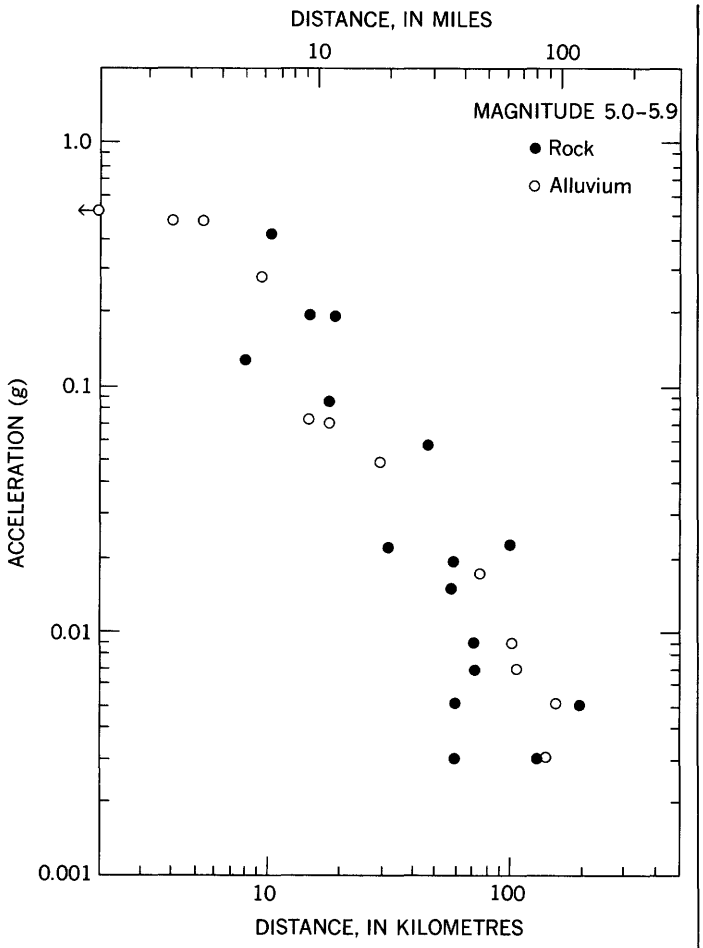

FIGURE 20.—Peak horizontal ground acceleration in relation to shortest distance to slipped fault for earthquakes of magnitude 5.0 to 5.9 as a function of site geology. Data from figure 19. Rock site is underlain by less than 5 m (16 ft) of alluvium; alluvium site by more than 5 m (16 ft). Arrow as in figure 19.

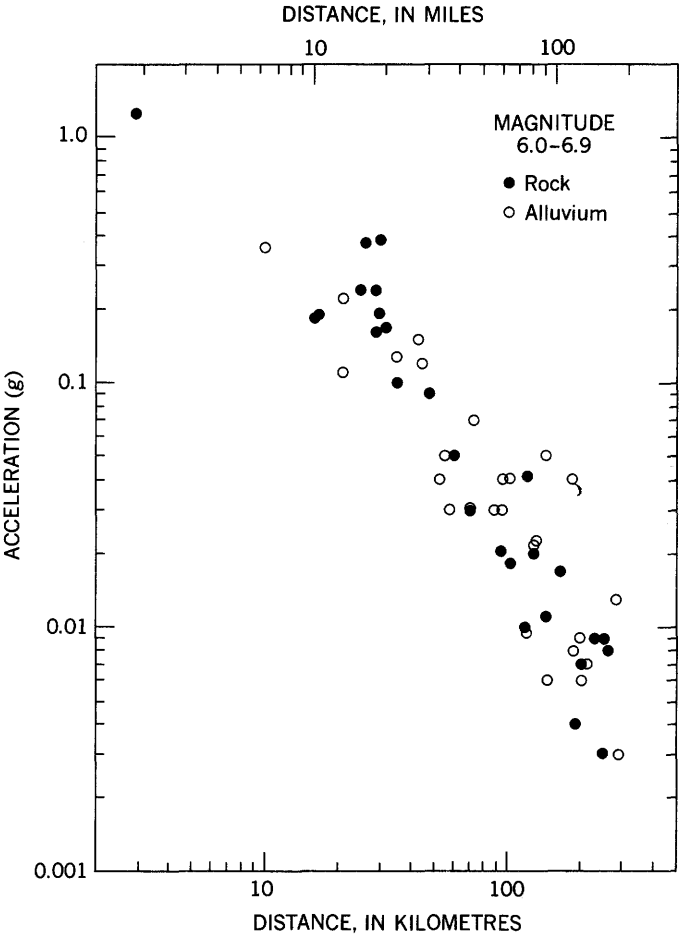

FIGURE 21.—Peak horizontal ground acceleration in relation to shortest distance to slipped fault for earthquakes of magnitude 6.0 to 6.9 as a function of site geology. Data from figure 19. Rock site is underlain by less than 5 m (16 ft) of alluvium; alluvium site by more than 5 m (16 ft).

expected on bedrock, the overall damage potential is likely to be greater on the soft ground than on rock, because of possible ground failure (see Youd and others, this report), possible extended duration of shaking, and possible ground-motion amplification at the lower frequencies (see Borcherdt, Joyner, and others, this report).

From the data presented, it is clear that the dependence of peak acceleration a upon distance r can be represented by an inverse power law, $a = kr^{-\beta}$, where k is a factor depending on magnitude. Within the uncertainty of the data, the exponent β is independent of magnitude and ranges from 1.4 to 1.7. This relation applies outside the immediate vicinity of the fault, that is, at distances greater than one fault depth or width. Within the immediate vicinity of the fault, the rate of attenuation must be less. Although there is considerable scatter in the peak-acceleration data (figs. 19, 20, 21), it is clear that useful statistical predictions of peak acceleration can be made now for sites on rock and competent alluvium at distances greater than 10, 20, and 40 km (6, 12, and 25 mi) for magnitude 5.0–5.9, 6.0–6.9, and 7.0–7.9 earthquakes, respectively.

PEAK GROUND VELOCITY

Standard strong-motion seismographs produce accelerograms, that is, graphical records of ground acceleration as a function of time. Ground velocity and displacement are calculated by integrating accelerograms once or twice, respectively. Because of the data processing involved, both velocity and displacement data are scarce compared with acceleration data, which are scaled directly from accelerograms. Recently established programs for routine computer processing of digitized accelerograms (Hudson and others, 1971) are beginning to provide the velocity and displacement data required to establish the dependence of peak ground velocity and displacement upon magnitude, distance,

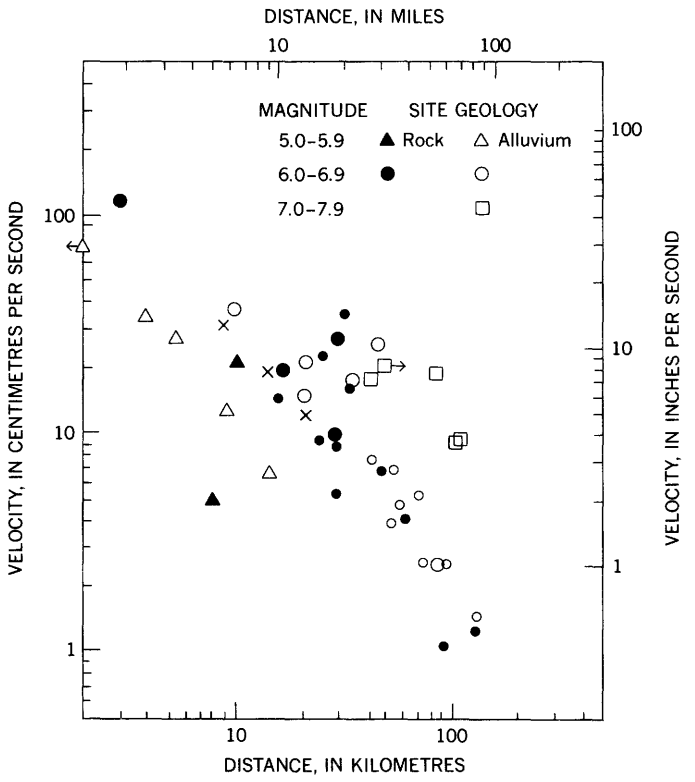

FIGURE 22.—Peak horizontal ground velocity in relation to shortest distance to slipped fault as a function of magnitude and site geology. Data from free-field sites, including buildings up to two stories high. Solid symbols for rock sites (underlain by less than 5 m (16 ft) of alluvium); open symbols for alluvium sites (more than 5 m (16 ft) of alluvium). Large symbols for velocities from integrated accelerograms; small symbols for velocities estimated by approximate integration techniques typically accurate to 10 to 20 percent. Distances accurate to 5 km (3 mi) or less with one exception, for which the minimum value is plotted. Crosses are interpolated values for postulated earthquake (see Borcherdt, Brabb, and others, this report). Arrow as in figure 19.

and site conditions.

In many respects the behavior of peak horizontal ground velocity parallels that of peak acceleration. Peak velocity increases with magnitude at all distances for which data are available and attenuates with distance from the slipped fault (fig. 22) following an inverse power law. The rate of attenuation, however, is slightly less than that for peak acceleration. The scatter in the velocity data is comparable to that observed in the acceleration data (compare fig. 19). Within the data shown, which includes sites on rock and firm alluvium only and corresponds only to low-strain levels of ground motion, there is no clear dependence of peak velocity upon site geology.

PEAK GROUND DISPLACEMENT

The displacement parameter discussed in this chapter is the peak horizontal dynamic ground displacement

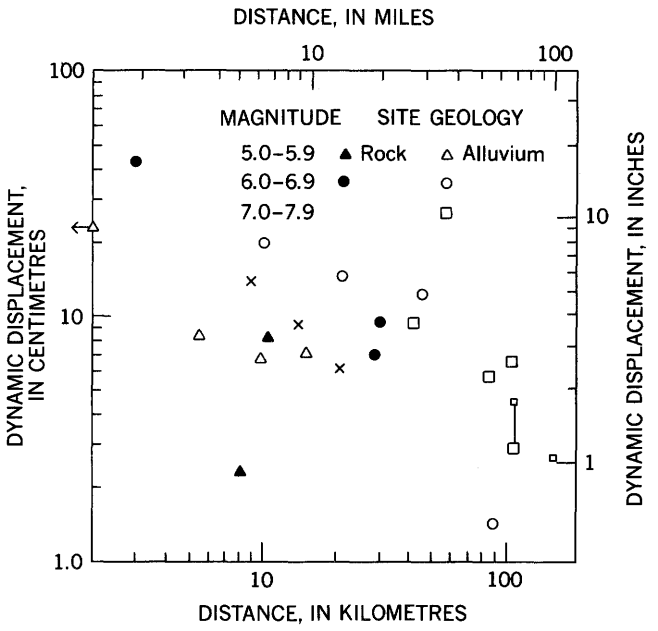

FIGURE 23.—Peak horizontal ground displacement in relation to shortest distance to slipped fault as a function of magnitude and site geology. Data from free-field sites, including buildings up to two stories high. Solid symbols for rock sites (underlain by less than 5 m (16 ft) of alluvium), open symbols for soil sites (more than 5 m (16 ft) of alluvium). Large symbols for displacements from twice-integrated accelerograms; small symbols for values from 10-second displacement meters. Distances accurate to 5 km (3 mi) or less. Crosses are interpolated values for postulated earthquake (see Borcherdt, Brabb, and others, this report). Arrow as in figure 19.

obtained from double integration of accelerograms or recorded directly by strong-motion displacement meters with natural periods of 10 s (seconds) and does not contain spectral components longer than about 10–15 s. Because the resonant periods of structures are usually less than a few seconds, even for very large structures, no significant information is lost by using this measure of displacement rather than the actual ground displacement.

A plot of peak dynamic displacement versus distance as a function of magnitude (fig. 23) shows that peak dynamic displacement increases with magnitude and attenuates with increasing distance from the fault at a rate probably less than those observed for the acceleration and velocity data. The data are scanty, and no inference is made regarding the effects of site geology.

DURATION OF SHAKING

Within the seismic engineering literature, no single measure of duration of shaking is in common usage and, in fact, discussion of duration is often not based on a quantitative definition. A crude but useful measure of duration is the time interval between the first and last peaks equal to or greater than 0.05 g on the accelero-

gram. This measure roughly corresponds to the "intense" or "strong" phase of shaking witnessed close to the fault during moderate-sized earthquakes and defines the time interval during which significant damage results from shaking. Durations of shaking for several earthquakes in the magnitude range 5.0–7.9 increase with magnitude and with decreasing distance to the fault (Page and others, 1972). The dependence of duration on magnitude reflects the increase in fault length with magnitude and the finite velocity at which rupture propagates along the fault.

EXTRAPOLATION BEYOND EMPIRICAL DATA BASE

The existing strong-motion data provide an empirical basis for predicting surface bedrock motion from earthquakes in the magnitude range 5.0–6.9 at distances greater than 10 to 20 km (6 to 12 mi) and at distances beyond 40 km (25 mi) for magnitude 7.0–7.9 shocks. There is, however, little observational data from which to predict motion in the immediate vicinity of the causative fault for earthquakes in the magnitude range 5.0–6.9 and no observational basis for predicting motion within 40 km (25 mi) of a magnitude 7.0–7.9 earthquake or within more than 100 km (60 mi) of a magnitude 8 shock. Thus for purposes of design or zonation, it is necessary to extrapolate from the existing base of data to small distances and to larger magnitudes. We briefly discuss some of the theoretical and numerical studies of the fault process and of the attenuation of ground motion with distance that can be used to guide extrapolations of recorded data.

Extrapolation of the apparent power-law attenuation of peak acceleration, velocity, and displacement with distance (figs. 19 through 23) to within a kilometre of the fault surface suggests unrealistically large ground motions; hence the attenuation curves must flatten close to the fault to reflect finite limits of motion at the fault surface. Values for such limits have been obtained for various simplified models of the fault mechanism (Housner, 1965; Ambraseys, 1969; Brune, 1970; Dieterich, 1973; Ida, 1973) and are shown in normalized form in figure 24. Peak velocity depends on the density and rigidity of the material surrounding the fault and on the driving stress (also referred to as stress drop) causing the fault to slip. Peak acceleration depends on these parameters and also on the high-frequency limit or cutoff in the frequency content of the motion. The high-frequency cutoff may arise from the mechanics of rupture (Ida, 1973) and the inelastic absorption of energy in highly sheared rock present in major fault zones (Boore, 1973). Estimates of the driving stress operating during earthquakes are as much as a few hundred bars and according to various fault models (for example, Brune, 1970) suggest peak velocities at the fault surface in excess of 100 cm/s (40 in./s) and peak accelerations in excess of 2 g as recorded on a standard strong-motion accelerometer with a natural frequency of 16 hertz. Whether these peak values of ground motion will occur at a particular site depends on the shear strength of the underlying geologic material. On competent rock such values are expectable, whereas on unconsolidated alluvium the strength may be insufficient to transmit such intense motion to the surface (Ambraseys, 1973).

The attenuation of these ground motions with distance close to the fault can be studied with numerical simulations of the faulting process using finite-element models. The results of such a study (Dieterich, 1973) have been used to derive scaling laws that relate peak ground-motion parameters to the stresses acting at the fault surface and to the dimensions of the fault. The acceleration data (fig. 19), normalized accordingly, are plotted together with attenuation curves computed from several different finite-element models (fig. 24). The model results are in reasonable agreement with the data. The more rapid rate of attenuation in the empirical data at distances greater than a few minimum fault dimensions reflects inelastic absorption of energy, a process that is not included in the model.

The use of this numerical model for the prediction of ground motion from an assumed earthquake requires a knowledge of both the stresses acting at the fault surface and the dimensions of the fault surface. At present, stress estimates for a given earthquake are uncertain by factors as large as five; as knowledge of the mechanics of faulting increases, the uncertainty in stress estimates should decrease. Although the intensity of ground motion is physically dependent upon the stresses acting at the fault surface, the current uncertainties in stress estimates are such that magnitude is currently a more satisfactory parameter than stress for scaling ground motion for purposes of seismic design.

SUMMARY

Strong-motion recordings of earthquakes currently provide a suitable basis for predicting peak parameters and duration of ground motion at sites on rock and firm alluvium at distances greater than 10, 20, and 40 km (6, 12, and 25 mi) for earthquakes of magnitudes 5.0–5.9, 6.0–6.9, and 7.0–7.9, respectively. There are still, however, very few recordings of ground motion from the critical region close to the fault, where earthquake damage is intense, and there are no recordings from within 100 km (60 mi) of an earthquake larger than magnitude 8.0. Simplified physical models of faulting provide theoretical estimates of ground motion close to the fault inside the distance range of existing observa-

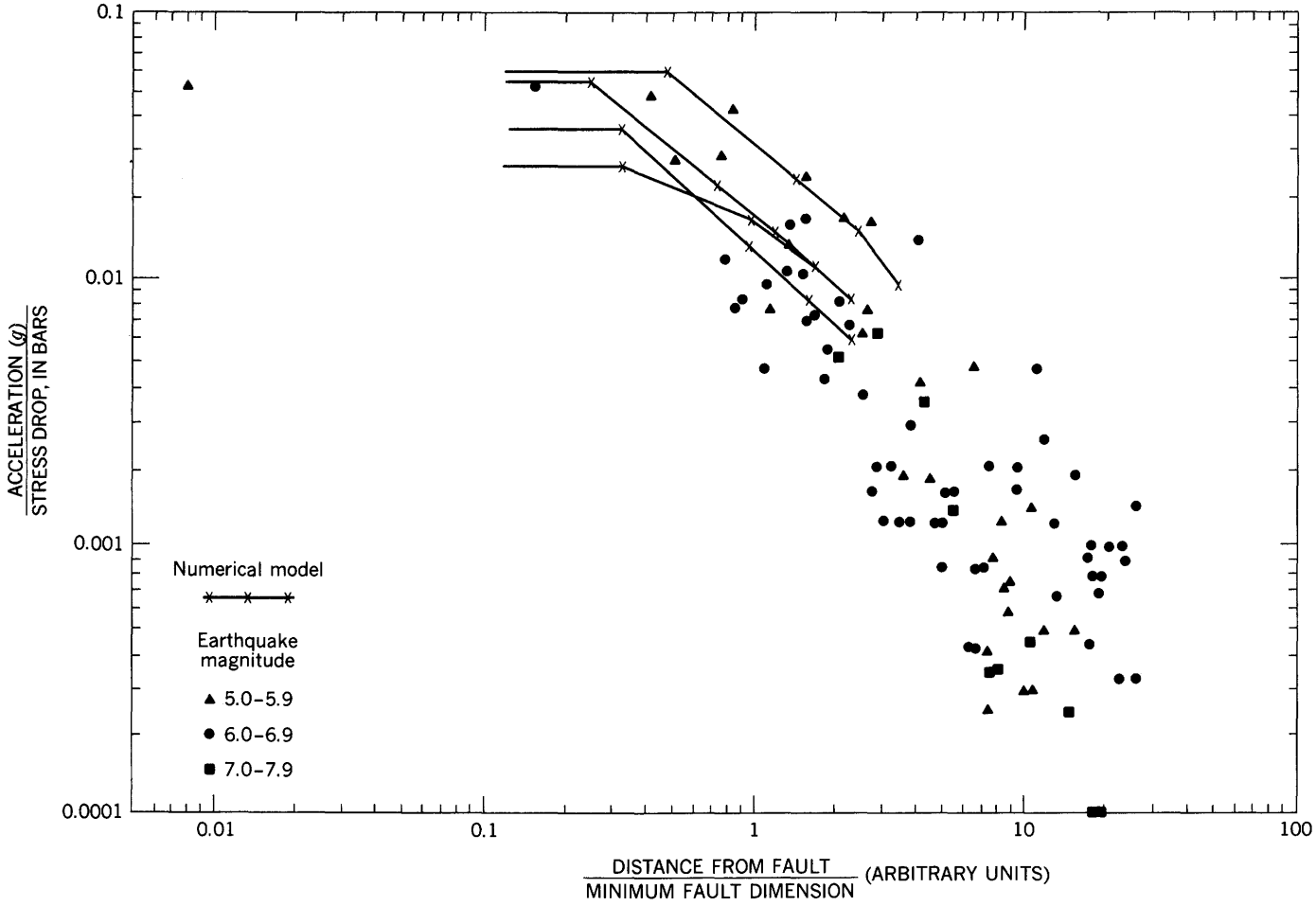

FIGURE 24.—Comparison of attenuation curves for four representative finite-element models of strike-slip faulting with peak acceleration data of figure 19. The data are normalized by dividing ground acceleration by stress drop and distance to the fault by minimum dimension of faulting (L_{min}) as suggested by the scaling relation of Dieterich (1973). Attenuation curves give peak accelerations along lines oriented perpendicular to fault and originating at point of initial surface rupture and assume a 10-hertz high-frequency cutoff of the ground motion. Locations of grid points at which accelerations were computed are shown as X. At distances less than 0.2 L_{min} all curves extend uniformly to fault. Differences between attenuation curves reflect differences in source geometry and point of origin for the four models.

tional data; however, the reliability of such estimates is determined by the accuracy of both the model and its input parameters and can be ultimately tested only by comparison with observational data.

There are two indications that the intensity of ground motion close to the fault in the zone of destructive shaking is significantly greater than that which was widely assumed for seismic design prior to 1971. One is the sparse but growing number of accelerograms recorded close to the fault, which have caused significant upward revision of acceleration-distance relations (compare Seed and others, 1969; Schnabel and Seed, 1973). The other indication is the extensive damage caused by recent moderate-sized earthquakes occurring in or on the edge of urban areas. For example, the 1969 Santa Rosa, Calif., earthquakes (magnitudes 5.6 and 5.7) caused $6 million damage to buildings (Steinbrugge and others, 1970), and the San Fernando, Calif., earthquake (magnitude 6.6) resulted in $500 million damage (Housner and Jennings, 1972). Another sobering example of extensive damage in an urban area is the Managua, Nicaragua, earthquake of 1972 (Brown, Ward, and Plafker, 1973).

In the next several years estimates of surface bedrock motion near to the fault where damage is intense will become more reliable as strong-motion recordings are collected at a growing rate and as more refined and complete theoretical and numerical models of the faulting processes are developed. Advances in techniques of processing strong-motion records will provide many more reliable data on velocity, displacement, and duration.

DIFFERENTIATION OF SEDIMENTARY DEPOSITS FOR PURPOSES OF SEISMIC ZONATION

By K. R. Lajoie and E. J. Helley

INTRODUCTION

Geologic data are the basis for special-purpose interpretive maps such as ground-response maps, liquefaction-potential maps, and slope-stability maps. However, most standard geologic maps do not, in themselves, contain sufficient data for these purposes, particularly in areas underlain by unconsolidated sedimentary deposits. For example, most geologic maps differentiate bedrock units in considerable detail but only crudely differentiate young, unconsolidated deposits. Yet, large historic earthquakes (for example, those that occurred near San Francisco, in Mexico City, and in Anchorage) demonstrate that some of the greatest structural damage and resultant loss of life due to high amplitudes of ground shaking and extensive ground failure occur in areas underlain by unconsolidated sedimentary deposits. The potential for such damage is greatest in flat lowlands because these areas generally are underlain by thick unconsolidated sedimentary deposits are are often highly developed and densely populated; parts of the San Francisco Bay region are examples of such areas.

The present distribution and physical properties of the various unconsolidated sedimentary deposits are controlled by their age and depositional environment. Geologic units defined and mapped on the basis of temporal, genetic, and physical criteria, therefore, can be used to outline regions of potential earthquake-induced hazards such as liquefaction, seismic amplification, and ground failure. The primary physical properties used to differentiate, map, and then regroup the unconsolidated deposits into broader units with similar seismic behavior include thickness, bedding, density, induration, texture (grain size), and porosity. These primary parameters control secondary parameters, such as seismic velocities and penetrometer resistance, which are useful to predict general behavior during earthquakes. Because none of these parameters were measured systematically in the present reconnaissance mapping project and some were estimated, the range of physical properties within each geologic unit is not precisely known. Therefore, the derivative maps based on these units, for example, the liquefaction-potential map (fig. 50) shows only in a general manner those areas where a particular seismic hazard most likely exists. Presently, the main applications of such maps are to call attention to areas where land users and planners should consider certain problems and to provide a base for future, more rigorous studies of seismic behavior.

This paper describes the reconnaissance techniques used for rapidly differentiating and mapping unconsolidated sedimentary deposits in the San Francisco Bay region and briefly discusses the physical parameters used to regroup these deposits for delineating areas where liquefaction and ground-motion amplification might occur.

GEOLOGIC MAPPING TECHNIQUES

One of the main efforts in the current geologic study of the San Francisco Bay region has been to differentiate into geologically distinct and seismically significant units the alluvial deposits underlying the gently sloping sedimentary plain between the bay and the surrounding hills. Shortcuts and specialized mapping techniques have been used because of the large area (approximately 19,300 km^2 (7,450 mi^2)) and short time (3 years) involved. The alluvial units are defined by various combinations of geologic and genetic criteria such as depositional environment, geomorphic expression, soil-profile development, age, induration, compaction, and texture. The distribution of the units is determined primarily from topographic maps, published soil series maps, and aerial photographs. The evolution of such a geologic map for the area of detailed study shown in figure 25 is illustrated in figures 26, 27, 28, and 29.

The contour lines on the topographic map (fig. 26) clearly reveal the major geomorphic features such as the hilly uplands, the flat marshlands adjacent to the modern bay, and the broad alluvial plain sloping gently from the hills to the bay. The contour lines also reveal smaller geomorphic features such as distinct alluvial fans, stream levees, and flood plains, all of which were formed by separate but closely related alluvial processes and which reveal the distribution of genetically related deposits.

On the basis of relative soil-profile development, the 18 alluvial soil series described in the Soil Conservation Service report on the region (fig. 27) fall into two distinct groups that reflect some basic difference in the deposits

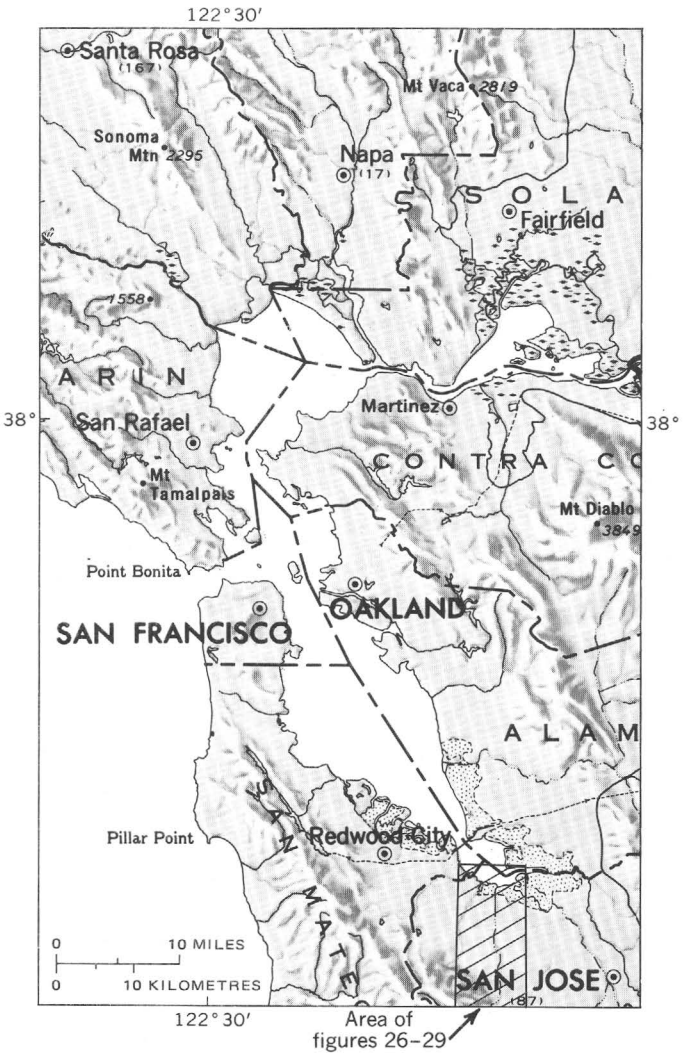

FIGURE 25.—Location of detailed study area.

on which they are developed. The soil units having strongly developed weathering profiles constitute one group, and those having weakly to moderately developed weathering profiles constitute the other. Soil profiles are developed by physical and chemical weathering processes at the surface of the earth; therefore, well-developed soil profiles generally indicate that the materials on which they are formed have been exposed to either intense weathering conditions or moderate weathering conditions for a considerable length of time. Because the weathering conditions in the bay region are moderate and relatively uniform, the alluvial deposits having strongly developed weathering profiles were inferred to be significantly older than the deposits having weakly to moderately developed profiles. This inferred age relation was used to differentiate younger and older alluvial deposits (fig. 28).

The younger deposits make up the alluvial fans being formed under the existing hydrologic regime. The streams forming these young fans are graded to present sea level. These younger deposits and the bay mud into which they grade are informally referred to as Holocene deposits (fig. 29). The older alluvial deposits, now partly covered by the Holocene deposits, make up alluvial fans formed by these same streams when they were graded to lower stands of sea level during the late Pleistocene (prior to about 10,000 years before present). These older deposits are informally referred to as late Pleistocene alluvium (fig. 29).

The Holocene alluvium is differentiated further into (1) depositional facies (fig. 29) on the basis of textural characteristics (that is, gravel, sand, silt, and clay) derived primarily from published soil reports and unpublished engineering foundation reports and (2) depositional environment (that is, stream levees and flood basins) determined from geomorphic expression as revealed on topographic maps and aerial photographs. These facies grade from coarse-grained gravel and sand deposits, which form prominent stream levees at the highest parts of the alluvial fans, into medium-grained sand and silt deposits, which form broad flood plains and subdued levees along the lower margins of the alluvial fans. These stream deposits grade into and interfinger with fine-grained silt and clay deposits that form the flat floors of flood basins between stream levees on the outer margins of the alluvial fans directly adjacent to the bay marshlands. These fine-grained basin deposits and some of the medium-grained levee deposits interfinger with and grade into the bay mud, the carbonaceous silty clay deposited in the marshes and on the mudflats of San Francisco Bay during Holocene time (approximately the past 10,000 years).

This gradation from coarse-grained to fine-grained sediment in the Holocene alluvium is a natural consequence of very recent stream erosion, transportation, and deposition. The coarsest rock debris eroded from the bedrock uplands is deposited near the base of the hills where the rapidly flowing streams enter the broad, gently sloping alluvial plain. Only the finer grained debris is carried by the ever-slackening water to the lower parts of the alluvial fans and eventually into the bay itself, where it is deposited as bay mud. The landward extent of the saturated plastic bay mud underlying the former marshes and tidal mudflats of San Francisco Bay (fig. 26) was inferred from early (ca. 1850) U.S. Coast and Geodetic Survey hydrographic charts (Nichols and Wright, 1971) rather than from direct field observation because cultural activity over the past 50 years has obscured its original distribution.

Long exposure to erosion and weathering processes has altered the original geomorphic expression and physical character of the late Pleistocene alluvium, thus it has not been separated into depositional facies

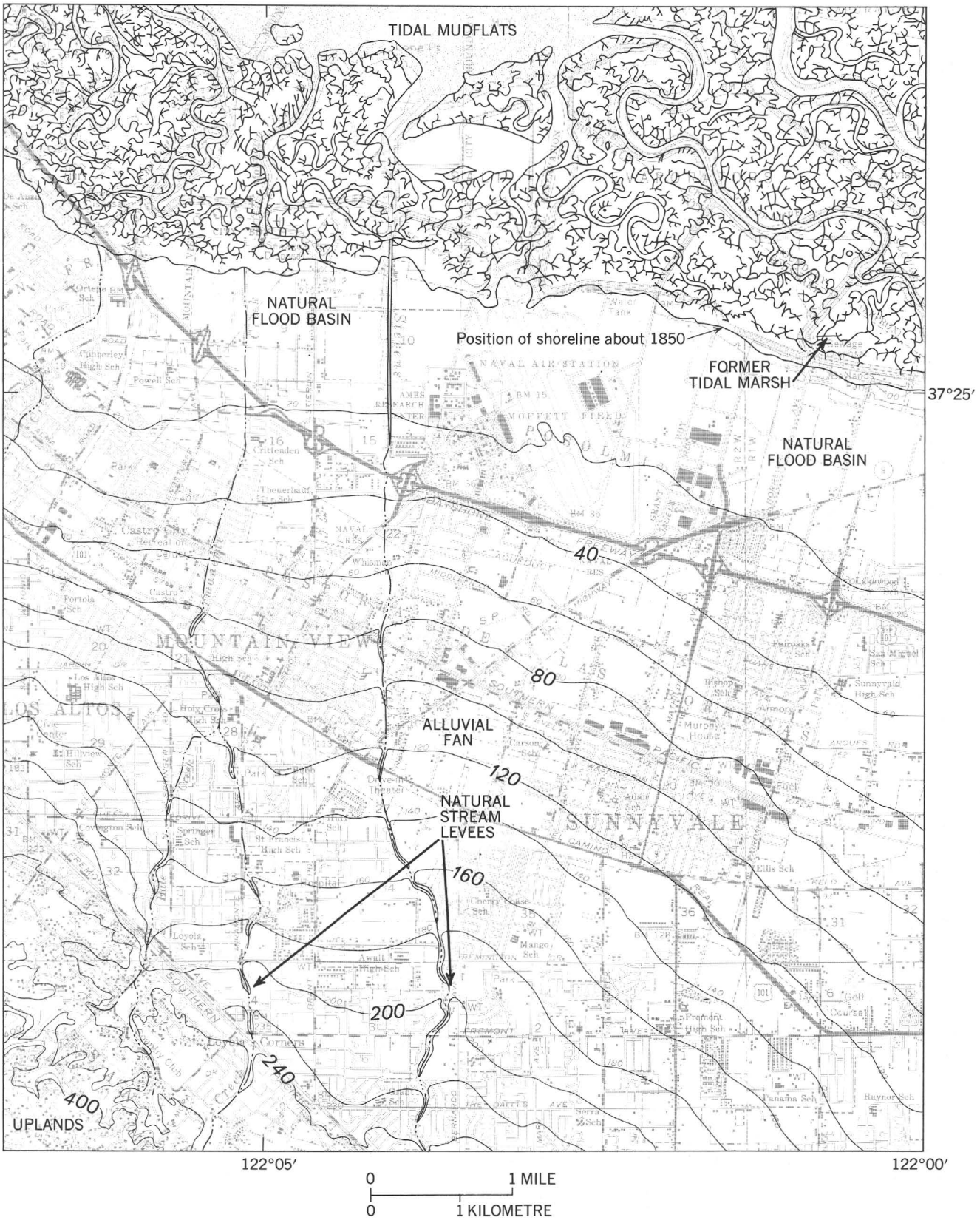

FIGURE 26.—Topographic map of the Mountain View–Sunnyvale area, Mountain View 7½-minute quadrangle. The enhanced contour lines show the irregular topography of the bedrock uplands and fluvial geomorphic features on the broad alluvial plain such as alluvial fans, stream levees, and flood basins. Distribution of former tidal marshland from Nichols and Wright (1971).

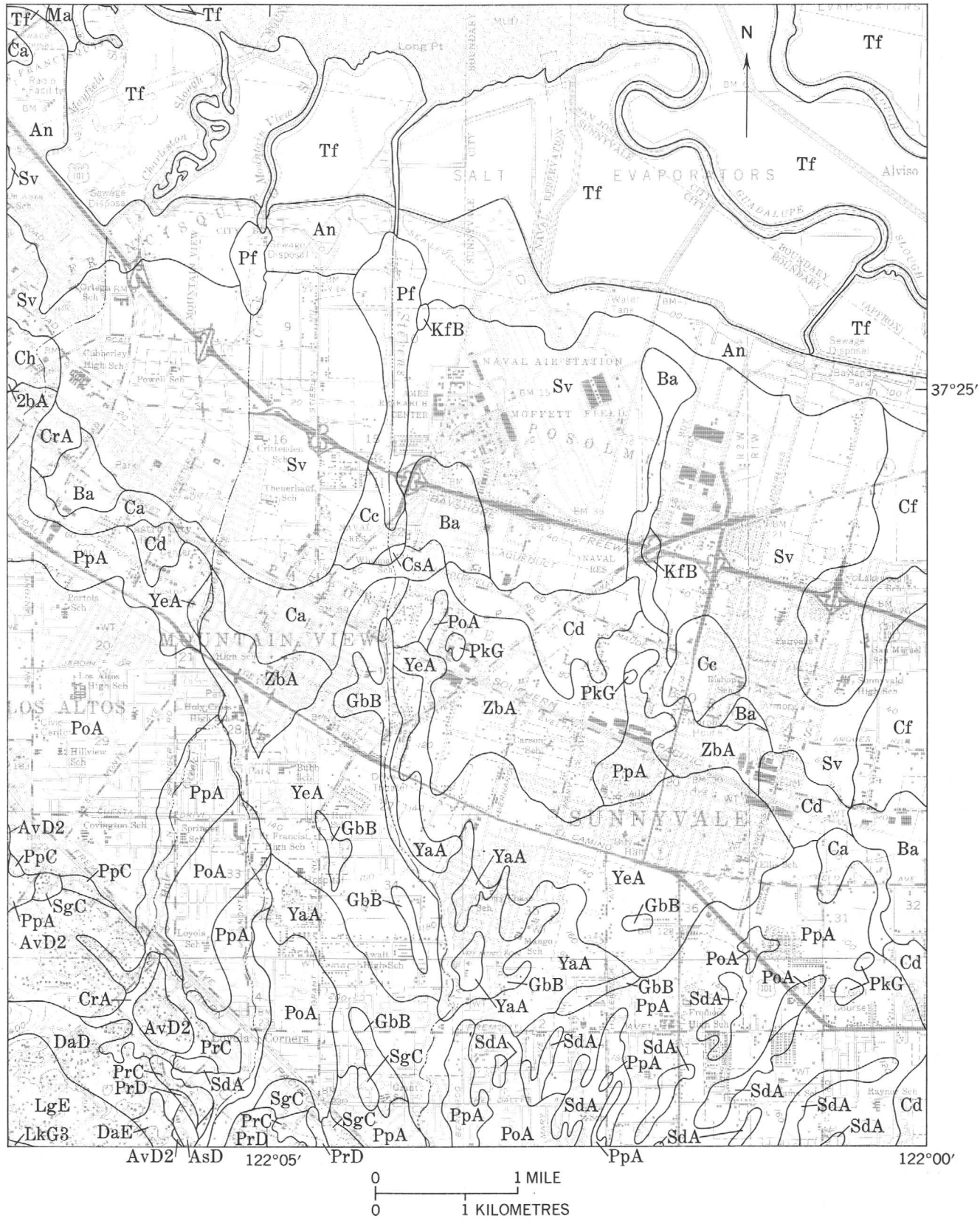
N
37°25′
122°05′
122°00′
0 1 MILE
0 1 KILOMETRES
MOUNTAIN VIEW
LOS ALTOS
SUNNYVALE
MOFFETT FIELD
NAVAL AIR STATION
SALT EVAPORATORS
Tf
Ma
Ca
An
Sv
Ch
2bA
CrA
Ba
Cd
PpA
YeA
ZbA
PoA
AvD2
PpC
SgC
DaD
PrC
PrD
LgE
LkG3
DaE
AsD
Pf
KfB
Cc
CsA
PkG
GbB
YaA
SdA
Cf

similar to those of the Holocene alluvial deposits.

In the areas of the bay region where detailed soils data are not available, the alluvial deposits have been differentiated using geomorphic and genetic criteria derived from aerial photographs and extrapolated from areas where detailed soils data provide the main and most reliable means of recognition. Fossils, archeological remains, and radiometric ages corroborate the relative ages and correlations based on these limited data. The upper part of the late Pleistocene alluvium contains a Rancholabrean fossil vertebrate fauna containing mainly extinct species (for example, camel, bison, mammoth, and ground sloth), whereas the Holocene alluvial deposits contain a fossil fauna completely modern in aspect (for example, deer and elk).

EXPLANATION

Soil Series in the Mountain View-Sunnyvale area*

Alluvial soil series with weakly to moderately developed weathering profiles:

An	Alviso clay
Ba	Bayshore clay loam
Ca	Campbell silty clay loam
Cc	Campbell silty clay loam, clay substrate
Cf	Castro clay
Ch	Clear Lake clay, drained
Cra	Cropley clay, 0- to 2-percent slopes
GbB	Garretson gravelly loam, 0- to 5-percent slopes
Pf	Pacheco loams, clay substrate
Sv	Sunnyvale silty clay, drained
YaA	Yolo loam, 0- to 2-percent slopes
YeA	Yolo silty clay loam, 0- to 2-percent slopes
Zbz	Zamora clay loam, 0- to 2-percent slopes

Alluvial soil series with strongly developed weathering profiles:

PoA	Pleasanton loam, 0- to 2-percent slopes
PoC	Cropley clay loam, 0- to 2-percent slopes
PpA	Pleasanton gravelly loam, 0- to 2-percent slopes
PpC	Pleasanton gravelly clay loam, 2- to 9-percent slopes
SdA	San Ysidro loam, 0- 2-percent slopes

Upland soil series (nonalluvial soils):

AsE	Ayer clay, 15- to 30-percent slopes
AuG	Azule clay loam, 30- to 75-percent slopes
AvE	Azule silty clay loam, 15- to 30-percent slopes
AvD2	Azule silty clay loam, 9- to 15-percent slopes
AvE2	Azule silty clay loam, 15- to 30-percent slopes
DaD	Diablo clay, 9- to 15-percent slopes
DaE	Diablo clay, 15- to 30-percent slopes
FbG	Felton-Ben Lomond complex, 50- to 70-percent slopes
LGE	Los Gatos clay loam
LGE2	Los Gatos clay loam, 15- to 30-percent slopes
LKG3	Los Gatos and Maymen, 50- to 75-percent slopes
MEF2	Maymen fine sandy loam, 15- to 30-percent slopes
PhG3	Permanente stony loam, 50- to 75-percent slopes
PRC	Positas-Saratoga loam, 2- to 9-percent slopes
PRD	Positas-Saratoga loam, 9- to 15-percent slopes
SgC	Saratoga-Positas loam, 2- to 9-percent slopes
ShE2	Soper gravelly loam, 15- to 30-percent slopes
ShF	Soper gravelly loam, 30- to 50-percent slopes

Miscellaneous map symbols:

KfB	Kitchen middens, archeological site
LfF	Landslides
Ma	Made land
Tf	Tidal flats

*From U.S. Soil Conservation Service (1968)

FIGURE 27.—Soil units in Mountain View–Sunnyvale area. Soil units are defined primarily on the basis of profile development, texture, and slope. Soil-profile development is controlled by many factors including time, climate, parent material, slope, and biological activity. In an area such as this, where weathering conditions and parent material are relatively uniform, the time factor is clearly expressed by relative development of soil profiles, which can be used as a means of differentiating alluvial deposits on the basis of relative age (fig. 28).

The upper part of the late Pleistocene alluvium contains fossil wood and fresh-water molluscan shells that yield radiocarbon ages of about 22,000 years before present. Holocene alluvial deposits contain fossil wood, shells, and archeological remains that yield radiocarbon ages of about 5,000 years before present and younger. Peat and shell deposits in the bay mud yield radiocarbon ages that range from about 9,600 years before present at the base of the unit in the lowest parts of the basin to modern at the top of the unit. These ages from the bay mud date the latest marine transgression into the basin, which agrees very well with the post-Pleistocene rise in sea level established from worldwide data (Milliman and Emery, 1968). In general, the partial flooding of the basin caused by this rise in sea level raised the base level of the local streams and began the present depositional cycle represented by the Holocene alluvial deposits. The fact that the Holocene alluvial deposits around the margins of the bay are graded to the present sea level is used as one means of identifying these deposits and adds credence to the relative ages and correlations based on other criteria.

Most of the age control used for establishing an absolute chronology and for correlating sedimentary deposits in the bay region was gleaned from published and unpublished geologic, archeologic, and engineering reports. These diverse and readily available sources provided the data for constructing an initial geologic model and determined where subsequent dating control was needed. Many of the samples dated specifically for this study were obtained from the numerous drill cores collected over a period of 25 years for engineering foundation studies of various proposed or existing transbay bridges.

PHYSICAL PARAMETERS OF GEOLOGIC UNITS

Physical parameters of the various geologic units such as texture, thickness, bulk density, induration, and seismic velocity are needed to assess their

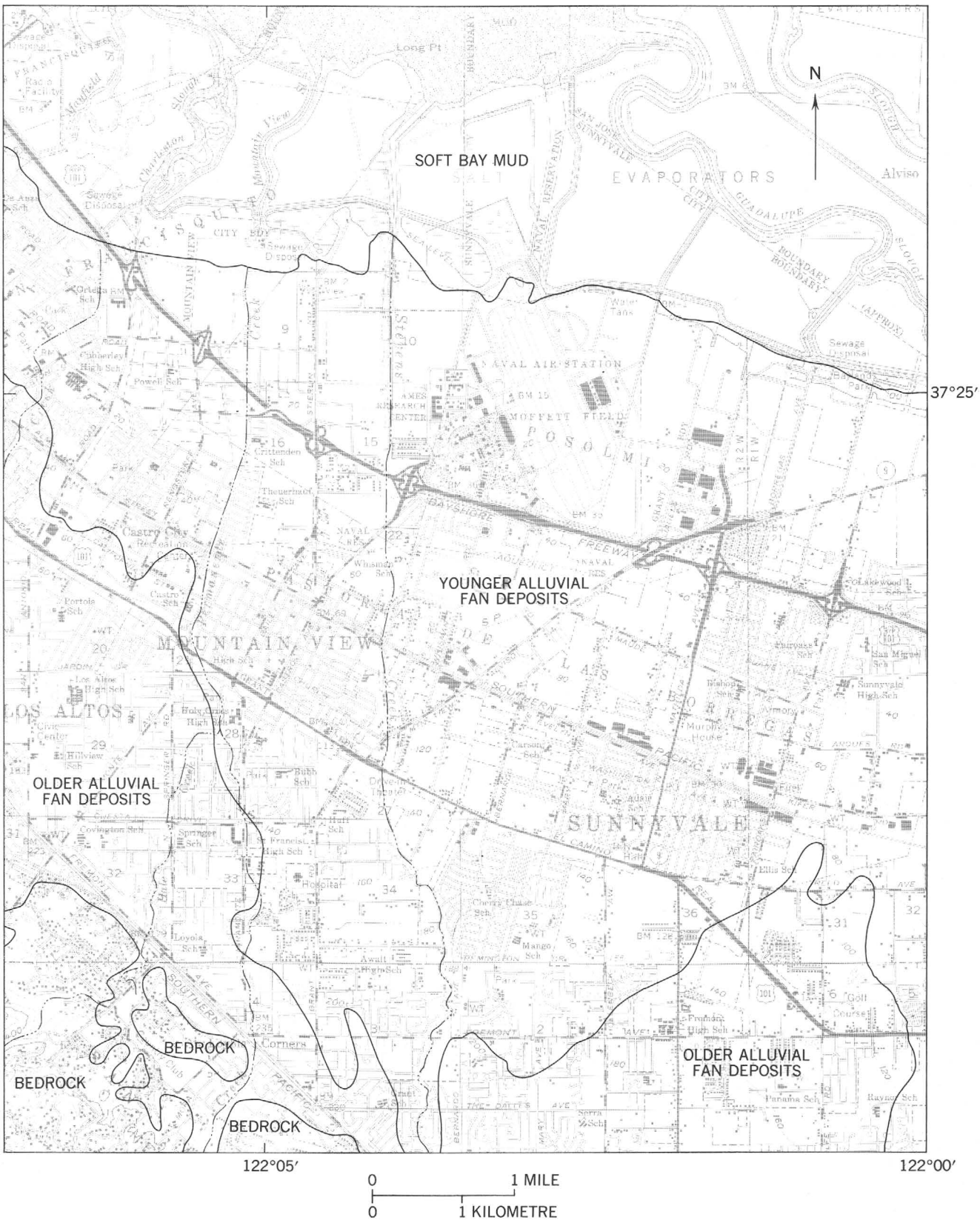
N
SOFT BAY MUD
YOUNGER ALLUVIAL FAN DEPOSITS
OLDER ALLUVIAL FAN DEPOSITS
OLDER ALLUVIAL FAN DEPOSITS
BEDROCK
BEDROCK
BEDROCK
37°25′
122°05′
122°00′
0 1 MILE
0 1 KILOMETRE

seismic-hazard potential. These parameters were compiled and interpreted from readily available sources (fig. 30) that were augmented by direct measurement where no data existed or where verification of existing data was needed. This information also was used to differentiate units where soil series data were ambiguous or did not exist.

Very few data are available on the total thickness of the unconsolidated and semiconsolidated deposits filling the bay basin. A few deep drill holes and several seismic profiles (Hazelwood, 1974) indicate that these sediments are probably more than 600 m (1,970 ft) thick in San Jose and thin irregularly northward from 60 to 90 m (200–300 ft) near San Francisco (see generalized cross section in figure 68 for data on sediment thickness in the Palo Alto–Coyote Hills area).

The thickness of the younger units is fairly well known from numerous shallow bore holes described in engineering reports (fig. 30) and from shallow seismic surveys where bore-hole data are lacking. The Holocene alluvium (fig. 29) generally ranges in thickness from about 15 m (50 ft) near the heads of alluvial fans to about 3 m (10 ft) near the margins of the bay. The Holocene bay mud ranges in thickness from 0 to as much as 37 m (120 ft).

The thickness of the late Pleistocene alluvium (fig. 29) is not precisely known because its base is not well defined in the thick sedimentary section beneath the bay and the surrounding alluvial plain. Where the base of the late Pleistocene alluvium can be seen on stream terraces in narrow valleys, these sediments are about 3 m (10 ft) thick. They are probably as much as 46 m (150 ft) thick beneath the bay where they overlie old estuarine mud, as identified by saltwater fossils brought up from that depth in a drill sample. Still older Pleistocene alluvial deposits probably underlie these deeply buried estuarine muds, but their total thickness is not known. In the southern bay area these deposits may grade downward into Pliocene and early Pleistocene alluvial deposits of the Santa Clara Formation or may lie unconformably on them.

Published soils maps and unpublished engineering reports (fig. 30) are the main sources of data on the physical properties of the various geologic units. Each unit generally has a distinctive range of values for properties such as grain size, sorting, bulk density, compaction, induration, and moisture content. These properties have been used in defining and delineating some of the units, in particular the late Pleistocene alluvium and the three facies of Holocene alluvium (see figs. 29, 30).

The primary physical properties such as grain size and sorting are controlled by the depositional environment, whereas the secondary properties such as induration, compaction, and bulk density are related to (and generally increase with) the age of the geologic units. This variation of the secondary physical properties with age is reflected in the resistance to penetration, which increases from low values for the Holocene deposits to high values for the various bedrock units (col. 4, fig. 31). The very low resistance to penetration of the bay mud is attributable to its extremely high water content and loose packing, which reflect its youthful age. Older deeply buried estuarine muds would have higher resistances to penetration owing to compaction. Penetrometer resistance can be used to estimate relative densities that, with data on grain size, sorting, and moisture content, can be used to evaluate liquefaction potential in shallow, unconsolidated deposits (see Youd and others, this report).

The velocities of seismic waves in geologic materials are determined by various primary and secondary physical properties and therefore can be used as a rough index of these properties and as a means of evaluating seismic behavior. The seismic wave velocities in the sedimentary units and some bedrock units are listed in figure 31. The compressional, or P-wave, velocities (V_P) were obtained primarily from shallow seismic refraction surveys conducted to identify or determine stratigraphic thicknesses of the younger sedimentary units and from deep seismic refraction surveys conducted to determine the total thickness of sedimentary material in the bay basin (Hazelwood, 1974). The shear, or S-wave, velocities (V_S) of the bay mud and alluvial units were derived from limited surface surveys by the authors and down-hole experiments by Warrick (1974;

FIGURE 28.—Distribution of younger and older alluvial deposits in Mountain View–Sunnyvale area as determined primarily from relative development of soil profiles, based on soil series as mapped by Soil Conservation Service (fig. 27). Alluvial deposits on which weak to moderate weathering profiles are developed were initially inferred to be younger than alluvial deposits on which strong weathering profiles are developed. Radiocarbon and fossil data have confirmed this relative age classification. The younger alluvial deposits contain modern vertebrate and invertebrate fossils and organic remains that yield radiocarbon ages of about 5,000 years before present and younger. Therefore, these deposits and the bay mud with which they interfinger are informally referred to as Holocene deposits (see figure 29). The older alluvial deposits locally contain extinct late Pleistocene vertebrate fossils such as camel, sloth, bison, and mastodon and organic remains that yield radiocarbon ages of about 20,000 years before present. Therefore, these older deposits are informally referred to as late Pleistocene alluvium (see figure 29).

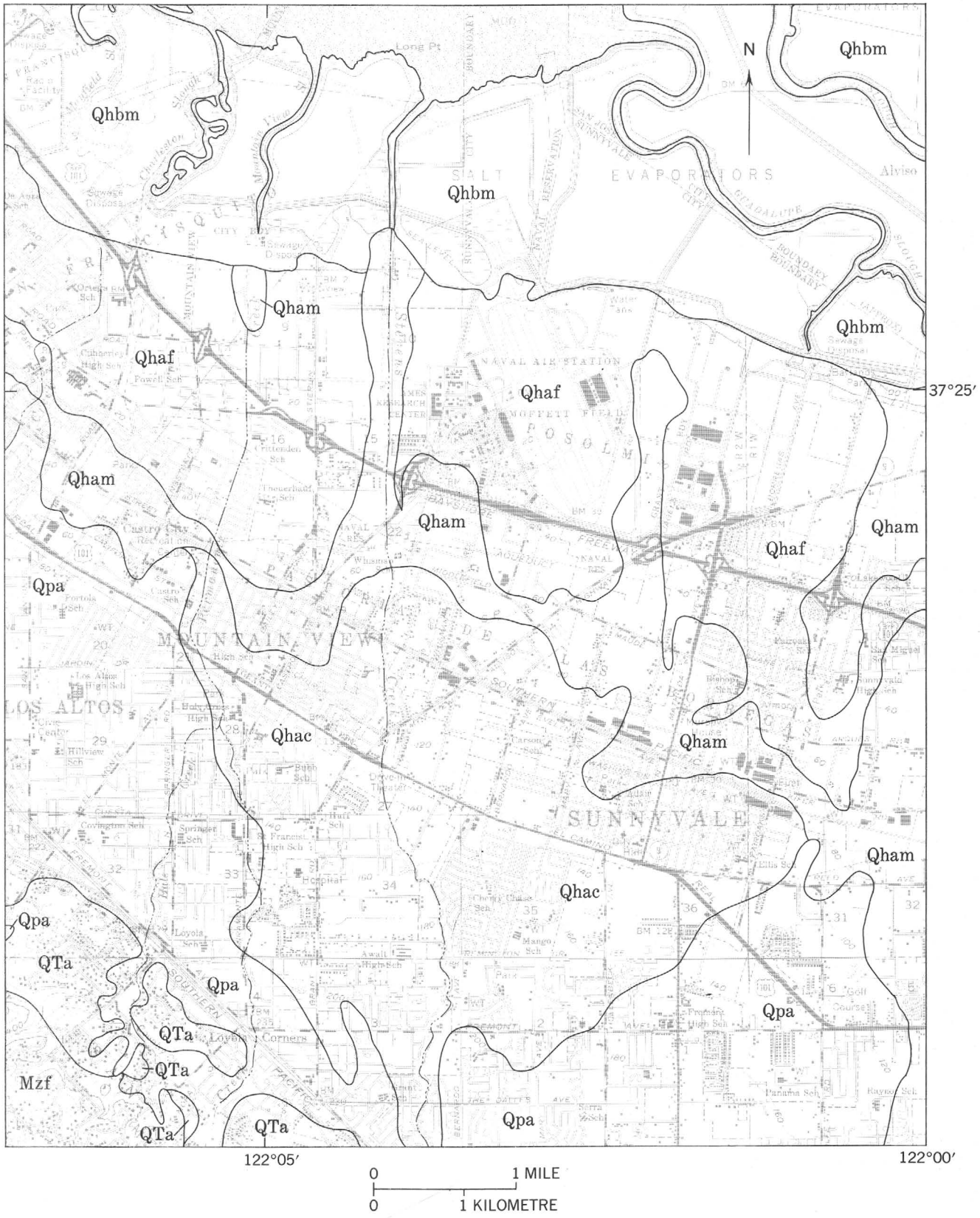

FIGURE 29.—Geologic map of the Mountain View–Sunnyvale area.

oral commun., 1974). The S-wave velocities of the bedrock units were not measured directly but were estimated using the relation $Vs \approx Vp/2$.

EXPLANATION
DESCRIPTION OF MAP UNITS

Holocene deposits (less than 10,000 years old):
Holocene estuarine deposits (0–9,000 years old):
Qhbm Bay mud. Water-saturated estuarine mud; predominantly clay and silty clay underlying marshlands and tidal mudflats of San Francisco Bay. Occasional lenses of well-sorted fine sand and silt; occasional shelly and peaty layers. Interfingers with and grades into fine-grained and medium-grained alluvium; generally overlies early Holocene alluvium or late Pleistocene alluvium 0–40 m (0–120 ft) thick
Holocene alluvial deposits (0–5,000 years old):
Qhaf Fine-grained alluvium. Plastic, poorly sorted carbonaceous clay and silty clay in poorly drained interfluvial basins marginal to bay marshlands. Locally contains thin beds of well-sorted silt, sand, and fine gravel; contains modern vertebrate fossils and freshwater gastropod and pelecypod shells. Interfingers with and grades into bay mud and medium-grained alluvium; overlies late Pleistocene alluvium. Generally less than 5 m (15 ft) thick
Qham Medium-grained alluvium. Loose, moderately drained, moderately sorted sand forming alluvial plains and stream levees. Locally contains beds of well-sorted clay, silt, and gravel; contains modern vertebrate fossils and fresh water gastropod and pelecypod shells. Intermediate in character and lateral extent between fine-grained and coarse-grained alluvium with which it interfingers; generally overlies late Pleistocene alluvium. Generally less than 7 m (21 ft) thick.
Qhac Coarse-grained alluvium. Loose, well-drained, moderately sorted, permeable sand and gravel forming stream levees and flood plains on higher parts of alluvial fans; gravel becomes dominant toward fan heads. Locally contains beds of well-sorted silt, sand, and gravel; contains modern vertebrate fossils and fresh water pelecypod and gastropod shells. Thickness ranges from as much as 15 m (50 ft) at fan heads to 6 m (20 ft) where these deposits interfinger with and grade into medium-grained alluvium; overlies late Pleistocene alluvium and bedrock
Pleistocene deposits (10,000–3,000,000 years old):
Qpa Late Pleistocene alluvium (10,000–70,000? years old). Weathered, slightly consolidated and indurated alluvial fan deposits consisting primarily of gravel and sand with some silt. Less permeable than Holocene alluvium. Locally contains fresh water pelecypod and gastropod shells and extinct late Pleistocene vertebrate fossils. Overlain by Holocene deposits on lower parts of alluvial plain; incised by channels that are partly filled with Holocene alluvium on higher parts of alluvial plain. Maximum thickness unknown but at least 45 m (150 ft) near margins of present bay where these deposits overlie deeply buried Pleistocene estuarine deposits
Bedrock:
QTa Pliocene and early Pleistocene alluvium. Tectonically deformed alluvial fan deposits with local minor amounts of shallow-water marine deposits. Weakly to moderately indurated gravel, sand, and silt with subordinate amounts of lacustrine silt and clay; local thin tuff beds; contains late Pliocene and early Pleistocene vertebrate fossils. Underlies late Pleistocene alluvium; overlies or is in fault contact with Franciscan Formation. Consists of the Santa Clara Formation in southwestern part of bay area
Mzf Mesozoic Franciscan Formation. Well-indurated sandstone, chert, and altered volcanic rocks. In map area underlies or is in fault contact with Pliocene and early Pleistocene alluvium

FIGURE 29.—Continued.

The P-wave velocity is low in loosely packed materials such as the Holocene alluvial deposits, which can be easily compressed, and high in hard materials such as the Franciscan Formation, which cannot be easily compressed. Within the Holocene alluvium the P-wave velocities are strongly dependent on water content. Above the water table the P-wave velocity is lower than that of water, whereas below the water table it is virtually that of water. The S-wave velocity is low in materials with low shear strengths, such as the saturated bay mud, and high in materials with high shear strengths, such as the well-indurated Franciscan rocks. In general, the P-wave and S-wave velocities systematically increase with induration and compaction of the geologic materials, and because these two properties generally increase with age of the geologic units, the seismic velocities increase in a similar manner. Also, within an individual geologic unit both the P-wave and S-wave velocities tend to increase with depth owing to increasing compaction and induration.

DELINEATING AREAS OF SEISMIC HAZARDS

Once the unconsolidated deposits have been differentiated into map units whose distribution and general physical properties are known or can be reasonably inferred, these units can be combined in various ways on the basis of particular similarities for specific seismic zonation purposes. Figure 32 shows how the sedimentary units delineated in this chapter have been recombined to reflect liquefaction potential and possible relative ground response.

LIQUEFACTION POTENTIAL

Liquefaction is defined as the transformation of a granular material from a solid state to a liquefied state as a consequence of increased pore-water pressure (Youd and others, this report). If shear stresses resulting from sloping terrain or nonuniform loading are present, the liquefied sediment may flow, generating ground failures that could result in serious damage to manmade structures. One cause of liquefaction is ground shaking during earthquakes. Seismic shaking tends to compact granular sediments, which causes a transfer of load from intergranular contacts to the interstitial pore water, thereby increasing the pore-water pressure.

Seismically induced liquefaction is most likely to occur in beds of loose, water-saturated, well-sorted silt and sand within 30 m (100 ft) of the ground surface. Geologic and engineering data indicate that these conditions exist to varying degrees in all five Holocene and

late Pleistocene sedimentary units (fig. 29). These five units were recombined to delineate three zones of different liquefaction potential in the southern bay region (fig. 50).

Beds of loose well-sorted silt and sand within and directly beneath the bay mud have the highest liquefaction potential because they lie below sea level and are permanently saturated. The distribution of bay mud therefore defines a zone of moderate to high liquefaction potential (zone 1, fig. 50). Similar beds occur in the Holocene alluvium but are not permanently saturated because of the fluctuating ground water table. The distribution of the Holocene alluvium therefore defines a zone of moderate liquefaction potential (zone 2, fig. 50) that is divided into two subzones (2a and 2b, fig. 50) on the basis of depth to the water table. In subzone 2a the depth to the water table is less than 3 m (10 ft). These areas are underlain by the fine-grained Holocene alluvium and medium-grained alluvium that form the low, poorly drained parts of the Holocene alluvial fans. In subzone 2b the depth to the water table is greater than 3 m (10 ft). These areas are underlain by the

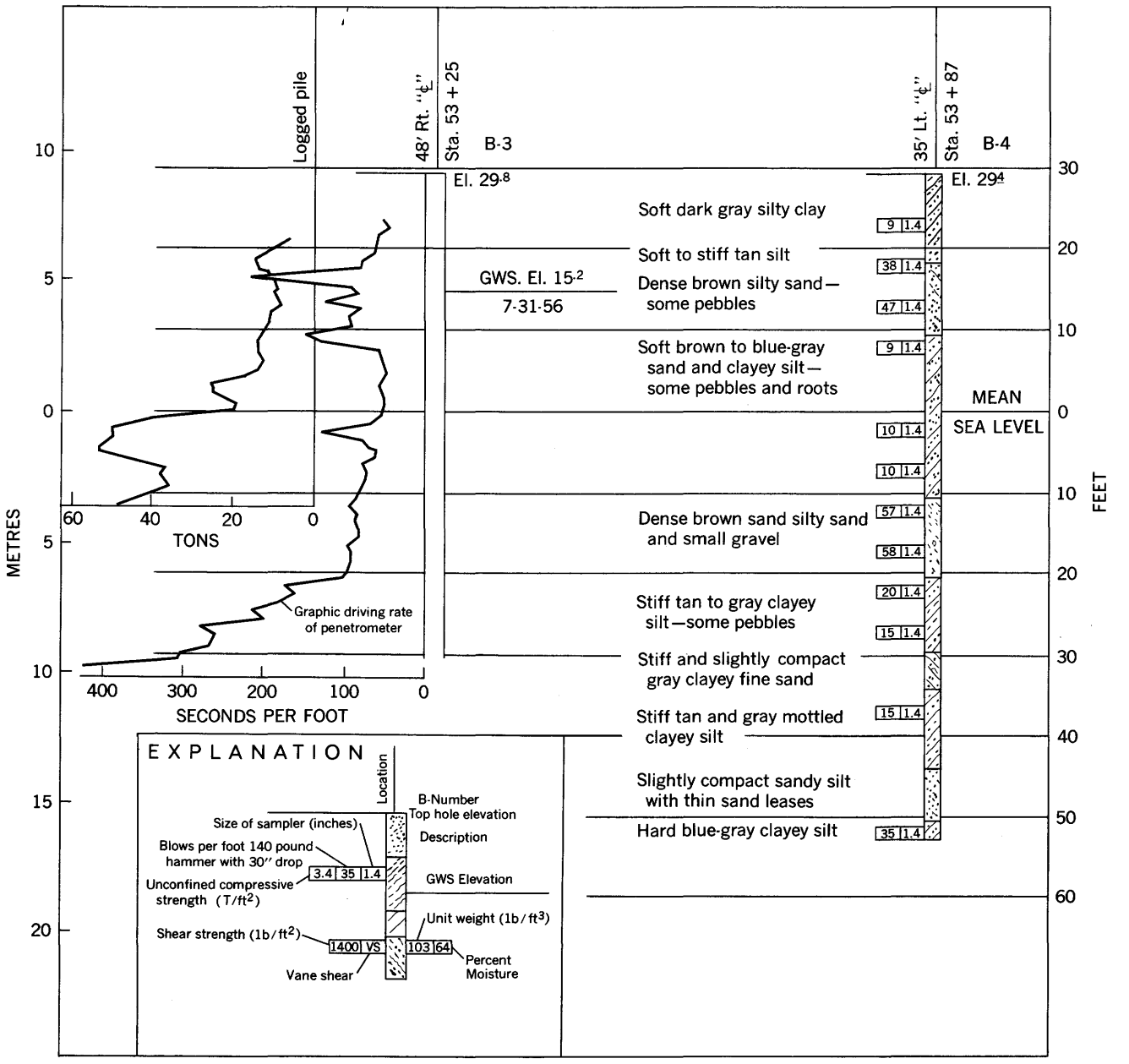

FIGURE 30.—An example of unpublished engineering data from which thickness and physical properties of alluvial deposits were partly derived. The abrupt decrease in driving rate of the penetrometer at about 6 m (20 ft) below sea level is interpreted to reflect the stratigraphic contact between the Holocene alluvium and the late Pleistocene alluvium.

coarse-grained Holocene alluvium and some of the medium-grained Holocene alluvium that together form the high, well-drained parts of the Holocene alluvial fans. These deposits are only seasonally saturated and are not subject to liquefaction during much of the year. Therefore, the beds of well-sorted silt and clay that may exist in subzone 2a are water saturated for a greater part of the year and have a slightly higher liquefaction potential than similar beds that may exist in subzone 2b.

Most beds of well-sorted silt and sand in the late Pleistocene alluvium are slightly compacted or chemically altered and are not as likely to liquefy as similar deposits in the loose Holocene alluvium. The surface distribution of Pleistocene alluvium therefore defines a zone (zone 3, fig. 50) of low liquefaction potential. The bedrock units are generally too well indurated to liquefy, and so their distribution delineates a zone of negligible liquefaction potential.

The liquefaction-potential map based on the above criteria does not outline areas where liquefaction, with or without resultant ground failure, will occur. It merely outlines those areas where units occur that may contain potentially liquefiable materials and where liquefaction and resultant ground failure may be expected during moderate or large earthquakes. Therefore, this map highlights those areas where liquefaction potential exists and should be evaluated prior to various types of land use.

GROUND RESPONSE

Medvedev (1965) showed that seismic impedance (defined as the product of S-wave velocity and bulk density, $V_s \rho$) can be used to make rough estimates of relative ground response. The potential for seismic amplification increases as the impedance contrast between an overlying and an underlying unit increases if other parameters such as stratigraphic thickness are con-

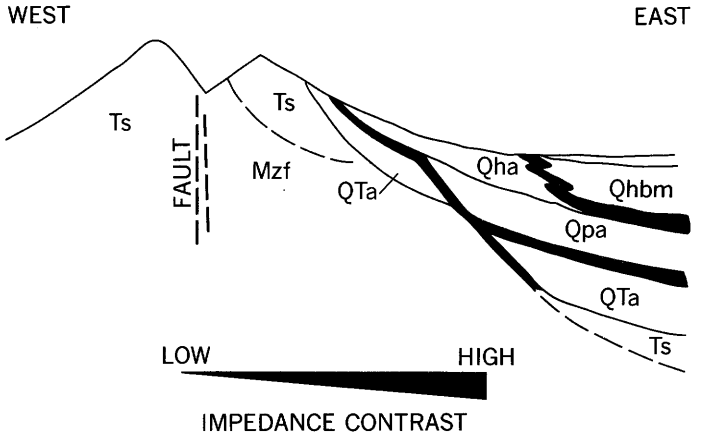

Unit	Thickness (m)	Relative bulk density, ρ (g/cm^3)	Penetration resistance[1] (blows/ft)	P-wave velocity, V_p (m/sec)	S-wave velocity, V_s (m/sec)	Impedance, $V_s \rho$
Qhbm	0-36	1.3-1.7	0	*1400* [4]	90-130 [2]	117-153
Qha	0-15	1.9	20-80	300-600 [3]	*200-300*	380-*570*
Qpa	10-45	2.1	100	1500-2100	200-400 [5]	420-*630*
QTa	0-250?	2.0	100-refusal	2500	*1200*	*2400*
Ts	0-*300*	2.4	Refusal	1500-3300	500-*1400*	*1200-3360*
Mzf	------	2.7	Refusal	2800-4000	*1400-2000*	*3780-5400*

[1] Test used 140-lb hammer dropped 30 in.
[2] From Warrick (1974)
[3] Above water table. Below water table $V_p = 1500-1700$
[4] Figures in italics are estimated values
[5] Warrick (oral commun., 1974)

FIGURE 31.—Schematic cross section of southern San Francisco Bay region and description of certain physical properties of the generalized geologic units. Qhbm, bay mud; Qha, Holocene alluvium; Qpa, late Pleistocene alluvium; QTa, early Pleistocene and Pliocene alluvium; Ts, Tertiary sandstone; Mzf, Franciscan Formation.

Geologic unit		Lajoie and Helley, this report		Borcherdt, Joyner, and others, this report		Youd and others, this report	
							Liquefaction potential zone
Bay mud	Qhbm	Holocene bay mud	Qhbm	Bay mud	Qhbm	Bay mud	1
Alluvium	Qal						
Holocene alluvium	Qha						
Fine grained	Qhaf	Holocene alluvium	Qhaf			Holocene alluvium	2a
Medium grained	Qham		Qham				
Coarse grained	Qhac		Qhac	Alluvium Qal	Qal		2b
Late Pleistocene alluvium	Qpa	Late Pleistocene alluvium	Qpa			Late Pleistocene alluvium	3
Bedrock	TMz b						
Pliocene-Pleistocene alluvium	QTa		QTa				
Merced Formation	QTm			Santa Clara Formation			
Santa Clara Formation	QTsc						
Tertiary rock	Ts	Bedrock	Ts	Pre-Tertiary and Tertiary bedrock		Bedrock	
Pre-Tertiary rock	Mz b						
Granite	Mz g						
Great Valley sequence	Mz gv						
Franciscan Formation	Mz f		Mz f	Franciscan Formation			

FIGURE 32.—Correlation diagram showing groupings of geologic units for evaluating ground response (Borcherdt, Joyner, and others, this report) and liquefaction potential (Youd and others, this report).

stant. The table in figure 31 lists the generalized geologic units in the southwestern bay area in increasing age, which is roughly proportional to density and S-wave velocity and therefore to impedance (column 7). The Holocene bay mud has the lowest impedance owing to both its low density and its low S-wave velocity. The three facies of the loose Holocene alluvium (fig. 29) have very similar physical properties and therefore are combined into one geologic unit that has only slightly lower impedance values than the weakly consolidated late Pleistocene alluvium. The variability of physical properties within and between bedrock units is reflected in their relatively wide range of moderate to high impedance values.

The schematic cross section (fig. 31) shows the generalized stratigraphic relations in the southwestern bay region with the high contrasts in impedance between units represented by slightly heavier contact lines. Considering only the impedance contrasts, amplification of bedrock motion is expected to be highest where bay mud overlies late Pleistocene alluvium or where Holocene alluvium overlies Pliocene and early Pleistocene alluvium. The impedance data suggest that the highest levels of amplification would occur where thick deposits of bay mud directly overlie Franciscan bedrock.

Because seismic amplification is dependent on frequency, and therefore controlled by other factors such as stratigraphic thickness, predicted amplification potential using only impedance data is neither very precise nor directly applicable to engineering design. These crude predictions are consistent, however, with comparative low-strain ground-motion measurements (Borcherdt, Joyner, and others, this report) that show that the highest amplifications occur on bay mud sites. It is probably significant that four of the generalized geologic units with distinct low-strain amplifications (table 5) roughly correspond to the four groups of geologic units with similar impedance values (groups separated by heavy lines in column 7 of fig. 31; correlation shown in fig. 32).

Combining the geologic units into groups with similar impedance values provides a useful means of evaluating data on earthquake intensity and low-strain-level response. For example, if deposits with similar impedance values behave differently in an earthquake, other parameters such as variation in stratigraphic thickness might be investigated as the causative factor.

SUMMARY

The alluvial deposits in the San Francisco Bay region, which in the past were usually treated as one geologic

unit, are differentiated into two main units, Holocene alluvium and late Pleistocene alluvium, primarily on the basis of soil profile development. The Holocene alluvium is further differentiated into three textural units, coarse-, medium-, and fine-grained alluvium, on the basis of depositional environment as determined from aerial photographs, soils reports, and engineering data. The fine-grained alluvium interfingers with and grades into the Holocene bay mud. Physical properties such as relative bulk density, compaction, and induration as expressed by penetrometer resistance and seismic velocities are generally lowest in the bay mud, intermediate in the Holocene alluvium, and highest in the late Pleistocene alluvium.

These sedimentary units may be regrouped in various ways for purposes of seismic zonation on the basis of similar physical properties. For example, all the unconsolidated sediments contain some potentially liquefiable beds of loose well-sorted fine sand and silt. Therefore, zones of different liquefaction potential based on the moisture content, relative compaction, and distribution of the geologic units can be delineated. The Holocene bay mud delineates a zone of high liquefaction potential because the beds of loose sand and silt within these estuarine sediments are permanently saturated. The beds of loose silt and sand in the Holocene alluvium are only seasonally saturated, and these three geologic units are grouped together. Their distribution delineates a zone of moderate liquefaction potential. This zone is subdivided into two subzones; one where the ground water table is less than 3 m (10 ft) deep has slightly higher liquefaction potential than the other. The beds of well-sorted silt and fine sand within the late Pleistocene alluvium are slightly compacted and indurated, and so they are not as susceptible to liquefaction as similar beds in the Holocene deposits. The distribution of the late Pleistocene alluvium therefore delineates a zone of low liquefaction potential (Youd and others, this report).

For purposes of comparing ground amplification, the sedimentary deposits and bedrock units can be grouped into four units according to similarities in seismic impedance ($V_s \rho$). The bay mud forms a unit with the lowest impedance, and the late Pleistocene and Holocene alluvium are combined to form a unit of low to moderate impedance. The bedrock units in the south bay region fall into two groups with higher seismic impedances than the sedimentary deposits. The early Pleistocene and Tertiary sandstones form a unit with moderate to high impedance, and the Franciscan Formation forms a unit with the highest impedance (fig. 31). Medvedev (1965) pointed out that the highest levels of seismic amplification can be expected where the impedance contrast between overlying and underlying geologic units is greatest. This relation suggests that the highest seismic amplifications in the bay region would be expected where thick deposits of bay mud directly overlie Franciscan bedrock. In the southern bay region the highest seismic amplifications would be expected where bay mud overlies the late Pleistocene alluvium or where deposits of late Pleistocene and Holocene alluvium overlie bedrock. This appraisal does not consider other factors, such as stratigraphic thickness, that will greatly affect seismic amplification. Data on contrasts in impedance do, however, provide means of evaluating these other parameters.

RESPONSE OF LOCAL GEOLOGIC UNITS TO GROUND SHAKING

By R. D. BORCHERDT, W. B. JOYNER, R. E. WARRICK and J. F. GIBBS

INTRODUCTION

The most widespread earthquake damage to man-made structures is generally a direct result of ground shaking. Local geologic conditions can change the characteristics of earthquake ground shaking. In particular, the intensity of shaking in certain frequency bands can be amplified by thick deposits of unconsolidated materials. Such materials exist over a large proportion of the San Francisco Bay region, and after the 1906 earthquake, effects of exaggerated ground shaking were documented at sites underlain by these materials (Lawson, 1908). For example, violent effects were observed on the muds near San Francisco Bay and on the thick alluvial deposits underlying San Jose and Santa Rosa. Lawson (1908, p. 160–253) reported evidence for exaggerated shaking on alluvial deposits in 18 other communities. This phenomenon is not considered in present building codes, partly because observations of damage are not sufficiently quantitative to be incorporated easily into designs for earthquake-resistant structures and partly because data on the seismic response of different geologic units are limited. However, recent increases in the number of comparative seismic recordings and advances in numerical models for the dynamic response of surficial geologic deposits are yielding improved quantitative data. This chapter summarizes these data for the San Francisco Bay region and examines their usefulness for purposes of seismic zonation.

OBSERVED GROUND-MOTION AMPLIFICATIONS FROM NUCLEAR EXPLOSIONS IN NEVADA

Comparative ground-motion measurements of a single seismic event provide quantitative estimates for the effects of various geologic units on ground shaking. Comparative measurements of ground motion generated by distant nuclear explosions in Nevada have been made at 99 sites in the San Francisco Bay region (fig. 33). Nuclear explosions in Nevada are especially useful for such studies in the bay area, since at these distances (approximately 530 km (330 mi)) source characteristics and travel paths are nearly the same for each recording site. In addition, most of the ground-motion energy is in the frequency band for which the effects of the local geologic units are greatest. This coincidence of frequency bands causes the amplification effects of the geologic units to be readily apparent on the analog recordings of ground velocity.

Detailed analyses of these ground-motion data were presented by Borcherdt (1970) and Gibbs and Borcherdt (1974). Results of these analyses are summarized here.

A brief summary of the geology aids in understanding these results. The numerous geologic units in the region can be grouped into three general categories on the basis of gross physical properties (see Lajoie and others, this report, for a discussion of methods for differentiating sedimentary deposits and a discussion of the physical parameters used in regrouping them). The three general categories determined to have distinctly different seismic properties (Borcherdt, 1970) are as follows:

1. Bay mud (equivalent to the younger bay mud unit of Borcherdt, 1970) consists mostly of recently deposited soft plastic carbonaceous clay, silt, and minor sand containing more than 50 weight percent water; thickness as much as 40 m (130 ft); shear velocities 90 to 130 m/s (290 to 430 ft/s).
2. Alluvium (equivalent to the older bay sediment unit of Borcherdt (1970) and the late Pleistocene and Holocene alluvium of Lajoie and Helley (Lajoie and Helley, this report) consists mostly of silty sandy clay, silty clayey sand, and sand and gravel with less than 40 weight percent water; thickness as much as 600 m (2,000 ft); shear velocity approximately 200 m/s (660 ft/s) at the surface, increasing with depth.
3. Bedrock consists of Pliocene and early Pleistocene alluvium of Lajoie and Helley (this report), which includes the Santa Clara Formation, consisting of semiindurated and indurated sandstone, siltstone, and mudstone; Tertiary rocks, consisting of marine sandstone and shale of Eocene, Miocene, and Pliocene age; the Page Mill Basalt, lava flows and pyroclastic rocks of Miocene age; and pre-Tertiary rocks, which include the Franciscan Formation, consisting mostly of sandstone, shale, radiolarian chert, and greenstone (volcanic rocks), minor amounts of granitic rocks, and the Great Valley sequence, consisting of indurated

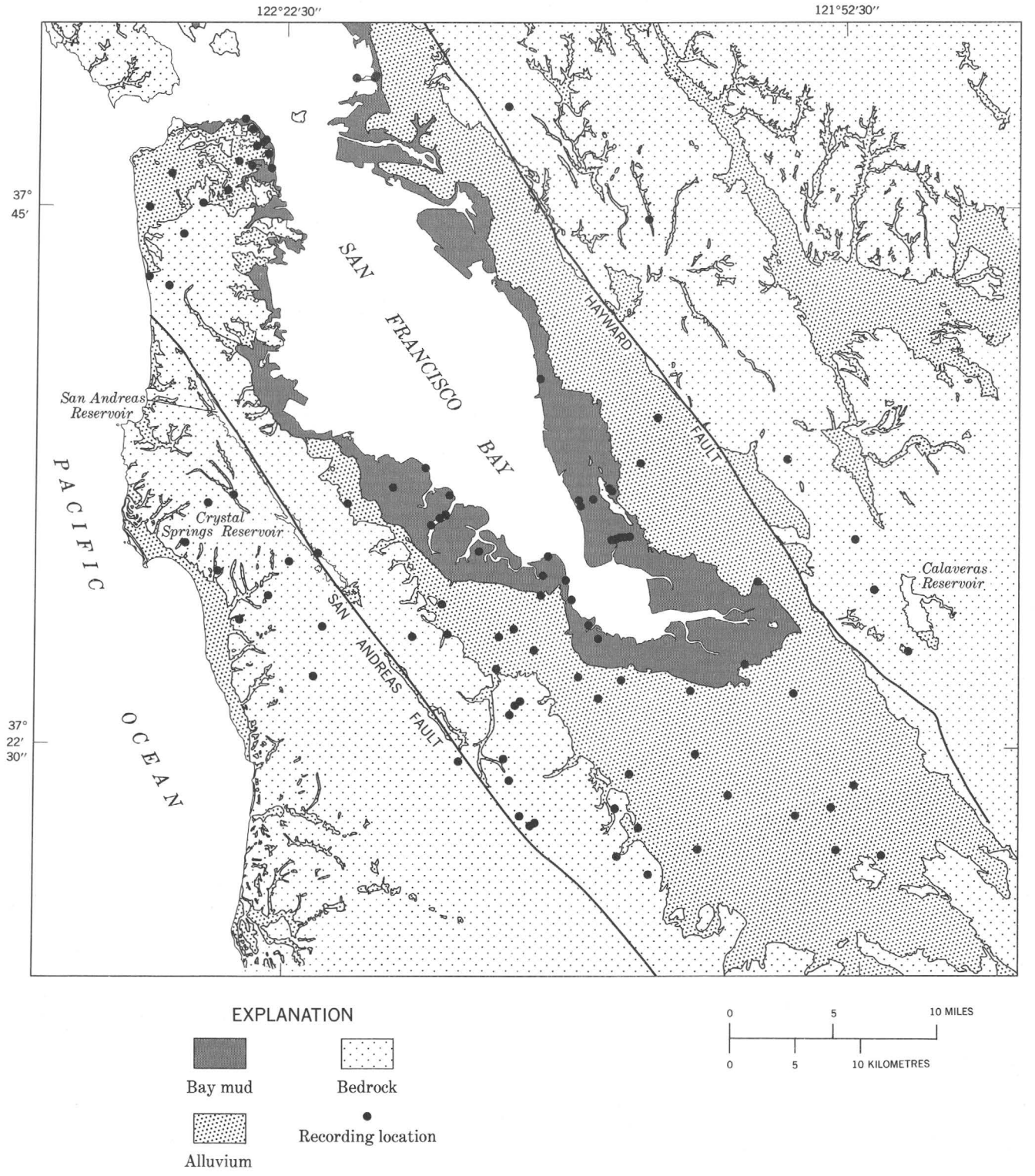

FIGURE 33.—Distribution of generalized geologic units and locations where three components of ground motions generated by nuclear explosions were recorded.

sandstone and siltstone; thicknesses vary; shear velocities estimated to range from 500 to 2,000 m/s (1,600–6,600 ft/s).

Examples of horizontal ground-velocity recordings obtained on each of these three units are shown on figure 34*A*. All the recordings were made at sites within

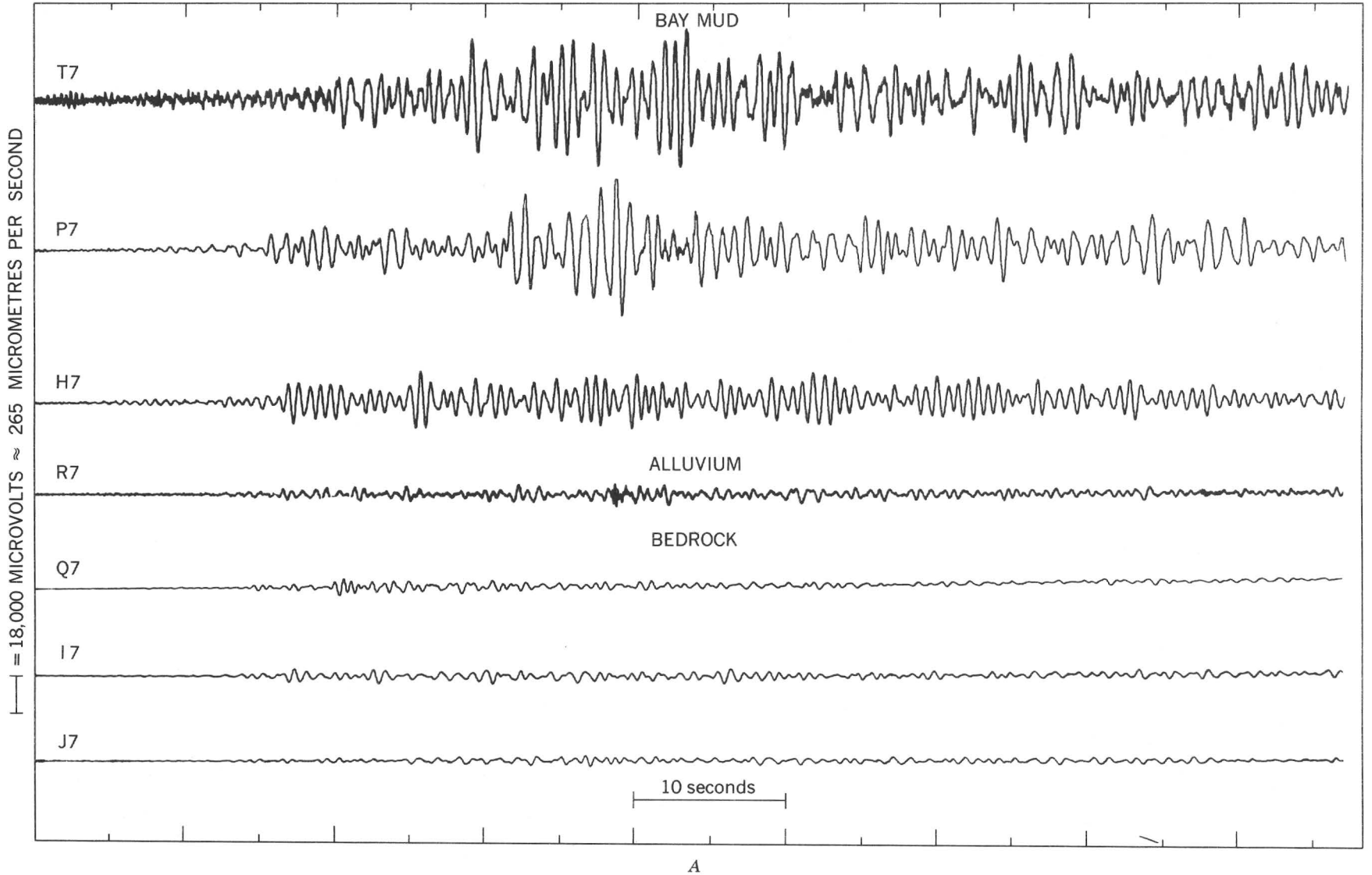

FIGURE 34.—Recordings of horizontal ground motion generated by two nuclear explosions. The recordings are grouped according to the type of geologic unit at the site. *A*, Equiscaled recordings of nuclear explosion 7 at sites in San Francisco. *B*, Equiscaled recordings of nuclear explosion 11.

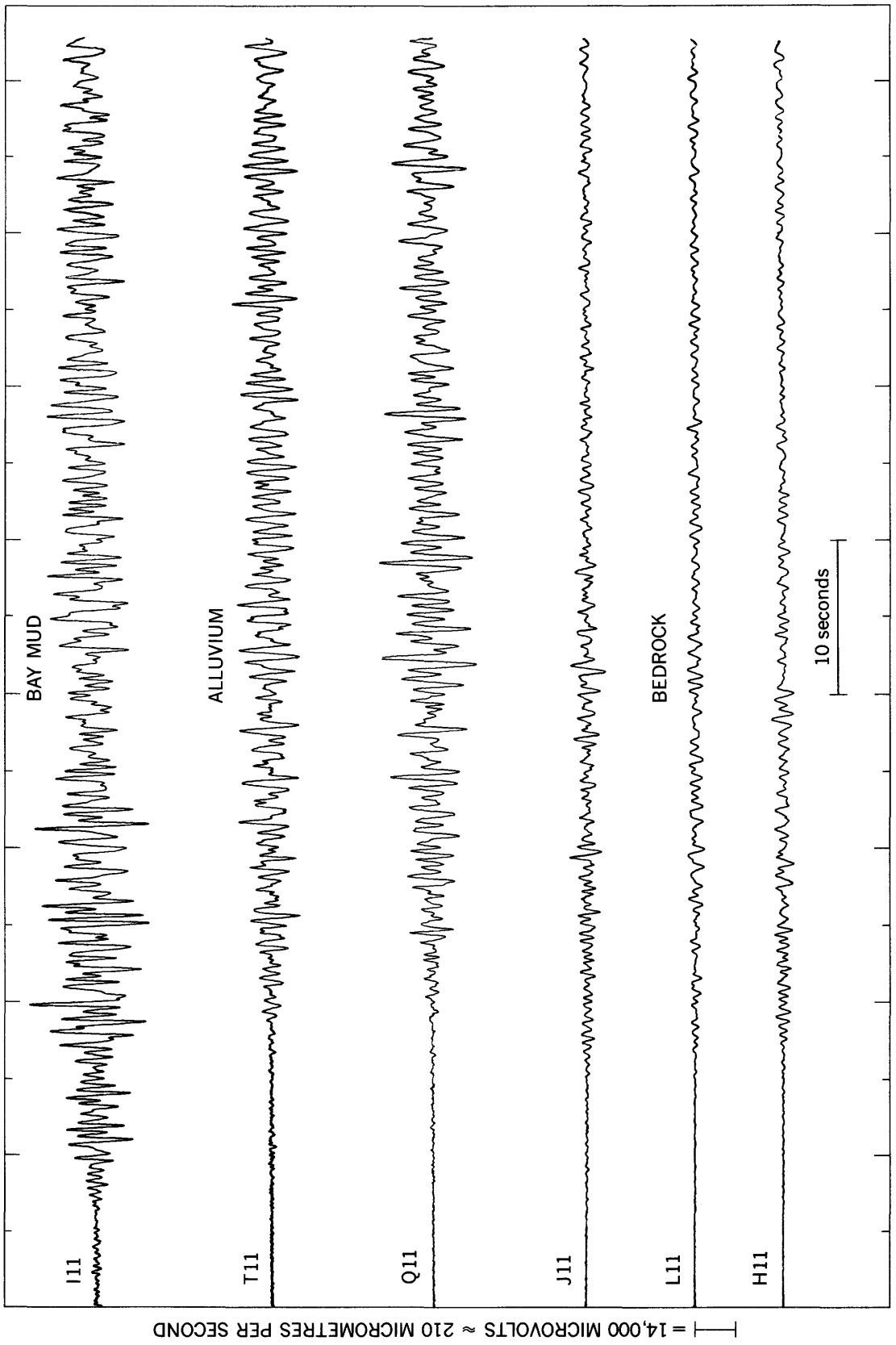

B

FIGURE 34.—Continued.

the city limits of San Francisco from the same nuclear event. Comparison of the recordings clearly illustrates the large amplifications of horizontal ground velocity due to differences in local geology. The maximum amplitudes recorded on sites underlain by bay mud are five to eight times larger than those recorded on nearby bedrock sites. Recordings from another nuclear event (fig. 34*B*) show similar large amplifications for sites underlain by bay mud and thick sections of alluvium (see Borcherdt, 1970, for geologic profiles of some of the sites).

Similar analyses have been made of vertical ground motion recorded at each of the sites. Most of the observed variations in vertical ground motion are less than the observed variations in horizontal motion (Borcherdt, 1970). As a result, this summary is concerned principally with horizontal motion, which is of most interest for the design of earthquake-resistant structures.

The characteristics of the seismic amplitude response of local geologic units can be approximated by computing the ratio of the absolute value of the Fourier transform for a recording to that obtained from a simultaneous recording at a nearby bedrock location. The ratios over the frequency band for which there is a good signal-to-noise ratio provide an estimate of the response characteristics of the local geologic unit with the effects of the source, travel path, and the recording instruments removed. The spectral ratios computed for the 13 recording sites in San Francisco (fig. 35) are grouped according to the type of underlying geologic unit.

The characteristics of the spectral ratios show several correlations with the type of underlying geologic unit. For sites underlain by bedrock, the spectral amplification curves are approximately constant as a function of frequency, with minor variations about 1. For sites underlain by alluvium, the spectral amplification curves are generally greater than 1, with irregular variations as a function of frequency and with peak values that may exceed 5. For sites underlain by bay mud, pronounced peaks exist in the spectral amplification curves, with much larger peak values than observed on either the bedrock sites or the alluvial sites.

To summarize these data, average horizontal spectral amplifications (AHSA) have been computed over the frequency band for which the signal-to-seismic-background-noise ratio is greater than 2. (The seismic background noise was determined from spectral analyses of the seismic noise recorded immediately prior to the arrival of the seismic energy generated by the nuclear explosions.) The AHSA values for all sites have been normalized by the average value obtained from sites underlain by granitic rock. Histograms for these average values (fig. 36) show that there are significant differences in the seismic response of the bay mud unit, the alluvial unit, and the bedrock unit. The mean and standard deviations for the three samples are, respectively, 1.3 and 0.6 for bedrock, 4.4 and 1.9 for alluvium, and 11.3 and 6.0 for bay mud. The standard deviations are partly dependent on variations in amplification caused by variations in thickness of the corresponding geologic units.

In summary, the spectral amplifications show that there are significant differences between the seismic responses of the three types of geologic units in the San Francisco Bay region. Of particular interest for the design of earthquake-resistant structures are the predominant periods and corresponding large amplifications observed on nearly all the bay mud sites and some of the alluvial sites.

For purposes of seismic zonation it is important to know to what extent these spectral amplifications can be extrapolated to describe quantitatively the amplification effects of local geologic units in the event of another large earthquake. To examine this question, the results from the nuclear explosions are compared with those from the March 22, 1957, San Francisco earthquake, data from the April 18, 1906, California earthquake, and numerical models of the dynamic response of surficial geologic units at high strain levels.

COMPARISON OF NUCLEAR EXPLOSION DATA WITH THE 1957 AND 1906 EARTHQUAKE DATA

The epicenter of the San Francisco earthquake of March 22, 1957, (magnitude 5.3) was located approximately 17 km (10 mi) southwest of downtown San Francisco. Four strong-motion recordings were obtained in San Francisco, one on bedrock, two on alluvium, and one on bay mud. An estimated $1 million of damage, limited principally to single-family dwellings in the immediate vicinity of the epicenter (Westlake-Palisades area), resulted from the earthquake (Oakeshott, 1959). Varying degrees of minor damage were reported in the buildings containing the strong-motion instruments. As part of this investigation, a nuclear explosion was recorded at each of the four locations occupied by the strong-motion recorders. The instruments used to record the nuclear explosion were placed within 3 m (10 ft) of the strong-motion instruments.

Samples of the spectral amplifications computed from the two events for the site underlain by bay mud (fig. 37) differ in detail, but their gross features are similar. In particular, the predominant frequencies agree to within 0.2 hertz, the average amplification to within 32 percent, and the maximum spectral amplification to within 36 percent. These comparisons suggest that the princi-

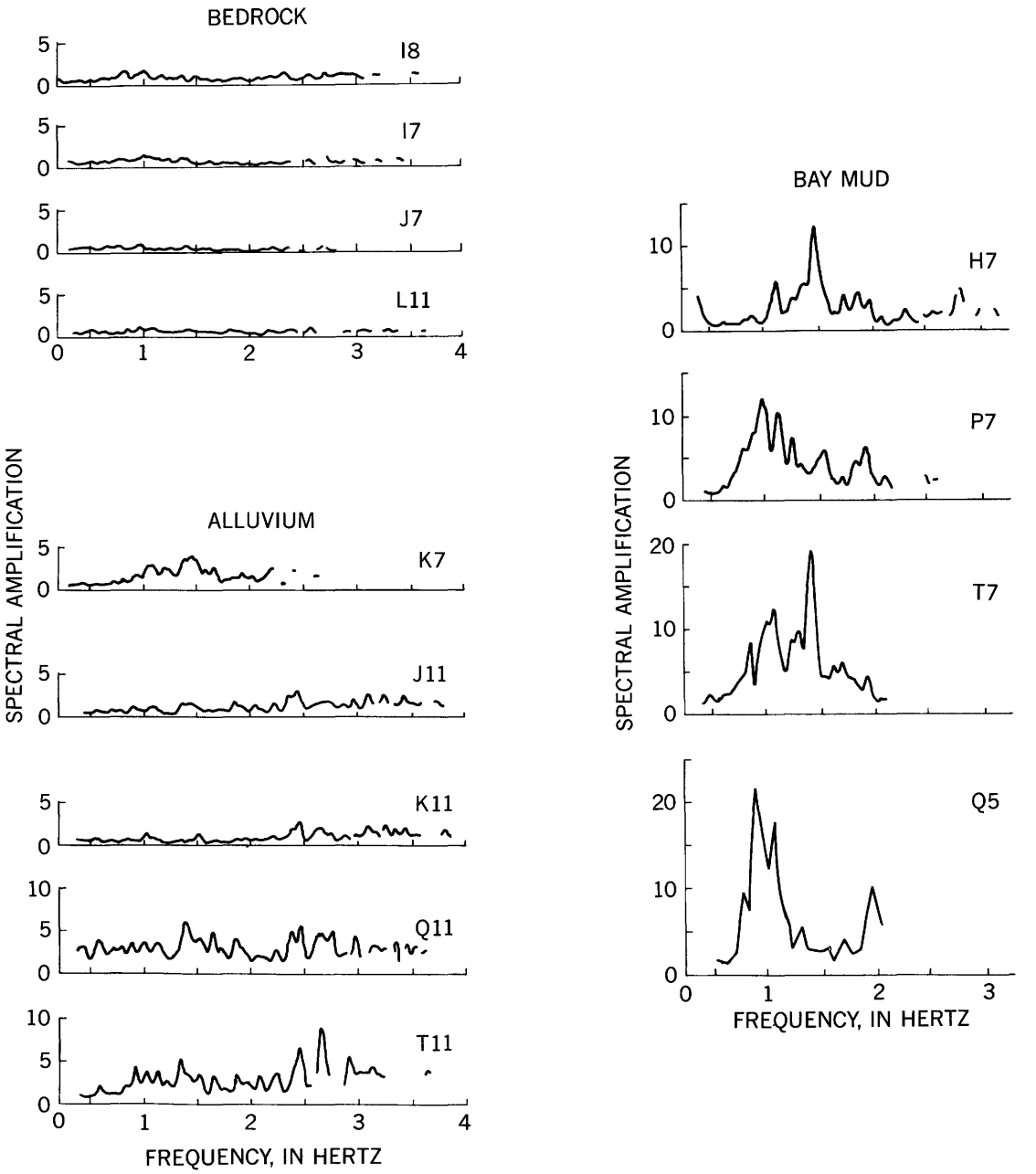

FIGURE 35. Horizontal spectral amplification curves computed for 13 recording sites in San Francisco.

pal amplification effects of the local geologic deposits could have been predicted quantitatively for this earthquake by analyzing the nuclear explosion recordings.

The other set of observational data for the San Francisco Bay region that bears on the extrapolation problem is the intensity data from the 1906 earthquake. Wide variations in the amounts of damage were observed in the city of San Francisco after the 1906 earthquake (fig. 1). Wood (1908) attributed these wide variations to the geologic character of the ground. Wood concluded "***Where the surface was of solid rock, the shock produced little damage; whereas upon made land great violence was manifested***." This dependence on the geologic character of the ground can be due to both increased levels of shaking and an increased number of ground failures. In many places, the surficial geologic deposits most likely to amplify shaking are also those with least strength. Buildings on such deposits are especially susceptible to failure during earthquakes.

The 1906 intensity maps prepared for the San Francisco Bay region (maps 19, 21, and 22, Lawson, 1908) show that for similar geologic units the observed intensity values generally decrease with increasing perpendicular distance from the San Andreas fault. Borcherdt

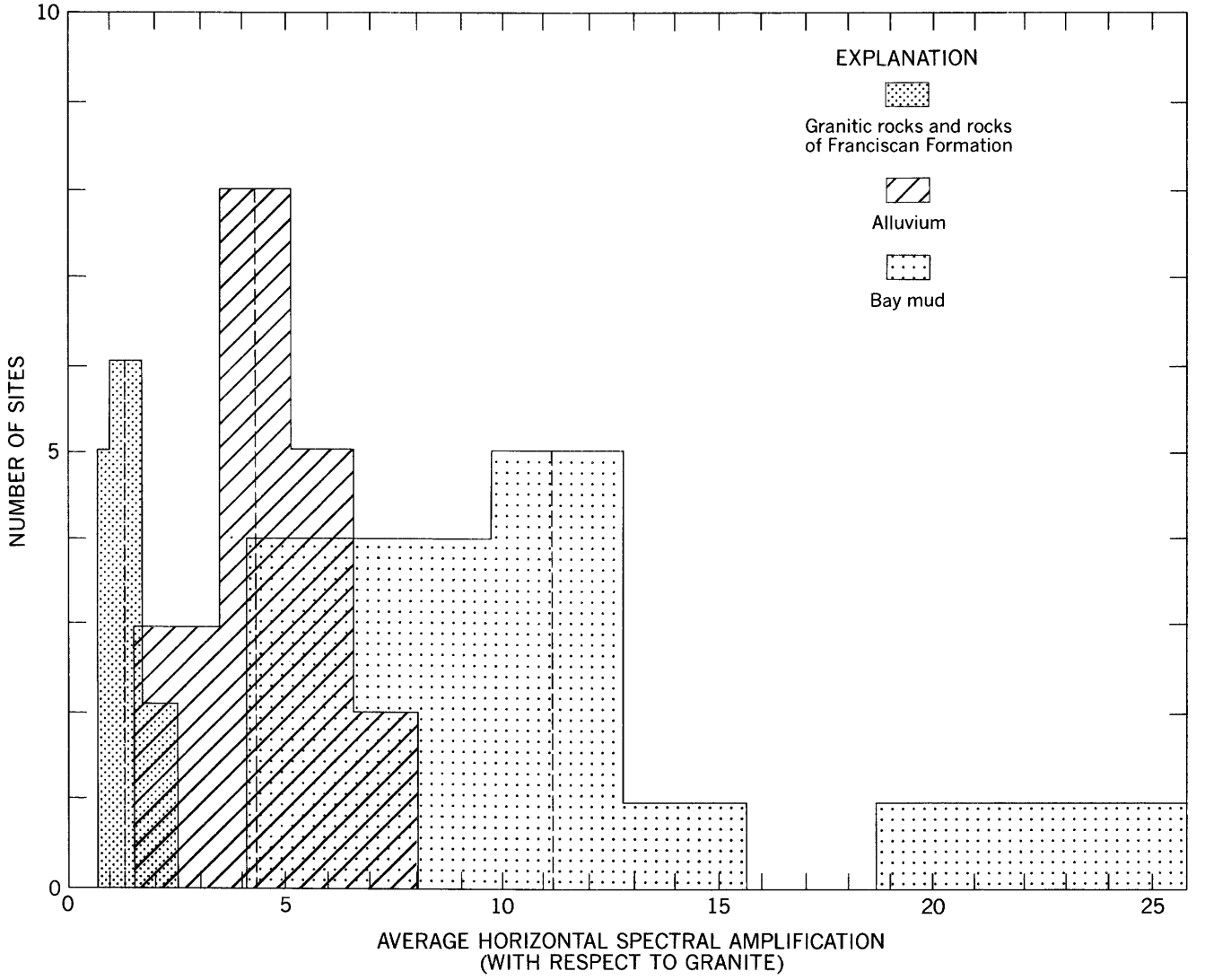

FIGURE 36.—Histograms of average horizontal spectral amplification values computed for sites underlain by bay mud, alluvium, and either granitic rocks or rocks of Franciscan Formation. Dashed line indicates mean value for each geologic unit.

and Gibbs (1975) derived an empirical relation between the 1906 intensities and distance for sites underlain by the Franciscan Formation (fig. 38). The resulting relation (intensity = 2.69 − 1.90 log (distance (km))), derived from only those sites (approximately one square city block in size) for which there was good evidence for the ascribed degree of intensity, shows that intensity for sites on the Franciscan Formation generally decreases as the logarithm of distance (fig. 38).

For each site Borcherdt and Gibbs (1975) determined an intensity increment between the observed 1906 intensity value and that predicted at the same distance by the logarithmic relation for the Franciscan Formation. These intensity increments were plotted as a function of the AHSA values computed from the nuclear data at corresponding sites (fig. 39). (The plotted AHSA values were normalized to the average value determined for the Franciscan Formation.)

The correlation coefficient of 0.95 computed for the empirical relation ($\delta I = 0.27 + 2.70$ log(AHSA)) shows that a strong correlation exists between the computed intensity increments and amplifications observed at low-strain levels. The physical basis of this empirical relation is complex and does not necessarily indicate that amplifications observed at low-strain levels can be extrapolated directly to high-strain levels. However, two interpretations of the amplifications obtained from small motions may be useful for predicting areas of high intensity in future large earthquakes: (1) For levels of ground shaking that would not cause ground failure, the higher amplifications characterize those sites most likely to sustain the higher levels of ground shaking and (2) for levels of ground shaking that would induce ground failure, the higher amplifications characterize

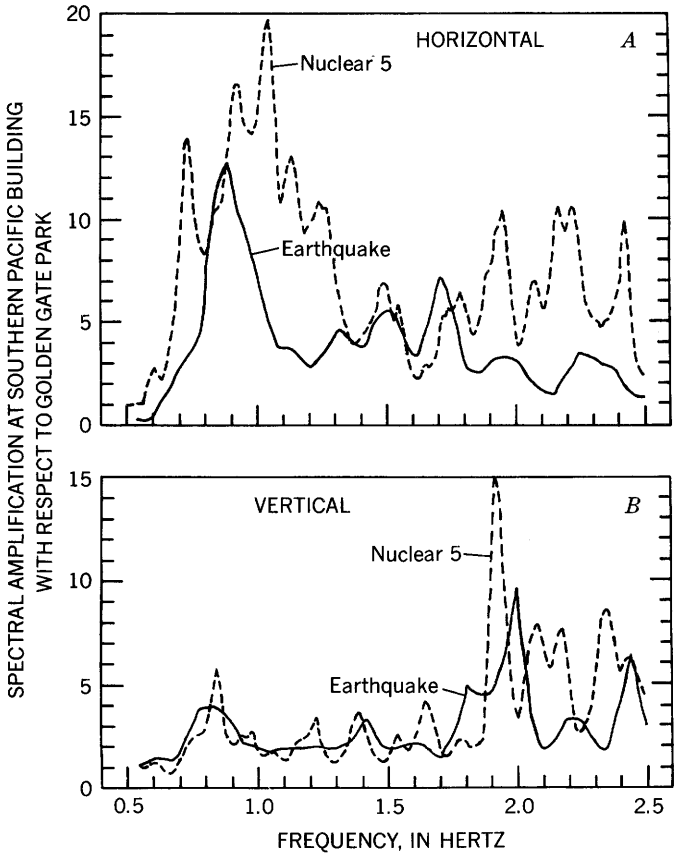

FIGURE 37.—Comparison of spectral amplification curves computed from recordings of a nuclear explosion with those computed from recordings at the same sites of the San Francisco earthquake of March 22, 1957. The curves show the spectral amplification of a bay mud site (Southern Pacific Building) with respect to a bedrock site (Franciscan Formation; Golden Gate Park). *A*, Spectral amplification curves computed for horizontal motions from the N. 45° W. recordings at the Southern Pacific Building and the S. 80° E. recordings at Golden Gate Park. *B*, Spectral amplification curves computed from the recordings of vertical motion at the two sites.

those sites most susceptible to ground failure (see Youd and others, this report). Such predictions are especially useful for evaluating the general earthquake hazard in currently urbanized areas not developed at the time of the 1906 earthquake.

On the basis of the empirical relation $\delta I = 0.27 + 2.70 \log(\text{AHSA})$, which is based only on intensity data in San Francisco for which there is "unequivocal evidence," Borcherdt and Gibbs (1975) predicted intensity increments for each of the 99 sites at which amplification values have been measured from the nuclear explosion data. The resulting average intensity increments, together with the average low-strain amplifications computed for each of the various geologic units with respect to the Franciscan Formation, are given in table 4. The average intensity increments range from −0.29 for granite to 2.43 for bay mud.

Utilizing the computed average intensity increments for the various geologic units (table 4), the empirical relation between intensity and distance (fig. 38), and a generalized geologic map (K. R. Lajoie, oral commun., 1974), Borcherdt and Gibbs (1975) predicted intensities on a regional scale (1:125,000) for the San Francisco Bay region. An insert from their map shows the intensities predicted for San Francisco (fig. 40). The map shows the maximum intensity predicted for a site that might result from an earthquake in the San Francisco Bay region on either the San Andreas fault or the Hayward fault. The map is useful for delineating general earthquake problem areas in the San Francisco Bay region; hence, the map is a preliminary form of seismic zonation that can be used to develop general land-use policies for reduction of future earthquake losses. For a more rigorous zonation of the San Francisco Bay region where additional data are available, the maps developed in other papers of this report can be used to further define the nature and potential severity of the problems in the various areas.

The design of critical structures such as hospitals, schools, and nuclear power plants requires quantitative estimates of ground shaking that the site might experience during a future strong earthquake. For soil sites such estimates require quantitative estimates of the shaking response of the underlying deposits. The analysis of the 1957 earthquake recordings suggests that the spectral amplification curves computed from the nuclear explosions could be used for such quantitative estimates of strain levels as much as approximately 10^{-4} in soil. However, for higher strain levels as occurred during the 1906 earthquake, there are no strong-motion records for a similar analysis. Another approach for developing improved quantitative estimates is through the use of numerical models and laboratory data on the behavior of surficial geologic units at high strain levels.

NUMERICAL MODELS FOR THE RESPONSE OF SURFICIAL GEOLOGIC UNITS

To develop improved numerical models, three-component seismometers were emplaced in drill holes at a site near the margin of San Francisco Bay. The three-component systems were placed in bedrock, at an intermediate depth in the alluvium, at the base of the bay mud, and at the surface (fig. 41). The output of the systems is recorded continuously on magnetic tape and used to analyze ground motions generated both by earthquakes and nuclear explosions. By using the motion recorded at depth in the bedrock as input, numerical models can predict the motions at other depths that in turn can be compared with the observed motions.

Horizontal ground motion produced by two earthquakes—one relatively near the recording site,

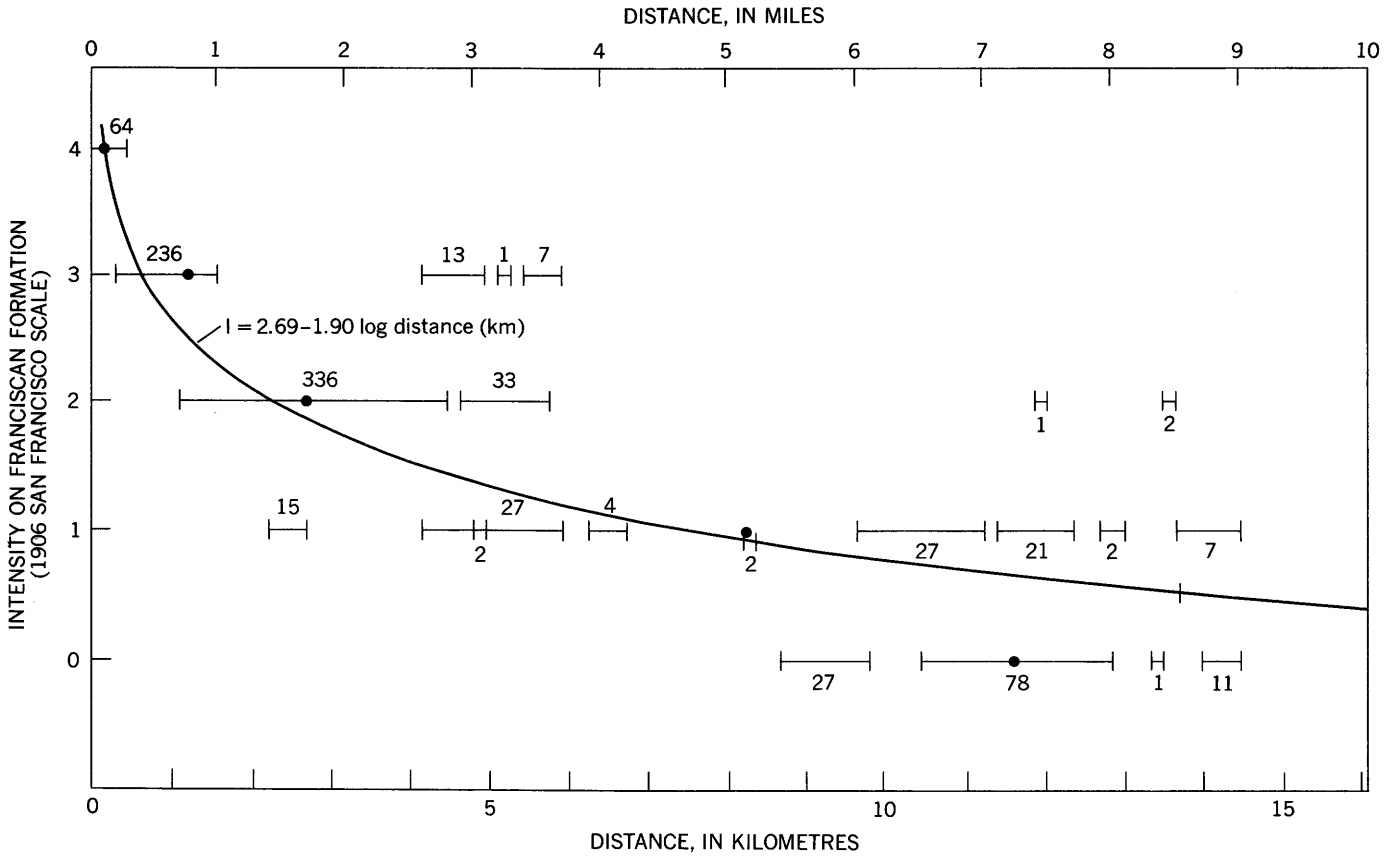

FIGURE 38.—Observed earthquake intensities for sites (one square city block in size) underlain by rocks of the Franciscan Formation as a function of perpendicular distance from the zone of surface rupture during the 1906 earthquake. For sites with "unequivocal evidence" in San Francisco (map 19, Lawson, 1908) the number of observed intensity values is shown below the corresponding distance interval. For sites intersected by an "examined route" south of San Francisco (maps 21 and 22, Lawson, 1908) the number of observed values is shown above the corresponding distance interval. The observed 1906 intensity values are expressed in terms of the 1906 San Francisco intensity scale with the letters A–E corresponding respectively to the numbers 4–0 (see section "1906 Intensity Scale for San Francisco").

the other farther away—was recorded on the down-hole systems. The recordings of both earthquakes (fig. 42) show that horizontal ground motion at the surface was substantially larger than that in bedrock. However, the depth range over which amplification took place differed for the two earthquakes. This observation is easily explained by the difference in the relative frequency content of the bedrock motions for the two events. The ground motion generated by the local earthquake was richer in higher frequencies, because the seismic waves did not travel as far from the source as they did for the San Fernando earthquake. The differences in the nature of the amplification, as apparent on the analog records for the two earthquakes, illustrate the need for characterizing the seismic response of local geologic units by spectral amplification curves rather than by ratios of maximum amplitudes measured from analog records. The ratios of maximum amplitude in general depend on the nature of the source, the length of the travel path, and the frequency response of both the local geologic units and the recording instruments. In contrast, the spectral amplifications are to a first approximation dependent only on the frequency response of the local geologic unit.

A comparison between the predicted and observed horizontal surface motions for the two earthquakes is shown in figure 43. Even though the relative frequency content of the bedrock motions for the two earthquakes is considerably different, the numerically predicted time histories agree reasonably well in both amplitude and relative frequency content with those actually observed.

The predictions of the numerical model are based on the solution for incident homogeneous plane *SH*-waves in plane-layered viscoelastic materials (Kanai, 1952). Kanai's solution was extended to multiple layers using the Thompson-Haskell (Haskell, 1953) matrix formulation and a viscoelastic constitutive law proposed by Chae (1968). The material parameters for the constitutive relation used in these calculations were determined from in situ seismic experiments (Warrick, 1974).

To characterize the seismic response at the surface

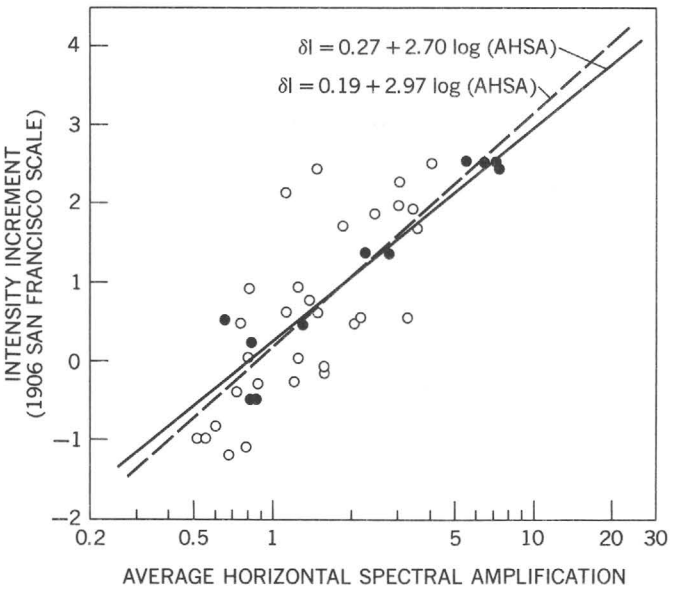

FIGURE 39.—Increments in 1906 intensities as a function of average horizontal spectral amplification computed at corresponding sites from recordings of nuclear explosions. Both the intensity increment values (δI) and the average spectral amplification values (AHSA) were computed with respect to the corresponding average value determined for sites underlain by rocks of the Franciscan Formation. The empirical relation (δI = 0.19+2.97 log(AHSA)) is based on the data from all sites for which there was an observed 1906 intensity value (circles and dots). The empirical relation (δI = 0.27+2.70 log(AHSA)) is based on only the data from sites in the city of San Francisco (dots) for which there was unequivocal evidence for the ascribed degree of intensity. (The second empirical relation is preferred, although intensity increments predicted from either relation differ by less than two-tenths of an intensity increment.)

TABLE 4.—*Statistics for samples of low-strain amplifications and intensity increments with respect to Franciscan Formation for various geologic units*

Geologic unit	Average horizontal spectral amplification		Intensity increment (1906 San Francisco scale)	
	Mean	Standard deviation	Mean	Standard deviation
Granite	0.63	0.11	−0.29	0.21
Franciscan Formation	1.00	0.38	0.19	0.47
Great Valley sequence	1.42	0.45	0.64	0.34
Santa Clara Formation	1.70	0.64	0.82	0.48
Alluvium	2.76	1.16	1.34	0.58
Bay mud	7.06	3.78	2.43	0.58

with respect to the bedrock, spectral amplifications were predicted with the numerical model. This prediction is compared with the amplifications observed from the recordings of the distant San Fernando earthquake (fig. 44). The fundamental frequency and the frequency of the first two higher modes for the computed response agree to within about 10 percent of those observed. The amount of amplification is also in reasonable agreement. The maximum computed amplification is about 35 percent less than the maximum observed. Such comparisons of low-strain amplifications (max. strain $\approx 10^{-6}$) are useful for understanding the amplification phenomena and for the development of numerical models. The corresponding low-strain parameters for the unconsolidated deposits can be determined satisfactorily both in the laboratory and in situ. However, estimates of high-strain parameters at present must result largely from laboratory measurement of soil parameters.

Using laboratory data on the dynamic behavior of bay mud and alluvium, a quasilinear procedure was applied to estimate the high-strain response of the surficial geologic deposits. The procedure is based on the assumption that the linear low-strain model is applicable, provided the model parameters are chosen in accord with high-strain data from laboratory studies. This assumption has been applied previously by Idriss and Seed (1968). The high-strain parameters were determined from curves presented by Hardin and Dernevich (1972) and from data on the properties of the unconsolidated deposits compiled by Harold Olsen (written commun., 1972).

Comparisons of the high-strain spectral response and the low-strain response for three sites are shown in figures 45, 46, and 47. The higher strain responses were computed using the bedrock motion from the San Fernando earthquake of February 9, 1971 at Pacoima Dam. The accelerogram was scaled according to the perpendicular distance of the sites from the San Andreas fault.

The model calculations suggest that the principal effect of high strain is to shift the frequencies of the higher modes to lower values and to reduce the amplification corresponding to these modes. For frequencies in the vicinity of the fundamental mode, there is only a slight change in the amount of amplification.

The high-strain responses of the two bay mud sites (figs. 46, 47) are distinctly different, even though the low-strain seismic models used for these two sites were identical. This difference is due to the difference in the input strain level at the two sites. The higher strain level (fig. 46) has two effects: (1) to increase the impedance contrasts at the bedrock-alluvium and alluvium-mud interfaces and (2) to increase the damping of the seismic waves. The first effect tends to increase the amount of amplification, and the second tends to decrease it. However, since the attenuation increases with frequency, the higher level of input strain results in less amplification at the higher modes but increased amplification for the fundamental mode.

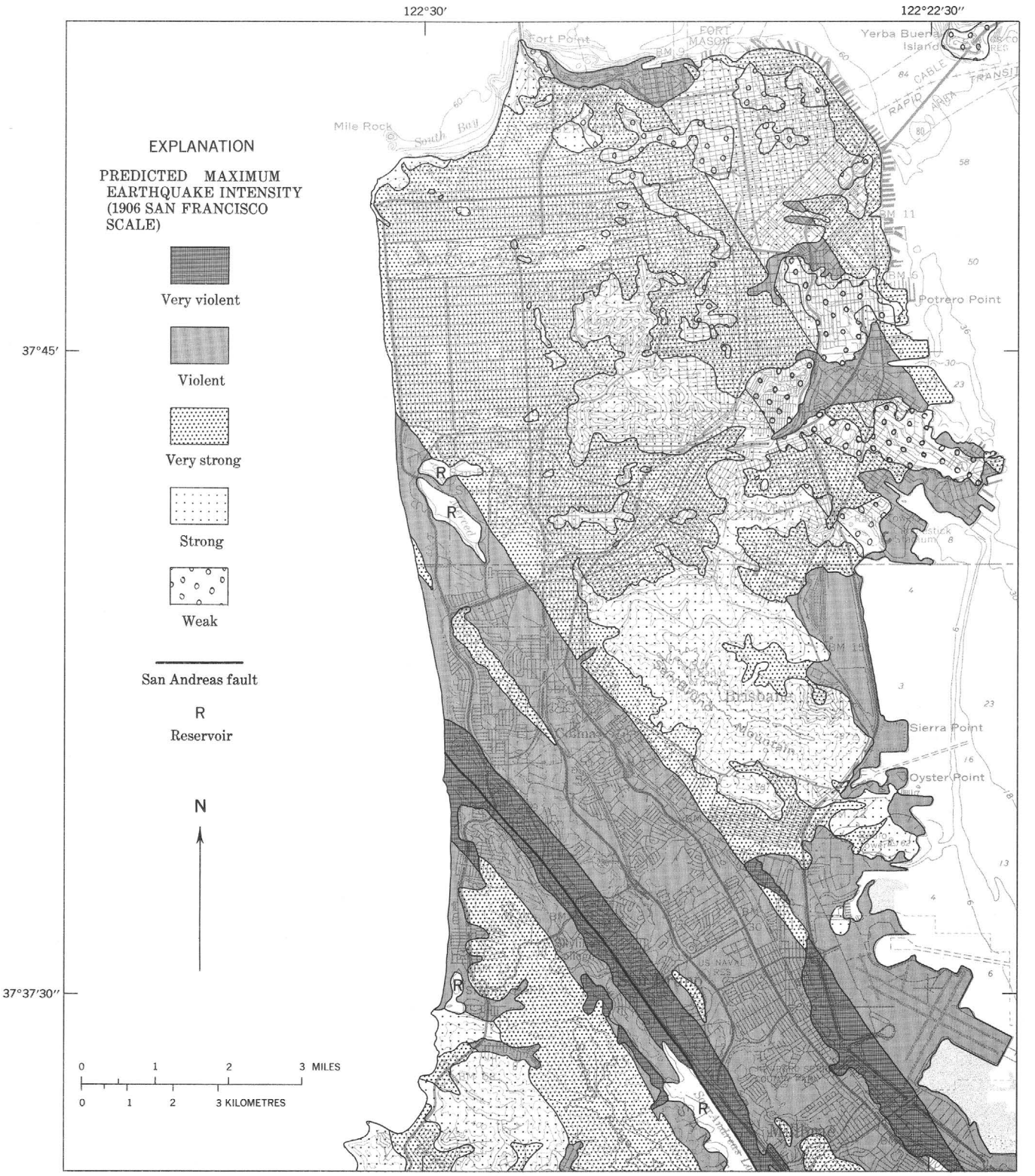

FIGURE 40.—Maximum earthquake intensities predicted for San Francisco. Each value is the maximum of those predicted assuming a large earthquake on the San Andreas fault or the Hayward fault. The intensity values are predicted from the empirical relations (figs. 38, 39) based on only the good intensity data for the 1906 earthquake together with a generalized geologic map compiled by K. R. Lajoie (written commun., 1974). Letters *A–E* indicate grades of the San Francisco intensity scale (see section "1906 Intensity Scale for San Francisco").

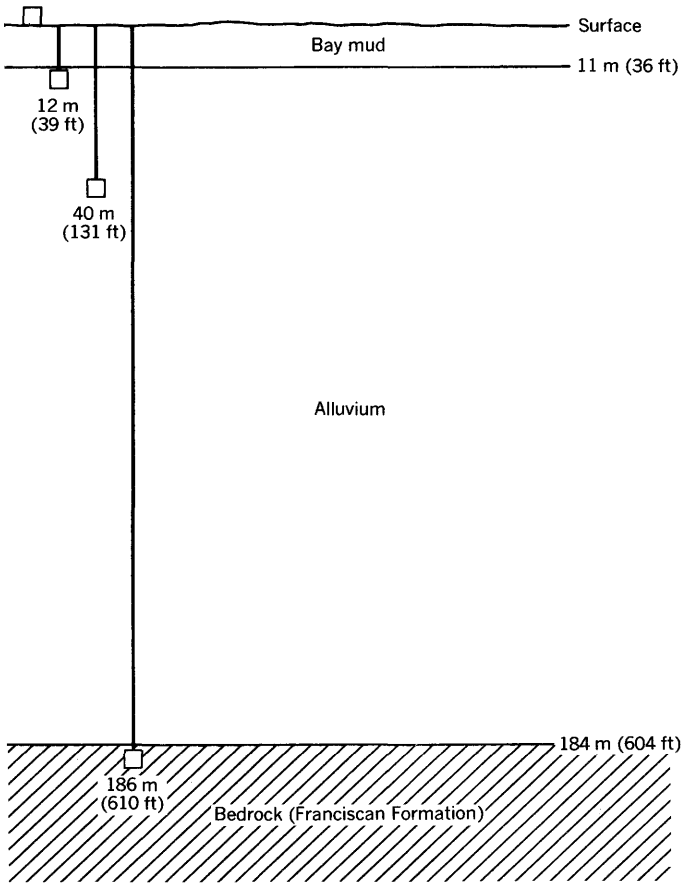

FIGURE 41.—Schematic geologic section at the site of the down-hole seismometer array.

In brief, these calculations show that an increase in level of input strain does not necessarily mean a decrease in amplification for all frequencies.

The model predicts that for the higher frequencies (frequencies more than about three times the fundamental) the corresponding levels of ground shaking can be substantially reduced. Part of this reduction in amplitude may be an artifact of the quasilinear model because the high-strain parameters are chosen for the dominant frequency in the strain history. This possibility has been raised by other researchers (for example, Dobry and others, 1971). Recent work with nonlinear models (W. B. Joyner, unpub. data) suggests that ground motions calculated using the quasilinear model are adequate for frequencies near the fundamental frequency, but at the higher frequencies the ground motions are underestimated by the quasilinear model. Further investigation of the problem is needed.

With the assumption that the high-strain modeling procedure is valid, it becomes possible to predict surface ground motions from postulated future earthquakes. Such predictions have been made at four different sites along a profile perpendicular to the San Andreas fault and are described in Borcherdt, Brabb, and others (this report).

SUMMARY

The amount of damage in San Francisco from the 1906 earthquake was observed to depend strongly on the geologic character of the ground. This dependence suggests the need for zonation maps to reduce losses from future earthquakes.

Comparative measurements of ground shaking generated by nuclear explosions and the 1957 earthquake show that there is a significant and consistent difference in the response to shaking of different geologic units in the San Francisco Bay region. Comparison of the measured amplifications with the 1906 intensities show that an increase in amplification corresponds to an increase in intensity. This correlation suggests that equidistant sites with large observed amplifications may also be sites of relatively high intensity in future earthquakes. These data together with available geologic information were used to predict the maximum intensity that sites in the San Francisco Bay region might sustain in another 1906-type earthquake on either the San Andreas fault or the Hayward fault (fig. 40; Borcherdt and Gibbs, 1975). Such a zonation, properly interpreted, is a useful first step toward predicting the earthquake hazard associated with various geologic conditions. Such a zonation does not provide quantitative estimates of ground shaking, nor does it necessarily define the nature of the problems in the various areas, such as surface faulting, liquefaction, or landsliding. It does delineate many potentially hazardous areas and provides a basis for development of general land-use policies to reduce the hazards of future earthquakes.

The data from the 1957 earthquake suggest that the response to shaking of the various geologic units, as based on data from nuclear explosions, can be extrapolated quantitatively to maximum strain levels of approximately 10^{-4}. For higher strain levels, the results of the numerical model suggest that there can be large amplification effects near the fundamental frequency of a site. However, further analysis of numerical procedures and more field data on the dynamic behavior of surficial geologic units at high-strain levels are needed before these preliminary model predictions can be used quantitatively with confidence in the design of earthquake-resistant structures.

In summary, certain qualitative conclusions can be drawn regarding expected intensities of shaking on a regional scale from future earthquakes. The data currently available for the San Francisco Bay region suggest that the level of ground shaking will vary substantially depending on the type of underlying geologic deposit. For sites equidistant from the fault, excluding

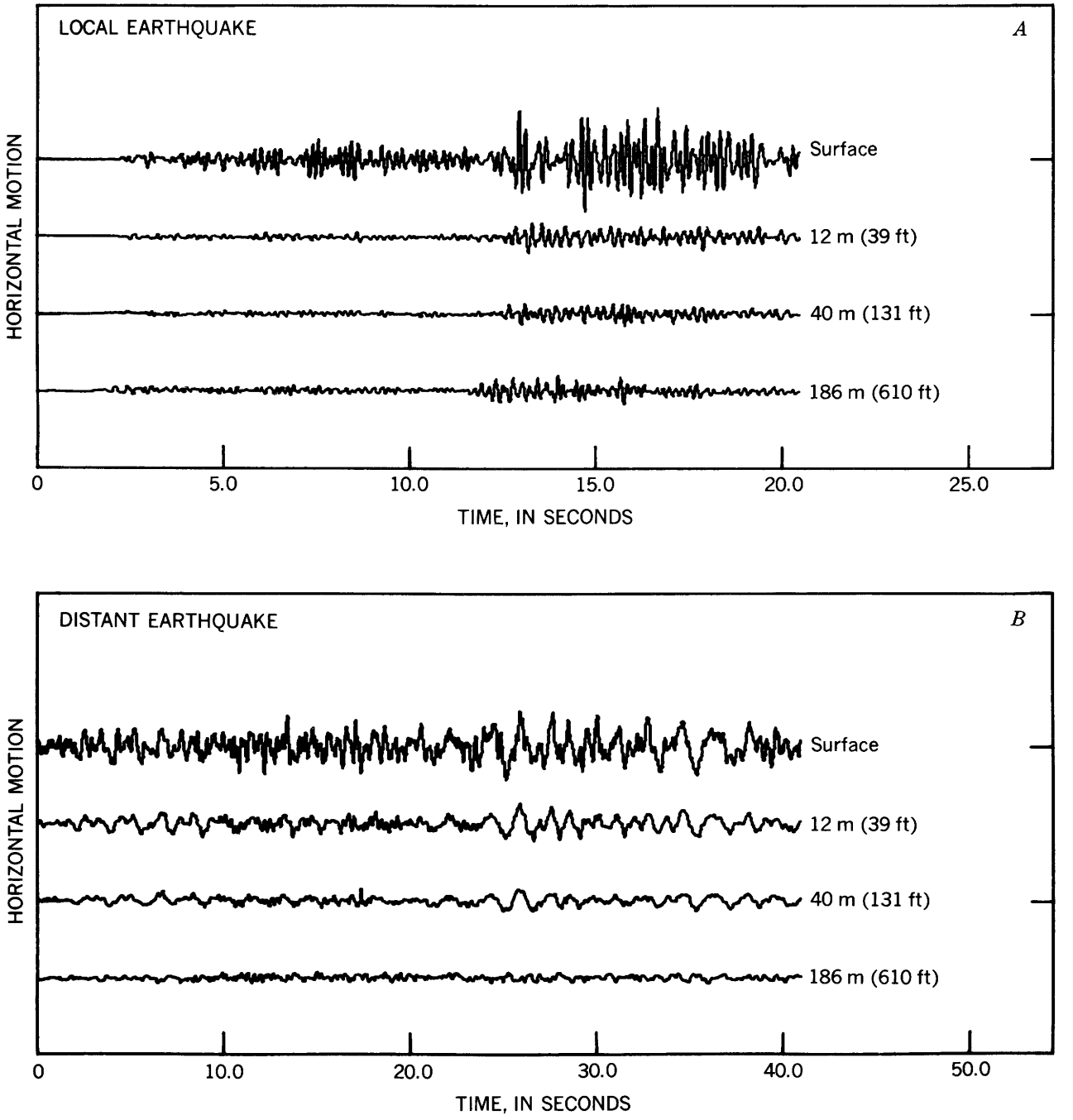

FIGURE 42.—Recordings of horizontal ground motion (N. 40° W. component) from a down-hole seismometer array near the margin of San Francisco Bay. Vertical scale within each set of records is the same to illustrate amplification effects of the soil profile. *A*, Local earthquake, magnitude 3.5, 79 km (49 mi) from recording site. *B*, Distant earthquake, magnitude 6.3, 480 km (298 mi) from site (San Fernando earthquake of February 9, 1971).

those in the immediate fault zone, the effects of amplified ground shaking are expected to be least for those sites underlain by bedrock, intermediate for those sites underlain by alluvium, and greatest for those sites underlain by artificial fill and bay mud. This qualitative classification of geologic units, together with the geologic maps of the San Francisco Bay region described in Lajoie and Helley (this report) provides a qualitative ground-response map of the San Francisco Bay region. The general areas for which the effects of amplified ground shaking are expected to be the greatest are also those areas that are generally considered to be most susceptible to liquefaction (see Youd and others, this report).

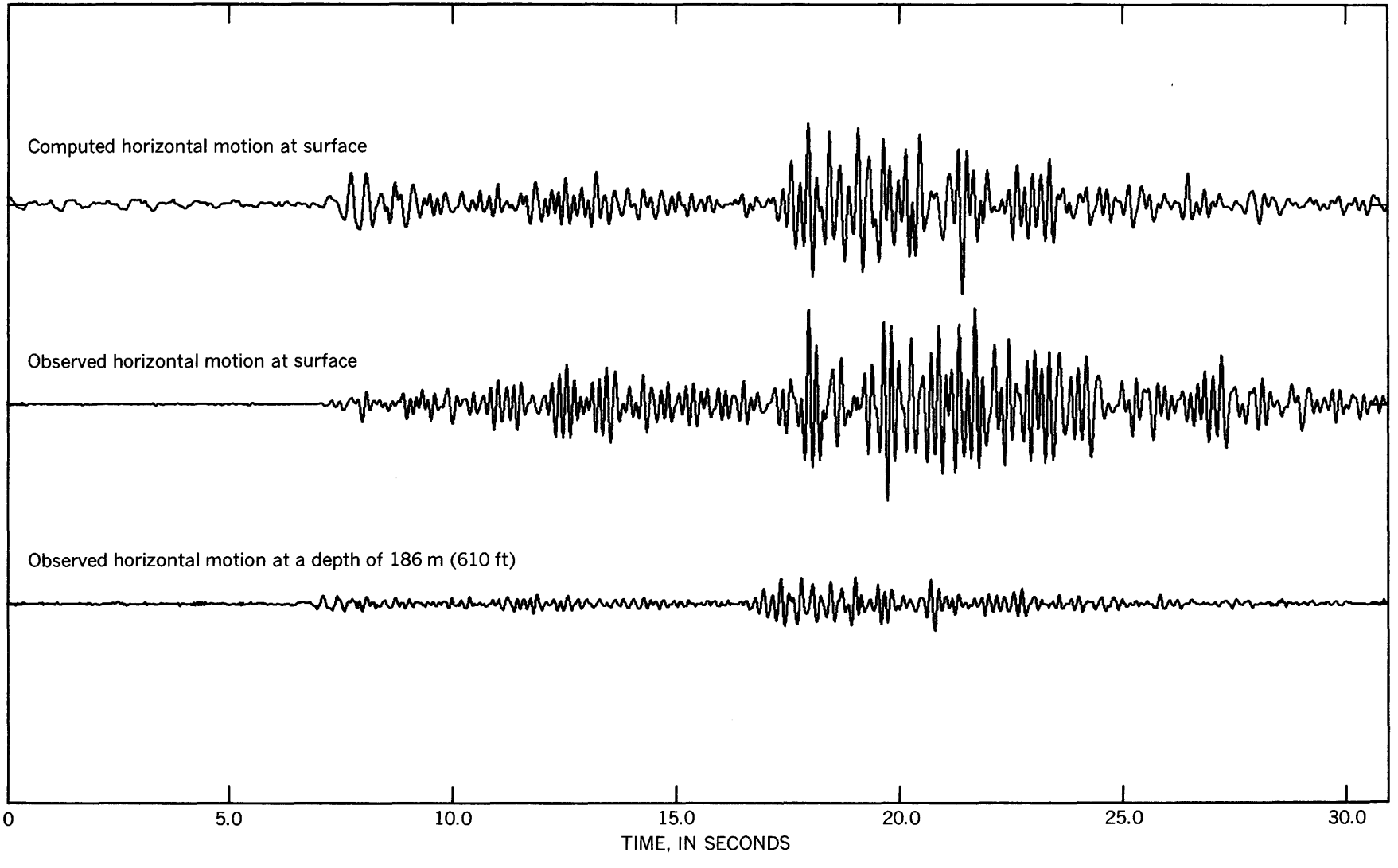

A

FIGURE 43.—Comparison of observed and computed surface ground motions determined from motion observed in bedrock at a depth of 186 m (610 ft). *A*, The observed motions were generated by a local earthquake (fig. 42*A*). *B*, The observed motions were generated by the distant San Fernando earthquake (fig. 42*B*).

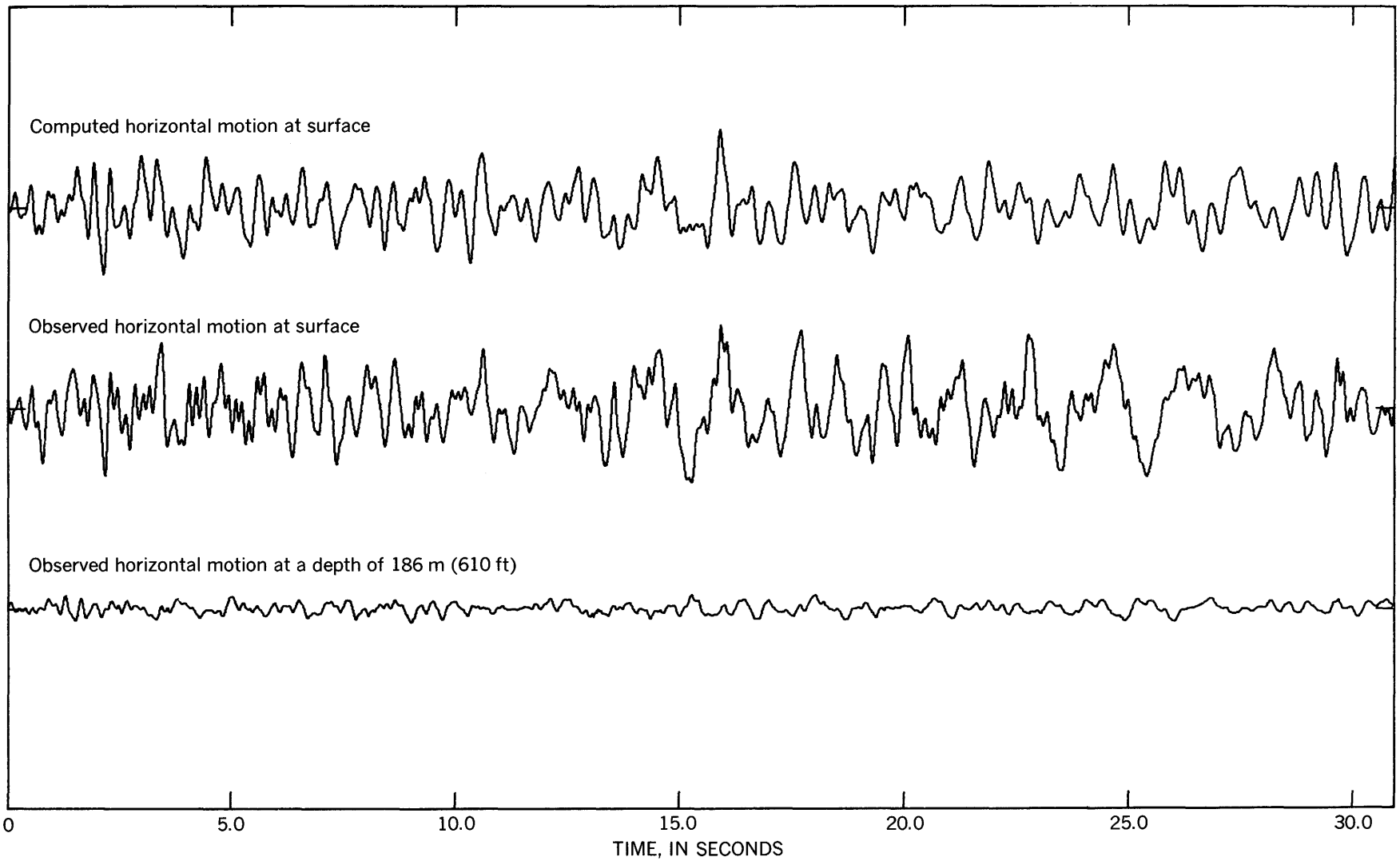

B

FIGURE 43.—Continued.

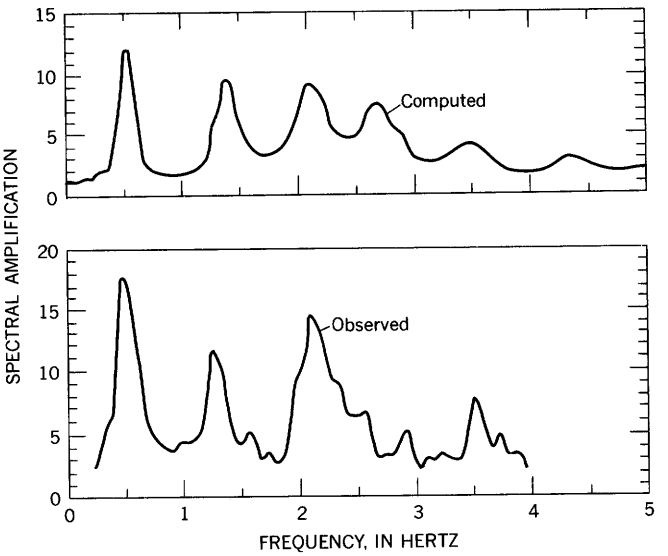

FIGURE 44.—Computed and observed spectral amplification curves for the site at the down-hole seismometer array. The curves were determined using the horizontal motion recorded in bedrock at a depth of 186 m (610 ft) from the San Fernando earthquake (fig. 42*B*).

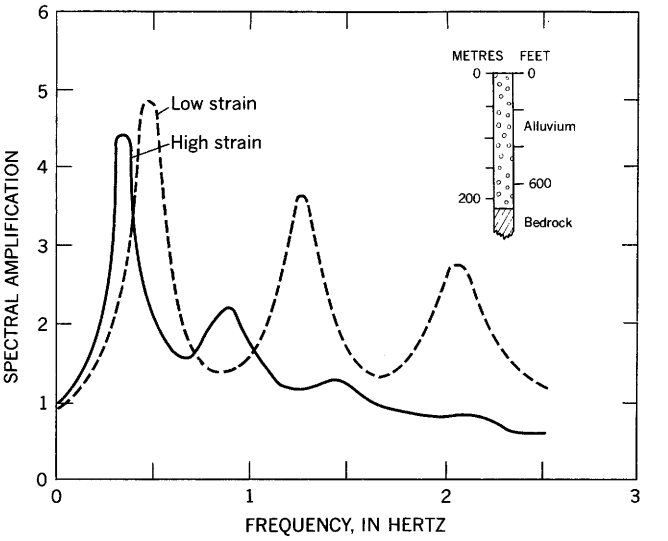

FIGURE 45.—Comparison of high- and low-strain spectral amplification for a site underlain by 220 m (722 ft) of alluvium. The high-strain spectral amplification was computed by using as input the bedrock motion recorded at Pacoima Dam, (San Fernando earthquake of February 9, 1971) scaled to a maximum velocity of 31 cm/s (12 in./s).

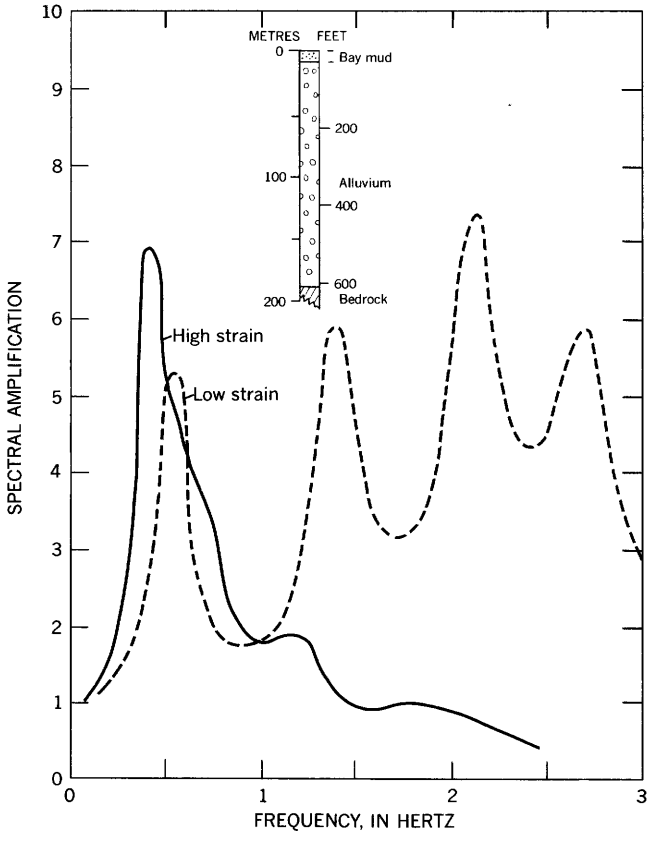

FIGURE 46.—Comparison of high- and low-strain spectral amplification for a site underlain by 11 m (36 ft) of bay mud and 173 m (567 ft) of alluvium. The high-strain spectral amplification was computed by using as input the bedrock motion recorded at Pacoima Dam, (San Fernando earthquake of February 9, 1971) scaled to a maximum velocity of 19 cm/s (8 in./s).

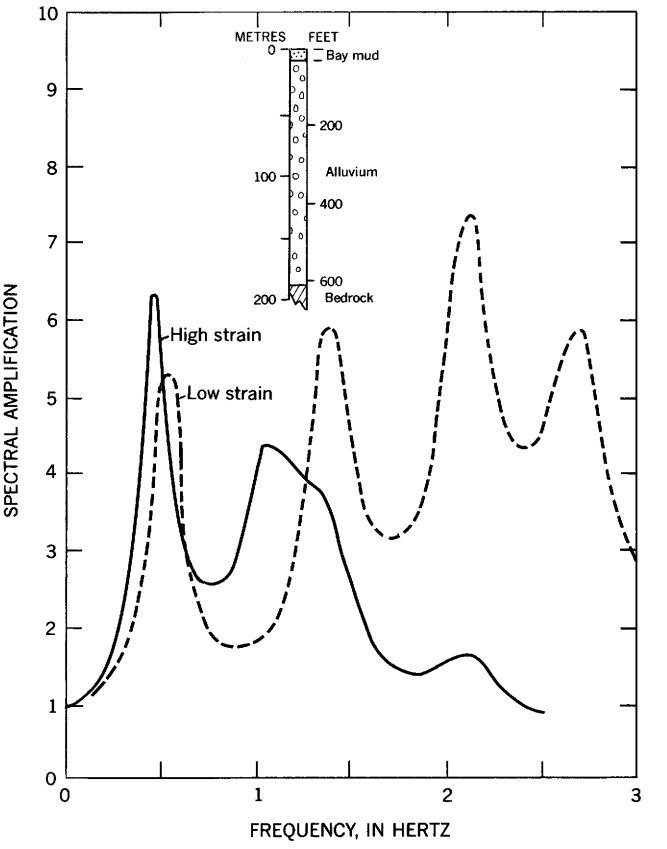

FIGURE 47.—Comparison of high- and low-strain spectral amplification for a site underlain by 11 m (36 ft) of bay mud and 173 m (567 ft) of alluvium. The high-strain spectral amplification was computed by using as input the bedrock motion recorded at the Pacoima Dam, (San Fernando earthquake of February 9, 1971) scaled to a maximum velocity of 12 cm/s (5 in./s).

LIQUEFACTION POTENTIAL

By T. L. Youd, D. R. Nichols, E. J. Helley, and K. R. Lajoie

INTRODUCTION

Liquefaction of clay-free granular layers has produced abundant and sometimes catastrophic ground failures during earthquakes and hence must be considered in assessing seismic risk or hazard. Conditions requisite for seismically induced liquefaction—saturated unconsolidated deposits and high seismicity—are widespread in the San Francisco Bay region. Evaluation of the liquefaction potential of these deposits thus forms an important element in mapping seismic hazards of the area.

This paper describes how a preliminary liquefaction-potential map of part of the San Francisco Bay region was made and describes types of ground failure commonly associated with liquefaction that might be expected to occur in that region. Map zones are based on detailed geologic studies of the unconsolidated sediments (Helley and Brabb, 1971; Helley and others, 1972; Lajoie and others, 1974; Nichols and Wright, 1971). Liquefaction potential is estimated from an analysis of maximum horizontal surface accelerations, duration of ground motion, depth of water table, and depth and standard penetration resistance of clay-free granular sediments. The analysis is based on the "simplified procedure for evaluating liquefaction potential" developed by Seed and Idriss (1971). The results were statistically averaged to provide an estimate of liquefaction potential for each zone.

Liquefaction is defined here as the transformation of a granular material from a solid state into a liquefied state as a consequence of increased pore-water pressures (Youd, 1973). This definition distinguishes liquefaction as a transformation process rather than liquefied flow or a type of ground failure. Hence, a potential for liquefaction does not necessarily indicate a similar potential for ground failure. However, ground failures are common consequences of liquefaction and hence can be expected to occur in areas susceptible to liquefaction.

GEOLOGY AND SEISMICITY OF STUDY AREA

The mapped area is bounded by the East Bay hills on the east, the Santa Cruz Mountains on the west, and by the cities of Oakland on the northeast, San Francisco on the northwest, and San Jose on the south. The area contains the broad alluvial plain surrounding the southern part of San Francisco Bay. This plain is underlain by late Cenozoic sediments that vary greatly in density and degree of consolidation. The sediments are subdivided into units with generally similar geotechnical properties, chosen for mapping liquefaction potential (see Lajoie and Helley, this report). Those sediments whose grain-size distribution (clay-free sand and silt) and degree of lithification (completely uncemented) make them potentially liquefiable occur within two units; the older of these was deposited during late Pleistocene time, and the younger, during Holocene time. Environments of deposition during both the late Pleistocene and Holocene were similar to those of today except that marine and estuarine conditions were absent during parts of the late Pleistocene.

The older deposits are denser and more consolidated and tend to be coarser grained. Because they have been long exposed to weathering processes and changing climatic regimes, they commonly contain well-developed soil profiles. Where exposed, the older deposits are expressed geomorphically as slightly dissected alluvial fans and aprons generally lying at higher altitudes near the margins of the plains, where they gradually merge into the surrounding foothills. Because these fans are in the highest part of the plain, ground-water levels are generally deep but may be temporarily high during wet seasons.

The younger alluvial deposits, which are much looser, wetter, and less consolidated than the older fan deposits on which they rest, grade into the modern sediments of San Francisco Bay. The interfingering of alluvial and estuarine (bay) sediments in these younger deposits reflects the post-Wisconsin marine transgression into the basin of San Francisco Bay.

The San Francisco Bay region is very active seismically, having been subjected to large historic earthquakes originating nearby on both the San Andreas and Hayward faults. For example, the 1906 earthquake (magnitude 8.2) was accompanied by a continuous 306

km (190 mi) surface rupture on the San Andreas fault. The 1868 (and possibly the 1836) earthquake on the Hayward fault also produced significant surface ruptures.

DESIGN EARTHQUAKES

Sediments are classified by liquefaction potential as follows: (1) Sediments likely to liquefy in the event of a moderate earthquake (magnitude 6.5) originating nearby on the San Andreas, Hayward, or other local fault are considered to have a high liquefaction potential; (2) sediments unlikely to liquefy even in the event of a major earthquake (magnitude 8.0) nearby on the San Andreas fault are considered to have a low liquefaction potential; and (3) sediments between these two extremes are considered to have moderate liquefaction potential dependent on earthquake size and duration and sediment properties such as grain size and degree of sorting. A moderate-size event would be characterized by approximately 10 significant strong-motion cycles (Seed and Idriss, 1971) with maximum horizontal surface accelerations of 0.2 g or greater (Page and others, 1972) over much of the area, and a large event by as many as 30 significant strong-motion cycles (Seed and Idriss, 1971) with maximum horizontal surface accelerations of 0.5 g or greater (Page and others, 1972). These parameters are used in the following analyses.

METHOD OF EVALUATING LIQUEFACTION POTENTIAL

The method used to estimate liquefaction potential is based on the "simplified procedure for evaluating liquefaction potential," which was developed for materials that underlie relatively level surfaces (Seed and Idriss, 1971, p. 1249) and have relative densities (D_r)[1] less than about 80 percent (p. 1256). Because slopes on the alluvial plain surrounding San Francisco Bay are small, the method can be applied over most of the area. However, because the large design earthquake could possibly produce liquefaction in sediments with relative densities greater than 80 percent, the procedure of Seed and Idriss was extended to permit evaluation of liquefaction potential for these extreme conditions.

The simplified procedure is based on two basic relations. First, the average cyclic shear stress (τ_{av}), developed during a given earthquake at a depth (h), beneath a level surface is estimated from the equation

$$\tau_{av} \approx 0.65 r_d \gamma h (a_{max}/g), \quad (1)$$

where r_d is an empirically determined stress reduction coefficient, γ is the unit weight of the soil, a_{max} is the maximum horizontal surface acceleration, and g is the acceleration of gravity. (Equation 1 is equation 4 of Seed and Idriss, 1971, p. 1256.) Second, the ratio of in situ cyclic shear stress (τ) required to produce liquefaction in a given number of cycles (l) on laboratory samples molded at the in situ relative density (D_r) to the effective overburden pressure (σ_o') is related to results of laboratory cyclical triaxial compression tests as

$$(\tau/\sigma_o')_{lD_r} \approx C_r (\sigma_{dc}/2\sigma_a)_{l50} (D_r/50) \text{ for } D_r < 80 \text{ percent}, \quad (2)$$

where C_r is a correction coefficient applied to triaxial compression test results, σ_{dc} is the cyclic deviator stress producing liquefaction in l cycles on a remolded sample of the in situ or similar material at a relative density of 50 percent, and σ_a is the initial effective confining pressure. (Equation 2 is equation 6 of Seed and Idriss, 1971, p. 1258.) Empirical curves have been constructed by Seed and Idriss (1971) for estimating C_r and $(\sigma_{dc}/2\sigma_a)_{50}$ from density state and gradational properties of the soil and the number of significant strong-motion cycles. Thus, by comparing the average cyclic shear stress (τ_{av}) developed at any given depth (equation 1) with the cyclic shear stress (τ) required to produce liquefaction of the materials at that depth (equation 2), a criterion is established for assessing liquefaction potential.

For the moderate-size design earthquake, the following parameters were used in equations 1 and 2 to estimate limiting values of relative density at which liquefaction would be likely to occur:

$a_{max} = 0.2\ g$,
$l = 10$ cycles,
$0.8 < r_d < 1.0$,
$0.6 < C_r < 0.7$,
1.44 g/cm^3 $< \rho <$ 1.76 g/cm^3 (90 lb/ft^3 $< \gamma <$ 110 lb/ft^3),
$0.2 < (\sigma_{dc}/2\sigma_a)_{l50} < 0.3$, and
0 m $< h_w <$ 3 m (0 ft $< h_w <$ 10 ft),

where ρ is the density of the material and h_w is depth to the water table. Substitution of reasonable combinations of these values into the equations shows that most granular soils with relative densities less than 65 percent that are located beneath the free water surface would have a high potential for liquefaction during the estimated moderate-earthquake conditions.

To evaluate liquefaction potential for the large design earthquake, it was necessary to extend the simplified procedure to relative densities greater than 80 percent. To do this, data presented by Peacock and Seed (1968) were used to evaluate stress conditions causing liquefaction at these higher densities. Average shear stress ratios (τ/σ_o') producing liquefaction in 30 loading cycles (simple shear) on samples with relative densities

[1]Relative density (D_r), in percent, is defined as

$$Dr = \frac{e_{max} - e}{e_{max} - e_{min}} (100),$$

where e_{max} and e_{min} are void ratios of a given granular material in its loosest and densest states, respectively, and e is the void ratio of the material at the density in question.

ranging from 50 to 90 percent (Peacock and Seed, 1968, p. 701) are

$\tau/\sigma_o' = 0.060$ for $D_r = 50$ percent,
$\tau/\sigma_o' = 0.093$ for $D_r = 80$ percent, and
$\tau/\sigma_o' = 0.152$ for $D_r = 90$ percent.

According to Seed and Peacock (1971, p. 1102), these stress ratio values should be increased 35 percent because of subsequent "improvements in sample preparation and cap seating techniques." They also stated (p. 1102) that the results should be increased by a compounded 15 percent to agree with results using rough platens. Even after applying these corrections, Seed and Peacock (1971, p. 1111) further increased the values by an additional factor (which varies with density) to bring the results into agreement with estimated field behavior. These factors (interpolated from data given by Seed and Peacock (1971, p. 1112)) are

22 percent for $D_r = 50$ percent,
46 percent for $D_r = 80$ percent, and
55 percent for $D_r = 90$ percent.

Thus, estimated stress ratios required to produce liquefaction in the field during 30 cycles of ground motion are

$\tau/\sigma_o' = 0.114$ for $D_r = 50$ percent,
$\tau/\sigma_o' = 0.211$ for $D_r = 80$ percent, and
$\tau/\sigma_o' = 0.366$ for $D_r = 90$ percent.

These data are plotted and a curve (reconstructed curve) drawn through them (fig. 48). A plot of equation 2 also is drawn on figure 48 for comparison. Parametric values used in constructing the latter curve include 30 cycles of ground motion, $(\sigma_{dc}/2\sigma_a) = 0.18$, a minimal (worst condition) value, (see Seed and Idriss, 1971, p. 1257), and C_r values taken directly from curves given by Seed and Idriss (1971, p. 1258).

To facilitate the use of the reconstructed curve for evaluating the liquefaction potential of granular sediments at relative densities greater than 80 percent, equation 2 was modified to

$$(\tau/\sigma_o')_{D_r} \approx M \text{ for } D_r > 80 \text{ percent}, \quad (3)$$

where the value of M is taken directly from the reconstructed curve. Next, τ in equation 3 was equated with τ_{av} in equation 1 to solve for limiting M values at which liquefaction could occur:

$$M \approx 0.65\, r_d (\gamma h/\sigma_o')\, (a_{max}/g). \quad (4)$$

For the large design earthquake, the following parametric values were used: $a_{max} = 0.5g$, $l = 30$ cycles, and other values as given for the moderate-size design earthquake. Substitution of reasonable combinations of these values into equation 4 yields limiting M values between 0.3 and 1.0. This corresponds to relative densities ranging from 87 to 92 percent. (The range is narrow because of the steep slope of the reconstructed curve, figure 48.) Thus, a limiting density of 90 percent was selected as the maximum at which liquefaction might be expected to occur during a large earthquake in the San Francisco Bay region.

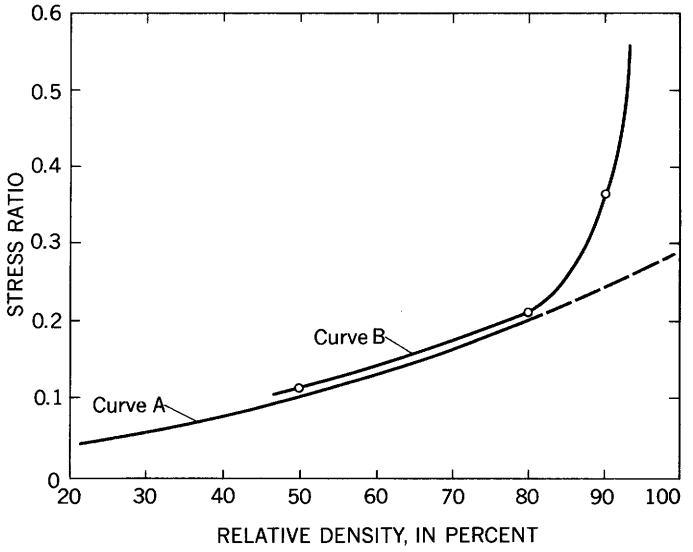

FIGURE 48.—Estimated stress ratio, $(\tau/\sigma_o')_{lD_r}$, required to produce liquefaction under field conditions during 30 cycles of seismic loading. Curve A, plot of equation 2 (equation 6 of Seed and Idriss, 1971). Curve B, reconstructed curve plotted from data given in Seed and Peacock (1971).

The liquefaction-potential criteria can now be summarized as follows: Saturated clay-free granular sediments with relative densities less than 65 percent are considered to have high liquefaction potential, even in a moderate earthquake; clay-free granular sediments with relative densities greater than 90 percent are considered to have low liquefaction potential, even in a major earthquake; and saturated clay-free granular sediments with relative densities between 65 and 90 percent have moderate liquefaction potential that depends on intensity and duration of ground shaking and textural properties of the sediments.

To facilitate application of the liquefaction criteria to field observations, relative densities were estimated from data on standard penetration tests using relations developed by Gibbs and Holtz (1957). This procedure also was used by Seed and Idriss (1971). Standard penetration versus depth curves taken from the relations of Gibbs and Holtz are plotted in figure 49 for relative densities of 65 and 90 percent. Assumed parameters used in constructing these curves include a water-table depth of 3 m (10 ft) at the time of drilling and a dry density of 1.6 g/cm^3 (dry unit weight=100 lb/ft^3).

MAPPING OF LIQUEFACTION POTENTIAL

Boring logs from throughout the study area were collected from numerous private consultants and governmental agencies. Standard penetration data from clay-free granular deposits within 15 m (50 ft) of the

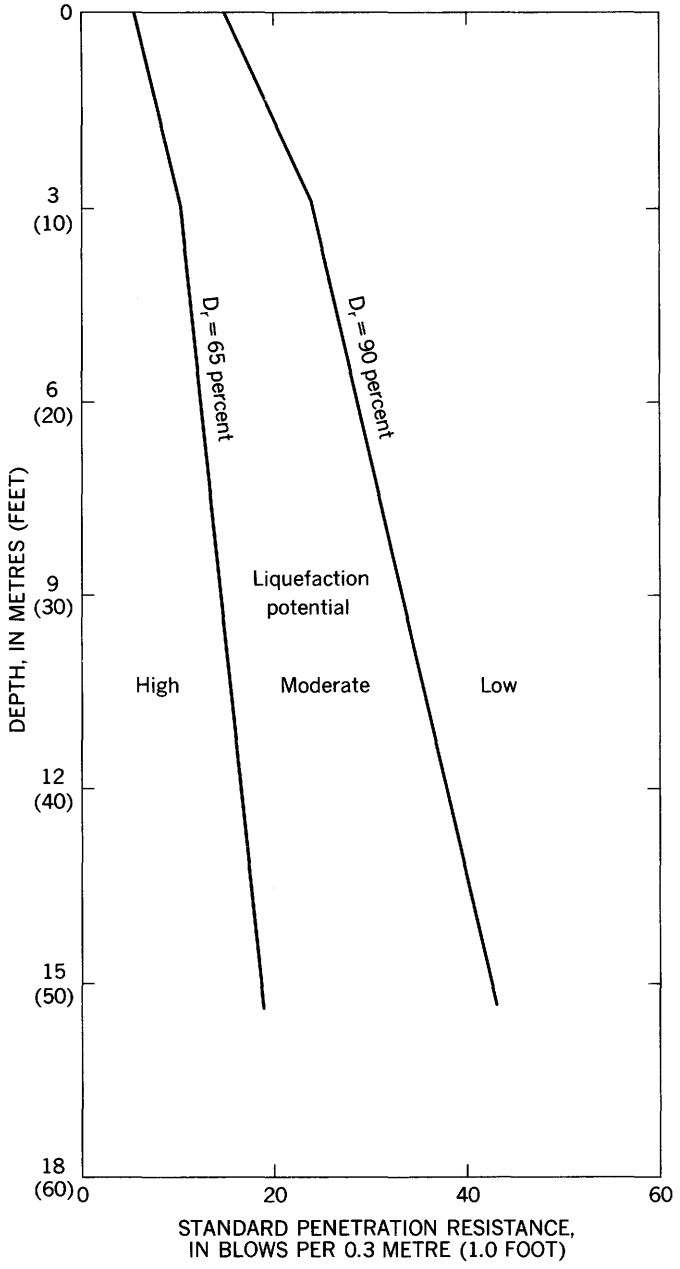

FIGURE 49. Criteria used for estimating liquefaction potential in the field. Based on a correlation between standard penetration resistance and relative density developed by Gibbs and Holtz (1957). Curves are based on the assumption that the water table was 3 m (10 ft) deep when penetration data were obtained from exploratory borings.

surface were compiled and statistically analyzed in each of the generalized map zones shown in figure 50. These zones were derived from geologic maps of unconsolidated sediments (Helley and Brabb, 1971; Helley and others, 1972; Nichols and Wright, 1971; Lajoie and others, 1974.) Zone 1 is an area of bay mud (9,000 years and younger) overlying Holocene and late Pleistocene alluvium. Clay-free granular layers are not generally present in the bay mud but do occur locally near present and former stream channels. Clean granular layers are rather common, however, in the Holocene alluvium and the late Pleistocene alluvium beneath the bay mud. The surficial deposits in zone 2 are Holocene alluvium (less than 10,000 years old) overlying late Pleistocene alluvium. This zone is subdivided on the basis of water-table depth. Areas in which the water table is normally at 3 m (10 ft) or less are labeled 2a. Areas with a deeper water table are labeled 2b. The Holocene alluvium is generally greater than 3 m (10 ft) thick in subzone 2a and thus extends below the water table. Hence, the Holocene alluvium in this zone has a continual potential for liquefaction. In subzone 2b, the Holocene alluvium is generally less than 3 m (10 ft) thick and thus is normally above the water table. It therefore has at most only a seasonal potential for liquefaction. Zone 3 is an area of late Pleistocene alluvium consisting of overconsolidated alluvial-fan deposits that extend to a considerable depth.

Table 5 summarizes the percentages of available standard penetration test data plotting in each category of liquefaction potential for each geologic unit. The data show that granular layers within the bay mud (zone 1) have a generally high potential for liquefaction. Seventy-three percent of the penetration data from these layers indicate high potential for liquefaction, and an additional 21 percent indicate moderate potential. Only 6 percent of the penetration data indicate low potential.

The granular layers beneath the bay mud (zone 1) show a much lower, but still significant, potential for liquefaction. Thirty-three percent of the data from these layers indicate high potential for liquefaction, and an additional 28 percent suggest moderate potential. The overall liquefaction potential of this unit is classed as moderate. Virtually all the bay mud and the deposits underlying the bay mud lie below the normal groundwater table; thus, they present a persistent potential for liquefaction.

Clay-free granular layers within the Holocene alluvium in zone 2 show on the average less potential for liquefaction than those within or beneath the bay mud because of both their greater density and the greater depth of the water table. Their potential, however, is still classed as moderate. Twenty-two percent of the penetration values for these sediments indicate high potential for liquefaction, an additional 33 percent indicate moderate liquefaction potential, and 45 percent indicate low potential. The Holocene alluvium of subzone 2b would be, at most, seasonally or intermittently liquefiable because it is normally above the water table. Although not specifically shown in figure 50 or table 5, granular layers in the relatively recent channel and

overbank deposits along present drainage ways are generally characterized by lower penetration resistance and, consequently, higher liquefaction potential than deposits in the adjacent alluvial plains.

Liquefaction potential of granular layers in the late Pleistocene alluvium (zone 3) is generally low. Only 11 percent of the penetration values from these sediments indicate high potential for liquefaction, whereas 60 percent indicate low potential. Liquefaction potential in this zone is further diminished by a relatively high topographic position and hence a deep water table.

TABLE 5.—*Summary of the analysis of liquefaction potential using standard penetration data and criteria plotted in figure 49*

[Two probable local earthquakes are considered; (1) a moderate event (magnitude ≈6.5) and (2) a large event (magnitude 8.0). Sediments likely to liquefy during a moderate event are classified as having high liquefaction potential; those unlikely to liquefy during a large event are classified as having low liquefaction potential; and those between these two categories are classified as having moderate liquefaction potential]

Zone	Sedimentary unit	Standard penetration test data			
		Percent indicating			Number of tests
		D_r<65 percent (high liquefaction potential)	65 percent<D_r<90 percent (moderate liquefaction potential)	D_r>90 percent (low liquefaction potential)	
1	Deposits within bay mud	73	21	6	53
1	Deposits underlying bay mud	33	28	39	155
2a, 2b	Holocene alluvium	22	33	45	708
3	Late Pleistocene alluvium	11	29	60	357

GROUND FAILURES ASSOCIATED WITH LIQUEFACTION

Three types of ground failure are commonly associated with liquefaction (Seed, 1968; Youd, 1973). (1) Flow landslides are failures that generally occur on moderate to steep slopes underlain by loose granular deposits. In this case, once liquefaction has occurred, flow deformation commences and continues unabated until the driving shear forces are reduced (as by slope reduction) to a value less than the viscous shear resistance of the liquefied soil. When that state is reached, the material stops flowing and solidifies, usually far from the point of origin. Loose granular deposits on moderately to steeply sloping hillsides in the San Francisco Bay region could be susceptible to this type of failure if they were saturated. Such failures occurred on San Bruno Mountain near Colma and near Half Moon Bay during the 1906 San Francisco earthquake (Crandall, in Lawson, 1908, p. 249; Anderson, in Lawson, 1908, p. 395). Because of the generally small slopes, it is unlikely that this type of failure would occur on the broad alluvial plain surrounding San Francisco Bay.

(2) Lateral-spreading landslides are failures that occur most commonly on gentle to nearly horizontal slopes underlain by loose to moderately dense granular deposits or layers. In this type of failure, liquefaction occurs and flow commences; however, after a finite displacement, flow is arrested by a drop in pore-water pressure resulting from the tendency for all but very loose granular sediments to dilate during shear. Continued shaking may cause reliquefaction (provided the shaking causes reversals in shear stress (Seed and Lee, 1969; Youd, 1973)), and a second episode of flow displacement may occur followed by restabilization. This sequence may continue as long as strong shaking continues. Displacements ranging from nearly zero to tens of metres have been produced by these kinds of failures (Varnes, 1958; Youd, 1973). Factors that contribute to greater displacement include greater duration of shaking, loose sediments, and optimal slope conditions. (Slopes that are too flat inhibit movement, and slopes that are too steep inhibit reversals in shear stress necessary for the generation of repeated episodes of liquefaction (Youd, 1973).) Cracks, fissures, and differential settlement are common on, and especially at the margins of, lateral-spreading failures. Although these features and accompanying slide movements may appear rather inconsequential in open terrain, they have proved to be very damaging and disruptive to structures and utilities constructed across, on, or within the slide mass.

Lateral spreading probably would be the most pervasive type of ground failure associated with liquefaction on the broad alluvial plain surrounding San Francisco Bay. Sediments containing granular layers, especially the bay mud and recent channel and overbank deposits in the Holocene alluvium, probably would be the materials most susceptible to this type of failure because of their greater potential for liquefaction and generally uncompacted state, which would permit greater slide movement after liquefaction. Least susceptible to this type of failure would be the late Pleistocene alluvium (zone 1) because of its low potential for liquefaction and generally dense state, which in turn would prevent significant displacements from occurring even if liquefaction should develop.

Evidence of lateral spreading was reported at several places within the study area during the 1906 San Francisco earthquake. Most of these slides occurred in the susceptible areas listed above. For example, lateral ground movements, some as large as 2 m (6 ft), occurred in several areas of San Francisco where artificial fill is underlain by bay mud (zone 1) (Wood, in Lawson, 1908, p. 220–245). In addition, lateral displacement of floodplain deposits toward the depressions of Alameda and Coyote Creeks was mentioned specifically (Lawson, 1908, p. 400). Many lateral-spreading landslides generated by the 1906 earthquake may not have been re-

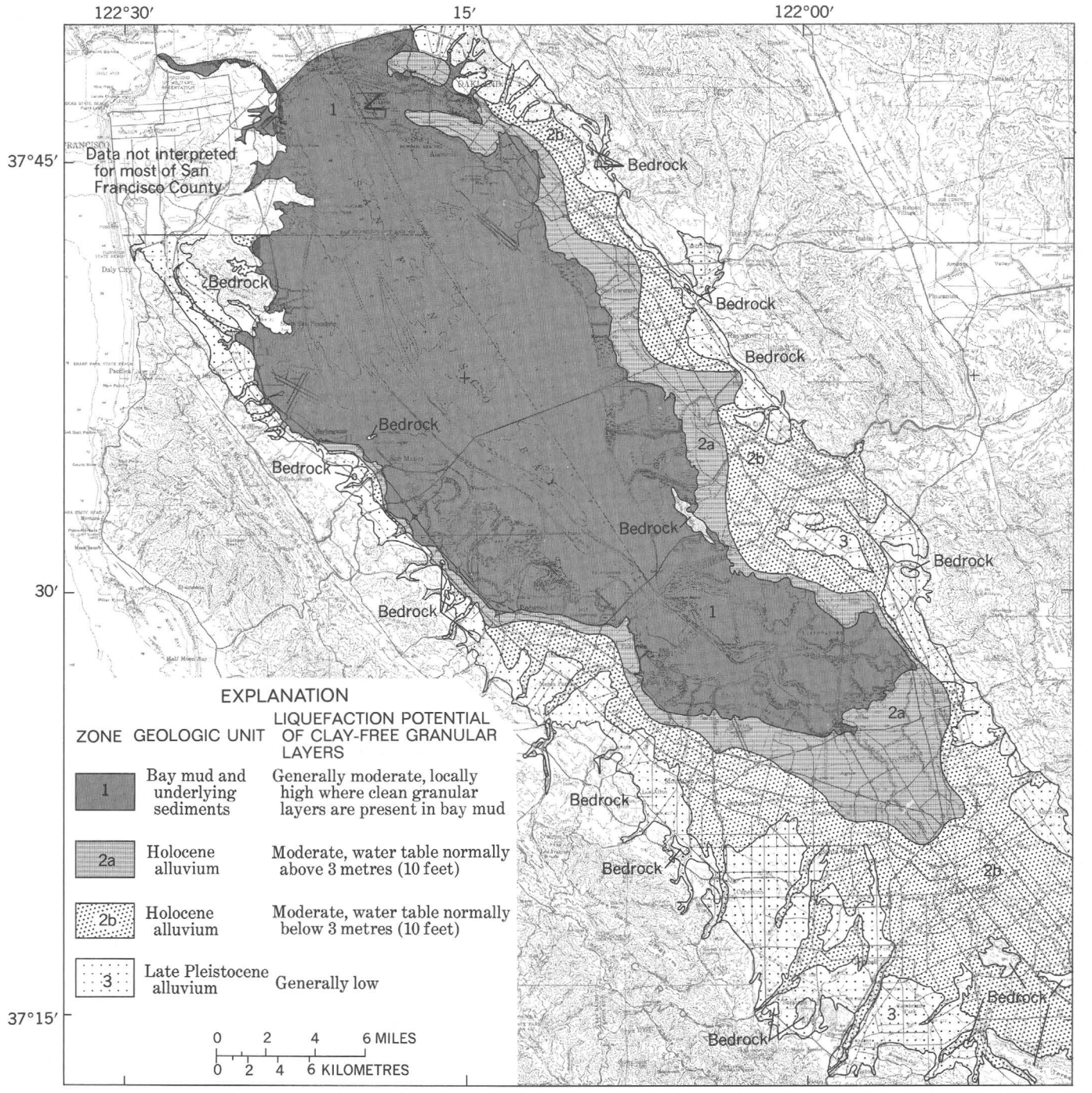

FIGURE 50.—Preliminary map showing liquefaction potential for the southern San Francisco Bay region. The map shows generalized liquefaction potential of granular layers in each map zone but does not delineate locations of these layers. Hence, the map is useful for designating zones where special consideration should be given to the possibility of liquefaction but is not valid for assessing the liquefaction potential of a given site.

corded, especially in undeveloped areas near the bay that were not thoroughly investigated.

(3) Quick-condition failures have occurred historically most often in flat areas with high water tables and loose to moderately dense granular sediments extending from near the surface to substantial depths. In this situation liquefaction may lead to a quick condition and often to the loss of bearing capacity with the result that structures, embankments, or other loads founded on the surface sink into the liquefied sediments. At the same time buried tanks or other vessels may rise buoyantly. Other than subsidence of several roadway fills in San

Francisco, which may or may not have been due to liquefaction, the authors have found no reports that this type of failure occurred in the study area during the 1906 San Francisco earthquake.

SUMMARY

A preliminary map of liquefaction potential has been compiled for the southern San Francisco Bay region. This map delineates zones in which existent clay-free granular layers are estimated to have low, moderate, or high liquefaction potential. The map zones are derived from detailed geologic studies of the unconsolidated sediments in the region. Liquefaction potential of the granular layers is estimated from an analysis of lithologic, water table, standard penetration, and seismic data.

Areas underlain by bay mud containing clay-free granular layers have a generally high potential for liquefaction. Granular layers underlying the bay mud have a significant but lower potential, which is classed herein as moderate. Granular layers within the Holocene alluvium have an even lower, but still moderate, potential; furthermore, most of this unit is normally above the water table and thus, at most, is only seasonally or intermittently susceptible to liquefaction. Clay-free granular layers within channel and recent overbank deposits of the Holocene alluvial unit generally are characterized by a greater liquefaction potential than adjacent deposits in the alluvial plain. Granular layers in the late Pleistocene alluvium generally have low potential for liquefaction.

Zones delineated in this study as having significant liquefaction potential indicate areas in which the liquefaction process may occur in existing clay-free granular layers; unfortunately, insufficient data are presently available to plot the actual locations of these layers. The data also give no indication of type or amount of ground failure, if any, that might follow liquefaction. However, lateral-spreading landslides are a common consequence of liquefaction beneath gentle slopes. Hence, in the event of a major earthquake, this type of failure is likely to be a result of liquefaction beneath the alluvial plain surrounding San Francisco Bay. Reports from the 1906 San Francisco earthquake verify this conclusion.

The criteria used for evaluating liquefaction potential are based on empirical procedures formulated by Seed and Idriss (1971) and approximate estimates of ground-motion parameters and geotechnical properties. In addition, the estimated potential of each zone is based on somewhat limited data generalized to include the entire map unit. Thus, the map of liquefaction potential must be considered preliminary and approximate and not valid for direct determination of liquefaction potential at any specific site. However, despite its limitations, the map should serve the intended purpose of generally delineating areas where the probability that liquefaction will occur during a major earthquake is greatest and hence areas where special attention is required.

LANDSLIDES

By T. H. Nilsen and E. E. Brabb

INTRODUCTION

Landslides are characteristically abundant in areas of high seismicity and steep slopes. Landslides associated with earthquakes may cause as many or more fatalities as the initial fault rupture and shaking of the ground. They may also occur long after an earthquake, having been caused or aided by the loosening, shaking, and disruption of the deposits on slopes during the earthquake. As a result, the landslide hazards related to earthquakes may persist long after the ground has stopped shaking and therefore can be a long-term problem.

Some of the major earthquakes that have occurred during the past 15 years have vividly demonstrated the hazards of seismically triggered landslides. The Hebgen Lake, Mont., earthquake of 1959 triggered a very large landslide (fig. 51) that killed and injured many people, formed a temporary lake, and blocked travel in the area (Hadley, 1964, fig. 54). The Anchorage, Alaska, earthquake of 1964 triggered both extensive subaerial (fig. 52) and submarine landslides; tsunamis (seismic sea waves) generated by the submarine landslides caused extensive damage and many fatalities in coastal areas (Hansen and others, 1966). The earthquake in western Peru in 1970 triggered a massive debris avalanche (fig. 53) that destroyed the cities of Yungay and Ranrahirca; it caused probably about one-half of the 38,000 fatalities attributed to the earthquake (Plafker and others, 1971). The San Fernando, Calif., earthquake of February 9, 1971, triggered more than 6,000 individual landslides in the surrounding upland areas, most of them of small size (fig. 54); however, only a few damaged manmade structures because residential and industrial development had been restricted almost wholly to the relatively flat floor of the San Fernando Valley (Morton, 1971; oral commun., September 1973).

Each of the major earthquakes described above had magnitudes greater than 6.5. Although smaller earthquakes may cause less damage (or none) to manmade structures by ground shaking, they are capable of triggering slope failures in hillside areas, especially renewed movements of old, marginally stable landslide deposits. For example, an earthquake in February 1972, with magnitude 5.0 and epicenter located 37 km (23 mi) south of Hollister, Calif., triggered considerable downslope movement on a large old landslide deposit on Halls Ranch, near Paicines (fig. 55; Rogers, 1972). Had

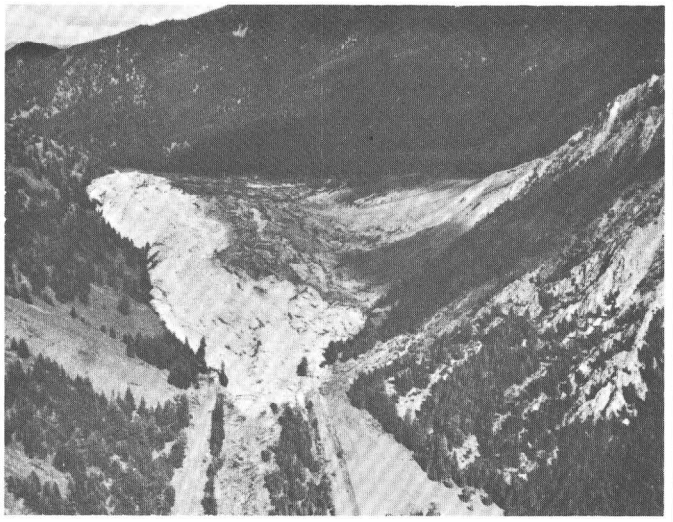

Figure 51.—Earthquake-generated landslide at Hebgen Lake, Mont. This landslide, one of the largest ever recorded in the United States, was responsible for 26 fatalities and many injuries during the August 17, 1959, earthquake (magnitude 7.1). Photograph by U.S. Forest Service.

Figure 52.—Oblique aerial view of Turnagain Heights landslide in Anchorage, Alaska, triggered by earthquake of March 27, 1964 (magnitude 8.4). The landslide destroyed more than 75 homes. Photograph by U.S. Army.

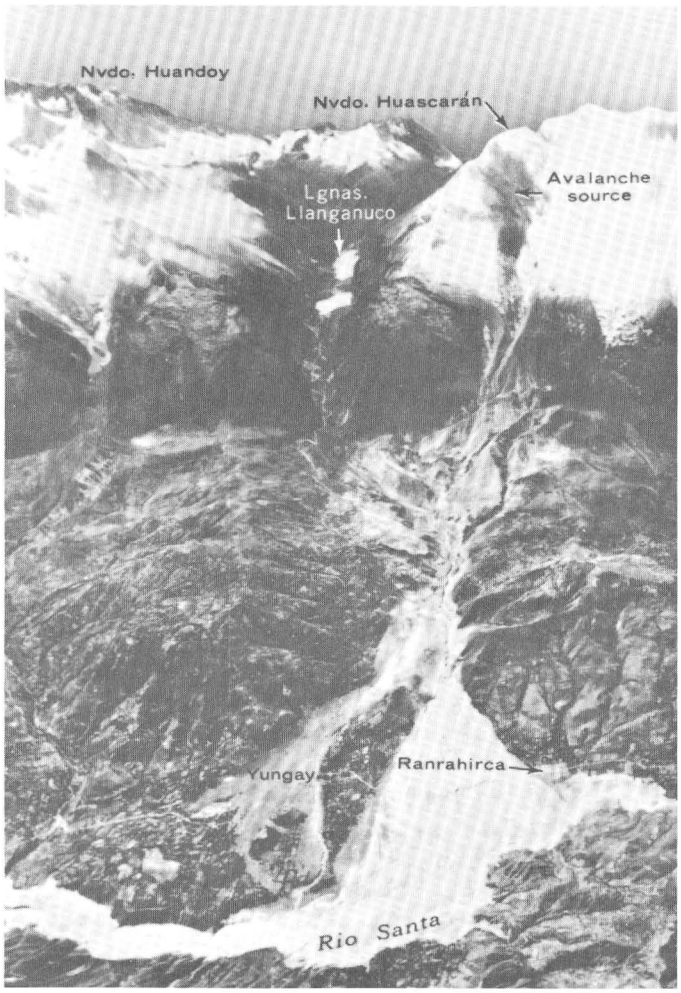

FIGURE 53.—Oblique aerial view of debris avalanche that destroyed the towns of Yungay and Ranrahirca in western Peru during the earthquake of May 31, 1970. The avalanche originated at an altitude between 5,500 and 6,400 m (18,000 and 21,000 ft) and moved 2.4 km (1.5 mi) downslope to the Rio Santa at a speed in excess of 280 km/hr (175 mi/hr) (Plafker and others, 1971, p. 550–558). More than 18,000 people were killed by the avalanche, and an additional 20,000 persons were killed by other effects of the earthquake.

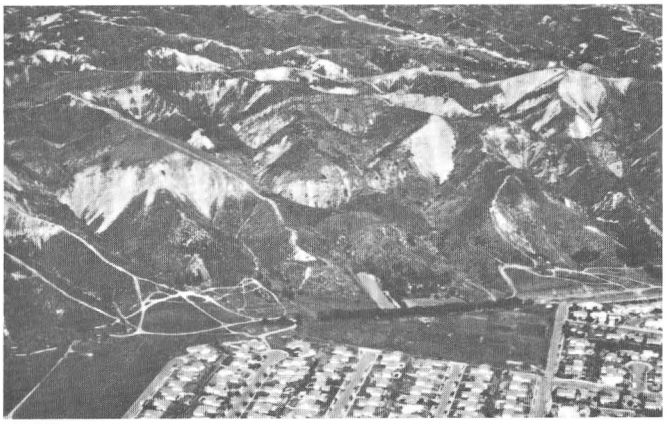

FIGURE 54.—Oblique aerial view of landslides (white patches) in Lopez Canyon area, north of San Fernando, Calif., triggered by the earthquake of February 9, 1971 (magnitude 6.6). Photograph by D. M. Morton.

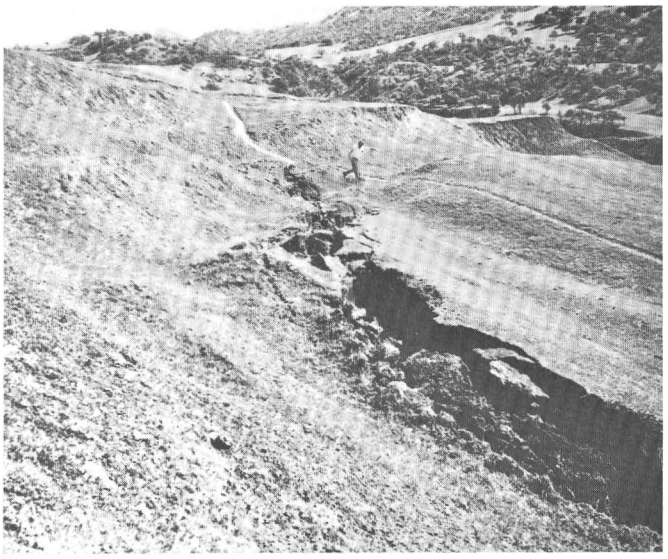

FIGURE 55.—Transverse cracks formed in upper part of old landslide deposit on Halls Ranch near Paicines, central California, by renewed movement during a moderate earthquake (magnitude 5.0) in February 1972. Photograph by T. H. Nilsen.

the hillside area been developed for residential purposes at the time of the earthquake, considerable damage might have resulted.

The most extensive records of seismically triggered landslides in the San Francisco Bay region are descriptions of the California earthquake of April 18, 1906, and the San Francisco earthquake of March 22, 1957. The 1906 earthquake triggered many landslides throughout the bay region (Lawson and others, 1908, p. 389–399). Photographic evidence and eyewitness accounts indicate that the earthquake triggered many different types of landslides, resulting in several fatalities and major damage to nearby manmade structures. Fortunately, in 1906 most of the residential and industrial development was concentrated along the gently sloping margins of San Francisco Bay and in some interior valleys, and so the total amount of damage caused by the numerous landslides was not catastrophic.

Some landslides that occurred in 1906 provide useful background data for predicting slope failures in future earthquakes. Earthflow-type landslides were triggered locally on very gently sloping surfaces where the ground moisture content was high (fig. 56*A*); under normal conditions, very few landslides in the San Francisco Bay region develop on slopes of less than 15 percent (Bonilla, 1960a; Brabb and others, 1972; Nilsen and others, 1974). Other earthflow-type landslides developed on steeper slopes, and some were observed to have moved during short periods of time (figs. 56*B, C*). Because the

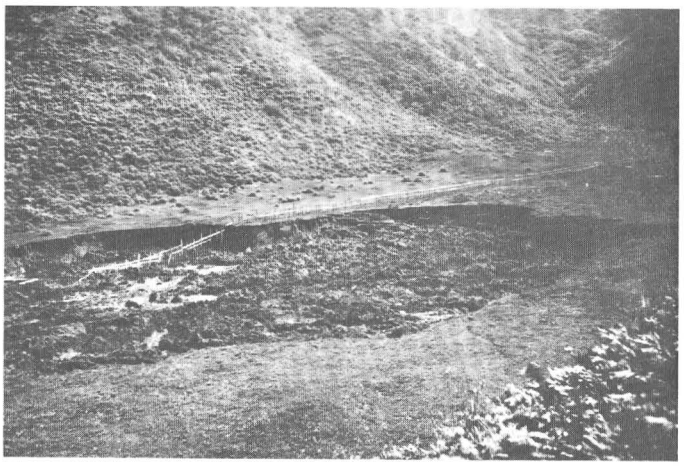

A

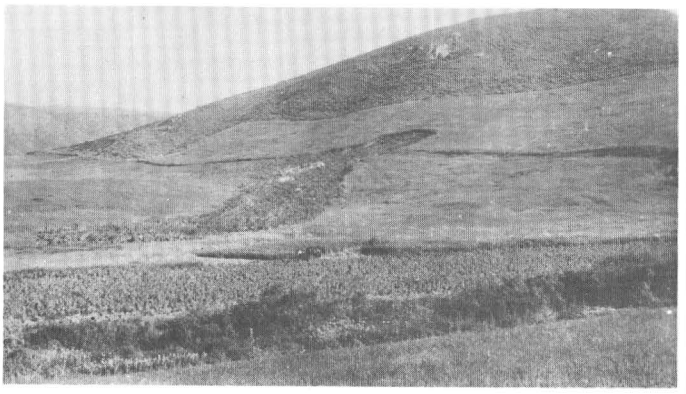

B

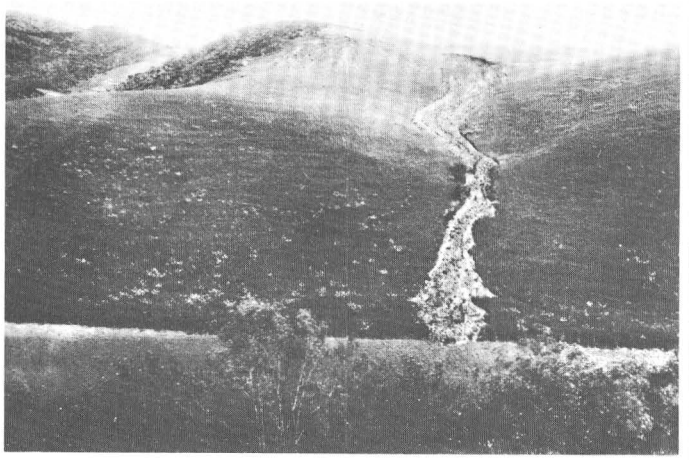

C

FIGURE 56.—Earthflow-type landslides triggered by the earthquake of April 18, 1906 (magnitude 8.3), near Half Moon Bay, Calif. *A*, Landslide on very gentle slope in water-saturated ground. The scarp is about 3 m (10 ft) high. Photograph 66 of J. C. Branner collection. *B*, Landslide on steeper slope in same general area as *A*. Photograph 69 of J. C. Branner collection. *C*, Landslide at Nunez Ranch. The flow originated about 150 m (500 ft) above the valley floor and took about half an hour to reach the base of the hill (Lawson and others, 1908, p. 397). Photograph 64 of J. C. Branner collection. Note: This photograph and others from the Branner and Gilbert collections are available for inspection at the U.S. Geological Survey library, Menlo Park, Calif.

1906 earthquake occurred in April, at the end of the rainy season, the ground probably was particularly susceptible to failure by earthflow processes because of high moisture content.

Other landslides triggered in 1906 damaged manmade structures such as railroads located in coastal areas (fig. 57). Some landslides that occurred a year or more after the earthquake were probably initiated by the earthquake. In one such example from the northern San Francisco Bay region (fig. 58), open fractures in the ground appeared immediately after the earthquake, but massive failure did not occur until the next rainy season.

The 1957 earthquake occurred near Daly City. Although the earthquake was of only moderate magnitude (5.3), it triggered landslides that caused considerable damage to manmade structures (fig. 59; Bonilla, 1959).

Landsliding is a severe and continual problem in the

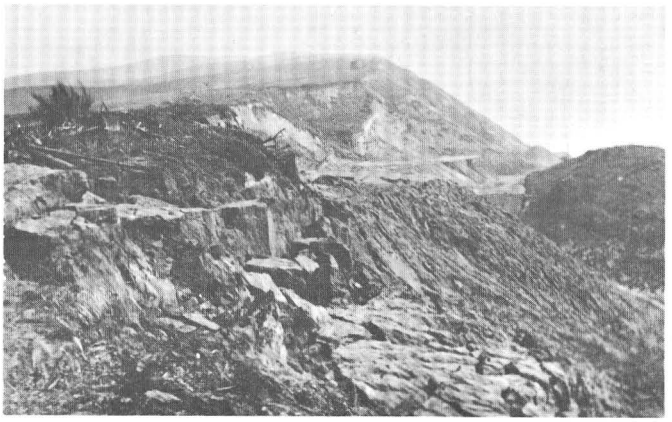

FIGURE 57.—Roadbed of the coastal Ocean Shore railroad, south of San Francisco, damaged by landslides triggered by the 1906 earthquake. Photograph 78 of J. C. Branner collection.

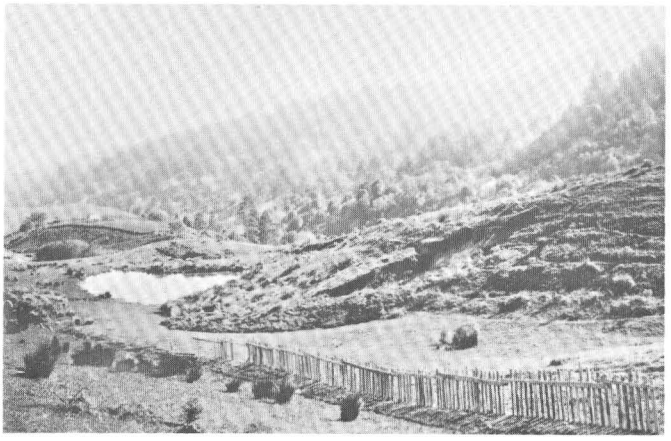

FIGURE 58.—Landslide located about 6 km (4 mi) north of Bolinas Lagoon, Marin County, Calif., generated in March 1907. Cracks that formed during the earthquake of April 1906 contributed to the triggering of this landslide. Photograph 34 of the G. K. Gilbert collection.

FIGURE 59.—Landslides in artificial fill along the shore of Lake Merced, near San Francisco, triggered by the San Francisco earthquake of March 22, 1957 (magnitude 5.3). Photograph by M. G. Bonilla.

San Francisco Bay region, as indicated by the high annual costs of landslide damage. Taylor and Brabb (1972) estimated an overall public and private cost in the bay region of more than $25 million from landslides generated during the rainy season of 1968–69. In another study Nilsen and Brabb (1972) determined that a single landslide, which has been active over a period of at least 10 years, cost the city of San Jose more than $750,000.

This brief review of the effects and history of landsliding in the San Francisco Bay region and other areas points out the severity of the problem and the magnitude of the potential hazard. However, we are only beginning to understand many aspects of the problem and are only in the early phases of developing methods for predicting the location, distribution, and types of landslides that would be triggered by a major earthquake in the bay region. Prediction of an individual slope failure for a given earthquake requires an understanding of all the factors that contribute to the slope-failure process and detailed investigations of specific site characteristics. Such detailed information is not available on a regional scale in the San Francisco Bay region. Our work has included (1) historical studies of landsliding during past earthquakes, (2) mapping of old landslide deposits, (3) study of bedrock units that are susceptible to landsliding, (4) studies of recent landsliding and its relation to slope, bedrock geology, rainfall, and areas underlain by old landslide deposits, (5) the effects of development and construction activities on landsliding, and (6) some of the economic costs associated with landsliding.

This report briefly describes landslide processes, discusses basic data pertinent to analyzing the landslide problem on a regional scale, and utilizes these data to delineate areas within the San Francisco Bay region with various levels of landslide susceptibility during earthquakes.

PREVIOUS WORK

Most previous geologic studies in the bay region have focused on bedrock units and their structural and stratigraphic relations rather than on surficial deposits and their slope-stability characteristics. Consulting engineering geologists have examined the slope-stability characteristics of many small parcels of land in detail, but little of this work has been published; moreover, few regional studies have been undertaken by either consultants or governmental agencies. Some of the earlier studies concerned with landslides, slope-stability characteristics, and engineering properties of bedrock and surficial units provided data and valuable contributions to our studies. These include studies by Schlocker, Bonilla, and Radbruch (1958), Bonilla (1960a, 1960b, 1971), Radbruch (1957, 1969), Radbruch and Weiler (1963), Kojan, Foggin, and Rice (1968), Harding (1969), Clague (1969), Pampeyan (1970), Rogers (1971), Waltz (1971), Huffman (1972a, b), Rice and Strand (1972), Burnett (1972), Radbruch and Wentworth (1971), Taylor and Brabb (1972), Nilsen and Turner (1974), and Nilsen, Taylor, and Brabb (1974). These and current studies have yielded important data for analyzing the landslide problem on a regional scale.

LANDSLIDE PROCESSES

Landslides are the downward and outward movement of slope-forming materials composed of natural rock, soils, artificial fill, or combinations thereof (Eckel, 1958, pl. 1). They move along surfaces of separation by falling, sliding, and flowing, giving rise to many characteristic features (fig. 60).

Landslide deposits range in appearance from clearly discernible, largely unweathered and uneroded topographic features to indistinct, highly weathered and eroded features recognizable only by their characteris-

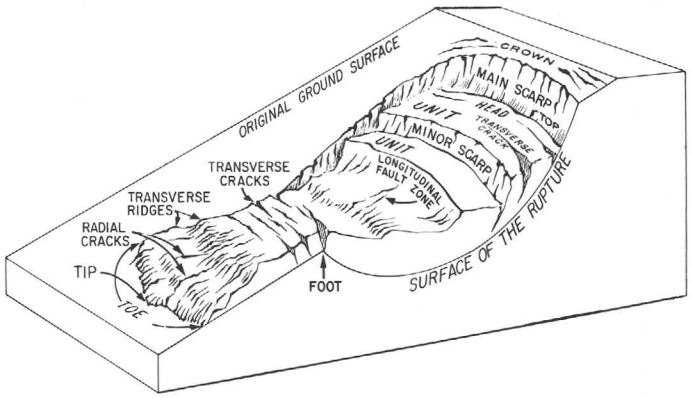

FIGURE 60.—Nomenclature of parts of a landslide (from Eckel, 1958).

tic topographic configurations. Topographic and associated features useful in recognizing landslide deposits include (1) small isolated ponds, lakes, and other closed depressions, (2) abundant natural springs, (3) abrupt and irregular changes in slope and drainage pattern, (4) hummocky irregular surfaces and flat or backtilted areas, (5) smaller landslide deposits that are commonly younger and form within older and larger landslide deposits, (6) steep, arcuate scarps at the upper edge of the deposit, (7) irregular soil and vegetation patterns, and (8) disturbed vegetation.

Landslides commonly are classified by the type of material underlying the slope before it moved, by the type of movement, and by the amount of water in the material. Four common types of landslides found in the San Francisco Bay region are shown in figure 61.

The formation of landslides under national conditions is affected by (1) type of earth materials—unconsolidated, soft sediments or surficial deposits will move downslope easier than consolidated, hard bedrock; (2) structural properties of earth materials—the orientation of the layering of some rocks and sediments relative to slope directions, as well as the extent and type of fracturing and crushing of the materials, will affect landslide potential; (3) steepness of slopes—landslides occur more readily on steeper slopes; (4) water—

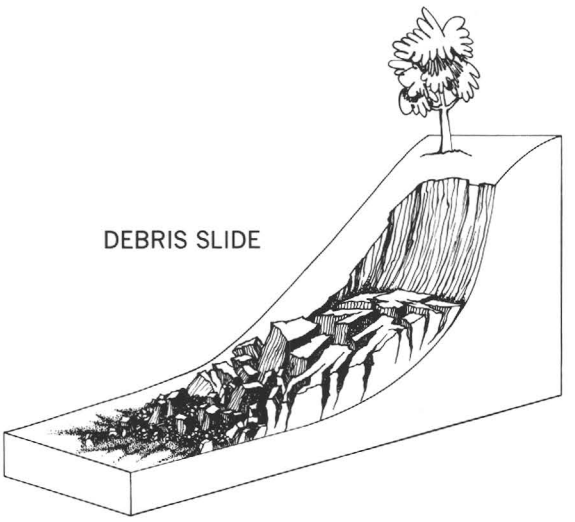

Incoherent or broken masses of rock and other debris that move downslope by sliding on a surface that underlies the deposit

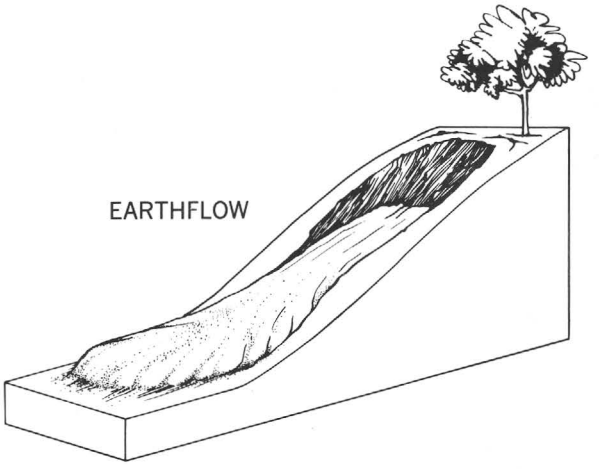

Colluvial materials that move downslope in a manner similar to a viscous fluid

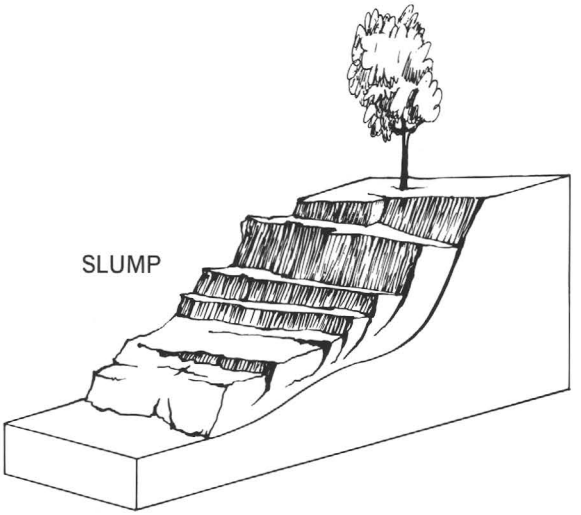

Coherent or intact masses that move downslope by rotational slip on surfaces that underlie as well as penetrate the landslide deposit

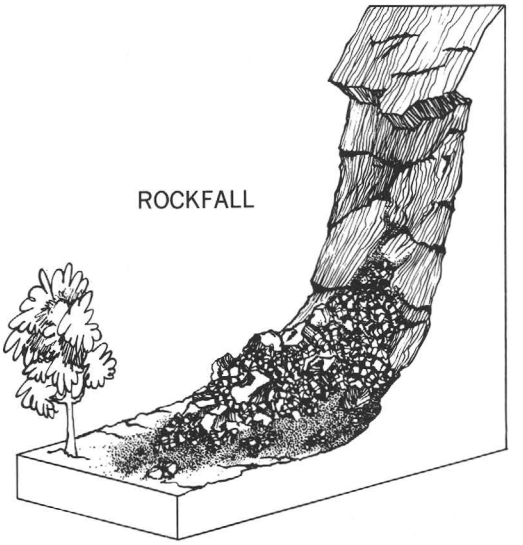

Rock that has moved primarily by falling through the air

FIGURE 61.—Common types of landslides in the San Francisco Bay region.

landsliding is generally more frequent in areas of seasonally high rainfall because the addition of water to earth materials commonly decreases their resistance to sliding; water decreases cohesive forces that bind clay minerals together, lubricates surfaces along which slippage may occur, adds weight to surficial deposits and bedrock, reacts with some clay minerals, causing volume changes in the material, and mixes with fine-grained unconsolidated materials to produce wet, unstable slurries; (5) type of vegetation—trees with deep penetrating roots tend to hold bedrock and surficial deposits together, thereby increasing ground stability; (6) proximity to areas undergoing active erosion —rapid undercutting and downcutting along stream courses and shorelines makes slopes in these areas particularly susceptible to landsliding; (7) earthquake-generated ground shaking—strong ground shaking can trigger failures at the time of the earthquake and can jar and loosen hillside materials leading to failure at some later time.

These are some of the many complex interrelated factors that may contribute to the formation of landslides, with earthquake-generated ground shaking being only one of several possible triggering mechanisms. The prediction of a slope failure at a specific site from a specified level of ground shaking requires an analysis of all such factors, as well as very detailed and expensive onsite investigations. Because such information is not available on a regional scale and we are only beginning to understand the landslide problem, we have approached the study of earthquake-induced landslides on a regional scale by trying to delineate relative slope stability on the basis of physical properties. Because landslides triggered by the 1906 earthquake occurred throughout the San Francisco Bay region, delineation of unstable areas according to their physical characteristics provides a guide to those areas most susceptible to earthquake-induced landsliding.

SLOPE STABILITY ANALYSIS ON A REGIONAL SCALE

Relative slope stability maps can be prepared in various ways and from various types of information. No generally applicable formula or technique has been developed that covers all situations and all areas. Different techniques have been used to prepare relative slope stability maps for different areas, at different scales, for different purposes, and from different types of information. Many examples of the widely divergent form and style of such maps have been published in recent years for California (Blanc and Cleveland, 1968; Johnson and Ellen, 1965; Johnson and Lobo-Guerrero, 1968; Rogers, 1971; Brabb and others, 1972; Rice and Strand, 1972; Huffman, 1972a, 1972b, 1974; Burnett, 1972; Frame, 1973; Radbruch and Wentworth, 1971; Saul, 1972) and for other parts of the United States (Bailey, 1971; Van Horn, 1972a, b, c; Williams, 1972; Scott, 1972; Maberry, 1972a, 1972b; Simpson, 1973a, 1973b).

Complexly interrelated factors contribute to the generation of landslides, and engineering geologists commonly spend months preparing sophisticated analyses of soil and rock-strength parameters, precipitation records, slope geometry, and other factors to determine the causes of individual landslides. To cover an area as large as the San Francisco Bay region (19,300 km^2) (7,450 mi^2), no such detailed analysis could be made owing to limitations of time, personnel, and available data. Instead we utilized data that (1) were available at the present, (2) were available throughout the entire map area, (3) could be incorporated easily into the slope-stability analysis, and (4) yielded information about some of the most important factors that control slope stability. The only data that met all these criteria were landslide distribution, slope, and bedrock geology.

LANDSLIDE DISTRIBUTION

Numerous studies in the bay region and elsewhere have shown that most landslides in a particular year occur in areas of previous landsliding (Nilsen and Turner, 1974; Kojan, 1973; Bailey, 1971). Commonly the new landsliding consists of renewed movements of old landslides triggered by earthquakes, unusually intense rainfall, and (or) man's activities. Hence, the preparation of maps showing the distributuion of present landslide deposits is a first step toward delineating areas likely to fail in the future. In addition, such maps are useful for identifying major factors contributing to the formation of landslides.

Maps showing the distribution of landslides in most of the San Francisco Bay region have been prepared for this purpose at a scale of 1:62,500, primarily by photointerpretation with a minimum of field checking. This technique is necessary because of the large size of the area, the inaccessibility of much of it, and time limitations. The photointerpretive techniques depend upon the recognition of scarps, anomalous bulges and lumps, hummocky topography, ridge-top depressions and trenches, terraced or backtilted slopes, abrupt changes in slope, altered stream courses, discontinuous drainage patterns, closed depressions, springs, and anomalous color, texture, shade, vegetation, and bedrock patterns. A number of maps have been published, and many others are in preparation (Brabb and Pampeyan, 1972; Nilsen, 1971, 1972a, b, c, d, 1973a, b, c; Sims and Nilsen, 1972; Burnett, 1972; Rice and Strand, 1972).

An example of the landslide distribution in San

Mateo County as mapped by Brabb and Pampeyan (1972) is shown in figure 62. The inventory shows the presence of more than a thousand landslide deposits in the region and indicates that landsliding is one of the major erosional processes. Recently, a map of the distribution of landslide deposits in the nine-county San Francisco Bay region was compiled at a scale of 1:125,000 for a slope-stability analysis of the entire region by Nilsen and Wright (unpub. data). An example from the northeastern bay region is shown in figure 63.

Although the type of movement, date of most recent activity, and nature of landslide materials were not determined, the maps by themselves can be used as a general guide to areas where landslides may be a problem; they provide a regional picture of the past history of landsliding, and they are useful to planners and engineering geologists in making preliminary appraisals of building sites.

In addition to the landslide-distribution maps, an isopleth map has been prepared for the southern San Francisco Bay region (Wright and Nilsen, 1974; Wright and others, 1974). This map shows contours depicting variations in geographic density of landslide deposits and permits rapid, quantitative evaluations of the abundance of landslide deposits in different areas.

Landslide deposits are abundant along some active faults or parts of active faults and uncommon along others. Where abundant, they may be related to either seismicity along the fault zone, the weak, crushed rocks found in the fault zone, or both. Abundant landslide deposits have been mapped along the Calaveras fault and along some parts of the San Andreas and Hayward faults. The maps of landslide deposits permit correlations and comparisons of the distribution of landslide deposits with other factors, but so far they have not in themselves permitted the recognition of those landslide deposits that were originally triggered by earthquakes.

SLOPE

Degree of slope is an important parameter controlling the stability of hillside materials. A slope map of the San Francisco Bay region has been prepared by the U.S. Geological Survey (1972) at a scale of 1:125,000.

Studies by Bonilla (1960a), Brabb, Pampeyan, and Bonilla (1972), and Nilsen, Taylor, and Brabb (1974) showed that in the bay region most landslides occur on slopes greater than 15 percent, with very few on slopes of 5–15 percent and virtually none on slopes less than 5 percent. As part of the current study, Nilsen and Wright (unpub. data) have prepared a generalized slope map of the San Francisco Bay region at a scale of 1:125,000 showing the slope intervals 0–5 percent, 5–15 percent, and greater than 15 percent. (An insert from their map is shown in fig. 64.) The generalized slope map shows only areas wider than about 300 m (1,000 ft) and eliminates the thousands of very small, discontinuous areas shown on the original slope map. The generalized map provides an important element for evaluating slope stability on a regional scale.

BEDROCK GEOLOGY

Certain bedrock units are more susceptible to landsliding than others because of their physical and chemical characteristics, as well as the types and thicknesses of soils that tend to develop over these rock types. Thus, two adjacent areas that may appear to be similar in most resepcts may differ greatly in landslide susceptibility because of the type of bedrock underlying them (Radbruch and Weiler, 1963; Radbruch and Case, 1967; Brabb and others, 1971).

For purposes of evaluating slope stability, a map showing the distribution of geologic units in the San Francisco Bay region was prepared at a scale of 1:125,000. On the basis of discussions with geologists at the U.S. Geological Survey responsible for bedrock mapping and research into the physical properties of hillside materials, certain of these units were judged to be especially susceptible to landsliding; these units are shown in figure 65 for an area in the northeastern bay region.

RELATIVE SLOPE STABILITY OF THE SAN FRANCISCO BAY REGION

Nilsen and Wright (unpub. data) prepared a slope stability map of the nine-county San Francisco Bay region at a scale of 1:125,000. An example for a part of the northeastern bay region is shown in figure 66. The map delineates areas according to five categories of relative slope stability ranging from generally highly stable to generally unstable. The five categories are defined and tabulated (fig. 66).

The map incorporates the most recent data on mapped landslide deposits, slope, and bedrock geology (refer to figs. 63, 64, 65, respectively) and delineates areas in more detail than an earlier map showing relative abundance of landslides at a scale of 1:500,000 (Radbruch and Wentworth, 1971); it does not incorporate as much detailed data, especially from field investigations, as earlier slope-stability maps of smaller areas prepared at larger scales (for example, Brabb, Pampeyan, and Bonilla, 1972). The map can be used only for regional scale investigations and not for slope-stability analyses of individual lots or small subdivision areas.

The map provides a generalized regional representation of relative slope stability in the San Francisco Bay region. Although it does not predict that particular slopes will fail during future earthquakes of specific size

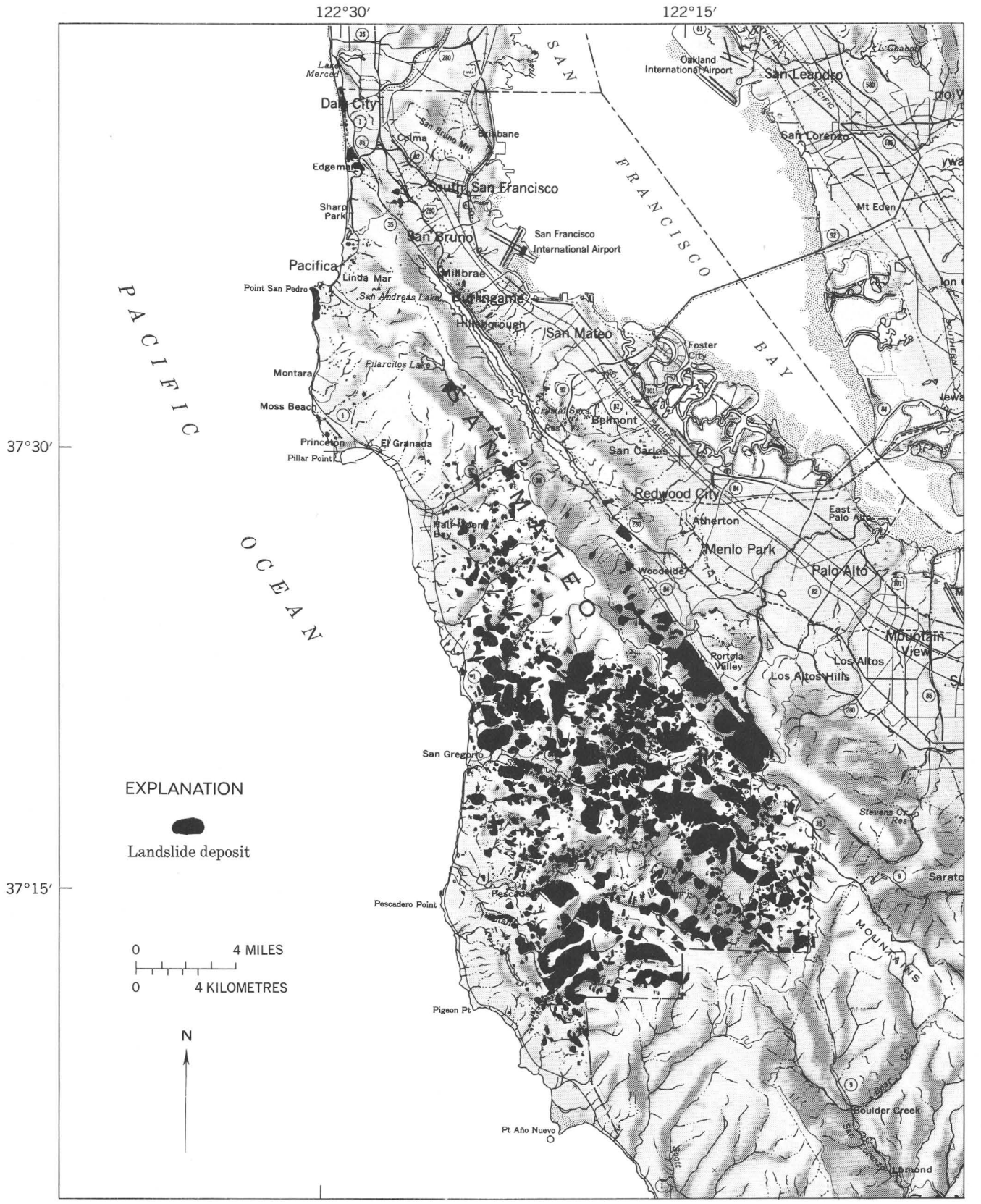

FIGURE 62.—Landslides in San Mateo County, Calif. More than 1,000 landslides have been mapped in this area. From Brabb and Pampeyan (1972).

and location, the map is useful for delineating areas according to their potential for earthquake-induced landslides. It defines the relative slope stability of general areas on the basis of existing physical characteristics. Because the 1906 earthquake generated landslides throughout the region and because most of the more unstable areas are concentrated along the ridges paralleling the San Andreas and Hayward faults, these areas must be considered most susceptible to landsliding during moderate to large earthquakes. Delineation of such areas is a basic tool for the development of land-use policies for reducing the hazards associated with

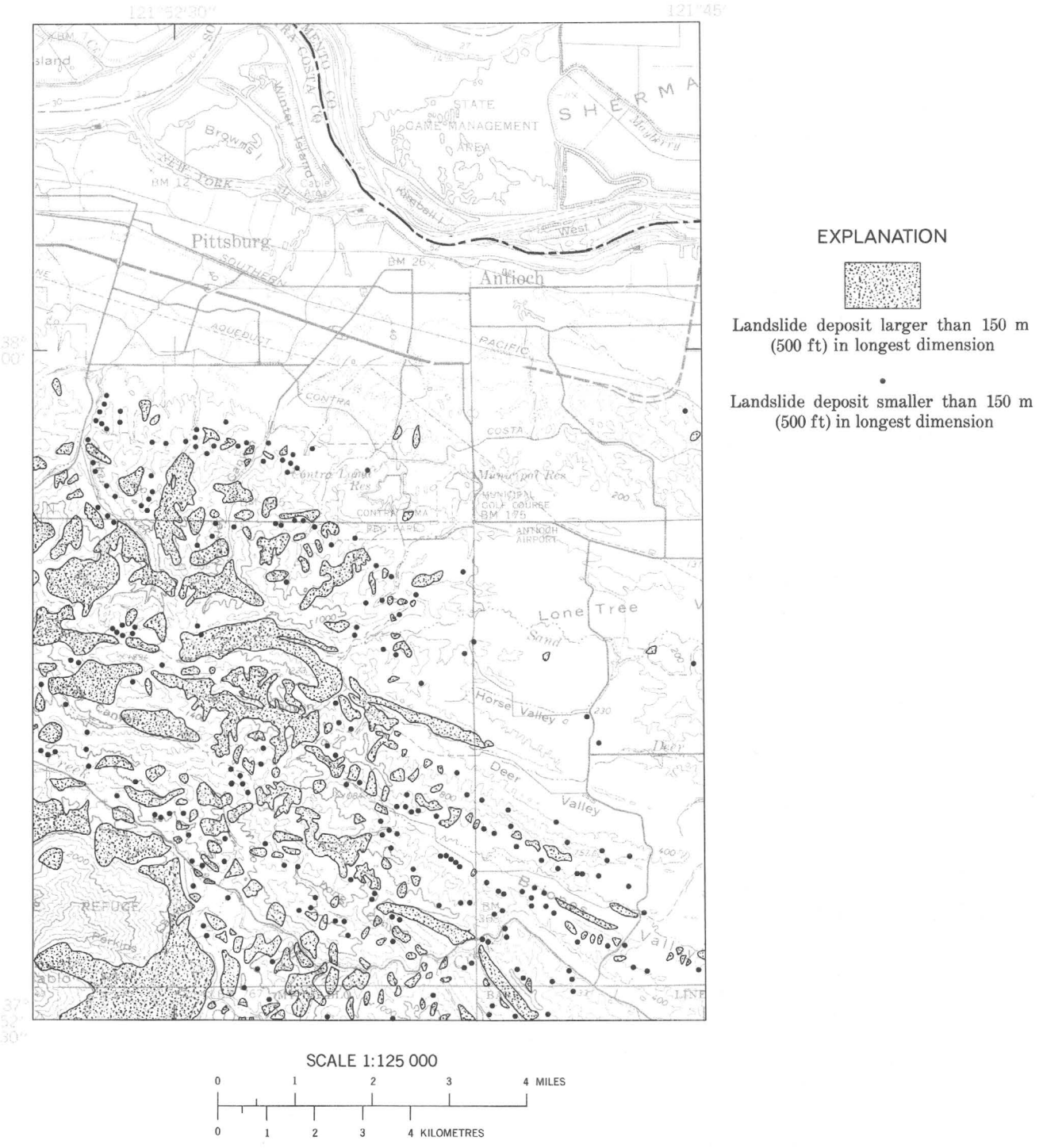

FIGURE 63.—Distribution of landslide deposits in part of northeastern Contra Costa County, Calif. After Sims and Nilsen (1972) and Nilsen (1971).

earthquake-induced landslides. Because the relative-slope-stability map is based on bedrock geology, slope, and the distribution of past landslide deposits, the map also defines general areas susceptible to landsliding triggered by other mechanisms such as rainfall and man's activities.

SUMMARY

Landsliding is continually a major hazard to life and property in the San Francisco Bay region. Studies of landslide cost showed that at least $25 million was spent in 1968–69 on landslides triggered by processes

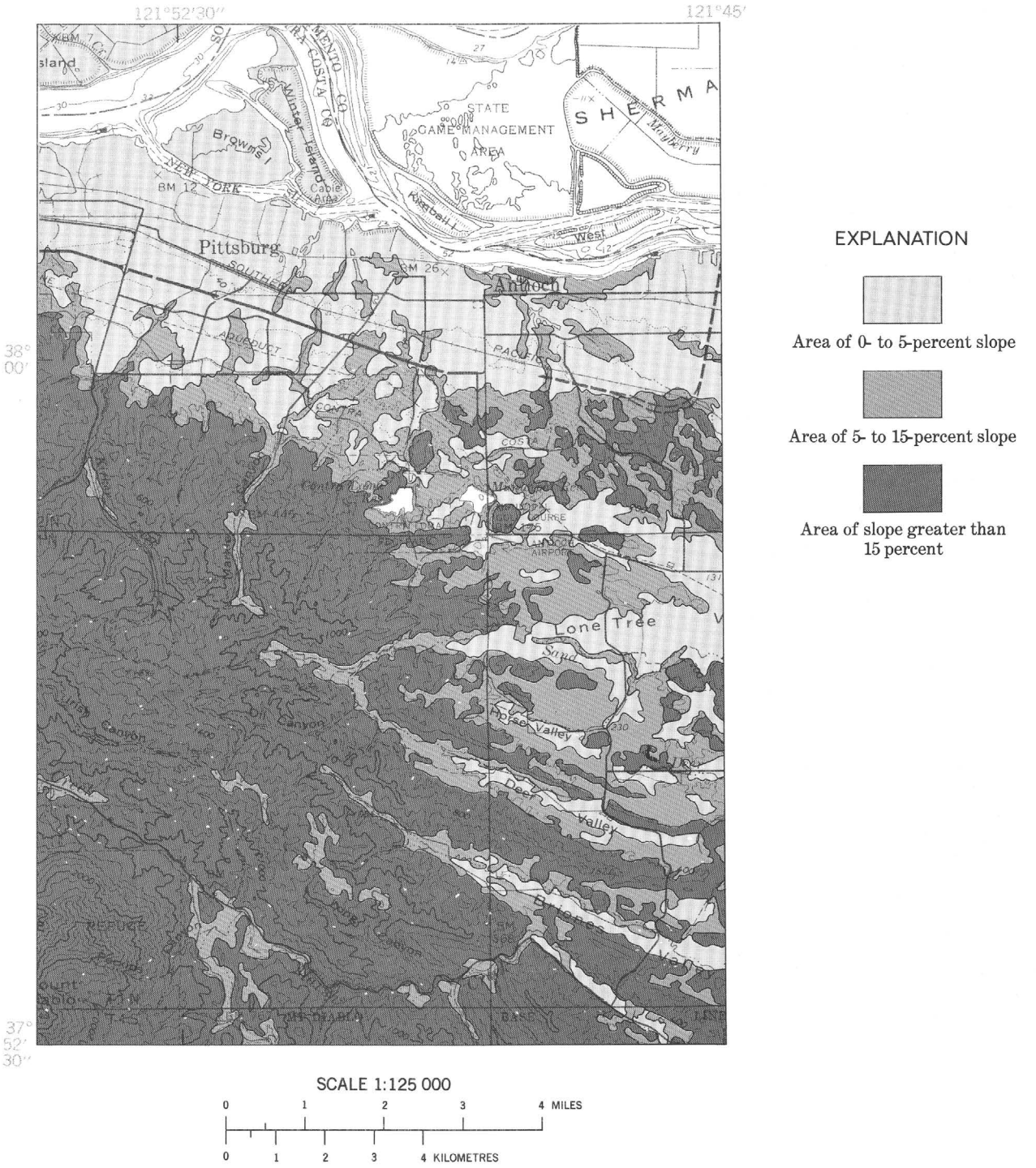

FIGURE 64.—Generalized slope map of part of northeastern Contra Costa County, Calif. Modified from U.S. Geol. Survey (1972) by T. H. Nilsen and R. H. Wright.

such as rainfall and man's construction activities. The number of landslides generated by the 1906 earthquake suggests that in the event of another such earthquake thousands of additional landslides would be triggered, costing possibly billions of dollars and untold loss of life because of extensive development of the hillside areas.

Evaluation of the landslide problem on a regional scale requires more generalized data and permits less specific conclusions than evaluation of the problem at specific sites. At present it is not possible to predict particular slope failures on a regional scale from specified levels of earthquake-induced ground shaking. Nevertheless, sufficient data exist in the San Francisco Bay region on a regional scale to provide a basis for

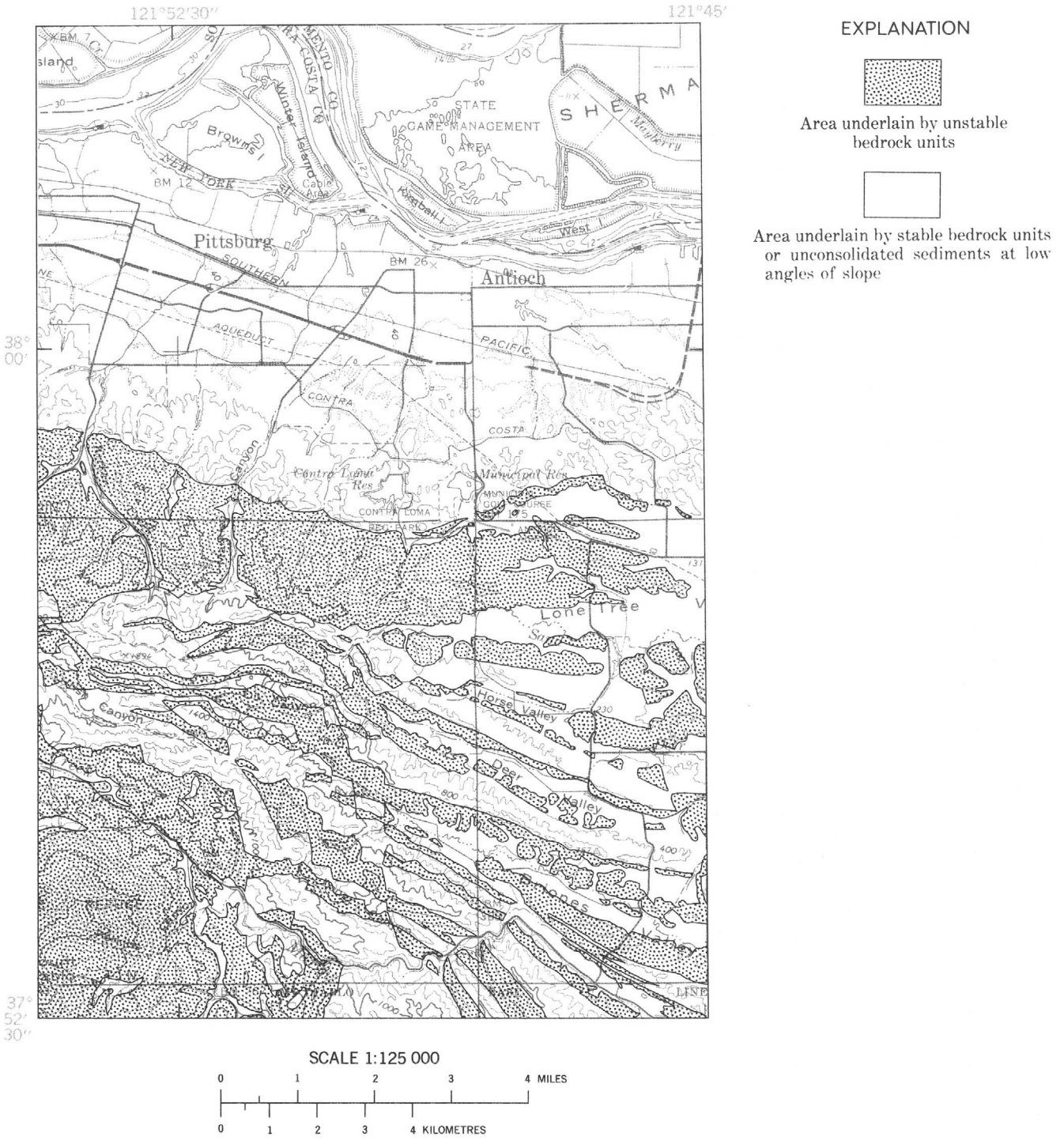

FIGURE 65.—Distribution of geologic units susceptible to landsliding in part of northeastern Contra Costa County, Calif.

substantially reducing the hazards associated with landsliding, both that occurring on a continuing basis and that triggered by earthquakes.

The relative-slope-stability map compiled at a scale of 1:125,000 of the San Francisco Bay region delineates areas according to five categories of estimated relative slope stability (Nilsen and Wright, unpub. data; fig. 66). The map indicates the stability of areas on the basis of landslide distribution, slope, and bedrock geology. The least stable areas are located mainly on the steep slopes of the ridges roughly paralleling the major San Andreas and Hayward faults. The map is preliminary and represents an initial attempt at analyzing the landslide problem of the entire region on a scale useful for land-use

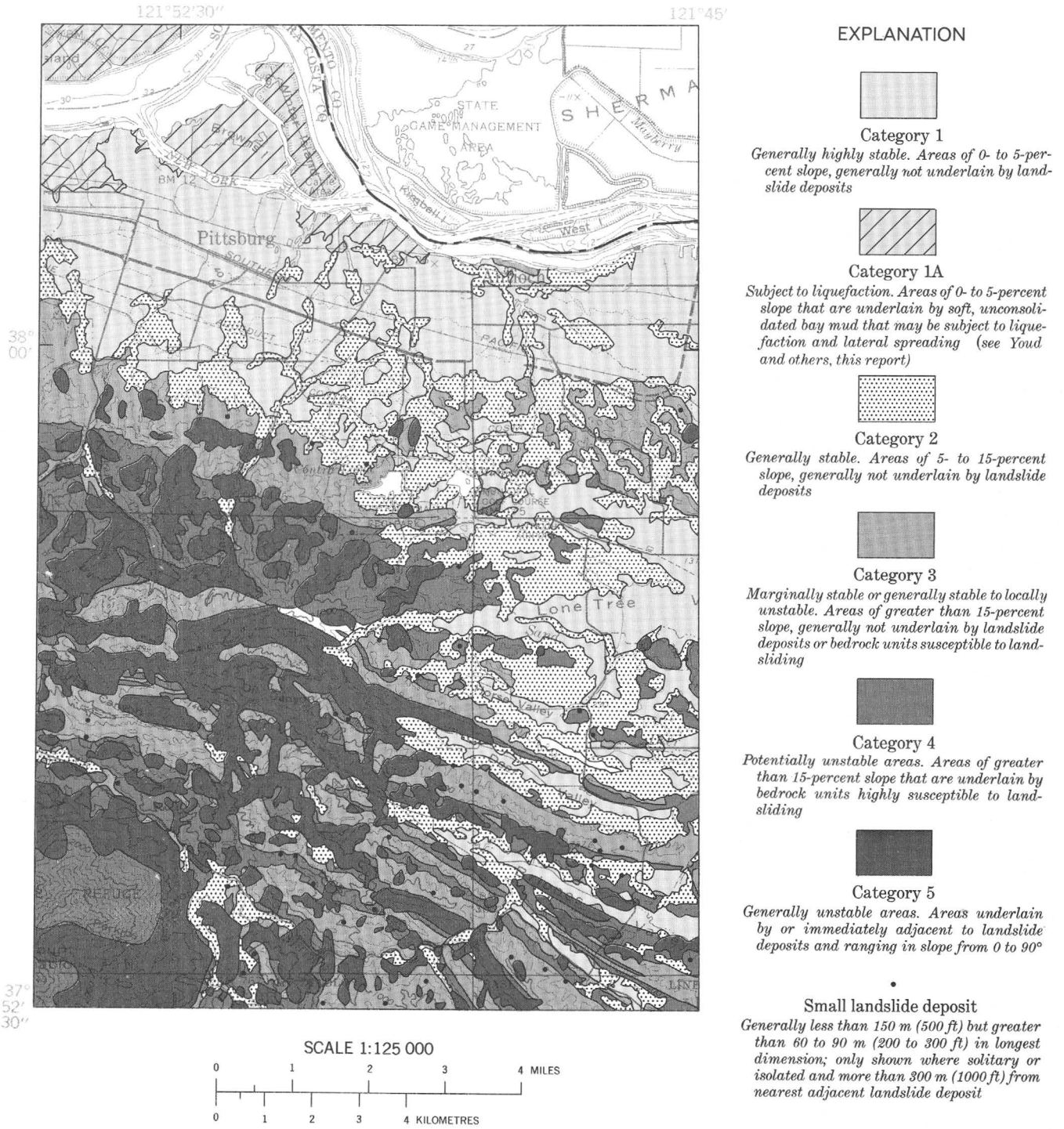

FIGURE 66.—Relative slope stability of part of northeastern Contra Costa County, Calif.

planning. In addition to those regional factors incorporated into the map, numerous other factors are known to influence slope stability, This preliminary map provides a basis for analyzing the importance of these factors and for developing future maps which incorporate improved data and techniques. The present map, even with its limitations, is a first step toward delineating .hose general areas most susceptible to landsliding during future earthquakes and, as such, provides an essential tool for seismic zonation of the San Francisco Bay region.

PREDICTED GEOLOGIC EFFECTS OF A POSTULATED EARTHQUAKE

By R. D. BORCHERDT, E. E. BRABB, W. B. JOYNER, E. J. HELLEY, K. R. LAJOIE, R. A. PAGE, R. L. WESSON, and T. L. YOUD

INTRODUCTION

The analyses presented in the preceding six papers show that the geologic setting of the San Francisco Bay region has a dominant influence on potential earthquake hazards. The strong correlation between geologic conditions and the amount of earthquake damage in 1906 emphasizes the importance of this influence and demonstrates the need for seismic zonation. Seismic zonation can provide the logical basis for preparation of special-purpose land-use maps that, with appropriate public policy, would be a significant step toward reducing the currently expected catastrophic effects of another great earthquake (Algermissen, 1972).

Seismic zonation requires a set of integrated multidisciplinary predictions about the geologic effects of potential earthquakes. To illustrate a strategy for making such predictions, a demonstration profile has been chosen perpendicular to a segment of the San Andreas fault, along which a magnitude 6.5 earthquake has been postulated. This profile includes a wide variety of geologic conditions and provides a means for application of the analyses presented in the preceding six papers.

Earthquake hazards to life and property originate from (1) surface faulting, (2) ground shaking, (3) flooding, (4) liquefaction, and (5) landsliding. The extent to which each of these geologic effects can be predicted for an earthquake of a given magnitude and location depends on the current state of the art. To illustrate techniques and data currently available, each effect is considered for the postulated earthquake.

This paper does not provide final estimates for the total earthquake hazard along the demonstration profile. Such an objective would require analysis of individual manmade structures as well as consideration of earthquakes of other sizes and locations. Instead, this paper illustrates the extent to which the above effects can be predicted for an earthquake of this given size and location. Such an analysis demonstrates a methodology for seismic zonation based on available data.

A POSTULATED EARTHQUAKE

For illustrative purposes, an earthquake of magnitude 6.5 is assumed to occur on the San Andreas fault. The location and estimated length of fault rupture are shown in figure 67. Previous large earthquakes associated with rupture of the ground surface along this section of the fault occurred in 1838 (magnitude >6.5) and in 1906 (magnitude 8.3). The moderate 1957 earthquake (magnitude 5.3) occurred approximately 25 km (15 mi) north of the postulated surface rupture, but with no associated surface faulting on land.

The assumed 6.5 magnitude is moderate in comparison with the 8.3 magnitude of the 1906 earthquake. However, the damage resulting from the recent San Fernando and Managua earthquakes suggests that damage from a moderate earthquake can be very intense but of smaller areal extent that that of a great earthquake.

GEOLOGY ALONG DEMONSTRATION PROFILE

The demonstration profile extends northeasterly from the community of Sky Londa, across the San Andreas fault zone, through the city of Menlo Park, and across San Francisco Bay to the southern tip of Coyote Hills (fig. 67). A brief summary of the geology along the profile will aid in understanding the potential geologic effects of the postulated earthquake.

The demonstration profile includes seven geologic units that are grouped into five units on the basis of physical properties. In order of increasing age, these units are as follows:

1. Bay mud; mostly recently deposited soft clay, silt, and minor sand; contains more than 50 weight percent water;
2. Holocene alluvium; poorly consolidated clayey silt, sand, and gravel; contains less than 40 weight percent water;
3. Late Pleistocene alluvium; primarily same material composition as Holocene alluvium, but contains less water and is more consolidated; in some places overconsolidated (soil-engineering sense);
4. Pliocene and early Pleistocene deposits; primarily continental Santa Clara and marine Merced Formations consisting of semiconsolidated and consolidated sandstone, siltstone, and mudstone; and
5. Pre-Tertiary and Tertiary bedrock; includes Franciscan Formation, consisting mostly of sandstone

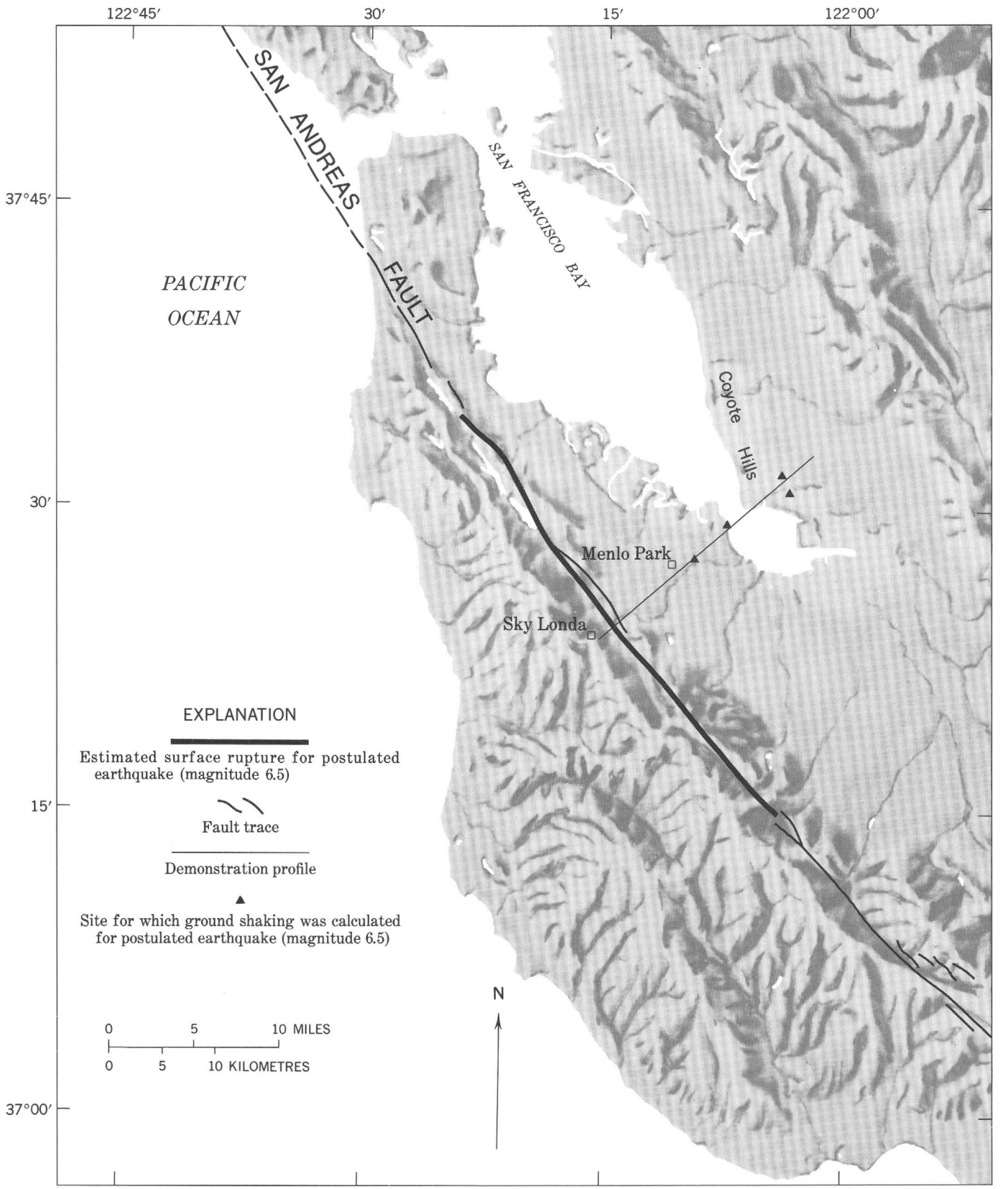

FIGURE 67.—Location of demonstration profile and estimated length of surface rupture associated with a postulated earthquake of magnitude ≈6.5 on the San Andreas fault, southwestern San Francisco Bay region.

and shale with lesser amounts of radiolarian chert, greenstone, limestone, and serpentine; marine sandstone and shale of Eocene, Miocene, and Pliocene age; and Page Mill Basalt, consisting of lava flows and pyroclastic rocks of Miocene age.

The general stratigraphic relations of the five geologic units are illustrated in figure 68 (more detailed descriptions are given in Lajoie and Helley, this report).

PREDICTED GEOLOGIC EFFECTS

The potential effects of the postulated earthquake are dependent on the distribution of the five geologic units with respect to the San Andreas fault. A generalized prediction for each geologic effect along the profile is presented in figure 68 and discussed in the following sections.

SURFACE FAULTING

Historically, the larger earthquakes of the San Francisco Bay region have been associated with surface ruptures localized along the main surface traces of strike-slip faults. The resulting displacements of the ground surface along the faults have been mainly horizontal, with only minor vertical displacements. They are typically expressed as an en echelon pattern of ground fractures that trend obliquely to the overall fault trace. The en echelon fractures have exhibited displacements ranging from a few centimetres (a few inches) to a few metres (several feet) and have defined a surface fault zone ranging in width from a few metres (several feet) to several tens of metres (about 200 ft).

On the basis of past observation, the postulated magnitude 6.5 earthquake probably would be associated with right-lateral surface displacement along the San Andreas fault that may be as great as 1 m (3 ft) (fig. 67). The length of estimated surface rupture is 40 km (25 mi) plus or minus about 10 km (6 mi). This displacement is likely to be predominantly horizontal with the land west of the fault shifting toward the northwest relative to the land east of the fault. The main zone of surface rupture will range in width from a few metres (several feet) to several tens of metres (about 200 ft), but small fractures and permanent ground distortion may extend to much greater distances. Locally, branch and subsidiary faults, such as the Black Mountain fault, the Cupertino fault, and the Cañada fault, may also move, but movements on such lesser faults are much more difficult to predict. If sympathetic surface movements do occur along these lesser faults, they are expected to be less than those on the main fault rupture.

During the 1906 earthquake, horizontal displacements as large as 2.6 m (8.5 ft) were observed along this segment of the San Andreas fault. Branner (1908) reported for the 1906 earthquake possible evidence for slight sympathetic movement on the Black Mountain fault and prevalent ground cracking extending several tens of metres (a few hundred feet) from the main trace of the San Andreas fault. Most of the ground cracking was associated with small local ground failures. The maximum reported fault displacement on the San Andreas of 6.4 m (21 ft) occurred farther north in Marin County.

GROUND SHAKING

The characteristics of the ground shaking expected from the postulated earthquake depend on many factors. They depend on (1) characteristics of the earthquake source (for example, type of offset, magnitude, location, stress drop, and size of associated rupture surface), (2) distance from associated rupture surface, and (3) characteristics of the local geologic materials. Existing data on these factors are presented in the first four pages of this report. To illustrate a strategy for predicting ground shaking on the basis of these data, four sites along the demonstration profile (fig. 68) were selected to illustrate responses of the several geologic units to ground shaking.

The first step in predicting ground shaking for the postulated earthquake is to estimate the bedrock shaking at each site. The amplitude spectra for bedrock shaking (fig. 69) were approximated by using a technique proposed by Newmark and Hall (1969). (For discussion of technique see Page and others, this report.) The acceleration, velocity, and displacement values used in constructing the spectra (see table 6) were taken from a preliminary set of data (see Page and others, this report) and probably are more representative of a magnitude 6.0 earthquake than one of magnitude 6.5. These values are included to illustrate techniques, and it was not considered necessary to repeat the calculations for the larger values more appropriate for a magnitude 6.5 earthquake.

The second step is to estimate the response to shaking of the unconsolidated deposits at each site. By using the techniques discussed in Borcherdt, Joyner, and others (this report) these responses were estimated from the Pacoima Dam accelerogram (San Fernando earthquake, Feb. 9, 1971), scaled to the peak velocity values used in construction of the bedrock spectra. The final amplitude spectra for ground shaking at the surface were obtained at each site (fig. 69) by multiplying the amplitude response spectra of surficial deposits, computed at the appropriate high-strain levels, by the approximated bedrock spectra.

The estimates of ground shaking for the postulated earthquake (fig. 69) are tentative; however, they do suggest some general conclusions for the sites considered:

1. The bay mud and alluvium deposits substantially

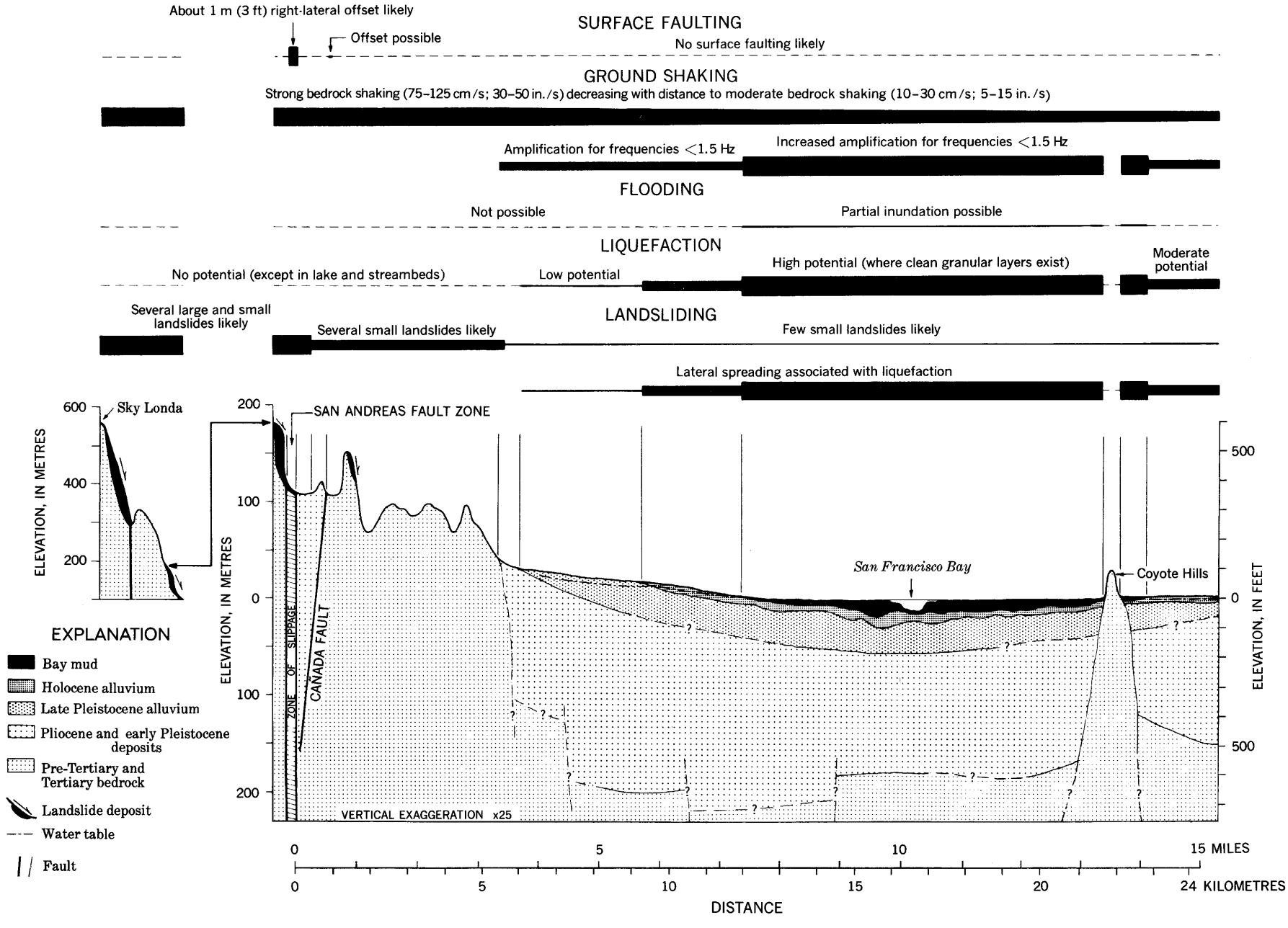

FIGURE 68.—Predicted geologic effects of a postulated earthquake (magnitude ≈6.5) on the San Andreas fault (see fig. 67 for location of demonstration profile and estimated length of surface rupture). The severity of each earthquake effect is indicated qualitatively by thickness of underlining and quantified to the extent permitted by the current state of the art for seismic zonation on a regional scale. The severity of the predicted earthquake effects generally depend on the type of underlying geologic material. Geologic cross section compiled by K. R. Lajoie.

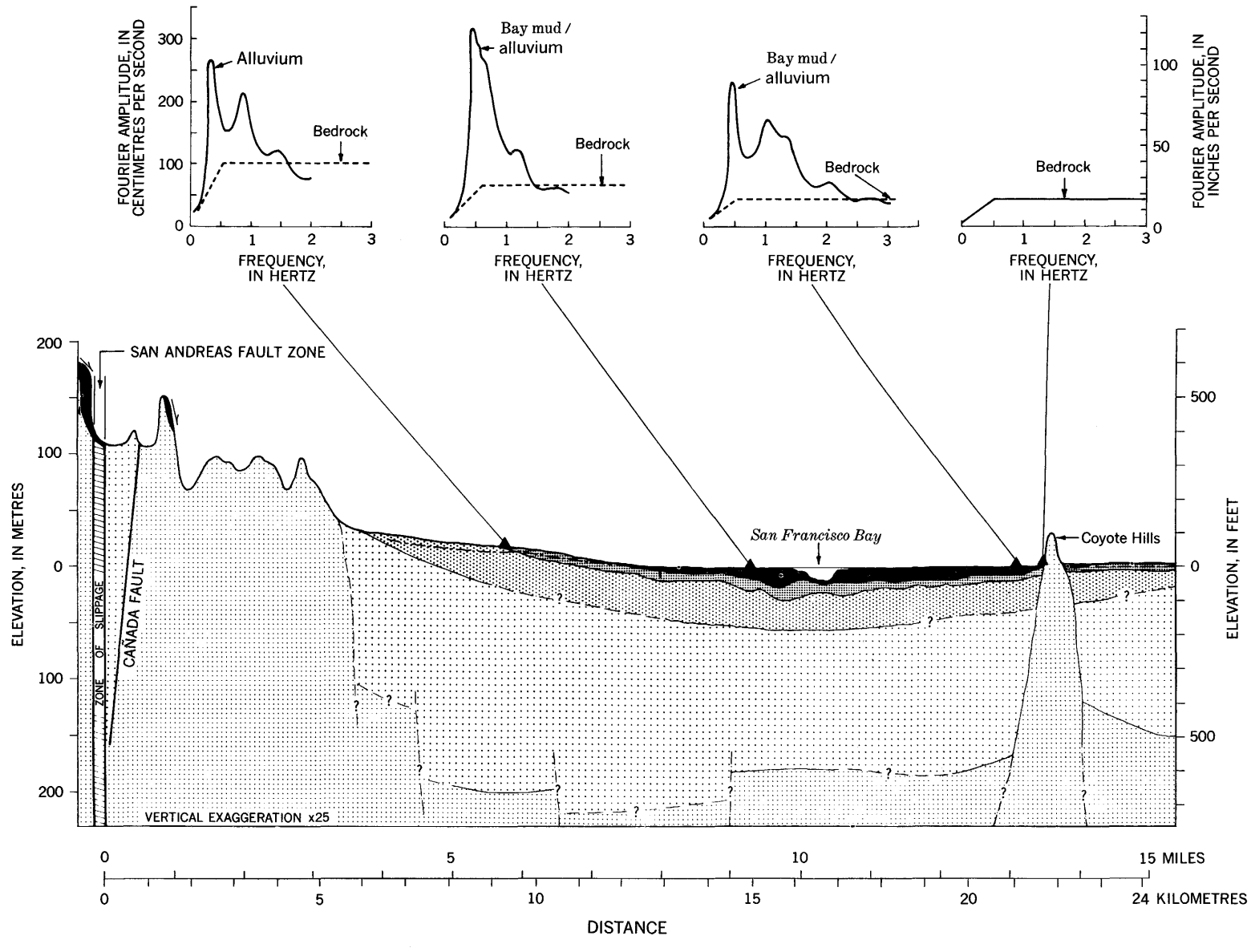

FIGURE 69.—Fourier amplitude spectra of surface ground shaking predicted at four sites along the demonstration profile for a postulated earthquake (magnitude ≈6.5). The estimated spectra suggest that even at high levels of strain local geologic units may substantially amplify frequencies of ground shaking near the fundamental frequency of the site (see Page and others; Borcherdt, Joyner, and others; Borcherdt, Brabb, and others, this report, for descriptions of techniques; see fig. 68 for explanation of geologic symbols).

TABLE 6.—*Parameters for estimating amplitude spectra for shaking of bedrock*

A. Time history parameters

Site	Distance (km)	Distance (mi)	Acceleration (g)	Velocity (cm/s)	Velocity (in./s)	Displacement (cm)	Displacement (in.)
1	9	5.6	0.40	31	12.2	14	5.5
2	14	8.7	0.22	19	7.5	9	3.5
3, 4	21	13.1	0.12	12	4.7	6	2.4

B. Estimated spectral parameters

Site	Acceleration (g) (factor 4.8)	Velocity (factor 3.0) (cm/s)	Velocity (factor 3.0) (in./s)	Displacement (factor 1.7) (cm)	Displacement (factor 1.7) (in.)
1	1.92	93	36.6	24	9.4
2	1.06	57	22.4	15	5.9
3, 4	0.58	36	14.2	10	3.9

amplify particular frequencies of bedrock shaking and attenuate others;

2. The amplification effect of the unconsolidated deposits is strongly dependent on frequency, which is partly due to input-strain level (compare the responses for the two sites on bay mud that have identical low-strain seismic models);
3. The amount of amplification near the fundamental frequency of the site in some places actually increases with increasing strain level; and
4. The amplification effect of the unconsolidated deposits in certain frequency bands is greater than the attenuation caused by increasing distance.

In general, strong shaking (50–125 cm/s (20–50 in./s)) could be expected from the postulated earthquake for all surface bedrock sites along the profile west of the bay plain (fig. 68). The model calculations suggest that a substantial amplification of bedrock shaking in the frequency range below 1.5 hertz could be expected for all parts of the demonstration profile underlain by alluvial deposits, with increased amplifications for the parts underlain by bay mud. The predicted amplifications are large enough to suggest that ground shaking for frequencies below 1.5 hertz may be stronger at the sites underlain by bay mud and alluvium than at sites underlain by bedrock much closer to the fault. Manmade structures with natural periods coinciding with those of the underlying unconsolidated geologic deposits are particularly susceptible to damage.

FLOODING

Areas of potential flooding have not been delineated in the San Francisco Bay region, except for the areas likely to be inundated by a tsunami-generated runup of 6.1 m (20 ft) (Ritter and Dupré, 1972). Analysis of the problem is not presented in the first six papers in this report; however, for completeness in considering those earthquake effects influenced by geologic conditions, a brief description of the problem is presented for the demonstration profile. For the postulated earthquake, the most probable cause of inundation by water is the failure of dams or dikes. Flood water from such failures could originate from either San Francisco Bay or upland reservoirs.

Southern San Francisco Bay is surrounded by a large number of dikes constructed mostly of fine-grained sediments dredged from the bottom of the bay. The continuous repair work necessary on many of the dikes suggests their vulnerability to failure, and their location on bay mud increases their vulnerability. Bay mud has both a high potential for amplifying particular frequencies of ground shaking (Borcherdt, Joyner, and others, this report) and a high potential for ground failure due to liquefaction (Youd and others, this report).

The area likely to be inundated because of possible dike failures depends on the tidal level at the time of the earthquake. The tidal range at the Dumbarton Bridge extends as much as 3.4 m (11 ft) above mean lower low water. For the postulated earthquake, partial inundation appears likely up to the 1850 shoreline (Nichols and Wright, 1971) and even farther in certain areas where the ground has subsided in recent years owing to the withdrawal of ground water. At the southern tip of the bay, for example, flooding could extend as much as 2 km (1.2 mi) beyond the 1850 shoreline.

Possible upland sources of flooding during the postulated earthquake are the Upper and Lower Crystal Springs Reservoirs and San Andreas Lake. Each of these bodies of water is in the San Andreas rift valley, which is drained by San Mateo Creek about 20 km (12 mi) north of the demonstration profile. Without a detailed engineering analysis of the associated dams, which is beyond the scope of this study, it is not possible to assess the resistance of the dams to the postulated earthquake. However, the areas of possible inundation can be outlined on a topographic map. None of the areas of possible inundation intersect the demonstration profile, even though they are of considerable size.

For the postulated moderate earthquake, the likelihood of a large vertical offset of the sea floor or large submarine landslide necessary to generate a tsunami seems remote. Ritter and Dupré (1972) reported that 19 tsunamis were recorded by the tide gage at the Golden Gate during the past 100 years. The maximum recorded wave height from a tsunami was only 2.3 m (7.5 ft). Tidal records within San Francisco Bay show that waves attenuate rapidly to less than 50 percent of their original height by the time they reach the area of the demonstration profile. For flooding to result from the unlikely possibility of a tsunami in San Francisco Bay, the corresponding earthquake would have to occur dur-

ing high tide when the tops of some of the dikes are less than 1 m (3 ft) above water level.

The postulated earthquake of magnitude 6.5 probably is not large enough to generate a seiche in San Francisco Bay. However, seiches could be generated in reservoirs close to the postulated surface faulting; thus, seiches might be generated in the Upper and Lower Crystal Springs Reservoirs.

The tectonic setting of the San Francisco Bay region suggests that large tectonic changes of land level and associated significant changes in sea level (such as occurred during the 1964 Alaska earthquake) are very unlikely to accompany the postulated earthquake. Only minor local changes in vertical elevation of about 0.3 m (1 ft) were produced by the 1906 earthquake.

LIQUEFACTION

By using the procedures discussed in Youd and others (this report), a cross section showing liquefaction potential was constructed along the demonstration profile for the postulated earthquake (fig. 68). Sediments with the greatest potential for liquefaction are the clay-free granular layers within the bay mud unit. Holocene alluvium has a generally moderate potential with locally high potential in some recent channel and overbank deposits. Late Pleistocene alluvium is generally dense and has a low potential for liquefaction. In addition, much of the Holocene and the late Pleistocene alluvium is normally above water table and thus has, at most, a seasonal potential for liquefaction.

The most common type of ground failure expected to result from liquefaction along the profile is that of lateral-spreading landslides (Youd and others, this report). In brief, this type of failure consists of movement of a soil mass down a mild slope with resulting cracks, fissures, and differential settlements within and near the margins of the slide mass. Relative displacements as large as tens of metres have been observed for such ground failures. Areas of the profile with the highest potential for this type of ground failure from the postulated earthquake are underlain by bay mud along the western margin of San Francisco Bay (fig. 68).

Evidence for lateral spreading during the 1906 earthquake was reported at several locations. For example, lateral ground movements as large as 2 m (6 ft) occurred in virtually every arm of bay mud extending beneath the city of San Francisco. Many more such ground failures may have been generated near the margins of southern San Francisco Bay but went unreported. Much of this area was marshland in 1906.

LANDSLIDING

The postulated magnitude 6.5 earthquake could be expected to generate several landslides along the demonstration profile. By using the techniques presented in Nilsen and Brabb (this report), a cross section showing general landslide susceptibility along the demonstration profile has been prepared (fig. 68). These approximate landslide susceptibilities are not specifically dependent on the postulated magnitude of 6.5 and would be equally applicable to any moderate earthquake in the same general location.

If the postulated earthquake were to take place during a wet season and high ground-water levels, many landslides could be expected along the profile. A few large (more than 150 m (500 ft) in maximum dimension) landslides and several small (10–150 m (30–500 ft) in maximum dimension) landslides are likely on the steep slopes between Sky Londa and the San Andreas fault. In this area, existing landslide deposits could be reactivated. Several small landslides could be generated in the area between the San Andreas fault and the western margin of the bay plain. Lateral-spreading landslides associated with liquefaction could be expected near the margins of San Francisco Bay.

If the postulated earthquake were to occur during a dry season and low ground-water levels, the amount of landsliding is expected to be much less. Some landsliding still could be expected between Sky Londa and the San Andreas fault, a few small landslides probably would occur in the other hilly areas along the profile, and lateral-spreading landslides associated with liquefaction still could be expected near the margins of San Francisco Bay.

The 1906 earthquake apparently generated hundreds of landslides throughout the hilly regions along the western margin of the bay plain. Numerous landslides were reported in the hilly regions between the San Andreas fault and Sky Londa. An exceptionally large mass (0.8 km (0.5 mi) across) near Black Mountain moved in 1906.

The epicenter for the 1957 earthquake (magnitude 5.3) was located approximately 25 km (15 mi) north of the location for the postulated earthquake. It generated about 15 small landslides along the steep coastal bluffs in the Daly City–San Francisco area (Bonilla, 1960a).

SUMMARY

Earthquake hazards to life and property originate from surface faulting, ground shaking, flooding, liquefaction, and landsliding. The extent to which the currently available data permit quantitative prediction of these effects on a regional scale, for an earthquake of a given size and location, is illustrated in figure 68. Along the demonstration profile, the predicted severity of the effects varies substantially depending on local geologic conditions.

In brief, and as shown in figure 68, the principal losses from the postulated earthquake could be expected to originate from the following factors:

1. Surface faulting, ground shaking, and landsliding in the distance interval 0 to 10 m (0 to 30 ft), underlain by pre-Tertiary and Tertiary bedrock and Pliocene and early Pleistocene deposits immediately adjacent to the San Andreas fault;
2. Ground shaking and landsliding in the distance interval 10 m to 5.2 km (30 ft to 3.2 mi), underlain by pre-Tertiary and Tertiary bedrock and Pliocene and early Pleistocene deposits;
3. Ground shaking in the distance interval 5.2 to 9.3 km (3.2 to 5.8 mi), underlain by Pliocene and early Pleistocene deposits and late Pleistocene alluvium;
4. Ground shaking and landsliding of the lateral-spreading type associated with liquefaction in the distance interval 9.3 to 12.0 km (5.8 to 7.4 mi), underlain by Holocene alluvium;
5. Ground shaking, flooding, and landsliding of the lateral-spreading type associated with liquefaction in the distance interval 12.0 to 21.0 km (7.4 to 13 mi), underlain by bay mud;
6. Landsliding in the distance interval 21.6 to 22.1 km (13.4 to 13.7 mi), underlain by pre-Tertiary and Tertiary bedrock; and
7. Ground shaking, flooding, and landsliding of the lateral-spreading type associated with liquefaction in the distance interval 22.1 to 22.8 km (13.7 to 14.2 mi), underlain by bay mud.

The strong dependence of the predicted effects on geology, together with the availability of extensive geologic and geophysical data, suggests the feasibility of extending this analysis to the entire San Francisco Bay region for other potential earthquakes. Such a regional analysis would provide a preliminary seismic zonation of the region from which special-purpose land-use maps could be constructed and then used to reduce earthquake hazards.

GENERAL CONCLUSIONS

The great California earthquake of April 18, 1906, demonstrated large variations in earthquake vulnerability for various areas of the San Francisco Bay region and provided basic data for the study of earthquakes and their effects. Extensive research facilities have been developed within the last decade to study the basic physical processes associated with earthquakes. These facilities have yielded important new geological and geophysical data, which when incorporated with data from the 1906 earthquake, provide the basis for development of guidelines to reduce future earthquake losses.

The analyses presented in this report show that the geologic setting of the San Francisco Bay region has a dominant influence on potential earthquake hazards. The geologic setting is shown to control the potential severity of the various earthquake effects from which losses of life and property originate; namely, surface faulting, ground shaking, flooding, liquefaction, and landsliding. The first step required to reduce earthquake hazards is seismic zonation, which requires prediction of the potential severity of these various geologic effects on a regional scale for future earthquakes of specific size and location. An example of such prediction as illustrated by a demonstration profile for a postulated earthquake (Borcherdt, Brabb, and others, this report) suggests that seismic zonation of the San Francisco Bay region is feasible using existing geological and geophysical knowledge. This example illustrates a methodology for seismic zonation at the current state of the art and demonstrates the extent to which the various effects can be predicted quantitatively on a regional scale using existing data.

Tools derived and discussed as a basis for seismic zonation are (1) a map showing active faults (fig. 3*A*), (2) data on attenuation of shaking in bedrock, (3) geologic data, (4) a map showing ground response, (5) a map showing liquefaction potential (fig. 50), (6) a map showing landslide susceptibility (fig. 66), and (7) a map showing areas that might be inundated by tsunamis (Ritter and Dupré, 1972). (This last map represents only part of the analyses necessary for a map of potential flooding.)

Application of these tools to the problem of seismic zonation shows that predictions on a regional scale for earthquakes of specific size and location are less quantitative than those that can be made at specific sites where additional data are available. Nevertheless, such predictions are useful for the development of regional land-use policies to reduce losses from future earthquakes. For example, although it is not possible to predict on a regional scale all those sites that will incur landsliding during the next earthquake of specific size and location, it is possible to delineate those general areas most susceptible to landsliding and hence those areas where special additional studies may be required to evaluate the landslide hazard for specific types of structures.

Until more detailed treatments of seismic zonation are avilable, it is hoped that these basic tools and analyses will be useful to a wide variety of users con-

cerned with reducing earthquake losses in the bay region. In general, the predicted maximum-intensity (fig. 40) map serves to delineate areas of potential earthquake problems, and the basic tools mentioned above help identify the nature and possible severity of the problems in each area. In particular and as an informal summary, the analyses presented in the various papers are useful for the following purposes:

1. Estimating the maximum size and location of future damaging earthquakes and delineating areas of potential surface faulting and the locations of potential sources of strong ground shaking (Wesson and others).
2. Estimating the degree of bedrock shaking at various distances from earthquake sources of various sizes (Page and others).
3. Interpreting basic geologic data pertinent to extrapolating results of specific site studies to a regional scale (Lajoie and Helley).
4. Estimating the shaking response of various geologic units at specific sites and delineating those geologic units (defined by Lajoie and Helley) for which the effects of amplified ground shaking at equidistant sites are likely to be least, intermediate, and greatest (Borcherdt, Joyner, and others).
5. Estimating the general liquefaction potential of various geologic units and delineating those geologic units (defined by Lajoie and Helley) for which the liquefaction potential of existent clay-free granular layers is low, moderate, and high (Youd and others).
6. Evaluating on a regional scale the vulnerability of various areas to landsliding and delineating those areas with various degrees of landslide susceptibility (Nilsen and Brabb).
7. Applying the various basic tools to the problem of predicting the geologic effects of potential earthquakes of specific size and location for purposes of seismic zonation (Borcherdt, Brabb, and others).

These analyses are preliminary and represent a first attempt at the required multidisciplinary analysis of the seismic-zonation problem. There are still many problems associated with seismic zonation, and the state of the art is rapidly changing. Nevertheless, it is hoped that this effort will serve as a useful first step toward the reduction of earthquake hazards on a regional scale.

1906 INTENSITY SCALE FOR SAN FRANCISCO

The following grades of apparent intensity were used by Wood (1908, pp. 224–225) in the city of San Francisco after the California earthquake of April 18, 1906:

Grade A. Very violent. Comprises the rending and shearing of rock masses, earth, turf, and all structures along the line of faulting; the fall of rock from mountainsides; numerous landslips of great magnitude; consistent, deep, and extended fissuring in natural earth; some structures totally destroyed.

Grade B. Violent. Comprises fairly general collapse of brick and frame buildings when not unusually strong; serious cracking of brickwork and masonry in excellent structures; the formation of fissures, step faults, sharp compression anticlines, and broad, wavelike folds in paved and asphalt-coated streets, accompanied by the ragged fissuring of asphalt; the destruction of foundation walls and underpinning structures by the undulation of the ground; the breaking of sewers and water mains; the lateral displacement of streets; and the compression, distension, and lateral waving or displacement of well-ballasted streetcar tracks.

Grade C. Very strong. Comprises brickwork and masonry badly cracked, with occasional collapse; some brick and masonry gables thrown down; frame buildings lurched or listed on fair or weak underpinning structures, with occasional falling from underpinning or collapse; general destruction of chimneys and of masonry, brick, or cement veneers; considerable cracking or crushing of foundation walls.

Grade D. Strong. Comprises general but not universal fall of chimneys; cracks in masonry and brickwork; cracks in foundation walls, retaining walls, and curbing; a few isolated cases of lurching or listing of frame buildings built upon weak underpinning structures.

Grade E. Weak. Comprises occasional fall of chimneys and damage to plaster, partitions, plumbing, and the like.

REFERENCES CITED

Albee, A. L., and Smith, J. L., 1967, Geologic criteria for nuclear power plant location: Soc. Mining Engineers Trans., v. 238, p. 430–434.

Algermissen, S. T. (principal investigator), 1972, A study of the earthquake losses in the San Francisco Bay area: Natl. Oceanic Atmospheric Admin., U.S. Dept. Commerce, 220 p.

Allen, J. E., 1946, Geology of the San Juan Bautista quadrangle, California: California Div. Mines Bull. 133, 112 p., map scale 1:62,500.

Ambraseys, N. N., 1969, Maximum intensity of ground movements caused by faulting: World Conference on Earthquake Engineering, 4th, Santiago, Chile, Proc., v. 1, p. 154–171.

———1973, Dynamics and response of foundation materials in epicentral regions of strong earthquakes: World Conference on Earthquake Engineering, 5th, Rome, Italy, Proc., 23 p.

Anderson, F. M., 1899, The geology of the Point Reyes peninsula: California Univ. Pubs. Geol. Sci., v. 2, p. 119–153.

Atomic Energy Commission, 1973, Nuclear power plants, seismic and geologic siting criteria: U.S. Federal Register, v. 38, p. 31279—31285.

Bailey, R. G., 1971, Landslide hazards related to land-use planning in Teton National Forest, northwest Wyoming: U.S. Dept. Agriculture, Forest Service, Intermountain region, Ogden, Utah, 131 p.

Berkland, J. O., 1969, Geology of the Novato quadrangle, Marin County, California: San Jose State College, unpub. M. S. thesis, 146 p.

Bernreuter, D. L., and Tokarz, F. J., 1972, Design basis earthquakes for the Lawrence Livermore Laboratory site: California Univ. Lawrence Livermore Lab. Pub. UCRL–51193.

Blanc, R. P., and Cleveland, G. B., 1968, Natural slope stability as related to geology, San Clemente area, Orange and San Diego Counties, California: California Div. Mines and Geology Spec. Rept. 98, 19 p.

Blanchard, F. B., and Laverty, G. L., 1966, Displacements in the Claremont Water Tunnel at the intersection with the Hayward fault: Seismol. Soc. America Bull., v. 56, p. 291–293.

Bolt, B. A., 1973, Duration of strong ground motion: World Conference on Earthquake Engineering, 5th, Rome, Italy, Proc., p. 1304—1313.

Bolt, B. A., and Marion, W. C., 1966, Instrumental measurement of slippage on the Hayward fault: Seismol. Soc. America Bull., v. 56, p. 305–316.

Bonilla, M. G., 1959, Geologic observations in the epicentral area of the San Francisco earthquake of March 22, 1957: California Div. Mines and Geology Spec. Rept. 57, p. 25–38.

———1960a, Landslides in the San Francisco South quadrangle, California: U.S. Geol. Survey open-file rept., 44 p.

———1960b, A sample of California Coast Range landslides, *in* Geological Survey research 1960: U.S. Geol. Survey Prof. Paper 400–B, p. B149.

———1965, Geologic map of the San Francisco South quadrangle, California: U.S. Geol. Survey open-file map, scale 1:24,000.

———1966, Deformation of railroad tracks by slippage on the Hayward fault in the Niles district of Fremont, California: Seismol. Soc. America Bull., v. 56, p. 281–289.

———1970, Surface faulting and related effects, *in* R. L. Wiegel, ed., Earthquake engineering: Englewood Cliffs, N.J., Prentice-Hall, p. 47–74.

———1971, Preliminary geologic map of the San Francisco South and part of the Hunters Point quadrangles: U.S. Geol. Survey Misc. Field Studies Map MF–311, scale 1:24,000.

———1975, Trench exposures of parts of the February 9, 1971, surface faults in the San Fernando fault zone, *in* Geological and Geophysical Studies, v. 3, of San Fernando, California, earthquake of Feb. 9, 1971: Natl. Oceanic Atmospheric Admin., U.S. Dept. Commerce (in press).

Bonilla, M. G., and Buchanan, J. M., 1970, Interim report on world wide historic surface faulting: U.S. Geol. Survey open-file rept., 32 p.

Boore, D. M., 1973, Empirical and theoretical study of near-fault wave propagation: World Conference on Earthquake Engineering, 5th, Rome, Italy, Proc., p. 2397–2408.

Boore, D. M., and Zoback, M. D., 1975, Two-dimensional kinematic fault modeling of the Pacoima Dam strong-motion recordings of the February 9, 1971, San Fernando earthquake: Seismol. Soc. America Bull. (in press).

Borcherdt, R. D., 1970, Effects of local geology on ground motion near San Francisco Bay: Seismol. Soc. America Bull., v. 60, p. 29–61.

Borcherdt, R. D., and Gibbs, J. F., 1975, Prediction of maximum earthquake intensities for the San Francisco Bay region: U.S. Geol. Survey Misc. Field Studies Map (in press).

Brabb, E. E., 1970, Preliminary geologic map of the central Santa Cruz Mountains, California: U.S. Geol. Survey open-file map, 3 sheets, scale 1:62,500.

Brabb, E. E., and Pampeyan, E. H., 1972, Preliminary maps of landslides in San Mateo County, California: U. S. Geol. Survey Misc. Field Studies Map MF-344, scale 1:62,500.

Brabb, E. E., and Pampeyan, E. H., and Bonilla, M. G., 1972, Landslide susceptibility in San Mateo County, California: U.S. Geol. Survey Misc. Field Studies Map MF–360, scale 1:62,500.

Branner, J. C., 1908, The earth movement on the fault of April 18, 1906; Crystal Springs Lake to Congress Springs: Carnegie Inst. Washington Pub. 87, 104 p.

Brewer, W. H., 1930, Up and down California in 1860–64; the journal of William H. Brewer (F. P. Farquahar, ed.): New Haven, Yale Univ. Press, 601 p.

Brown, R. D., Jr., 1970a, Faults that are historically active or that shows evidence of geologically young surface displacements, San Francisco Bay region; A progress report—October 1970: U.S. Geol. Survey Misc. Field Studies Map MF–331, 2 sheets, scale 1:250,000.

———1970b, Map showing recently active breaks along the San Andreas and related faults between the northern Gabilan Range and Cholame Valley, California: U.S. Geol. Survey Misc. Geol. Inv. Map I–575, scale 1:62,500.

———1972, Active faults, probable active faults, and associated fracture zones, San Mateo County, California: U.S. Geol. Survey Misc. Field Studies Map MF–355, scale 1:62,500.

Brown, R. D., Jr., and Lee, W. H. K., 1971, Active faults and preliminary earthquake epicenters in the southern part of the San Francisco Bay region: U.S. Geol. Survey Misc. Field Studies Map MF–307, scale 1:250,000.

Brown, R. D., Jr., and Vedder, J. G., 1967, Surface tectonic fractures along the San Andreas fault, *in* The Parkfield-Cholame, earthquakes of June-August 1966: U.S. Geol. Survey Prof. Paper 579, p. 2–22.

Brown, R. D., Jr., Vedder, J. G., Wallace, R. E., Roth, E. F. Yerkes, R. F., Castle, R. O. Waananen, A. O., Page, R. W., and Eaton, J. P., 1967, The Parkfield-Cholame, California, earthquakes of June-August 1966—Surface geologic effects, water-resources aspects, and preliminary seismic data: U.S. Geol. Survey Prof. Paper 579, 66 p.

Brown, R. D., Jr., and Wallace, R. E., 1968, Current and historic fault movement along the San Andreas fault between Paicines and Camp Dix, California, *in* Dickinson, W. R., and Grantz, Arthur,

eds., Proceedings of conference on geologic problems of San Andreas fault system: Stanford Univ. Pubs. Geol. Sci., v. 11, p. 22–41.

Brown, R. D., Jr., Ward, P. L., and Plafker, George, 1973, Geologic and seismologic aspects of the Managua, Nicaragua, earthquakes of December 23, 1972: U.S. Geol. Survey Prof. Paper 838, 34 p.

Brown, R. D., Jr., and Wolfe, E. W., 1972, Map showing recently active breaks along the San Andreas fault between Pt. Delgada and Bolinas Bay, California: U.S. Geol. Survey Misc. Geol. Inv. Map I–692, scale 1:24,000.

Brune, J. N., 1970, Tectonic stress and the spectra of seismic shear waves from earthquakes: Jour. Geophys. Research, v. 75, p. 4997–5009.

Burke, D. B., and Helley, E. J., 1973, Map showing evidence for recent fault activity in the vicinity of Antioch, Contra Costa County, California: U.S. Geol. Survey Misc. Field Studies Map MF–533, scale 1:24,000.

Burnett, J. L., 1972, Geologic and slope stability maps of the Hayward hills, California: Hayward, California Planning Dept., Hayward Hills Study Area, scale 1:24,000.

California Department of Water Resources, 1966, Evaluation of ground water resources, Livermore and Sunol Valleys, Appendix A, Geology: California Dept. Water Resources Bull. 118–2, 153 p.

Chae, Y. S., 1968, Viscoelastic properties of snow and sand: Am. Soc. Civil Engineers Proc., Jour. Eng. Mechanics Div., v. 94, p. 1379—1394.

Clague, J. J., 1969, Landslides of southern Point Reyes National Seashore: California Div. Mines and Geology Mineral Inf. Service, v. 22, p. 107–110, 116–118.

Clark, M. M., 1972, Surface rupture along the Coyote Creek fault, *in* The Borrego Mountain earthquake of April 9, 1968: U.S. Geol. Survey Prof. Paper 787, p. 55–86.

Clark, M. M., Grantz, Arthur, and Rubin, Meyer, 1972, Holocene activity of the Coyote Creek fault as recorded in the sediments of Lake Cahuilla, *in* The Borrego Mountain earthquake of April 9, 1968: U.S. Geol. Survey Prof. Paper 787, p. 1112–1130.

Cluff, L. S., and Steinbrugge, K. V., 1966, Hayward fault slippage in the Irvington-Niles district of Fremont, California: Seismol. Soc. America Bull., v. 56, p. 257–279.

Cooper, Allan, 1971, Structure of the continental shelf west of San Francisco, California: California State Univ. San Jose, unpub. M.S. thesis.

Cummings, J. C., 1968, The Santa Clara formation and possible post-Pliocene slip on the San Andreas fault in central California, *in* Dickinson, W. R., and Grantz, Arthur, eds., Proceedings of conference on geologic problems of San Andreas fault system: Stanford Univ. Pubs. Geol. Sci., v. 11, p. 191–207.

Dibblee, T. W., Jr., 1966, Geology of Palo Alto quadrangle, Santa Clara and San Mateo Counties, California: California Div. Mines and Geology, Map Sheet 8, scale 1:62,500.

———1972a, Preliminary geologic map of the Lick Observatory quadrangle, Santa Clara County, California: U.S. Geol. Survey open-file map, scale 1:24,000.

———1972b, Preliminary geologic map of the San Jose East quadrangle, Santa Clara County, California: U.S. Geol. Survey open-file map, scale 1:24,000.

———1972c, Preliminary geologic map of the Milpitas quadrangle, Alameda and Santa Clara Counties, California: U.S. Geol. Survey open-file map, scale 1:24,000.

———1972d, Preliminary geologic map of the Calaveras Reservoir, Santa Clara County, California: U.S. Geol. Survey open-file map, scale 1:24,000.

———1973a, Preliminary geologic map of the Gilroy quadrangle, Santa Clara County, California: U.S. Geol. Survey open-file map, scale 1:24,000.

———1973b, Preliminary geologic map of the Gilroy Hot Springs quadrangle, Santa Clara County, California: U.S. Geol. Survey open-file map, scale 1:24,000.

———1973c, Preliminary geologic map of the Morgan Hill quadrangle, Santa Clara County, California: U.S. Geol. Survey open-file map, scale 1:24,000.

———1973d, Preliminary geologic map of the Mt. Madonna quadrangle, Santa Clara and Santa Cruz Counties, California: U.S. Geol. Survey open-file map, scale 1:24,000.

———1973e, Preliminary geologic map of the Mt. Sizer quadrangle, Santa Clara County, California: U.S. Geol. Survey open-file map, scale 1:24,000.

Dickinson, W. R., and Grantz, Arthur, 1968, Proceedings of conference on geologic problems of San Andreas fault system: Stanford Univ. Pubs. Geol. Sci., v. 11, p. 117–120.

Dieterich, J. H., 1973, A deterministic near-field source model: World Conference on Earthquake Engineering, 5th, Rome, Italy, Proc., p. 2385–2396.

Dobry, R. Whittman, R. V., and Roeset, J. M., 1971, Soil properties and the one-dimensional theory of earthquake amplification: Massachusetts Inst. Tech. Research Rept. R71–18, Soils Pub. 275, 347 p.

Dooley, R. L., 1973, Geology and land use considerations in the vicinity of the Green Valley fault, Solano County, California: California Univ. Davis, unpub. M.S. thesis, 47 p.

Eckel, E. B., ed., 1958, Landslides and engineering practice, *in* National Research Council, Highway Research Board Spec. Rept. 29: Dept. of Soils, Geology and Foundations, NAS–NRC Pub. 544, 232 p.

Fox, K. F., Jr., Sims, J. D., Bartow, J. A., and Helley, E. J., 1973, Preliminary geologic map of eastern Sonoma County and western Napa County, California: U.S. Geol. Survey, Misc. Field Studies Map MF–483, 4 sheets, scale 1:62,500.

Frame, P. A., 1974, Landslides in the Mt. Sizer area, Santa Clara County, California: California State Univ. San Jose, M.S. thesis, 67 p.

Gealey, W. K., 1951, Geology of the Healdsburg quadrangle, California: California Div. Mines and Geology Bull. 161, 76 p.

Gibbs, J. F., and Borcherdt, R. D., 1974, Effects of local geology on ground motion in the San Francisco Bay region—a continuing study: U.S. Geol. Survey open-file rept., 162 p.

Gibbs, H. J., and Holtz, W. G., 1957, Research on determining the density of sand by spoon penetration test: Internat. Conf. Soil Mechanics and Foundations Eng., 4th, London, Proc., v. 1, p. 35–39.

Gibson, W. M., and Wollenberg, H. A., 1968, Investigations for ground stability in the vicinity of the Calaveras fault, Livermore and Amador Valleys, Alameda County, California: Geol. Soc. America Bull., v. 79, p. 627–638.

Glen, William, 1959, Pliocene and lower Pleistocene of the western part of the San Francisco peninsula: California Univ. Pubs. Geol. Sci., v. 36, p. 147–198.

Greene, H. G., Lee, W. H. K., McCulloch, D. S., and Brabb, E. E., 1973, Faults and earthquakes in the Monterey Bay region, California: U.S. Geol. Survey Misc. Field Studies Map MF–518, 4 sheets, scale 1:250,000.

Griggs, G. B., 1973, Earthquake activity between Monterey and Half Moon Bay, California: California Geology, v. 26, p. 103–110.

Hadley, J. B., 1964, Landslides and related phenomena accompanying the Hebgen Lake earthquake of August 17, 1959: U.S. Geol. Survey Prof. Paper 435, p. 107–138.

Hall, Nelson T., Sarna-Wojcicki, Andre, and Dupré, William, 1974, Faults and their potential hazard in Santa Cruz County, California: U.S. Geol. Survey Misc. Field Inv. MF–626, scale 1:62,500.

Hanks, T. C., 1975, The faulting mechanism of the San Fernando earthquake: Jour. Geophys. Research (in press).

Hansen, W. R., 1964, Sewage effluent disposal and its effects on ground water beneath Livermore Valley: Assoc. Eng. Geologists Bull., v. 1, p. 22–36.

Hansen, W. R., Eckel, E. B., Schaem, W. E., Lyle, R. E., George, Warren, and Chance, Genie, 1966, The Alaska earthquake, March 27, 1964: Field investigations and reconstruction effort: U.S. Geol. Survey Prof. Paper 541, 111 p.

Hardin, B. O., and Dernevich, V. D., 1972, Shear modulus and damping in soils; design equations and curves: Am. Soc. Civil Engineers Proc. Soil Mechanics and Found. Div., p. 667–692.

Harding, R. C., 1969, Landslides—A continuing problem for Bay area development, *in* Danehy, E. A. (ed.), Urban environmental geology in San Francisco Bay region: Assoc. Eng. Geologists, San Francisco Section, Spec. Pub., p. 65–74.

Haskell, N. A., 1953, The disperson of surface waves on multilayered media: Seismol. Soc. America Bull., v. 43, p. 17–34.

Hazelwood, R. M., 1974, Preliminary report of seismic refraction survey along the east side of San Francisco Bay, Alameda County, California: U.S. Geological Survey open-file rept., 10 p.

Helley, E. J., and Brabb, E. E., 1971, Geologic map of late Cenozoic deposits, Santa Clara County, California: U.S. Geol. Survey Misc. Field Studies Map MF–335, 3 sheets, scale 1:62,500.

Helley, E. J., Lajoie, K. R., and Burke, D. B., 1972, Geologic map of late Cenozoic deposits, Alameda County, California: U.S. Geol. Survey Misc. Field Studies Map MF–429, scale 1:62,500.

Hudson, D. E., Brady, A. G., Trifunac, M. D., and Vijayaraghavan, A., 1971, Strong-motion earthquake accelerograms, corrected accelerograms and integrated ground velocity and displacement curves: California Inst. Tech., Earthquake Eng. Research Lab., EERL 71–51, v. 2, 321 p.

Huffman, M. E., 1972a, Geology for planning on the Sonoma County coast between the Russian and Gualala Rivers: California Div. Mines and Geology Prelim. Rept. 16, 38 p., scale 1:24,000.

———1972b, Geology for planning in the Sonoma Mountain and Mark-Riebli Road areas, Sonoma County, California: California Div. Mines and Geology open-file rept. 72–25, scale 1:24,000.

———1974, Geology for planning on the Sonoma County coast between the Russian River and Estero Americana: California Div. Mines and Geology Prelim. Rept. 20, 36 p.

Housner, G. W., 1965, Intensity of earthquake ground shaking near the causative fault: World Conference on Earthquake Engineering, 3rd, Wellington, New Zealand, Proc., v. 1, p. III–94–III–109.

Housner, G. W., and Jennings, P. C., 1972, The San Fernando, California earthquake: Earthquake Eng. and Structural Dynamics 1, p. 5–31.

Hudson, D. E., 1962, Some problems in the application of spectrum techniques to strong-motion earthquake analysis: Seismol. Soc. America Bull., v. 52, p. 417–430.

Ida, Y., 1973, The maximum acceleration of seismic ground motion: Seismol. Soc. America Bull., v. 63, p. 959–968.

Idriss, I. M., and Seed, H. B., 1968, Seismic response of horizontal soil layers: Am. Soc. Civil Engineers Proc., Soil Mechanics and Found. Div., v. 94, p. 1003–1031.

Iida, Numizi, 1965, Earthquake magnitude, earthquake fault and source dimensions: Nagoya Univ. Jour. Earth Sci., v. 13, p. 115—132.

Jack, Robert, 1968, Quaternary sediments of the Montara Mountain area, San Mateo County: California Univ., Berkeley, unpub. M.A. thesis.

Jahns, R. H., and Hamilton, D. H., 1971, Geology of the Mendocino Power Plant, *in* Mendocino Power Plant Preliminary Safety Analysis Report: U.S. Atomic Energy Comm., v. 1, appendix 2.5A, 61 p.

Johnson, A. M., and Ellen, S. D., 1965, Preliminary evaluation of the interaction between engineering development and natural geologic processes on the Bovet property, town of Portola Valley, California—with a section on the San Andreas fault by W. R. Dickinson: Report prepared for City of Portola Valley, California, scale 1:2,400.

Johnson, A. M., and Lobo-Guerrero, A. U., 1968, Preliminary evaluation of the relative stability of ground, Marianni property, town of Portola Valley, California—with a section on the San Andreas fault by W. R. Dickinson: Report prepared for the City of Portola Valley, California, 22 p.

Kanai, K., 1952, Relation between the nature of surface layer and the amplitudes of earthquake motions: Tokyo Univ. Earthquake Research Inst. Bull., v. 30, p. 31–37.

Kojan, E., Foggin, G. T., III, and Rice, R. M., 1972, Prediction and analysis of debris slide incidence by photogrammetry, Santa Ynez–San Rafael Mountains, California: Internatl. Geol. Congress, 24th, sec. 13, p. 124–131.

Lajoie, K. R., Helley, E. J., Nichols, D. R., and Burke, D. B., 1974, Unconsolidated and semi-unconsolidated sedimentary deposits, San Mateo County, California: U.S. Geological Survey Misc. Field Studies Map MF–575, scale 1:62,500.

Lawson, A. C., 1893, The post-Pliocene diastrophism of the coast of southern California: California Univ. Pubs. Geol. Sci., v. 1, p. 115–160.

———1895, Sketch of the geology of the San Francisco peninsula, Extract from the Fifteenth Annual Report of the U.S. Geol. Survey, 1893–94, Washington, Govt. Printing Office, p. 401–476.

Lawson, A. C., and others, 1908, The California earthquake of April 18, 1906—Report of the State Earthquake Investigation Commission: Carnegie Inst. Washington Pub. 87, 2 vols.

Lee, W. H. K., Eaton, M. S., and Brabb, E. E., 1971, The earthquake sequence near Danville, California, 1970: Seismol. Soc. America Bull., v. 61, p. 1771–1794.

Lee, W. H. K., Meagher, K. L., Bennett, R. E., and Matamoros, E. E., 1972, Catalog of earthquakes along the San Andreas fault system in central California for the year 1971: U.S. Geol. Survey open-file rept., 67 p.

Lee, W. H. K., Roller, J. C., Bauer, P. G., and Johnson, J. D., 1972, Catalog of earthquakes along the San Andreas fault system in central California for the year 1969: U.S. Geol. Survey open-file rept., 48 p.

Lee, W. H. K., Roller, J. C., Meagher, K. L., and Bennett, R. E., 1972, Catalog of earthquakes along the San Andreas fault system in central California for the year 1970: U.S. Geol. Survey open-file rept., 73 p.

Lindh, A. G., and Boore, D. M., 1973, Another look at the Parkfield earthquake using strong-motion instruments as a seismic array (abs.): Seismol. Soc. America, Earthquake Notes 44, p. 24.

Louderback, G. D., 1942, Faults and earthquakes: Seismol. Soc. America Bull., v. 32, p. 305–330.

———1947, Central California earthquakes of the 1830's: Seismol. Soc. America Bull., v. 37, p. 33–74.

Maberry, J. O., 1972a, Map showing landslide deposits and areas of potential landsliding in the Parker quadrangle, Arapahoe and Douglas Counties, Colorado: U.S. Geol. Survey Misc. Geol. Inv. Map I–770–E, scale 1:24,000.

———1972b, Slope map of the Parker quadrangle, Arapahoe and Douglas Counties, Colorado: U.S. Geol. Survey Misc. Geol. Inv. Map I–770–F, scale 1:24,000.

McEvilly, T. V., 1966, The earthquake sequence of November 1964 near Corralitos, California: Seismol. Soc. America Bull., v. 56, p. 755–773.

———1970, Magnitudes, epicenters, and fault plane solutions, *in* The Santa Rosa earthquakes of October 1969: Mineral Inf. Service, v. 23, p. 44–48.

McEvilly, T. V., and Casaday, K. B., 1967, The earthquake sequence of

September 1965 near Antioch, California: Seismol. Soc. America Bull., v. 57, p. 113–124.

McLaughlin, R. J., 1971, Geologic map of the Sargent fault zone in the vicinity of Mount Madonna, Santa Clara County, California: U.S. Geol. Survey open-file map, scale 1:12,000.

———1973, Geology of the Sargent fault zone in the vicinity of Mount Madonna, Santa Clara and Santa Cruz Counties, California: California State Univ. San Jose, unpub. M. S. thesis, 131 p.

McLaughlin, R. J., Simoni, T. R., Osbun, E. D., and Bauer, P. G., 1971, Preliminary geologic map of the Loma Prieta–Mount Madonna area, Santa Clara and Santa Cruz Counties, California: U.S. Geol. Survey open-file map, scale 1:24,000.

Medvedev, S. V., 1965, Engineering seismology: National Technical Inf. Service, NTIS No. TT65–50011, 260 p.

Milliman, J. D., and Emery, K. O., 1968, Sea levels during the past 35,000 years: Science, v. 162, p. 1121.

Morton, D. M., 1971, Seismically triggered landslides in the area above the San Fernando Valley, *in* The San Fernando, California, earthquake of February 9, 1971: U.S. Geol. Survey Prof. Paper 733, p. 99–104.

Murphy, L. M., and Cloud, W. K., 1957, United States earthquakes, 1955: U.S. Coast and Geodetic Survey, 83 p.

Nason, R. D., 1971, Measurements and theory of fault creep slippage in central California: Royal Soc. New Zealand Trans., v. 9, p. 181–187.

Newmark, N. M., and Hall, W. J., 1969, Seismic design criteria for nuclear reactor facilities: World Conference Earthquake Engineering, 4th, Santiago, Chile, Proc., v. 2, p. 37–50.

Nichols, D. R., and Wright, N. A., 1971, Preliminary map of historic margins of marshlands, San Francisco Bay, California: U.S. Geol. Survey open-file map, scale 1:125,000.

Nilsen, T. H., 1971, Preliminary photointerpretation map of landslide and other surficial deposits of the Mount Diablo area, Contra Costa and Alameda Counties, California: U.S. Geol. Survey Misc. Field Studies Map MF–310, scale 1:62,500.

———1972a, Preliminary photointerpretation map of landslide and other surficial deposits of parts of the Altamont and Carbona 15-minute quadrangles, Alameda County, California: U.S. Geol. Survey Misc. Field Studies Map MF–321, scale 1:62,500.

———1972b, Preliminary photointerpretation map of landslide and other surficial deposits of the Byron area, Contra Costa and Alameda Counties, California: U.S. Geol. Survey Misc. Field Studies Map MF–338, scale 1:62,500.

———1972c, Preliminary photointerpretation map of landslide and other surficial deposits of the Mount Hamilton quadrangle and parts of the Mount Boardman and San Jose quadrangles, Alameda and Santa Clara Counties, California: U.S. Geol. Survey Misc. Field Studies Map MF–339, scale 1:62,500.

———1972d, Preliminary photointerpretation map of landslides and other surficial deposits of parts of the Los Gatos, Morgan Hill, Gilroy Hot Springs, Pacheco Pass, Quien Sabe, and Hollister 15-minute quadrangles, Santa Clara County, California: U.S. Geol. Survey Misc. Field Studies Map MF–416, scale 1:62,500.

———1973a, Current slope stability studies by the U.S. Geological Survey in the San Francisco Bay region: Landslide, The Slope Stability Review, v. 1, no. 1, p. 2–10.

———1973b, Preliminary photointerpretation map of landslide and other surficial deposits of the Livermore and part of the Hayward 15-minute quadrangles, Alameda and Contra Costa Counties, California: U.S. Geol. Survey Misc. Field Studies Map MF–519, scale 1:62,500.

———1973c, Preliminary photointerpretation map of landslide and other surficial deposits of the Concord 15-minute quadrangle and the Oakland West, Richmond, and part of the San Quentin 7.5-minute quadrangles, Contra Costa and Alameda Counties, California: U.S. Geol. Survey Misc. Field Studies Map MF–493, scale 1:62,500.

Nilsen, T. H., and Brabb, E. E., 1972, Preliminary photointerpretation and damage maps of landslide and other surficial deposits in northeastern San Jose, California: U.S. Geol. Survey Misc. Field Studies Map MF–361, scales 1:12,000 and 1:24,000.

Nilsen, T. H., Taylor, F. A., and Brabb, E. E., 1975, Structurally damaging landslides in Alameda County, California, from 1940 to 1971—economic analysis and influence of ancient landslide deposits: U.S. Geol. Survey Bull. 1398 (in press).

Nilsen, T. H., and Turner, B. L., 1974, The influence of rainfall and ancient landslide deposits on recent landslides (1950–1971) in urban areas of Contra Costa County, California: U.S. Geol. Survey Bull. 1388.

Oakeshott, G. B., ed., 1959, San Francisco earthquake of March 1957: California Div. Mines Spec. Rept., v. 57, p. 73–123.

Page, R. A., Boore, D. M., Joyner, W. B., and Coulter, H. W., 1972, Ground motion values for use in the seismic design of the trans-Alaska pipeline system: U.S. Geol. Survey Circ. 672, 23 p.

Pampeyan, E. H., 1970, Geologic map of the Palo Alto 7.5-minute quadrangle, San Mateo and Santa Clara Counties, California: U.S. Geol. Survey open-file rept., scale 1:24,000.

Peacock, W. H., and Seed, H. B., 1968, Sand liquefaction under cyclic loading simple shear conditions: Am. Soc. Civil Engineers Proc., Jour. Soil Mechanics and Found. Div., v. 94, no. SM3, p. 689–708.

Plafker, George, 1969, Tectonics of the March 27, 1964 Alaska earthquake: U.S. Geol. Survey Prof. Paper 543–I, 74 p.

Plafker, G., Erickson, G. E., and Concha, F. J., 1971, Geological aspects of the May 31, 1970, Peru earthquake: Seismol. Soc. America Bull., v. 61, p. 543–578.

Radbruch, D. H., 1957, Areal and engineering geology of the Oakland West quadrangle, California: U.S. Geol. Survey Misc. Geol. Inv. Map I–239, scale 1:24,000.

———1967, Approximate location of fault traces and historic surface ruptures within the Hayward fault zone between San Pablo and Warm Springs, California: U.S. Geol. Survey Misc. Geol. Inv. Map I–522, scale 1:62,500.

———1968a, Map showing recently active breaks along the Hayward fault zone and southern part of the Calaveras fault zone, California: U.S. Geol. Survey open-file map, 2 sheets, scale 1:24,000.

———1968b, New evidence of historic fault activity in Alameda, Contra Costa, and Santa Clara Counties, California, *in* Dickinson, W. R., and Grantz, Arthur, eds., Proceedings of conference on geologic problems of San Andreas fault system: Stanford Univ. Pubs. Geol. Sci., v. 11, p. 46–54.

———1969, Areal and engineering geology of the Oakland East quadrangle, California: U.S. Geol. Survey Geol. Quad. Map GQ–769, scale 1:24,000.

Radbruch, D. H., Bonilla, M. G., and others, 1966, Tectonic creep in the Hayward fault zone, California: U.S. Geol. Survey Circ. 525, 13 p.

Radbruch, D. H., and Case, J. E., 1967, Preliminary geologic map and engineering geologic information, Oakland and vicinity, California: U.S. Geol. Survey open-file map, scale 1:24,000.

Radbruch, D. H., and Lennert, B. J., 1966, Damage to culvert under Memorial Stadium University of California, Berkeley, caused by slippage in the Hayward fault zone: Seismol. Soc. America Bull., v. 56, p. 295–305.

Radbruch, D. H., and Weiler, L. M., 1963, Preliminary report on landslides in a part of the Orinda Formation, Contra Costa County, California: U.S. Geol. Survey open-file rept., 49 p.

Radbruch, D. H., and Wentworth, C. M., 1971, Estimated relative abundance of landslides in the San Francisco Bay region, California: U.S. Geol. Survey open-file rept., scale 1:500,000.

Rice, S. J., and Strand, R. G., 1972, Geologic and slope stability maps of the Tennessee Valley, Lucas Valley and north coastal areas,

Marin County, California: California Div. Mines and Geology open-file rept. 72–22, scale 1:12,000.

Richter, C. F., 1958, Elementary seismology: San Francisco, W. H. Freeman, 768 p.

Reiche, Parry, 1950, Rio Vista, California, fault scarp (abs.): Geol. Soc. America Bull., v. 61, p. 1529–1530.

Ritter, J. R., and Dupré, W. R., 1972, Map showing areas of potential inundation by tsunamis in the San Francisco Bay Region, California: U.S. Geol. Survey Misc. Field Inv. Map MF–480, scale 1:125,000.

Rogers, T. H., 1971, Environmental geologic analysis of the Santa Cruz Mountain study area, Santa Clara County, California: California Div. Mines and Geology, San Jose, Calif., Santa Clara County Planning Dept., 64 p.

———1972, Bear Valley–Melendy Ranch earthquakes of 24–27 February 1972: California Geology, v. 25, p. 138.

Rogers, T. H., and Nason, R. D., 1971, Active displacement on the Calaveras fault zone at Hollister, California: Seismol. Soc. America Bull., v. 61, p. 399–416.

Saul, R. B., 1972, Geology and slope stability of the southwest quarter of the Walnut Creek quadrangle, Contra Costa County, California: California Div. Mines and Geology Map Sheet 16, scale 1:12,000.

Savage, J. C., and Burford, R. O., 1973, Geodetic determination of relative plate motion in central California: Jour. Geophy. Research, v. 78, p. 832–845.

Schlocker, J., Bonilla, M. G., and Radbruch, D. H., 1958, Geology of the San Francisco north quadrangle, California: U.S. Geol. Survey Misc. Geol. Inv. Map I–272, scale 1:24,000.

Schnabel, P. B., and Seed, H. B., 1973, Accelerations in rock for earthquakes in the western United States: Seismol. Soc. America Bull., v. 63, p. 501–516.

Schuyler, J. D., 1898, Reservoirs for irrigation, *in* Eighteenth Annual Report of the U.S. Geol. Survey for 1896–1897, Part IV: Washington, D. C., p. 711–713.

Scott, G. R., 1972, Map showing landslides and areas susceptible to landsliding in the Morrison quadrangle, Jefferson County, Colorado: U.S. Geol. Survey Misc. Geol. Inv. Map I–790–B, scale 1:24,000.

Seed, H. B., 1968, Landslides during earthquakes due to soil liquefaction: Am. Soc. Civil Engineers Proc., Jour. Soil Mechanics and Found. Div., v. 94, p. 1053–1122.

Seed, H. B., and Idriss, I. M., 1971, Simplified procedure for evaluating soil liquefaction potential: Am. Soc. Civil Engineers Proc., Jour. Soil Mechanics and Found. Div., v. 97, p. 1249–1273.

Seed, H. B., Idriss, I. M., and Kiefer, F. W., 1969, Characteristics of rock motions during earthquakes: Am. Soc. Civil Engineers Proc., Jour. Soil Mechanics and Found. Div., v. 95, p. 1199–1218.

Seed, H. B., and Lee, K. L., 1969, Pore-water pressures in earth slopes under seismic loading conditions: World Conf. on Earthquake Engineering, 4th, Santiago, Chile, Proc. V. 3, p. A–5–1 to A–5–11.

Seed, H. B., and Peacock, W. H., 1971, Test procedures for measuring soil liquefaction characteristics: Am. Soc. Civil Engineers Proc., Jour. Soil Mechanics and Found. Div., v. 97, p. 1099–1119.

Sharp, R. V., 1973, Map showing recent tectonic movement on the Concord fault, Contra Costa and Solano Counties, California: U.S. Geol. Survey Misc. Field Studies Map MF–505, scale 1:24,000.

Sharp, R. V., and Clark, M. M., 1972, Geologic evidence of previous faulting near the 1968 rupture on the Coyote Creek fault, *in* The Borrego Mountain earthquake of April 9, 1968: U.S. Geol. Survey Prof. Paper 787, p. 131–140.

Simpson, H. E., 1973a, Map showing landslides in the Golden quadrangle, Jefferson County, Colorado: U.S. Geol. Survey Misc. Geol. Inv. Map I–761–B, scale 1:24,000.

———1973b, Map showing areas of potential rockfalls in the Golden quadrangle, Jefferson County, Colorado: U.S. Geol. Survey Misc. Geol. Inv. Map I–761–C, scale 1:24,000.

Sims, J. D., Fox, K. F., Jr., Bartow, J. A., and Helley, E. J., 1973, Preliminary geologic map of Solano County and parts of Napa, Contra Costa, Marin, and Yolo Counties, California: U. S. Geol. Survey Misc. Field Studies Map MF–484, 5 sheets, scale 1:62,500.

Sims, J. D., and Nilsen, T. H., 1972, Preliminary photointerpretation map of landslides and other surficial deposits of parts of the Pittsburg and Rio Vista 15-minute quadrangles, Contra Costa and Solano Counties, California: U.S. Geol. Survey Misc. Field Studies Map MF–322, scale 1:62,500.

Slemmons, D. B., 1967, Pliocene, and Quaternary crustal movements of the Basin-and-Range Province, USA: Osaka City Univ. Jour. Geosciences, vol. 10, p. 1–11.

Smith, D. D., 1960, Geomorphology of the San Francisco peninsula: Stanford Univ., unpub. Ph.D. thesis, 433 p.

Steinbrugge, K. V., Cloud, W. K., and Scott, N. H., 1970, The Santa Rosa, California earthquakes of October 1, 1969: Washington, U.S. Govt. Printing Office, 99 p.

Steinbrugge, K. V., and Zacher, E. G., 1960, Fault creep and property damage, *in* Creep on the San Andreas fault: Seismol. Soc. America Bull., v. 50, p. 389–396.

Taylor, F. A., and Brabb, E. E., 1972, Map showing distribution and cost by counties of structurally damaging landslides in the San Francisco Bay region, California, winter of 1968–69: U.S. Geol. Survey Misc. Field Studies Map MF–327, scale 1:1,000,000.

Thatcher, W., and Hanks, T. C., 1973, Source parameters of southern California earthquakes: Jour. Geophys. Research, v. 78, p. 8547–8576.

Tocher, Don, 1958, Earthquake energy and ground breakage: Seismol. Soc. America Bull., v. 48, p. 147–153.

———1959, Seismic history of the San Francisco Bay region, *in* San Francisco earthquakes of March 1957: California Div. Mines Spec. Rept. 57, p. 39–48.

———1960, Creep on the San Andreas fault—creep rate and related measurements at Vineyard, California, *in* Creep on the San Andreas fault: Seismol. Soc. America Bull., v. 50, p. 396–404.

Trask, J. B., 1964, Earthquakes in California from 1800 to 1864: California Acad. Sci. Proc., v. 3, p. 130–153.

Trifunac, M. D., 1975, A three-dimensional dislocation model for the San Fernando, California, earthquake of February 9, 1971: Seismol. Soc. America Bull. (in press).

Trifunac, M. D., and Hudson, D. E., 1971, Analysis of the Pacoima dam accelerogram—San Fernando, California, earthquake of 1971: Seismol. Soc. America Bull. v. 61, p. 1393–1411.

Unger, J. D., and Eaton, J. P., 1970, Aftershocks of the October 1, 1969, Santa Rosa, California, earthquakes (abs): Geol. Soc. America Abs. with Programs, v. 2, p. 155.

U.S. Geological Survey, 1971a, Surface faulting, *in* The San Fernando California earthquake of February 9, 1971: U.S. Geol. Survey Prof. Paper 733, p. 55–76.

———1971b, Worldwide correlation of surface displacement and Richter magnitude, *in* Geological Survey research 1971; U.S. Geol. Survey Prof. Paper 750–A, p. 168.

———1972, Slope map of the San Francisco Bay region: U.S. Govt. Printing Office, 3 sheets, scale 1:125,000.

U.S. Soil Conservation Service, 1968, Soils of Santa Clara County, California: Washington, D. C., U.S. Govt. Printing Office, 227 p.

Van Horn, Richard, 1972a, Slope map of the Sugar House quadrangle, Salt Lake County, Utah: U.S. Geol. Survey Misc. Geol. Inv. Map I–766–C, scale 1:24,000.

———1972b, Landslide and associated deposit map of the Sugar House quadrangle, Salt Lake County, Utah: U.S. Geol. Survey Misc. Geol. Inv. Map I–766–D, scale 1:24,000.

———1972c, Relative slope stability of the Sugar House quadrangle, Salt Lake County, Utah: U.S. Geol. Survey Misc. Geol. Inv. Map

I–766–E, scale 1:24,000.

Varnes, D. J., 1958, Landslide types and processes, chap. 3, *in* Eckel, E. B., ed., Landslides and engineering practice: Natl. Research Council, Highway Research Board Spec. Rept. 29, NAS-NRC Pub. 544, p. 20–47.

Vedder, J. G., and Wallace, R. E., 1970, Map showing recently active breaks along San Andreas fault between Cholame Valley and Tejon Pass, California: U.S. Geol. Survey Misc. Inv. Map I–574, scale 1:24,000.

Wallace, R. E., 1968, Notes on stream channels offset by the San Andreas fault, southern Coast Ranges, California, *in* Dickinson, W. R., and Grantz, Arthur, eds., Proceedings of conference on geologic problems of San Andreas fault system: Stanford Univ. Pubs. Geol. Sci., v. 11, p. 6–21.

———1969, Planning along active strands of the San Andreas fault: Assoc. Eng. Geologists, National Meetings, San Francisco, 1969, Field Trips (Guidebook), p. E5–E6.

———1970, Earthquake recurrence intervals on the San Andreas fault: Geol. Soc. America Bull., v. 81, p. 2875–2890.

Waltz, J. P., 1971, An analysis of selected landslides in Alameda and Contra Costa Counties, California: Assoc. Eng. Geologists Bull., v. 8, p. 153–163.

Warrick, R. E., 1974, Seismic investigation of a San Francisco Bay mud site: Seismol. Soc. America Bull., v. 64, p.

Weaver, C. E., 1949, Geology of the Coast Ranges immediately north of the San Francisco Bay region, California: Geol. Soc. America Mem. 33, 242 p.

Weber, G. E., and Lajoie, K. R., 1974, Holocene movement on the San Gregorio fault zone near Año Nuevo, San Mateo County, California (abs.): Geol. Soc. America Abs. with Programs, v. 6, p. 273.

Wentworth, C. M., Bonilla, M. C., and Buchanan, J. M., 1973, Seismic environment of the Burro Flats site, Ventura County, California: U.S. Geol. Survey open-file rept., 35 p.

Wentworth, C. M., Ziony, J. I., and Buchanan, J. M., 1970, Preliminary geologic environmental map of the greater Los Angeles area, California: U.S. Atomic Energy Comm., TID–25363, 41 p., scale 1:250,000.

Wesson, R. L., Bennett, R. E., and Lester, F. W., 1972a, Catalog of earthquakes along the San Andreas fault system in central California, April–June, 1972: U.S. Geol. Survey open-file rept. 42 p.

Wesson, R. L., Bennett, R. E., and Meagher, K. L., 1972b, Catalog of earthquakes along the San Andreas fault system in central California, January –March, 1972: U.S. Geol. Survey open-file rept. 60 p.

Wesson, R. L., and Ellsworth, W. L., 1973, Seismicity preceding moderate earthquakes in California: Jour. Geophys. Research, v. 78, p. 8527–8546.

Wesson, R. L., Lester, F. W., and Meagher, K. L., 1974, Catalog of earthquakes along the San Andreas fault system in central California, October–December 1972: U.S. Geol. Survey open-file rept., 46 p.

Wesson, R. L., Meagher, K. L., and Lester, F. W., 1973a, Catalog of earthquakes along the San Andreas fault system in central California, July–September, 1972: U.S. Geol. Survey open-file rept., 49 p.

Wesson, R. L., Roller, J. C., and Lee, W. H. K., 1973b, Time-term analysis and geological interpretation of seismic travel-time data from the Coast Ranges of central California: Seismol. Soc. America Bull., v. 63, p. 1447–1471.

Whitney, J. D., 1865, Geology of California, vol. I, part I. Geology of the Coast Ranges: California Geol. Survey, p. 1–197.

Williams, P. L., 1972, Map showing landslides and areas of potential landsliding in the Salina quadrangle, Utah: U.S. Geol. Survey Misc. Geol. Inv. Map I–591–L, scale 1:250,000.

Wood, H. O., 1908, Distribution of apparent intensity in San Francisco, *in* The California earthquake of April 18, 1906, Report of the State Earthquake Investigation Commission: Carnegie Inst. Washington Pub. 87, p. 220–245.

Wright, R. H., 1971, Map showing locations of samples dated by radiocarbon methods in the San Francisco Bay region: U.S. Geol. Survey Misc. Field Studies Map MF–317, scale 1:500,000.

Wright, R. H., Campbell, R. H., and Nilsen, T. H., 1974, The preparation and use of isopleth maps of landslide deposits: Geology, Oct. 1974, p. 483–485.

Wright, R. H., and Nilsen, T. H., 1974, Isopleth map of landslide deposits, southern San Francisco Bay region, California: U.S. Geol. Survey Misc. Field Studies Map MF–550, scale 1:125,000.

Yerkes, R. F., Bonilla, M. G., Youd, T. L., and Sims, J. D., 1974, Geologic environment of the Van Norman reservoirs area, northern San Fernando Valley, California: U.S. Geol. Survey Circ., 691, pt. 1., 35 p.

Youd, T. L., 1973, Liquefaction, flow and associated ground failure: U.S. Geol. Survey Circ. 688, 12 p.

Ziony, J. I., Wentworth, C. M., and Buchanan, J. M., 1973, Recency of faulting; A widely applicable criterion for assessing the activity of faults: World Conference on Earthquake Engineering, 5th, Rome, Italy, Proc., p. 1680–1683.

☆U.S. GOVERNMENT PRINTING OFFICE: 1975-0-690-036/7

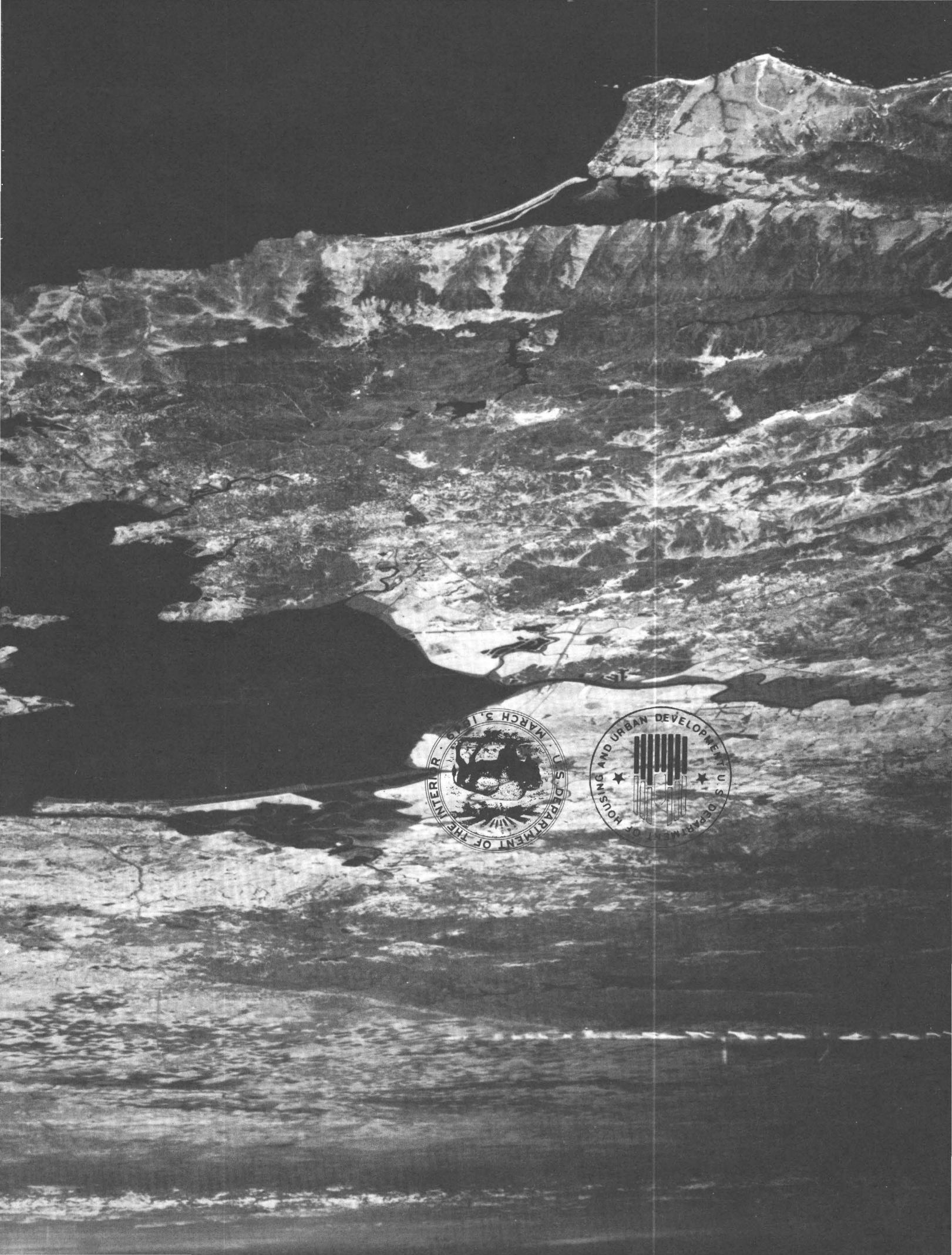
U.S. DEPARTMENT OF THE INTERIOR
MARCH 3, 1849
U.S. DEPARTMENT OF HOUSING AND URBAN DEVELOPMENT